

Winter 2008

Ion sequestration particles for naval anticorrosion coatings

Zachary Z. Zguris

University of New Hampshire, Durham

Follow this and additional works at: <https://scholars.unh.edu/dissertation>

Recommended Citation

Zguris, Zachary Z., "Ion sequestration particles for naval anticorrosion coatings" (2008). *Doctoral Dissertations*. 464.
<https://scholars.unh.edu/dissertation/464>

This Dissertation is brought to you for free and open access by the Student Scholarship at University of New Hampshire Scholars' Repository. It has been accepted for inclusion in Doctoral Dissertations by an authorized administrator of University of New Hampshire Scholars' Repository. For more information, please contact nicole.hentz@unh.edu.

ION SEQUESTRATION PARTICLES FOR NAVAL
ANTICORROSION COATINGS

BY

ZACHARY Z. ZGURIS

BS in Chemical Engineering, Minor in Dance, University of New Hampshire 1998

MS in Chemical Engineering, University of New Hampshire, 2000

DISSERTATION

Submitted to the University of New Hampshire
in Partial Fulfillment of
the Requirements for the Degree of

Doctor of Philosophy
in
Materials Science

December, 2008

UMI Number: 3348320

INFORMATION TO USERS

The quality of this reproduction is dependent upon the quality of the copy submitted. Broken or indistinct print, colored or poor quality illustrations and photographs, print bleed-through, substandard margins, and improper alignment can adversely affect reproduction.

In the unlikely event that the author did not send a complete manuscript and there are missing pages, these will be noted. Also, if unauthorized copyright material had to be removed, a note will indicate the deletion.

UMI[®]

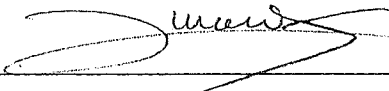
UMI Microform 3348320

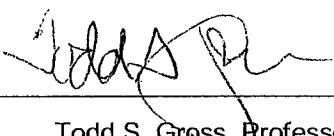
Copyright 2009 by ProQuest LLC.

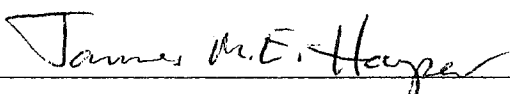
All rights reserved. This microform edition is protected against unauthorized copying under Title 17, United States Code.

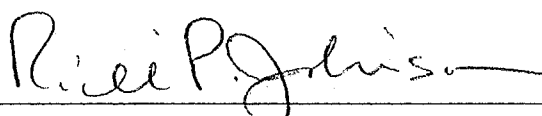
ProQuest LLC
789 E. Eisenhower Parkway
PO Box 1346
Ann Arbor, MI 48106-1346

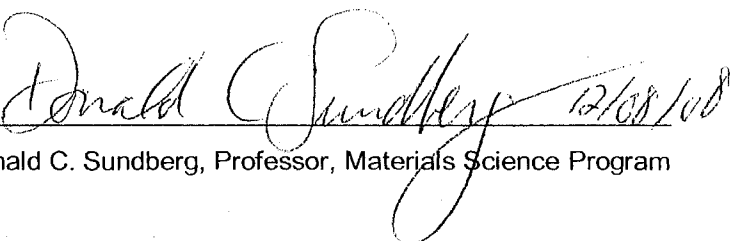
This dissertation has been examined and approved.


12.08.2008
Dissertation Director, Yvon G. Durant,
Research Associate Professor, Materials Science Program


Todd S. Gross, Professor, Mechanical Engineering


James M. Harper, Professor, Physics


Richard P Johnson, Professor, Chemistry


12/08/08
Donald C. Sundberg, Professor, Materials Science Program

DEDICATION

This dissertation is dedicated to my parents who have tolerated and supported me in all my endeavors throughout my life and to whom I am eternally grateful.

ACKNOWLEDGEMENTS

I would like to thank my advisor, Dr. Yvon Durant for his guidance and support over my many years working with him. Without his encouragement I would have likely pursued other interests before completing my graduate studies. I would also like to thank the other members of my committee, Dr. Todd Gross, Dr. James Harper, Dr Richard Johnson, and Dr. Donald Sundberg for their time, support, and advice.

I would like to thank my fellow NPRC members, past and present for their help and assistance with this research work. Many times they came to my assistance with advice and experimental aid for which I am very grateful.

I would like to thank the Office of Naval Research for their funding of this work. I would also like to thank the Naval Research Labs for their assistance and training. Especially Arthur Web and Ted Lemieux as both of them provided invaluable advice and experience that made this project successful.

TABLE OF CONTENTS

DEDICATION	iii
ACKNOWLEDGEMENTS	iv
LIST OF FIGURES	ix
LIST OF TABLES	xii
DEFINITION OF ABBREVIATIONS	xiii
ABSTRACT	xiv
INTRODUCTION	1
CHAPTER 1 BACKGROUND	5
1.1 Corrosion of Steel	5
1.1.1 Effect of Chloride Ions on Corrosion	9
1.1.2 Undercoating (Organic) Corrosion	10
1.2 Organic Anti-Corrosion Coatings	12
1.2.1 Binders	14
1.2.2 Anticorrosion Pigments	16
1.2.2.1 Barrier Pigments	17
1.2.2.2 Chemically Active Pigments	20
1.2.2.3 Electrochemically Active Pigments	29
1.2.3 Fillers	29
1.2.4 Additives	30
1.2.5 Solvent	32
1.3 Ion Sequestration Particles in the Anticorrosion Coating	33
CHAPTER 2 ISP SYNTHESIS	34

2.1	Evolution of the Synthesis of Ion Sequestration Particles	34
2.2	Synthesis of Ion Sequestration Particles	43
2.2.1	Encapsulation of Wet Ion Sequestering Core Material	44
2.2.1.1	Wet Ion Sequestration Material	44
2.2.1.2	Encapsulation of Wet Ion Sequestration Core Material	45
2.2.1.3	Drying of PMMA Encapsulated WISCM	48
2.2.1.4	WISCM Encapsulation Experimental Variations	50
2.2.1.5	Summary of WISCM ISP Experiments	53
2.2.2	Synthesis of a “Core Shell” ISP	54
2.2.2.1	Batch Process Synthesis	58
2.2.2.2	Semi-Batch Process Synthesis	62
2.2.2.3	Summary of Core Shell Experiments	65
2.2.3	Solid Ion Sequestration Core Material Encapsulation	66
2.2.3.1	Experimental Procedure	68
2.2.3.2	Variations in Solid Ion Sequestering Core Materials	70
2.2.3.3	Summary of SISCM Encapsulation Experiments	73
2.3	Summary of ISP Synthesis	75
CHAPTER 3 CHARACTERIZATION		77
3.1	Characterization of Monomers and Surfactants	77
3.1.1	Reaction Kinetics of DGEBA TEPA	78
3.1.2	Characterization of PMMA Produced by SISCM Encapsulation	80
3.1.3	Experimental Determination of PEI Amine Ratio	82
3.2	Characterization of ISPs	85

3.2.1	Particle morphology	86
3.2.2	Characterization of ISP Size	93
3.2.3	Characterization of PMMA Encapsulation of WISCM	97
3.2.4	SISCM Encapsulation	101
3.2.5	Characterization of Ion Exchange Capacity	102
3.2.6	Diffusion of Chloride Ions Through the MIL-DTL-24441 Coating	106
3.2.7	Diffusion Coefficient Determination by ATRIR	113
3.3	Summary of Characterization	124
CHAPTER 4 ANTICORROSION PROPERTIES		126
4.1	Preparation of Steel Coupons	127
4.1.1	Anticorrosion Coating for ISP Performance Evaluation	128
4.1.2	Coating Application	129
4.1.3	Interaction Between ISPs and Coating	134
4.2	Accelerated Corrosion Experiments	136
4.2.1	90 Day Cathodic Disbondment	136
4.2.2	1000 hrs Salt Fog Chamber (ASTM B117)	138
4.2.3	500 hrs Hot De-Ionized Water Immersion	146
4.3	Summary of Anticorrosion Properties	150
CHAPTER 5 CONCLUSIONS & RECOMMENDATIONS		152
5.1	Conclusions	152
5.2	Recommendations for Future Work	154
APPENDICES		157
APPENDIX 1 HOMOGENEOUS ISPs		158

A1.1	Introduction to Homogeneous ISPs	158
A1.2	Synthesis of Homogeneous ISPs	159
A1.3	Characterization of Homogeneous ISPs	161
A1.4	Synthesis Variations	163
A1.5	Summary of Homogeneous ISP Approach	164
APPENDIX 2 SOLVENT/NONSOLVENT POLYMER PRECIPITATION		165
A2.1	Introduction	165
A2.2	Solvent/Nonsolvent ISP Synthesis	166
A2.3	Characterization	170
A2.4	Bulk Ion Sequestering Core Based ISPs	175
A2.5	Summary of Solvent/Nonsolvent Synthesis	178
APPENDIX 3 SUPPLEMENTAL EXPERIMENTS		179
A3.1	Determination of Primary versus Secondary Amine Reactivity	179
A3.2	Development of Extended Amines	183
A3.3	Pre-Rusted Accelerated Corrosion	184
A3.4	Characterization of Ion Exchange by FTIR	185
A3.5	Other Techniques for Ion Exchange	186
APPENDIX 4 B117 SCRIBE EVALUATION DATA		188
APPENDIX 5 PHOTOGRAPHS OF SAMPLE COUPONS		197
REFERENCES		238

LIST OF FIGURES

Figure 1.1: Simplified Corrosion Cell	5
Figure 1.2: Corrosion Rate of Steel as a Function of pH.....	6
Figure 1.3: Schematic of polarization curves for steel in near neutral solution....	8
Figure 1.4: Reaction between Epoxide and Primary Amine	15
Figure 1.5: Urethane Formation from an Alcohol and Isocyanate	16
Figure 2.1: Ion Sequestration Particle in a coating matrix.....	35
Figure 2.2: Synthesis Scheme for Initial Core Shell Approach.....	36
Figure 2.3: Synthesis Scheme for Homogeneous ISPs.....	37
Figure 2.4: Synthesis Scheme for PEI Solvent/Non-Solvent Approach.....	39
Figure 2.5: Synthesis Scheme for WISCM based ISPs.....	41
Figure 2.6: Synthesis Scheme for SISCM based ISPs.....	42
Figure 2.7: Precipitation of Polymer on WISCM in Heptane	44
Figure 2.8: Chemical Structure of V-70	46
Figure 2.9: Experimental Apparatus for WISCM Drying	49
Figure 2.10: Comparison of encapsulated WISCM (left) and unencapsulated WISCM (right), both as suspensions in heptane.....	52
Figure 2.11: Depiction of an Ideal Core Shell ISP	55
Figure 2.12: Ionic Association of Monomers	56
Figure 2.13: Schematic of Batch Process.....	58
Figure 2.14: Cross section Showing Modified Continuous Cell.....	62
Figure 2.15: Process Schematic Semi-Batch Synthesis	63
Figure 2.16: Wako Chemical V-65 Azo-Initiator.....	68
Figure 2.17: Experimental Apparatus for Encapsulation of SISCM.....	68
Figure 2.18: Pebble like agglomerations of 90% phosphate SISCM.....	72
Figure 2.19: Final ISP Synthesis Scheme	75
Figure 3.1: Isothermal Heat Flow of DGEBA + TEPA at 30C.....	79
Figure 3.2: Isothermal Heat Flow of DGEBA + TEPA at 60C.....	80
Figure 3.3: GPC Results for ZZZONR040808.....	81
Figure 3.4: Structure of Polyethylenimine	83
Figure 3.5: Titration of PEI by Phosphoric Acid	85
Figure 3.6: SEM of ZZZONR070108, first successful ISPs	86
Figure 3.7: Cross Section Schematic of Occluded Morphology of ISPs.....	87
Figure 3.8: SEM image of a Semi-Batch Synthesized ISP	88
Figure 3.9: SEM micrograph of 50,000x magnification of a polyurea encapsulation experiment.....	89
Figure 3.10: SISCM ISP @13,000x and 50,000x.....	90
Figure 3.11: SEM of SISCM Synthesized ISPs.....	91
Figure 3.12: TEM of Microtomed ISP at 25,000 x Magnification.....	92
Figure 3.13: TEM of Microtomed ISP at 40,000 x Magnification.....	93
Figure 3.14: Microtrac Size Characterization Data for ZZZONR042508	94
Figure 3.15: Bimodal Distribution for ZZZONR010705 ISPs	95

Figure 3.16: Nanotracer Particle Size Distribution for PMMA encapsulated WISCM (ZZZONR120706)	97
Figure 3.17: TGA Data for WISCM and PMMA encapsulated WISCM.....	98
Figure 3.18: Light microscopy image of PMMA encapsulated WISCM.....	100
Figure 3.19: SEM of SISCAM pre and post encapsulation with PMMA.....	101
Figure 3.20: Titration Setup for ISP Capacity Determination.....	103
Figure 3.21: Ion Sequestering Capacity of Early ISPs	104
Figure 3.22: Ion Sequestering Capacity of Later ISPs.....	105
Figure 3.23: Concentration Profile for the Differential Cell.....	107
Figure 3.24: Diffusion Cell with Perspective, Front, and Top Views shown	108
Figure 3.25: Diffusion Cell Experimental Setup	110
Figure 3.26: Diffusion Cell Results for ISP containing sample (ZZZONR042908)	111
Figure 3.27: Sectional Diagram of Diffusion Cell on ATR Crystal.....	116
Figure 3.28: Overlay of IR Spectra for ZZZONR062408 (30 minute sampling interval)	118
Figure 3.29: Normalized Integral Plotted Versus Time for ATRIR Experiment ZZZONR062408	119
Figure 3.30: Linear Regression for OH band at $\sim 1600\text{ cm}^{-1}$ in ZZZONR062408	120
Figure 3.31: Normalized Phosphate Data Coupled (ZZZONR062408) and Uncoupled (ZZZONR091908) from Water	123
Figure 4.1: Edge Thinning of Epoxy Coating.....	127
Figure 4.2: Coupons by Different Application Techniques.....	130
Figure 4.3: Draw Bar Over Plate Mold with Dimensions	131
Figure 4.4: Application Defects on a Draw Bar Application	132
Figure 4.5: Spray Application Tools, Cressendo (left) and Mini Touch up (right)	133
Figure 4.6: Coating Containing Early ISPs	135
Figure 4.7: Cathodic Disbondment Tank Showing Central Anode and Sample Coupons	136
Figure 4.8: 90 Day Cathodic Disbondment Sample Pre and Post Testing.....	137
Figure 4.9: Q-Fog Salt Spray Chamber.....	139
Figure 4.10: Coupons Prepared for Salt Spray.....	140
Figure 4.11: Coupons Post 1000 hrs of Salt Spray Exposure	140
Figure 4.12: Salt Spray Exposure, left samples contains 5 wt % DETONR046 right samples are controls with no ISPs	143
Figure 4.13: Weight % ISPs vs Performance in B117	144
Figure 4.14: Images Hot DI Sample Coupons Showing the Effect if ISPs	148
Figure 4.15: Wt % ISP vs. Hot DI Performance	149
Figure A1.1: Synthesis Scheme for Homogeneous ISPs.....	159
Figure A1.2: Solid State NMR spectra of Polyallylamine ISPs	161
Figure A1.3: Aqueous GPC Results for ZZZONR110904.....	163
Figure A2.1: Synthesis Scheme for PEI Solvent/Non-Solvent Approach	1677
Figure A2.2: Histogram showing particle size for HDI/PEI ISPs (ZZZONR061506)	171

Figure A2.3:DSC plot for ZZZONR06166, HDI encapsulated PEI ISPs	172
Figure A2.4: DSC plot for ZZZONR072406, TDI encapsulated PEI ISPs	172
Figure A2.5: DSC showing Transition of PEI/Phosphoric Acid Core Material ..	173
Figure A2.6: SEM images of dried ZZZONR061506.....	174
Figure A2.7: Microtrac Particle Size Analysis for Ground Bulk PEI/H ₃ PO ₄	176
Figure A2.8: DSC for TDI encapsulate ground bulk PEI/H ₃ PO ₄ particles	177
Figure A3.1: H-NMR Spectra before Addition of Phosphoric Acid.....	181
Figure A3.2: H-NMR Spectra After Reaction with Phosphoric Acid.....	182
Figure A3.3: Reaction of TEPA with TDI to Synthesize a Larger Monomer.....	183
Figure A3.4: Pre-Rusted Plates Prior to Coating	184
Figure A3.5: Pre-rusted coupon post 1000 hrs B117.....	185

LIST OF TABLES

Table 1-1: Barrier Properties of Resin and Paint Films	10
Table 1-2: Grey Maintenance Epoxy Amine Coating System.....	13
Table 1-3: Results of Kalendova Anti-Corrosion Pigment Study.....	24
Table 2-1: WISCM Composition	45
Table 2-2: Experiments in the Investigation of Low Temperature Initiators	46
Table 2-3: Surfactants Studied for WISCM Dispersion Stabilization.....	47
Table 2-4: WISCM ISP Formulation.....	48
Table 2-5: Calculated Tg Values of Comonomer Shell Experiments	52
Table 2-6: Experimental Details for WISCM Based ISPs.....	54
Table 2-7: pKa's for ion sequestration core materials.....	56
Table 2-8: Experimental Details for Batch Process ISPs	65
Table 2-9: Experimental Details for Semi Batch Process ISPs	66
Table 2-10 Components used in ZZZONR010705.....	69
Table 2-11: PEI SISCM Compositions	71
Table 2-12: Experimental Data for SISCM Core Particle	74
Table 2-13: Experimental Data for SISCM Encapsulation	74
Table 3-1: SISCM Encapsulation Experiments.....	82
Table 3-2: Summary of Particle Size Analysis in μm	96
Table 3-3: ISP Capacity at pH = 12	106
Table 3-4: Diffusion Coefficient of NaCl through the MIL-DTL-24441 Coating	112
Table 3-5: Diffusion Coefficients Determined by the ATRIR Method	122
Table 4-1: Formulation of TEPA/DGEBA Coating System.....	129
Table 4-2: Rating of Failure at Scribe (Procedure A).....	141
Table 4-3: Evaluation Results for ZZZONR021207 by ASTM D 1654	142
Table 4-4: Evaluation Results for ZZZONR082007 by ASTM D 1654	142
Table 4-5: Summary of Salt Spray Plate Evaluations by ASTM D1654.....	146
Table 4-6: Scale and Description of Rust Ratings (ASTM D610)	147
Table 4-7: Results of Hot Deionized Water Immersion as per ASTM D610.....	150
Table A1-1: Experimental Details for ZZZONR110904	160
Table A1-2: Calibration Data for Aqueous GPC	162
Table A2-1: Nonsolvent of PEI Selection Experimental Observations.....	166
Table A2-2: Reactants Used for Solvent/Nonsolvent ISP Synthesis.....	168
Table A3-1: Composition for ZZZONR071504.....	180
Table A3-2 : Peak Integration Values from H-NMR	180

DEFINITION OF ABBREVIATIONS

ACN	–	Acetonitrile
ASTM	–	American Society of Test Methods
ATRIR	–	Attenuated Total Reflectance Fourier Transform Infrared Spectroscopy
CD	–	Cathodic Disbondment
CHT	–	Chemical Holding Tank
DGEBA	–	Di-Glycidyl Ether of Bisphenol A
DI	–	Deionized
DSC	–	Differential Scanning Calorimetry
EIS	--	Electrical Impedance Spectroscopy
ISP	–	Ion Sequestration Particle
NMR	–	Nuclear Magnetic Resonance Spectroscopy
NRL	–	Naval Research Laboratories
ONR	–	Office of Naval Research
PEI	–	Polyethyleneimine
SEM	–	Scanning Electron Microscopy
SISCM	–	Solid Ion Sequestration Core Material
SSPC	–	Society for Protective Coatings (formerly Steel Structures Painting Council)
TDI	–	Toluene Di-Isocyanate
TEM	–	Transmission Electron Microscopy
TEPA	–	Tetraethylenepentamine
TGA	–	Thermal Gravimetric Analysis
WISCM	–	Wet Ion Sequestration Core Material
WT	–	Weight

ABSTRACT

ION SEQUESTRATION PARTICLES FOR NAVAL ANTICORROSION COATINGS

BY

ZACHARY Z. ZGURIS

University of New Hampshire, December, 2008

Corrosion is the electrochemical process of a metal returning to its lower energy state, the metal oxide. The cost of corrosion is difficult to estimate. One area particularly susceptible to corrosion problems with high maintenance costs is that of the 20,000 tanks existent in the US Naval Fleet. The Navy is sponsoring the development of novel coatings and additives that can be used to decrease the rising corrosion related costs.

This dissertation describes in detail the synthesis of Ion Sequestration Particles (ISP) that when added to the standard MIL-DTL-24441 or potentially another coating system act to enhance the anticorrosion properties of the coating. A solid ion sequestration core material (SISCM) is first produced. The core is then encapsulated in a second stage forming a shell that protects the SISCM sufficiently from the harmful interactions with uncured epoxy based coatings.

ISPs were designed to sequester harmful ions while releasing passivating ions in their place. The passivating ions then migrate to defect sites at the coating interface where they act to inhibit corrosion. The anticorrosion

performance of ISPs in epoxy coatings has been demonstrated by both 500 hrs of hot deionized water immersion and 1000 hrs of salt spray exposure (ASTM B117). The best improvements in coating performance are attained with ISP content ranging from 5 -10 wt % loading in a coating.

ISPs were designed to limit the transport of harmful ions through the coating. However this work has determined high diffusion coefficients for ions (Cl^- and PO_4^{2-}) through the epoxy matrix. Without ISPs, the diffusion coefficient through the MIL-DTL-24441 coating was determined for phosphate to be $1.16 \times 10^{-7} \text{ cm}^2/\text{s}$ and for chloride to be in the range of 2.7×10^{-9} to $5.6 \times 10^{-10} \text{ cm}^2/\text{s}$. The addition of 5 wt % ISPs to the coating had the effect of decreasing the diffusion coefficient by an average of 25.5%. These results yield the conclusion that the enhanced anticorrosion properties of coatings containing ISPs is more likely due to the passivating effect of the released phosphate ions than due to the ISPs ability to sequester harmful ions.

INTRODUCTION

Corrosion is the electrochemical process of a metal returning to a lower energy state, that of a metal oxide. This process occurs naturally for most metals, with the metal oxide being the natural state found during mining operations. The metal ores are converted into pure metals or alloys during a refining process, consuming a large amount of energy in the process. Metals and metal refining has been the basis of modern society, dating back to the Chalcolithic period in the 5th millennium BC and advancing through to the current days.

The cost of corrosion is difficult to estimate. One large scale study initiated by the US Legislature in 1998, undertaken in cooperative agreement between NACE International and the Federal Highway Administration, looked at two separate issues in an attempt to estimate the national corrosion costs for the United States. Method 1 considered the total costs of corrosion control methods and services with a resultant total annual cost estimate at \$121 billion (1.38 % of the total US GDP in 1998). Method 2 was an industrial sector analysis of corrosion costs with a total annual cost for the five categorized sectors at \$137.9 billion. These two approaches were summed up to a total annual direct cost of corrosion in excess of \$276 billion. The study goes on to say that the total cost is more than twice the \$276 billion including the indirect costs¹.

In a 2003 report to congress by the US General Accounting Office on the corrosion costs to the DOD and Military services it is stated that the full impact of corrosion on defense management can not be quantified due to limited amount of data from these sources on the issue². The report goes on to state that corrosion costs represent the largest life cycle cost of components of military weapons systems (tanks, aircraft, ships ,etc). For example, in 1993 it was reported an estimated \$2-2.5 billion was spent for corrosion related repairs just on wheeled vehicles, including 5-ton trucks³.

One area particularly susceptible to corrosion problems with high maintenance costs is that of the 20,000 tanks (ballast, fuel, potable water, combined holding tanks, etc) existent in the US Naval Fleet. Approximately 4000 of these tanks are inspected annually with a total cost in excess of \$24 million⁴. Only a small fraction of these inspected tanks are in need of repair. The cost of refurbishment and repair of failed coatings in these tanks is approximated at \$250 million annually.

The Navy is taking a number of approaches to minimize the maintenance cost of the tanks. One of the Naval Research Laboratories (NRL) areas of research focus is "Solvent free high edge coverage ballast tank coatings increase current service life for increased cost savings, and reduction in hazardous material emission during ship's life"⁵. There is a largely financial motivation driving the service life of anticorrosion coatings used inside tanks from the current 5-7 years lifetime towards a 20+ year lifetime. To this end, there is an increase in funding and study of new anticorrosion coating systems to be

developed for and evaluated by the NRL for their ability to compete with and exceed the existent MIL-DTL-24441 coatings that have seen wide spread used throughout the fleet.

While the Navy is interested in the development of new low volatile organic compound long life anticorrosion coatings, it has also expressed interest in novel anticorrosion approaches. One such alternative approach to increased coating performance is an additive that can be used in existing as well as newly developed coating systems to increase their anticorrosion potential. This approach requires the development of an anticorrosion additive that offers increased corrosion protection to the coating without changing the basic chemistry or physical properties of the system.

The goal of this work was to develop a successful synthesis process for ion sequestration particles (ISPs) that provide enhanced corrosion protection upon dispersal in an anticorrosion coating. These ISPs are designed to sequester free ions, as they are generated during the corrosion process as in the case of hydroxyl ions or as they diffuse through the coating as in the case of chloride ions. In order to maintain charge neutrality, the particles will release phosphate ions which function as corrosion inhibiting anions. The driving force for the ion exchange is the concentration gradient differential of the ions between the particle and the coating, and can be considered a diffusion controlled process.

This dissertation describes in the following chapters the development of the synthesis of these ISPs, characterization of the ISPs, and testing of their

anticorrosion enhancing capabilities on steel substrates. Chapter 1 presents background information on corrosion and the anticorrosion coating to further aid in the readers understanding of this work. In Chapter 2 the synthesis evolution and experiments performed resulting in the final development of ISPs are explained. The details of each experimental procedure as well as the process changes made during development are discussed. Chapter 3 describes characterization of the ISPs and other materials used in this work. Chapter 4 discusses the evaluation of the anticorrosion properties of the synthesized ISPs. Chapter 5 provides conclusion and discusses the future continuation of this work.

CHAPTER 1

BACKGROUND

1.1 Corrosion of Steel

A plethora of texts have been written covering the many complex issues of corrosion. This section does not provide a thorough in depth understanding of all the issues related to corrosion. Instead it covers the essential information needed to understand the addressed problem of corrosion of steel substrates in an aqueous environment as would be found inside the ballast tanks of a naval vessel.

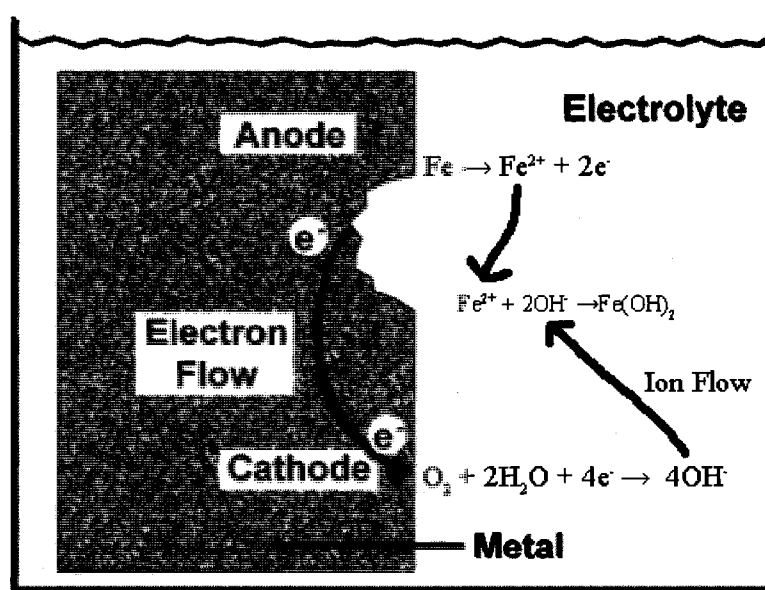


Figure 1.1: Simplified Corrosion Cell

Simply stated, corrosion is the electrochemical conversion of a metal into an oxide that, dependent on the pH of the system, can be either soluble or

insoluble. This is an electrochemical process which requires in essence a complete cell or circuit. In the corrosion “cell” illustrated in Figure 1.1, the electrons conduct through the metal while the ions are transported through the electrolyte.

Corrosion requires a conductive medium, the electrolyte, connecting the anodic and cathodic sites such that a complete circuit is formed. The electrolyte is typically water but in some cases other liquids or materials are utilized or encountered. The anode and cathode areas can be separated by distances ranging from angstroms up to meters. However the solution conductivity varies as the inverse of the conduction path and damage is more severe over shorter distances⁶.

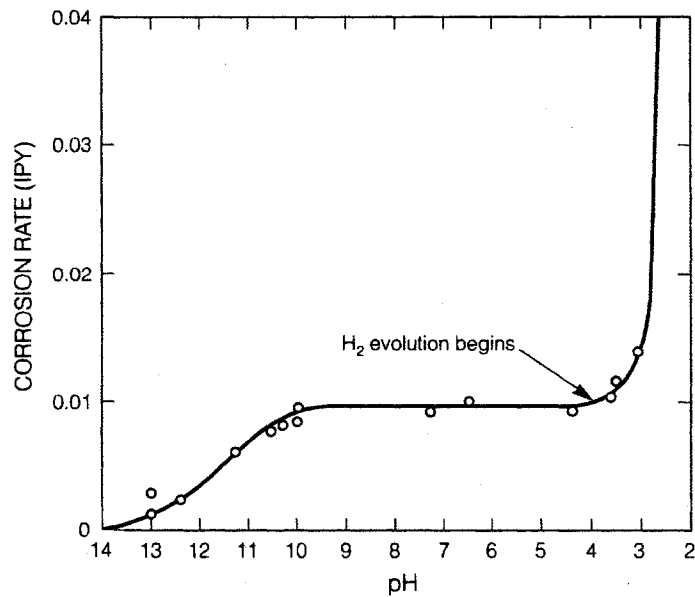
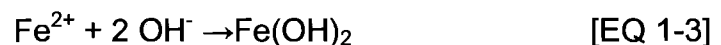
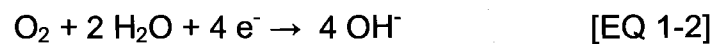


Figure 1.2: Corrosion Rate of Steel as a Function of pH⁷

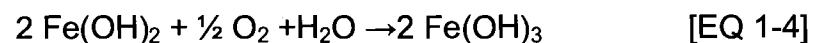
In aqueous environments in the range of pH 4-10, the corrosion rate is nearly constant, as can be seen in Figure 1.2 and is primarily controlled by the

rate of oxygen diffusion to the actively corroding surface⁸. For alkaline conditions above pH 10, the corrosion rate is retarded by the formation of a passive ferrous oxide film. At pH values below 4, the corrosion rate increases dramatically due the evolution of hydrogen and the solubility of the oxide formed.

The anodic reaction of iron into iron oxide is presented as EQ 1-1. The cathodic reaction for the reduction of oxygen dissolved in water is shown as EQ 1-2. The ferrous ions and the hydroxyl ions formed by these reactions then combine to form ferrous hydroxide as in EQ 1-3.



Given a sufficient oxygen and water supply in the region of the ferrous hydroxide precipitation, there is then a further oxidation as written in EQ 1-4 into a hydrated ferric oxide. This is the ruddy brown material deposited on the surface of corroding steel and is commonly referred to as "rust". While other oxides can form under varying conditions (ex. Fe_2O_3 and Fe_3O_4) this is the product of primary importance to this project.



It has been shown by more than one author that the oxide film formed on iron is of a hydrated gel like network of ferric oxides and that it is changed into the Fe_2O_3 form when removed from solution and dried⁹. The passive film network consists of a three different types of "bridges", $-\text{Fe}-\text{H}_2\text{O}-\text{Fe}-$, $-\text{Fe}-\text{HO}-\text{Fe}-$, and $-\text{Fe}-\text{O}-\text{Fe}-$. This ionic gel structure forms a much more efficient protective

passive film then does the perfect oxide film of Fe_2O_3 .¹⁰ For the case of internal tanks on Naval Vessels it is likely this drying and associated weakening of the protective oxide layer occurs during the logistical cycles of filling and emptying the tanks.

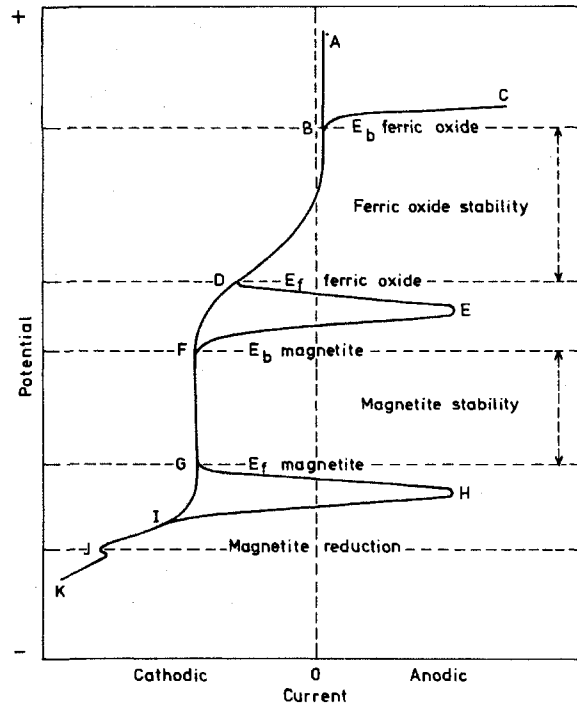


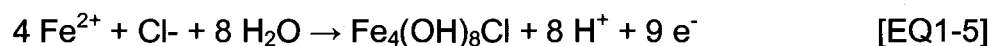
Figure 1.3: Schematic of polarization curves for steel in near neutral solution¹¹

The ferric oxide layer is one of two protective oxide layers formed for steel substrates, the other being the formation of a magnetite layer in an oxygen depleted solution as can occur in transport limited by localized corrosion conditions such as undercoating or pitting. Schematically, the two passive films for iron are represented in Figure 1.3. The Flade potential, E^f is the point where the reduction or dissolution of the passive film occurs at a greater rate than the formation. The breakdown potential, E_b is the point where more aggressive corrosion occurs; i.e. localized failures to the passive layer initiate pitting

corrosion. This breakdown potential and associated explosion of growth in pitting occurs due to a cooperative interaction caused by the increase in defect spacing from randomly distributed metastable pits transitioning from a dispersed to a more clustered arrangement¹². Inhibition of steel substrates by ionic species requires a concentration of anions, pH, and oxidizing agents resulting in a potential that falls in either of the stability regions of ferric oxide or magnetite¹³.

1.1.1 Effect of Chloride Ions on Corrosion

The presence of chloride ions alters the corrosion process considerably. The chloride ions and associated counter ion increase the conductivity of the solution. It has been repeatedly shown that the corrosion rate increases with an increase in conductivity of the electrolyte^{14,15,16,17}. Additionally, the chloride ions can form ferrous chloride at the anode, while sodium hydroxide is formed at the cathode. These two soluble intermediates meet away from the steel surface forming ferrous hydroxide that then undergoes further oxidation as in EQ1-4¹⁸. Chlorides drastically increase the corrosion rates due to this action which results in a dissolution of the oxide layer from the surface. The dissolution of the oxide layer results in a loss of any protective passivating or resistive effect the oxide layer as on the underlying metal. The chlorides can additionally become directly included into the corrosion products. EQ 1-5 shows a reaction with the additional products of H⁺ ions which results in a local acidic condition which further accelerates corrosion in the region¹⁹.



1.1.2 Undercoating (Organic) Corrosion

Coatings used for the prevention of corrosion can be thought of as acting as a resistor in the electrochemical circuit of the corrosion cell. The modern anticorrosion coating acts as a barrier to the transport of water, oxygen, and ions to the metal surface. However, all organic coatings are somewhat permeable to both oxygen and water at varying rates shown in Table 1-1. The diffusion rate of water through a coating is 10-100 times greater than the consumption rate at a freely corroding steel surface²⁰. Therefore the limiting of ion transport through a polymeric coating has more of an effect on the corrosion rate than does the limiting of oxygen and water transport²¹.

Table 1-1: Barrier Properties of Resin and Paint Films²²

Coating Type	Oxygen Permeability cc/m ² / 100 um /day 23C, 85% RH		Water Vapor Permiability g/m ² / 25um /day 38C, 95% RH	
	value	deviation	value	deviation
Epoxy Polyamide	130	33	62	8
Chlorinated Rubber Plasticized	183	7	38	2
Chloropolymer (solvent borne)	82	19	40	8
Styrene acrylic latex	1464	54	920	
vinyl chloride - vinylidene copolymer latex	22	9	11	4
Red lead heat treated linseed oil (BS 2523)	734	42	214	3
TiO ₂ Pigmented Alkyd	595	49	258	6
Aluminum Epoxy Mastic	110	37	42	6
Tar Coal Epoxy	213	28	30	1
Chlorinated Rubber unmodified	30	7	20	3
acrylic water borne primer	500		720	37
Copolymer Latex	12	5	27	5

Outside of gross defects or mechanical damage, corrosion of steel substrate protected by an otherwise intact and pore free organic coating occurs at the interface between the metal and the coating. In order for undercoating corrosion to occur there first needs to be a loss of adhesion between the metal

substrate and the coating. Typically this is initiated by the diffusion of water molecules through the coating into an area at the interface containing contaminants or corrosion products. Some instances of initiation of undercoating corrosion are caused by capillary forces, where water is drawn into the interfacial area due to a pre-existing lack of good adhesion. This lack of good adhesion is often due to a failure of the coating system as a result of poor mixing, improper drying/curing conditions or entrapment of air underneath the coating during application²³.

Undercoating corrosion has been theorized to follow one or a combination of three different perspectives comprising mechanical, chemical, or electrochemical²⁴. The mechanical approach looks at the defect as a pore with the anode and cathode inclusive. The corrosion products are formed and eventually block the pore. At which point the corrosion products continue to develop as water, oxygen and ions are transported through the coating to the corrosion site. These products result in an increase in pressure and a resultant mechanical force pushing the coating away from the metal substrate increasing the active corrosion area²⁵.

The chemical approach differs in that the anode and cathodes exist separately underneath the coating. The ion transport happens through the coating²⁶. The corrosion products generated result in an undercoating pH shift at both the anodic and cathodic sites²⁷. This resultant pH shift causes one of a number of possible effects to the coating/substrate interface, including precipitation of insoluble products, cathodic disbondment, polymer degradation²⁸,

and localized increase in ion transport through the coating²¹. This is an area that is not clearly understood since the failure mechanism is unique to each coating/substrate application.

Electrochemically a substantial potential difference can exist between the anode and cathode of the undercoating corrosion cell due to the resistive effect of the protective coating. This potential difference drives water transport into the coating by electro-osmosis²⁹. It follows that the increase in hydration of localized regions within the coating would yield a decrease in resistance and transport occurs initiating corrosion. This rapid ion migration leads to delamination of the coating³⁰. In addition, the increase in water in the coating can in and of itself result in a loss of adhesion between the coating and the substrate³¹.

1.2 Organic Anti-Corrosion Coatings

The existing anti corrosion coatings can be broken down into one of four categories: organic, inorganic, anodic, and cathodic. In regard to this work, due to the application of ion sequestration particles specifically to internal naval holding tanks and voids, the organic anti-corrosion coating is the only category of interest. These organic coatings are complex formulations consisting of multiple functional components that synergistically provide the best possible corrosion protection for a given application. Any one coating contains a combination of binders, pigments, fillers, additives, and solvents as can be seen in by the coating contents listed in Table 1-2 . This section contains a reasonably detailed review of organic coating formulation and the function of each component

therein. Emphasis of this review is on active anti corrosion compounds, especially active pigments as these will be the pigments replaced or augmented by the ion sequestration particles developed and discussed in the body of this dissertation.

Table 1-2: Grey Maintenance Epoxy Amine Coating System

Coating Component	wt %	Function
Rutile Titanium Dioxide	23.7%	filler
Lampblack	0.1%	inactive pigment
Chrome Yellow Medium	0.3%	anticorrosion pigment
Epoxy Resin MW900	38.6%	binder component
Methyl Isobutyl Ketone	3.9%	solvent
Ethoxyethanol	10.2%	solvent
Xylene	6.9%	solvent
Resin Leveling Agent	1.5%	additive
Amine adduct	14.9%	binder component
Pigment to binder wt ratio	40:60	
Nonvolatile content (wt%)	60	
Viscosity (Stormer-Krebs Units)	72	
Density (lb/gal)	10.2	

Throughout the literature the terminology differs between individual authors. In this text an anticorrosion pigment shall be designated as any solid and insoluble inorganic particle added to the binder for the purpose of enhanced corrosion protection. Organic inhibitive compounds added to the binder matrix will be classified as an additive as opposed to a pigment. Terminology often defines inhibitors as those soluble compounds which used in closed loop liquid systems to protect the internal metal surfaces from corrosion damage. This terminology will allow for a better report on the current technologies in the anticorrosion coating field.

1.2.1 Binders

Binders serve as the media that holds the other components of the organic coating together and adherent to the substrate. The binder also forms the bulk of the resistive properties of the coating. Binders for anti corrosion coatings primarily belong to the following characteristic families: drying oils, alkyd resins, polycondensation resins, coalescent film forming, and silicone organics. While upwards of 2/3 of all anti corrosion coatings sold are of the oil based alkyd type³² their use is primarily for the protection against atmospheric corrosion and they are unsuitable for continuous immersion and marine applications.

Coatings used on interior tanks for naval applications are almost exclusively of the polycondensation type, primarily utilizing either polyurethanes or epoxy/amide chemistries. Polycondensation type coatings form a tough highly crosslink network that is resistant to swelling, ion transport, water transport, and oxygen transport³³.

Epoxy Amine/Polyamide Binders

Epoxies react readily with a number of different functional groups, though the most significant in regards to the anticorrosion coatings is the reaction with a primary or secondary amine as in Figure 1.4. The most common di-epoxide produced and used is that of the coupling reaction of epichlorohydrin with bisphenol-A followed by dehydrohalogenation to produce, Diglycidyl Ether Bisphenol A or DGEBA as it is commonly named³⁴. More than 50% of epoxy

produced is used for anticorrosion coatings due to a high corrosion resistance and excellent adhesion to metal substrates³⁵.

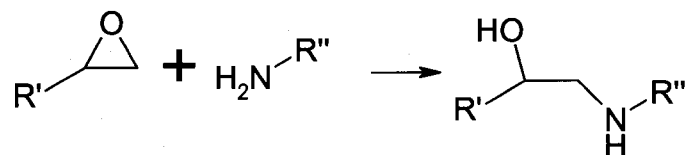


Figure 1.4: Reaction between Epoxide and Primary Amine

The properties derived from these binders come with a substantial increase in materials and application cost. For the case of naval applications, the savings from longer periods between maintenance and overhaul largely outweigh the additional material and application costs³⁶. Epoxy coating systems have the technical challenges of short pot life and narrow overcoat windows which require careful application techniques and regimens for success.

Polyurethane Binders

The urethane linkage is a chemical group formed between an isocyanate and an alcohol moiety shown in Figure 1.5. When these linkages exist in quantities averaging more than 2 per molecule a crosslinked network is formed. Polyurethanes can have an almost limitless number of properties dependent on their formulation. By controlling chain length, cross link density, and monomer polarity, polyurethanes can be produced with properties ranging from soft elastomers to tough rigid solids and hydrophilic to hydrophobic in nature, etc.

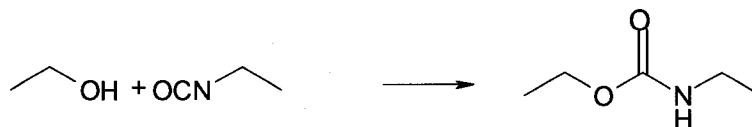


Figure 1.5: Urethane Formation from an Alcohol and Isocyanate

In addition to properties such as good adhesion, low permeability, and excellent film formation, urethane coatings have the advantage of speed over epoxy based coatings. Some urethane coating systems cure so rapidly it is possible to walk on the coated surface 30 to 60 seconds after application³⁷. This can shorten application time as there is no long wait between coats in applications requiring multiple coating layers to complete the protective system.

1.2.2 Anticorrosion Pigments

Pigments in anticorrosion coatings are not added for aesthetics but for the additional corrosion protection they bring to a coating system³⁸. Functional anticorrosion particles that are insoluble in the solvent and binder systems fall into this category. The mechanisms by which the various pigments affect corrosion differ but can be regarded as belonging to one of three functional types³⁹: barrier, chemically active, or electrochemically active. In regard to barrier mechanisms they provide either a decrease in transport through the coating (flake pigments) or they adsorb on the substrate during the coating process providing a physical barrier at the metal interface (blocking pigments)⁴⁰. The chemically active components react with the substrate, binder, or diffusing species to provide inhibition. The electrochemically active inhibitors are those

that affect the potential of the system directly by cathodic protection of the metal substrate.

Important for all pigment types is the pigment volume concentration (PVC) and the critical pigment volume concentration (CPVC). PVC is defined as:

$$\% \text{ PVC} = 100\% * V_{\text{pigment}} / (V_{\text{pigment}} + V_{\text{non-volatile binder}})$$

Where V_{pigment} is the total volume of the pigment and $V_{\text{non-volatile binder}}$ is the volume of the non volatile binder in the coating system⁴¹. In order for a coating to have good performance and low porosity there has to be sufficient binder to wet out all of the pigment particles.

The CPVC is the crossover point where the binder is in insufficient quantity to wet out the surface area of the pigments⁴². Above the CPVC coatings exhibit progressively decreasing performance due to an increase in voids, porosity, and permeability⁴³. For isometric particles the CPVC decreases with increasing particle size⁴⁴. Prediction of CPVC values has proven impossible and the methods used to determine it involve the production of sample plates at differing pigment concentration for subjection to an array of accelerated corrosion experiments⁴⁵.

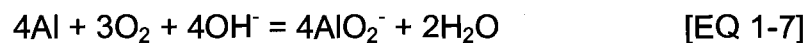
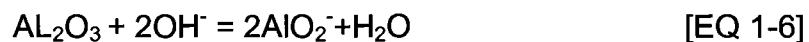
1.2.2.1 Barrier Pigments

Flakes are pigments which have large aspect ratios as a lamellar thin sheet with thickness of up to 5 microns⁴⁶. At application, the flakes align themselves parallel to the substrate forming a multilayer platelet barrier suspended in the binder⁴⁷. Flake pigments in anticorrosion coatings increase the resistance to water permeability by increasing the diffusion path length through

the coating⁴⁸. In aggressively abrasive environments the flakes also increase the erosion resistance of the coating⁴⁹. Flake pigments utilized for anticorrosion purposes are made of glass, aluminum, zinc, or micaceous iron oxide.

Glass flakes were first used in coatings by Owens Corning back in the late 1950s, but with the dawn of the high solids single coat market they are being revisited⁵⁰. In a 5 year oceanic exposure experiment off the shores of Dam Neck, VA and LaCosta Island, FL a glassflake coating system finished as a top performer out of 31 included coating systems based on corrosion protection⁵¹. Glass flakes are unique among the pigments used for anticorrosion coatings in that they only act as a physical barrier⁵².

While the glass flake pigments provide an increase in corrosion resistance they are not as efficient in their anticorrosion role as are the metal and metal oxide flakes⁵³. This is due to the metal flakes having an additional chemical effect when the flake containing coating is in direct contact with the metal. Aluminum flakes can consume oxygen or hydroxyl ions as they are generated by one of the two following equations⁵⁴:



Both of these reactions result in the decrease in cathodic disbondment at the coating/steel interface. The disadvantage of aluminum flakes is their susceptibility to cathodic alkali attack, making them poor performers for sea water immersion coatings as shown by B117 salt fog chamber experiments⁵⁵.

Zinc flakes have been successfully utilized as anticorrosion pigments where they create very good barrier effects resulting in coatings with high packing densities and mechanical properties without porous structure, blistering or other defects⁵⁶. Post accelerated salt spray exposure, zinc particles of lamellar structure showed an increased coating adhesion when tested side by side under identical conditions against spherical zinc particles⁵⁷. Lamellar zinc has an adverse reaction which takes place in water-borne coatings resulting in the generation of hydrogen. This adverse reaction can be prevented by a series of inhibitors containing a nitro-group ortho to an hydroxyl-group which acts as a potential chelating group⁵⁸.

Micaceous iron oxide pigments have been successfully used with their enhanced anticorrosion properties being attributed to the decrease in water permeation due to the orientation of the lamellar pigments in the coating⁵⁹. The anticorrosion performance of micaceous iron oxide pigments can be further enhanced by a zinc phosphate conversion coating process⁶⁰. Lamellar muscovite particles with a precipitated layer of hematite on their surface showed an 8% increase in anticorrosion efficiency over lamellar zinc, with a particular resistance to osmotic blistering of the coating⁶¹. The optimal pigment volume concentration for micaceous iron oxide has been shown to be in the range of 15% for maximum corrosion protection⁶².

Blocking pigments function by reducing the active metal surface area by adsorption without any additional chemical effects. This adsorbed pigment layer blocks the ionic transport at the metal surface resulting in inhibition of the

corrosion process⁶³. Pigments of this type include but are not limited to lead oxide (white lead), lead sulfate, cobalt oxide and zinc oxide. These are of limited use in naval anticorrosion coatings due to low corrosion protection efficiencies compared to active and lamellar pigments. One suggested possibility to increase the anticorrosion performance of the oxide (ZnO, Al₂O₃, Fe₂O₃, Fe₃O₄) blocking pigments is to impart onto them n-semiconductors properties⁶⁴.

1.2.2.2 Chemically Active Pigments

Chemically active pigments inhibit corrosion by retarding the anodic reaction, retarding the cathodic reaction, or limiting the ionic transport⁶⁵.

Modern inhibitive pigments are regulated globally and required to meet strict environmental and health regulations in the US. Many of the earlier pigments, most notably those based on hexavalent chromium and lead have been banned from the coatings industry due to their toxic nature as they eventually leech out into the environment⁶⁶. The “old” toxic pigments will be discussed only briefly with the focus of this section will be on the newer non toxic inhibitor pigments used in the anticorrosion industry.

Toxic Inhibitors

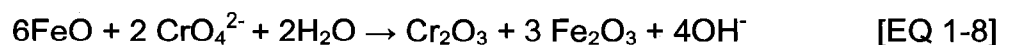
The toxic pigments used for anticorrosion are the traditional chrome and lead based pigments. Due to environmental and health concerns these are no longer in use with a few exceptions such as chromate coatings for specialized aircraft aluminum alloy protection. In the early days, these were reported as the

most effective corrosion inhibitors but more recent work has shown modern environmentally friendly pigments to have equal or even superior performance⁶⁷.

Chromate Pigments

The chromate based pigments are either categorized as known or suspected carcinogens. Environmental regulations and worker health and safety oversight groups have propagated legislation and laws that restrict the use of these heavy metal based pigments⁶⁸. Chromate leaches out of coatings when there is an increase in acidity inside defects of the coating, while in neutral environments there is no evidence of chromates escaping from the coating⁶⁹. Chromate replacement has been taking place steadily since the 1960's as new less toxic alternatives have been developed.

The chromate pigments provided anticorrosion protection at cathodic points by the reduction of Cr⁶⁺ to a solid species containing Cr³⁺ inhibiting the cathodic reaction⁷⁰. Additionally there is a formation of a passive layer on the iron surface. The passive layer contains a mixture of iron (II) and chrome (III) oxides formed by the reaction of EQ 1-8⁷¹. This oxide layer acts as a barrier to prevent ion transport thus inhibiting corrosion of the iron surface.



Zinc chromate (3ZnCrO₄•K₂CrO₄•Zn(OH)₂•H₂O) is historically one of the most frequently used anticorrosion pigments⁷². Other commonly used chromate

pigments are Barium Chromate (BaCrO_4), Calcium Chromate, Ammonium Chromate, Zinc Tetrachromate ($\text{ZnCrO}_4 \cdot 4\text{Zn(OH)}_2$), Lead Chromate (PbCrO_4), and Strontium Chromate (SrCrO_4).

Lead Pigments

Lead based pigments are one of the oldest synthetic pigments dating back to the second century BC⁷³. In the first half of the 20th century more than three million tons of lead pigment was produced for use in protective coatings⁷⁴. Lead has the heaviest laws and regulations prohibiting usage in modern coatings due to the widespread use in decades past. In addition to the ban of lead use in modern coatings, many states have laws requiring specialized removal and treatment of existing lead coatings in and on structures. Lead leaches out readily from coatings over the total range of pH with as much as 80% of the total lead escaping at low pH⁷⁵.

The common lead pigments used in coatings consist of powdered lead (Pb), calcium plumbate (Ca_2PbO_4), lead suboxide ($\text{Pb}+\text{PbO}$), red lead (PbOPbO_2), and white lead, (PbCO_3) 2Pb(OH)_2). Lead provides protection by a mechanism involving degradation of compounds and the formation of lead soaps. These then degrade in the presence of water and oxygen to yield a variety of compounds which are inhibitive. The most important being lead azelate⁷⁶. The resulting lead azelate and other lead compounds inhibit rust formation by blocking defects in the naturally occurring oxide film on the iron surface or possibly by interfering with the cathodic reduction of rust to magnetite⁷⁷.

Metallic lead can protect steel galvanically by acting as an anode and thereby limiting the steel surface to the cathodic reduction of oxygen eliminating damage to the surface⁷⁸. There is also anodic inhibition due to Pb(OH)_2 , and a scavenging of oxygen resulting in an oxygen deficient condition on the steel surface⁷⁹. Lead based anticorrosive paints have been developed specifically for ship hull and other in service use in the naval environment⁸⁰. Given the anti-lead legislation and strict regulation by the EPA as well as the Navy's goals of being ahead of the EPA in terms of coating compliance it is clear that there is no longer any place for the lead based pigments in Naval applications.

Non-Toxic Inhibitors

The area of non toxic environmentally friendly corrosion inhibitors is one of great interest. Efforts are put forth toward studying any compound with even a glimmer of hope as being functional in regards to corrosion protection. Any listing or tallying of pigments investigated for anticorrosion properties would be remiss in thinking that none had been overlooked. This section will cover the most widely accepted and used pigments as well as some of the newer pigment technologies.

It is often difficult to compare results between authors as both the methods used and the methods of reporting corrosion protection efficiency vary greatly. The most complete and recent comparison of anticorrosion pigments was reported by A. Kalendova⁸¹. It involved studying many of the most significant modern anticorrosion pigments under standardized conditions in accelerated

corrosion environments. The results of this work are presented in Table 1-3. The author concludes with two comments worth noting here. The first is that some pigments are sensitive to overdosing with drastic loss in performance with increased loading, including those used in the study. The other is that modern environmentally friendly pigments have excellent anticorrosion efficiencies compared with the chromate and lead based pigments of the past.

Table 1-3: Results of Kalendova Anti-Corrosion Pigment Study

Anticorrosion pigment	Ranking @	Ranking @
	PVC = 10%	PVC=CPVC
zinc phosphomolybdate	1 (best)	2
calcium hydrogen phosphate	2	5
organic modified zinc phosphate	3	4
calcium metaborate	4	8
zinc phosphate	5	3
zinc aluminum phosphate	6	1
strontium chromate	7	10
zinc dust	8	6
calcium ferrite	9	9
calcium borosilicate	10	7
strontium aluminum polyphosphosil	11 (worst)	11

Phosphates

By far the most commonly used and most effective* of the non toxic inhibitors are those belonging to the phosphate family. A number of different cations are available to make up the phosphate salt. These include aluminum, barium, calcium, potassium, zinc and others. Zinc phosphate, along with the

* although zinc molybdenum phosphate is discussed under molybdates it is a modified phosphate

other phosphate pigments have anticorrosion efficiencies that typically rise with an increase in pigment concentration⁸¹.

Zinc phosphate was one of the earliest non toxic replacements for the lead and chromate based pigments. It has been proven to be an efficient substitute for zinc chromate, especially for immersion applications⁸². The mechanism of zinc phosphate protection on steel is reportedly by phosphate ion donation⁸³. This phosphate ion is used to build up a protective film on the anodic area of the iron surface⁸⁴. This protective phosphate layer on steel consists of a mixture of hydrated insoluble metal phosphates: hopeite, $Zn_2(PO_4)_2 \cdot 4H_2O$ and phosphophyllite, $Zn_2(Fe,Mn)(PO_4)_2 \cdot 4H_2O$ ⁸⁵. In addition to the development of a protective ferric phosphate layer on the steel surface there is a blockage of pores caused by diffusion of free ferric phosphate precipitate reducing the transport of water and harmful ions to the corrosion sites to further inhibit damage⁸⁶.

Zinc phosphate pigment anticorrosion efficiencies can be increased by modification, especially in the neutral aqueous sodium chloride environment⁸⁷. The addition of calcium cations into the coating via calcium exchanged silica can produce a modified phosphate film containing calcium phosphate which imparts effective inhibition of corrosion by limiting oxygen access to the metal surface⁸⁸. Furthermore a synergistic effect between zinc phosphate and a modified zeolite rock allows for decrease in zinc phosphate content in a coating at the same protection levels.⁸⁹

Zinc aluminum polyphosphate, another modified zinc phosphate pigment, showed superiority over unmodified zinc phosphate in EIS data and polarization

experiments⁹⁰. Polyphosphates with cations of calcium, magnesium, or zinc protected steel in artificial sea water by the precipitation of a thin amorphous film on cathodic areas⁹¹. Polyphosphates represent the possibility of increasing the phosphate content and thereby increasing the efficiency of an anticorrosion pigment⁹². The most important polyphosphates are tripolyphosphate and hexametaphosphate⁹³.

Calcium acid phosphate, a cheaper pigment, has better corrosion protection under salt spray testing than zinc phosphate and comparable protection to zinc tetraoxochromate⁹⁴. Furthermore, polarization results show an almost complete inhibition of the cathodic oxygen reduction reaction by calcium acid phosphate ($\text{Ca}(\text{H}_2\text{PO}_4)_2$).

Molybdates

Molybdate based pigments are anodic passivators that form a ferric molybdate layer over the metallic substrate thereby inhibiting both the anodic and cathodic reactions of corrosion⁹⁵. The use of molybdates is somewhat limited due to their high price and they are often used in combination with other inhibitive pigments⁹⁶. The four most popular molybdates for anticorrosion pigments are basic zinc molybdate, basic calcium zinc molybdate, basic zinc molybdate phosphate, and basic calcium zinc molybdate phosphate⁶⁶.

Of the molybdates, zinc molybdenum phosphate has the highest reported corrosion control reportedly due to a synergistic effect between the phosphate and molybdate ions⁹⁷. Zinc molybdenum phosphate has higher anticorrosion

performance compared to zinc phosphate, zinc and iron phosphate, zinc aluminum phosphate, and basic zinc phosphate proven by salt chamber studies and EIS measurements where the capacitance for the molybdate was the lowest for the longest period of time⁹⁸. The protective characteristics of zinc molybdenum phosphate pigments have been reported to be close to those of strontium chromate pigments which make it a viable replacement for the toxic chromate⁹⁹. Performance of zinc molybdenum phosphates can be even further enhanced by the additional presence of zinc oxide pigments due to an electrostatic attraction between the molybdate anion and the positively charged surface of the zinc oxide particles¹⁰⁰.

Borates

Barium metaborate ($\text{Ba}(\text{BO}_2)_2 \cdot n\text{H}_2\text{O}$) is the most commonly used borate inhibitor industrially with application across a broad spectrum of binder systems⁶⁶. Alkalinity and anodic passivation from the metaborate ion are the primary modes of protection. These systems are considered environmentally acceptable due to relatively low acute and chronic toxicity of the barium ion and a low effect of barium and borates on the environment¹⁰¹. Peak anticorrosion performance has been reported at barium metaborate concentrations of 20 parts by weight¹⁰². The chief disadvantage of borate pigments is their high solubility which makes it unacceptable for use in some water borne binder systems.

Silicates

Silicates are not suitable for anticorrosion coatings that are meant for immersion applications⁶⁶. They are chiefly used in oleoresinous systems where they form inhibitive soaps with ions from other pigments in the system. Common anticorrosion silicate pigments are calcium borosilicate, calcium barium phosphosilicate, calcium silicate and calcium strontium phosphosilicate. They work as a blocking pigment as well as having some active functionality based on their ionic nature and in some cases their basicity¹⁰³. These pigments find use in light duty coatings due to their lower performance when compared to other anticorrosion pigments¹⁰⁴.

Ion Exchange Pigments

Few references have been found with mention of ionic exchange pigments or mechanism in regards to anticorrosion coating. The references found are vague mentioning a pigment consisting of a silicate anion and Ca^{2+} cations¹⁰⁵. The mechanism of ion exchange indicated is that the pigment exchanges Ca^{2+} with harmful species, the Ca/silica interacts with the binder and improves crosslinking, or the silica and calcium become mobile and form a protective layer on the metal surface¹⁰⁶. Shieldex is a commercially available pigment based on this principle¹⁰⁷. Shieldex is recommended for use in coil coating primers or one and two coat wash primers and does not find application in naval immersion coatings¹⁰⁸.

1.2.2.3 Electrochemically Active Pigments

The galvanic pigment acts as the sacrificial cathode in the coating, protecting the steel substrate. They are typically a powdered metal with the limiting conditions being the metal selected must be less noble than the metal substrate it is trying to protect. In addition to this criterion, the metal oxide of the pigment must also allow for electron conductivity. This limits the selection of available metals for use in this type of system on steel substrates to zinc based particles. Zinc particles are widely used in primer coatings, with some modern zinc rich coatings approaching 98% PVC. The zinc oxide layer that occurs during the corrosion of these particles conducts electrically, due to inclusions of zinc metal in the layer.

Zinc particles protect iron by a twofold process. First the zinc particles form a compact barrier to the ionic transport through the coating. Second, they protect by anodic zinc dissolution following the reaction shown in EQ 1-10¹⁰⁹.



This anodic dissolution leads to formation of zinc oxide at the site of the cathodic reaction, i.e. the surface of the iron substrate or the zinc salt precipitates in the pore of a coating defect¹¹⁰. This zinc oxide layer acts as an efficient protective barrier layer against further transport of ionic species to the corrosion site¹¹¹.

1.2.3 Fillers

Fillers are typically low cost materials added to a coating to lower the cost per volume, or in some cases to offer thixotropic control of coating viscosity. Talc

is very common as filler in anticorrosion coating systems. Other common fillers are titanium dioxide, magnesium aluminum silicate, and silica¹¹². There have been reported cases where careful selection of a lower cost filler material has shown a synergistic effect and increased the performance of an inhibiting pigment such that it can be used at lower concentrations of the more expensive pigment at the same effectiveness¹¹³.

1.2.4 Additives

Additives in the anti corrosion coating are soluble and sometimes reactive compounds used in small quantities to give the coating specific properties. The function an additive can bring to a coating is quite diverse. Some examples of additive function are antifouling, increase flow ability, enhance surface adhesion, anti foaming, fire resistance, thickeners, etc.

A few anticorrosion compounds are classified as an additive as opposed to a pigment. These organic anticorrosion additives are typically conducting polymers which are sometimes referred to as organic metals due to their ability to conduct electrons. The organic anticorrosion additive of primary interest is polyaniline (PANI) in the emeraldine (conductive) form.

The corrosion protection provided by PANI is attributed to the passivating effect caused by the oxidizing ability of the emeraldine form¹¹⁴. The efficacy of PANI as a corrosion inhibitor in organic coatings is as of yet not clearly defined. One author reports that there is no beneficial effect of the addition of PANI to epoxy and alkyd based coatings¹¹⁵. Instead they report a decrease in corrosion

protection for an epoxy coating containing 0.3% PANI that also utilizes zinc pigmentation due to an increase in the formation of zinc oxide caused by the conductive pathway formed by PANI between zinc particles. In a different work, PANI was shown to actually increase the corrosion rate of the steel plates, along with altering the uniform corrosion of the controls to a pitting regime¹¹⁶.

In stark contrast to these results, a more involved study showed across the board performance enhancement by the addition of PANI to epoxy based coatings containing differing inorganic anticorrosion pigments¹¹⁷. The best reported results were with PANI concentrations of 5 vol % for all pigments and a 100% protection efficiency (zero corrosion) when combined with zinc dust (@ pvc/cpvc=0.65) after approximately 1500 hrs of salt spray testing. Another study reported that an anticorrosion coating containing dispersed PANI had 5 times longer coating life and protected at 25-60% lower coating thickness than other materials¹¹⁸. A composite particle produced from TiO₂ and PANI shows improved results over PANI alone when utilized as anticorrosion additive in a coating and subjected to salt spray studies¹¹⁹.

Polydiphenylamine (PDPA) is another conductive polymer under consideration as an anticorrosion additive. Coatings with concentrations ranging from 0-5% PDPA in a vinyl resin were used to characterize the anticorrosion behavior. Coatings with PDPA concentrations greater than 3% showed excellent corrosion protection of steel¹²⁰.

1.2.5 Solvent

Solvents are used to increase flow ability of the anticorrosion coatings in order to aid in applications of a smooth defect free coating. Additionally, a decrease in coating viscosity has been proven to result in better adhesion between coatings and steel substrates¹²¹. Solvents used for anticorrosion coatings fall into two categories, inert and reactive. Traditionally the solvents used were volatile organic liquids that evaporated from the coating prior to the gel point was reached. However today there are numerous regulations that limit the amount of volatile organic compounds in coating systems to relatively low levels¹²².

Class I corrosion preventative compounds are identified by the US Navy as those with more than 340 g/L of VOC while Class II components have less than 340g/L¹²³. The Navy no longer allows the use of Class I components with the exception of application for spot touch up and repair work¹²⁴. They are currently striving to meet the reality of zero VOC anticorrosion coatings. The Navy has set the goal of exceeding current and future EPA regulations by adopting 100% solids anticorrosion coatings¹²⁵.

One solution to the zero solvent regulations is the use of reactive solvents. These are low molecular weight molecules with at least one functional group that is reactive and completely miscible with the coating system chemistry¹²⁶. By this method it is possible to achieve a low viscosity in order to achieve adequate film formation and adhesion at application while still maintaining a 100% solids content of the coating to meet regulations and standards¹²⁷. High solids anti-

corrosion coatings have the additional benefit of being better at protecting against corrosion¹²⁸. This increase in resistance is due to a more homogeneous film formation in solvent free systems¹²⁹.

1.3 Ion Sequestration Particles in the Anticorrosion Coating

The ISPs developed as discussed in this dissertation would take on the roll of an active pigment in an anticorrosion coating. They could be utilized as a total or partial substitution for the current active pigments used for corrosion inhibition. ISPs added should not interfere with other aspects of the coatings to which they are added, such as their adhesion to the substrate, film forming characteristics, etc. Given the complex nature of the interaction between the various components (binder, active pigments, fillers, additives, and solvents) of the anticorrosion coating formulation, it is likely that the addition of ISPs at the commercial level would require some slight reformulation.

CHAPTER 2

ISP SYNTHESIS

This chapter describes in detail the synthesis evolution and experiments performed resulting in the final development of ISPs. The details of each experimental procedure as well as the process changes made during development are discussed here. Synthesis composition is covered in this chapter with the specific details of each chemical reaction performed during the course of this work provided in tabulated form for reference. Chapter 3 will describe characterization of the particles, and Chapter 4 will discuss the anticorrosion properties of the synthesized ISPs.

2.1 Evolution of the Synthesis of Ion Sequestration Particles

The goal of this work was to develop a successful synthesis process for ion sequestration particles (ISPs) that provide enhanced corrosion protection upon dispersal in an anticorrosion coating. These ISPs are designed to sequester free ions, as they are generated during the corrosion process as in the case of hydroxyl ions or as they diffuse through the coating as in the case of chloride ions. In order to maintain charge neutrality, the particles will release phosphate ions which function as corrosion inhibiting anions. The driving force for the ion exchange is the concentration gradient differential of the ions between the particle and the coating, and can be considered a diffusion controlled

process. This system is illustrated in Figure 2.1 where you see a particle in a coating matrix on a steel substrate and some possible ion exchange schemes.

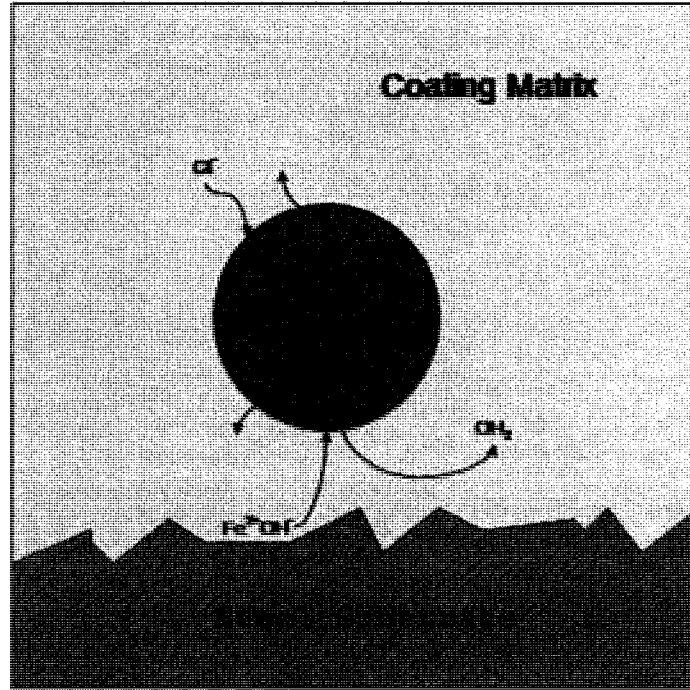


Figure 2.1: Ion Sequestration Particle in a Coating Matrix

There has been considerable evolution of the ISP synthesis. Initially there were two congruent synthesis approaches proposed and investigated. One was based on the development of a core shell based ISP while the other aimed to develop a homogeneous ISP.

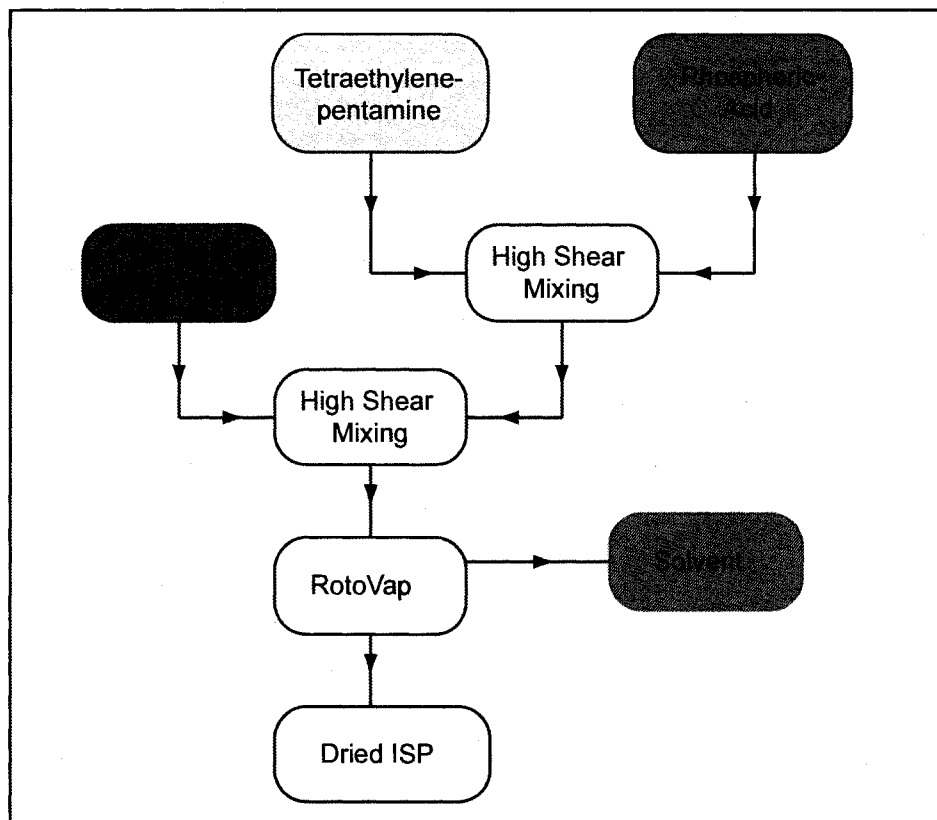


Figure 2.2: Synthesis Scheme for Initial Core Shell Approach

The initial core shell approach as illustrated in Figure 2.2 utilized ionic bonding of short chain polyamines and phosphoric acid to make an ion sequestration core particle. Due to the rapid reaction between the acid and base this required development of an atypical dispersion method. The particles were made by drop wise addition of dilute monomers directly into a high shear field. Originally it was hoped that these core particles would be stable and useable on their own. Unfortunately this was not the case and the ionic core required further protection. The ionic coupled core particles were then stabilized by interfacial polymerization with either a multifunctional isocyanate or a multifunctional epoxide. Both of these monomers react by condensation polymerization with an excess of the amine functionality that was designed in to the core particles.

This technique synthesized solid ISPs that were dried into free flowing powders with particle sizes ranging from 1-100 um. However, the encapsulation of the ionic core material was incomplete and far from the desired core shell morphology. Upon mixing these particles with a MIL-DTL-24441 standard coating there was reaction causing a gelation of the liquid. Initially it was assumed that this was related to pigment shock. Further investigation revealed the problem to be more fundamental in nature. The ISPs were exchanging ions with amine components of the liquid monomers, in effect adding ionic crosslinks to the coating components. This rendered the coating system unusable by changing the liquid into a viscous slurry/loose gel.

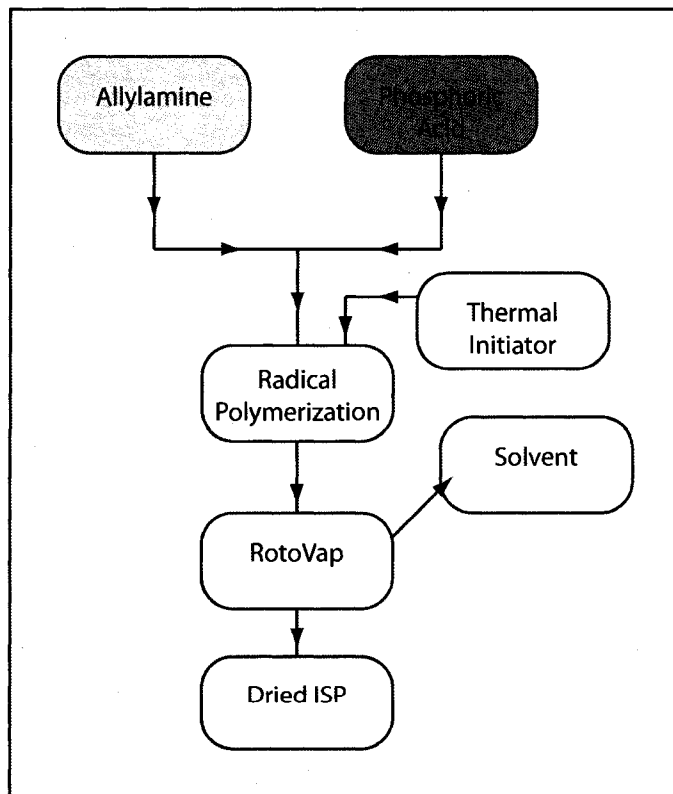


Figure 2.3: Synthesis Scheme for Homogeneous ISPs

The alternate homogeneous ISP relied on a different synthesis route illustrated in Figure 2.3. The mechanism of this approach was to create an ionic coupled droplet of phosphoric acid and an amine containing monomer capable of radical polymerization. A dispersion of phosphoric acid in heptane was coupled with allylamine and other monomers including a crosslinker. The polymerization should have resulted in a homogeneous crosslinked polymer network bound to phosphate. This method produced ISPs for characterization, but was abandoned after 18 months due to difficulties stemming from the inability to produce allylamine based polymer chains beyond oligomeric length. This work is not presented in the body of this dissertation. The details are presented in Appendix I.

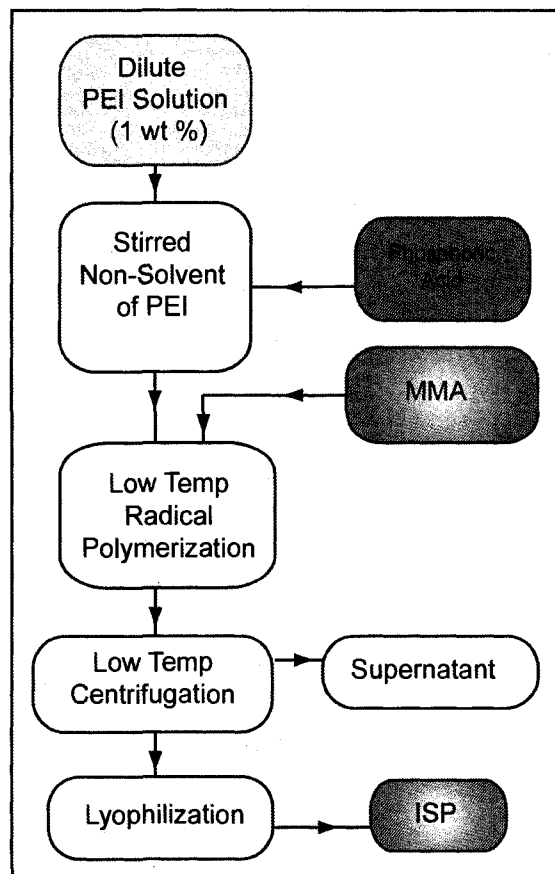


Figure 2.4: Synthesis Scheme for PEI Solvent/Non-Solvent Approach

Figure 2.4 illustrates a third synthesis scheme that was investigated after abandoning the homogeneous route and the inability of the core shell synthesis to successfully encapsulate the core. This approach was an alternative method to produce a core shell ISP. The concept was to use a solvent/nonsolvent system for polyethylenimine to produce core particles. Polyethylenimine ($M_w=60,000$) was dissolved, at dilute concentration, in a good solvent. During slow drop wise addition of the solution into a miscible liquid that was a nonsolvent of the polymer the good solvent disperses and the polymer precipitates as a “dried” polymer particle. The dispersed particles were then

encapsulated. Fine dispersions of particles in the 100-200 nm range were synthesized by this method. This method required difficult drying schemes involving low temperature centrifugation and lyophilization due to low temperature transitions of the synthesized particles. It was considered unsuccessful and offers little in regards to the successful synthesis route of this work. At this time it was also attempted to produce particles by fine mechanical grinding of bulk dry ion sequestering core material based on PEI, but this was also unsuccessful. Detailed discussion of this work is left out of the body of this dissertation, but is available in APPENDIX 2.

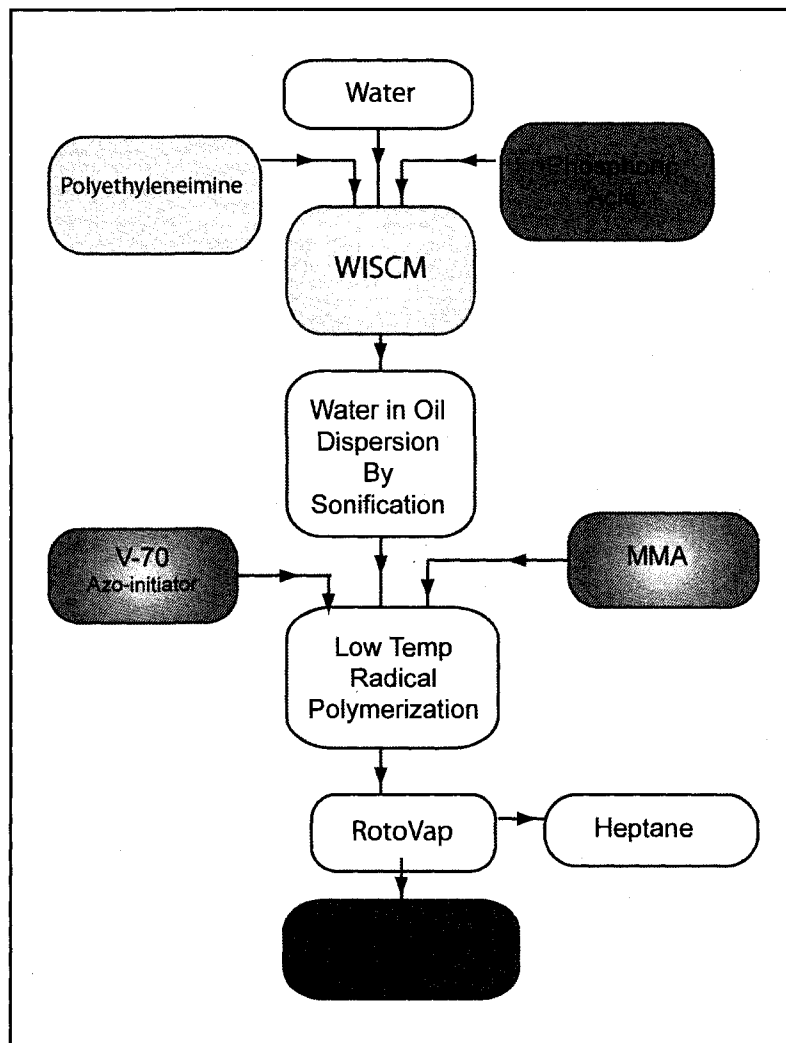


Figure 2.5: Synthesis Scheme for WISCAM based ISPs

In the face of failure, a step back was taken to garner a fresh perspective on the development of a new synthesis scheme for ISPs as seen in Figure 2.5. This new scheme utilizes a wet ion sequestration core material (WISCAM) encapsulated by a layer of polymethylmethacrylate (PMMA). Then by a controlled drying process the water was removed from the core. This method produced the first viable ISPs capable of incorporation into an anticorrosion coating. However this does not represent the final evolution of the ISP synthesis.

The drying process was difficult and resulted in ruptured capsules if not carried out precisely.

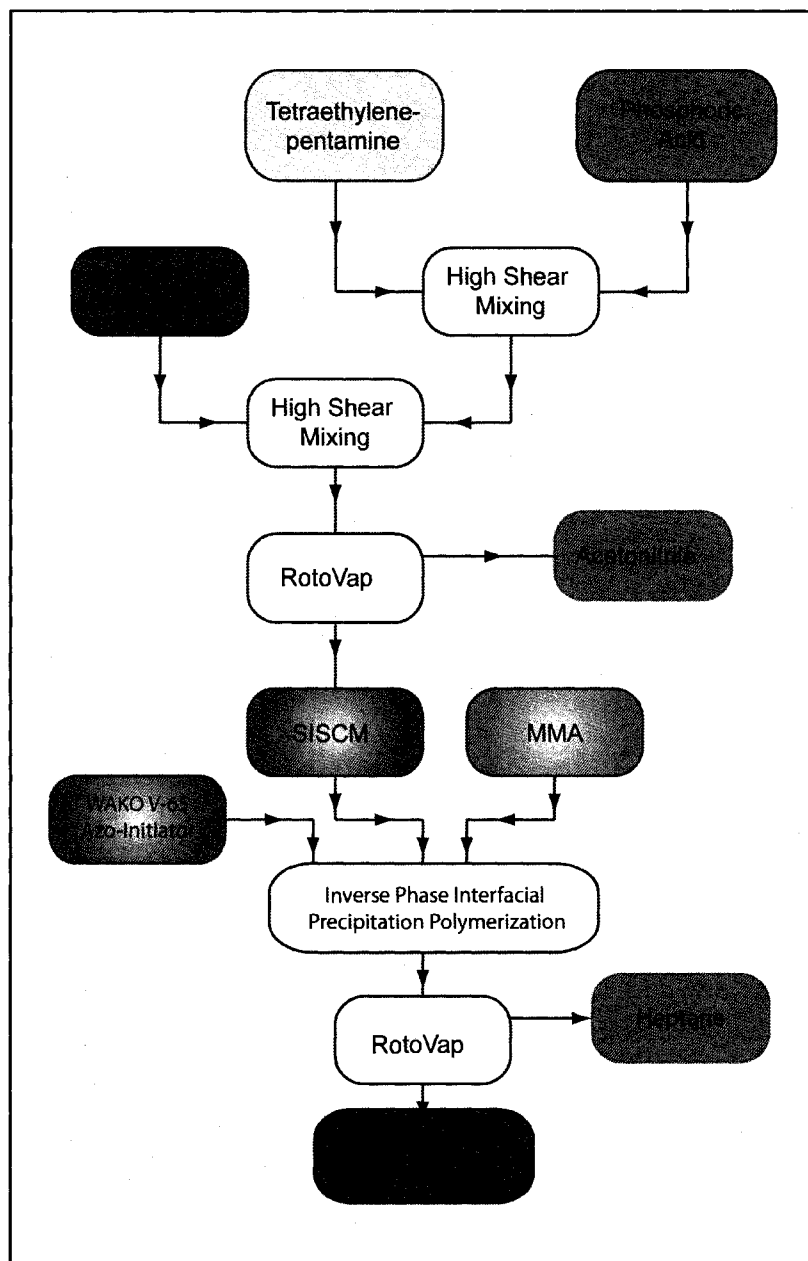


Figure 2.6: Synthesis Scheme for SISCM based ISPs

Upon successfully synthesizing WISCM based ISPs, it was deduced that if a WISCM could be encapsulated and protected by this technique the same could

be done with a solid core. The best particles from the initial synthesis scheme were selected and dispersed in heptane. They were encapsulated with PMMA in an inverse phase precipitation interfacial polymerization. These particles were viable as they were successfully incorporated into an anticorrosion coating. This final synthesis is more somewhat straightforward, reproducible, and produces ISPs that when then mixed with an anticorrosion coating system results in improved corrosion protection, as seen in later chapters of this text. The synthesis scheme is presented in Figure 2.6 and the details are presented fully in the following sections of this chapter.

2.2 Synthesis of Ion Sequestration Particles

This section will describe the details of the experimental procedures used to synthesize the ISPs. This will be discussed in three parts. First the WISCM process is discussed in detail. Next the initial unsuccessful core shell synthesis is described, as these particles were later used as the solid ion sequestration core material (SISCM) in the final evolved synthesis. Finally, the successful combined synthesis utilizing the particles made in the initial process and the encapsulation developed as part of the WISCM synthesis is described.

2.2.1 Encapsulation of Wet Ion Sequestering Core Material

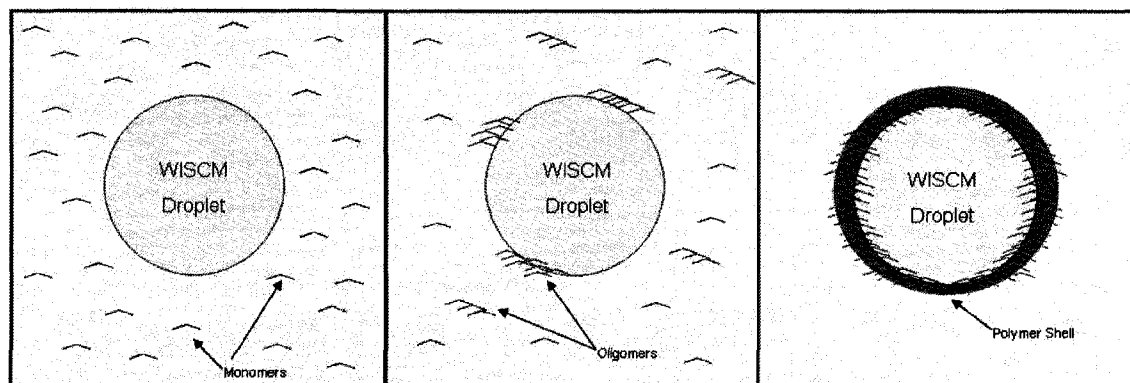


Figure 2.7: Precipitation of Polymer on WISC M in Heptane

This synthesis of an ISP differed from other approaches in that the initial encapsulation was of a liquid phase. Wet ion sequestration core material (WISC M) was dispersed in heptane by sonification. Then the droplets were encapsulated by an inverse phase precipitation polymerization of methylmethacrylate (MMA) in heptane as represented in Figure 2.7. The encapsulated ion sequestering liquid needed to be dried after the encapsulation. Successful drying was achieved by a controlled low pressure distillation process that allows the water to be separated from the distillate while refluxing the heptane.

2.2.1.1 Wet Ion Sequestration Core Material

The WISC M developed is chemically similar to previous ISP core materials. The primary difference is that it is solvated with water. WISC M consists of polyethyleneimine ($M_w = 60,000$) ionically associated with phosphoric

acid. For all of the experimental work done with this method the WISCM is of the composition shown in Table 2-1.

Table 2-1: WISCM Composition

Component	Mass	%
Water	140	90%
PEI	10	6%
H3PO4	6	4%

WISCM is prepared by first diluting 10g of PEI into 90mL water and 6g of phosphoric acid into 50 mL of water. The two solutions are then mixed together. The resultant liquid is a transparent solution. The solution is then boiled under reflux for one hour with an argon purge to remove any dissolved oxygen.

2.2.1.2 Encapsulation of WISCM

Previous attempts at ISP synthesis (see APPENDIX 2) provided the knowledge of a low temperature transition in the PEI (@ ~25C) which required the temperature to be kept to a minimum during the encapsulation process. If the encapsulation was attempted at a temperature above 50 C there was agglomeration to the point of almost complete separation (ZZZONR020107). To meet this requirement low temperature radical generating initiators for the polymerization of MMA were investigated with the results presented in Table 2-2.

Table 2-2: Experiments in the Investigation of Low Temperature Initiators

Experiment ID	Low Temperature Initiator	Description of Result
ZZZONR092906	benzoyl peroxide - phosphoric acid	no precipitate
ZZZONR100206	benzoyl peroxide - triethylamine	amber discoloration, no precipitate
ZZZONR100306	benzoyl peroxide - ascorbic acid	no precipitate
ZZZONR110306	benzoyl peroxide - cobalt naphthanate	solid polymer formed
ZZZONR110606	WAKO Chemical V-70	white polymer precipitate
ZZZONR110806	benzoyl peroxide-cobalt naphthanate	solution browned, polymer precipitate

The first successful system (ZZZONR110306) for low temperature radical polymerization of MMA for encapsulation utilized a redox couple of benzoyl peroxide with cobalt naphthenate. This system successfully polymerized MMA at room temperature but PMMA was not produced under WISCM encapsulation conditions utilizing this system. It was suspected that the core material was interfering in the redox couple of the initiator system preventing or scavenging the low temperature generation of radicals.

A low temperature initiator made by WAKO Chemicals Inc has been successfully utilized in other unrelated projects and was selected as the initiator for the polymerization of MMA for WISCM encapsulation. WAKO's V-70 (**Error! Reference source not found.**) has a half life of 10 hrs at 35C and is the lowest temperature solvent soluble azo-initiator commercially available. V-70 was successful in polymerizing MMA which in turn precipitated at the interface encapsulating the WISCM droplets.

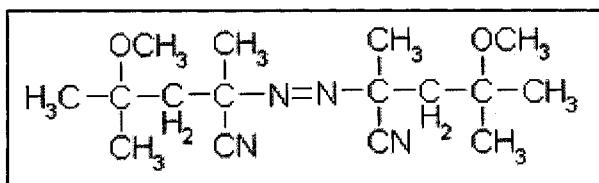


Figure 2.8: Chemical Structure of V-70

The procedure (ZZZONR120706) used to successfully encapsulate the WISCM in PMMA was as follows. Into a three neck round bottom flask is placed 200mL of heptane, 20mL of WISCM solution, and 3g of SPAN83 surfactant. The temperature is maintained at 35C with a temperature probe inside the flask. A condenser at 5C is used to minimize the loss of heptane as vapor. A Branson Sonifier 450 with a ½” diameter tip is used to sonicate the solution for 20 minutes at an 80% duty cycle and output power of 7. The sonifier disperses the WISCM solution in the heptane. The sonifier power, duty cycle, tip size, and sonification time control the size of the droplets of WISCM produced.

WISCM droplets produced by the sonifier were not stable on their own. A low HLB surfactant was needed to help stabilize this water in oil emulsion. Investigation (ZZZONR102306 & ZZZONR112807) of several likely candidates for the best surfactant was performed by producing dispersions of WISCM in heptane and then observing the stability of the suspension with different surfactants. The results are presented as Table 2-3. SPAN 83 was selected as the surfactant for use for the WISCM process as it maintained the suspension for a period of several hours.

Table 2-3: Surfactants Studied for WISCM Dispersion Stabilization

Surfactant	HLB	Effect on Dispersion
Symperonic PE/F68	N/A	separation by 15 min
Span 60	4.7	separation at 3 min
Span 83	3.7	stable for several hours
Tween 80	15	settling after 5 to 10 minutes

Agitation was supplied at 300 rpm by an overhead shaft mixer after the generation of the inverse phase emulsion by the sonifier. Next 5g of MMA was

added to the flask and the system purged with argon for 30 minutes. Then 0.050 g of V-70 dissolved in 2 mL of toluene was added and the system was allowed to react for approximately 48 hrs under nitrogen. Table 2-4 shows a summary of the components used in this experiment, the quantity used, and the weight percentage of the total mass.

Table 2-4: WISCM ISP Formulation

Chemical	Mass (g)	Weight %
Heptane	200	88.1%
WISCM	20	8.8%
Span 83	2	0.9%
MMA	5	2.2%

2.2.1.3 Drying of PMMA Encapsulated WISCM

The encapsulated WISCM next underwent a process for removal of water from the core. The technique developed to remove the water utilized a controlled partial vacuum at slightly elevated temperatures. Initial drying attempts using high temperatures ($T > 100^{\circ}\text{C}$) resulted in vaporization of the water in the WISCM and destruction of the PMMA capsules due to rupture.

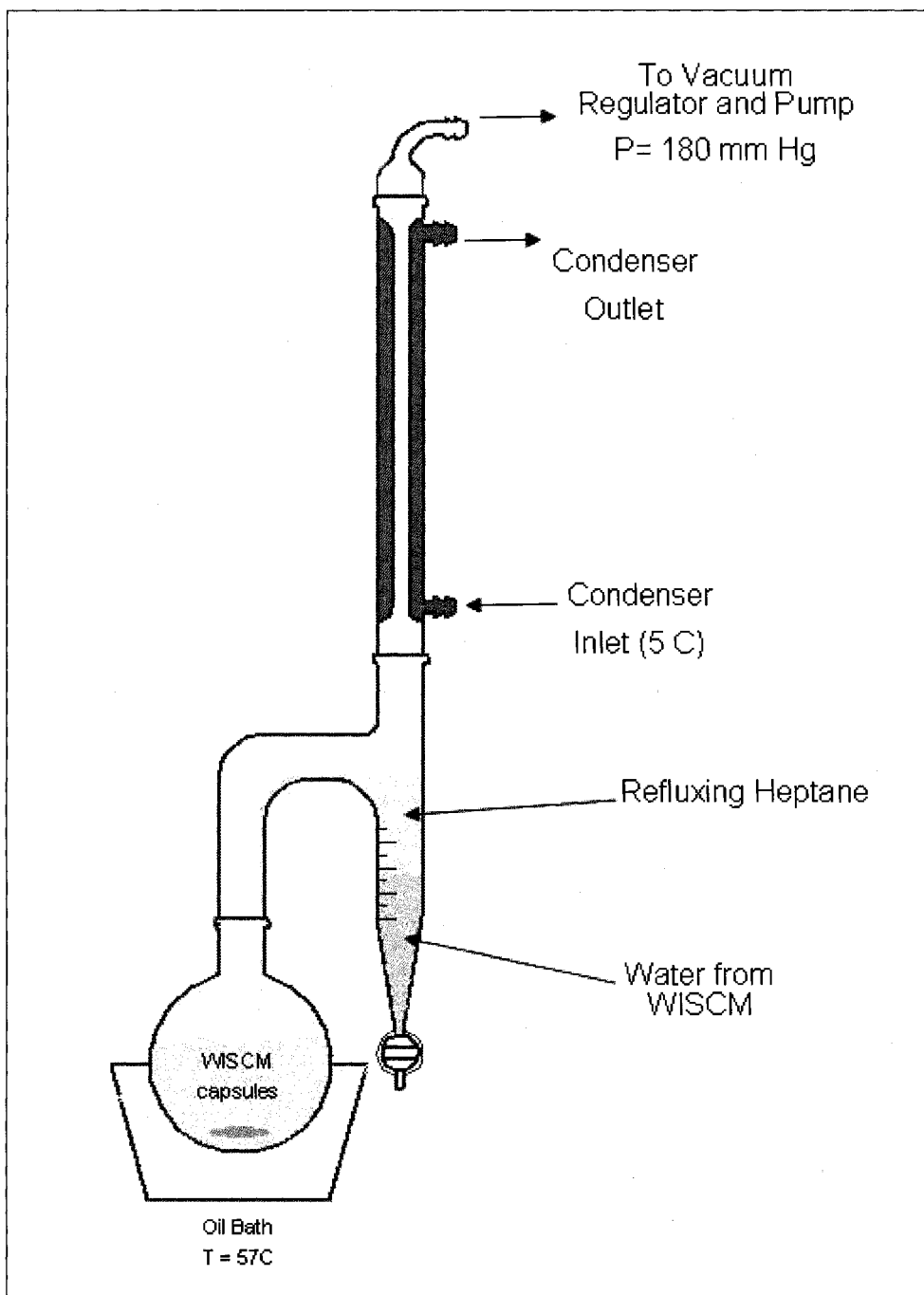


Figure 2.9: Experimental Apparatus for WISCAM Drying

A 10mL distilling receiver was used in this step to collect the water removed from the encapsulated WISCAM. The experimental set up shown in Figure 2.9 consisted of an oil bath, round bottom flask, distillate receiver,

condenser, vacuum pump, and digital vacuum regulator. As the heptane and water condense they run down collecting in the receiver. The heptane being less dense and immiscible with water separates to the top in the receiver. As the condensate fills the receiver flask the heptane being on top was refluxed back into the RBF. The water is collected in the bottom of the receiver. The amount was quantified by reading the graduations or by drainage after bringing the system back to atmospheric pressure and opening the valve at the base of the receiver. The drying was stopped when the volume of water in the receiver no longer increased.

The experimental parameters identified to yield a successful drying process were a temperature of 57C with the vacuum regulator set at 180 mm Hg. This provides conditions where the water was slowly removed through the PMMA wall. If too rapid a drying process was used the capsules ruptured resulting in failure to synthesize ISPs. This happened in the earlier high temperature drying experiments that resulted in agglomeration and degradation of the ISPs.

2.2.1.4 WISCM Encapsulation Experimental Variations

After the first successful encapsulation and drying of WISCM based ISPs(ZZZONR120706)), the experiment was repeated. The process succeeded in being reproduced one additional time showing that the encapsulation of the WISCM is reproducible. However two of the repeated experiments failed to produce particles resulting in a 50% success rate for the synthesis process.

The next evolution involved changing the agitation in the experimental apparatus. In the first successful WISCM synthesis, agitation was provided by a 25mm football shaped magnetic stir bar in the RBF. One of the reproducibility failures was suspected to be due to an unstable suspension. If this was the case it was likely caused by a lack of sufficient agitation from the magnetic stir bar. The WISCM suspensions generated by the sonifier were not stable for more than a period of hours without continued agitation. The experimental set up was then changed to one that utilizes an overhead mechanical stirrer with a hemispherical mixing blade which results in an increased agitation in the flask and the suspension was better maintained.

This process change once again failed to yield a successfully encapsulated WISCM particle. The oligomer chains did not seem to be precipitating at the WISCM droplet surface as the polymerization progressed, possibly due to the increased shear field generated by the mechanical mixer. Instead there was a formation of new particles of polymer in the bulk phase leaving the WISCM unencapsulated. Failure to encapsulate the WISCM was easily detected as unencapsulated WISCM yellows rapidly after only a few days when not protected by encapsulation. This can be seen in Figure 2.10, where the right hand jar contains unencapsulated WISCM solution which has yellowed as amines are known to when unprotected¹³⁰.

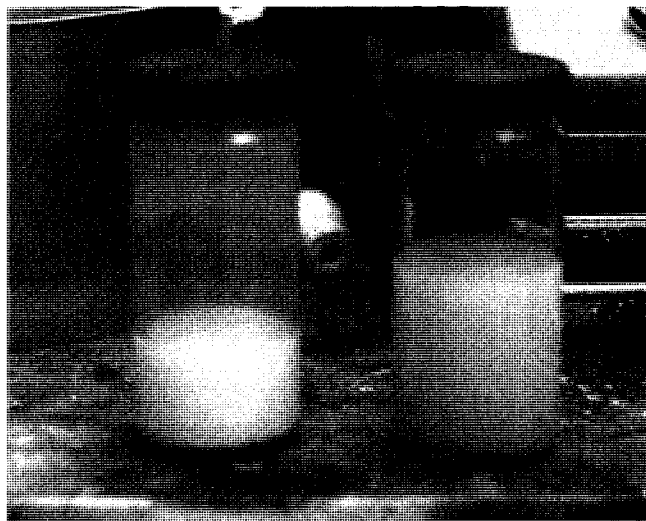


Figure 2.10: Comparison of encapsulated WISCM (left) and unencapsulated WISCM (right), both as suspensions in heptane

Attempts to vary the shell wall composition were made by copolymerizing MMA with BA and BMA. This was done in an attempt to be able to decrease the glass transition temperature (T_g) of the shell material from the 105 C T_g of PMMA. The lowering of the glass transition temperature would result in a softer shell which in turn would allow for the more rapid transport of water and ions through the shell wall. Towards this a number of experiments were performed where co-monomers were used to produce lower T_g which was predicted by the Fox equation. The results of this are shown in Table 2-5.

Table 2-5: Calculated T_g Values of Comonomer Shell Experiments

Experimental ID	Monomer A	Monomer B	W_A	W_B	T_g (K)
ZZZONR041907	MMA	BA	0.480	0.520	274
ZZZONR050107	MMA	BMA	0.252	0.748	311
ZZZONR051507	MMA	BMA	0.332	0.668	317
ZZZONR052207	MMA	BMA	0.335	0.665	317

The result of these experiments was that it was not readily possible to encapsulate the WISCM successfully with a copolymer. While copolymers were made during these experiments, they did not encapsulate the WISCM. This is likely due to the low temperature polymerization scheme used, coupled with the different reaction rates for the copolymerizations. Additionally the copolymers might not be as thermodynamically driven to the interface between the WISCM and the heptane as was the PMMA homopolymer due to polarity differences or changes in the zeta potential of the system.

2.2.1.5 Summary of WISCM ISP Experiments

The WISCM encapsulation was capable of producing ISPs with a limited 50% success rate (ZZZONR120706 and ZZZONR010307). The success of the dried ISPs was shown when they were mixed with the amine component of a Mil P-24441 epoxy coating. After a week the mixture was still liquid, transparent, and there was no observable viscosity increase. The amine was then mixed with the epoxy component and cured. This was the first successful dispersion of an ISP into the MIL-DTL-24441 coating.

Table 2-6 contains the experimental data in a compact form for the synthesis experiments done under the WISCM encapsulation presented in this section.

Table 2-6: Experimental Details for WISCM Based ISPs

Experimental ID	Solvent (mL)	WISCM (mL)	Surfactant (g)	MMA (g)	Temp. (C)
ZZZONR111406	100	20	3	5	45
Span 83 as surfactant. Result was a solid mass of polymer. Possibly temperature related					
ZZZONR112706	200	20	1.2	5.031	35
Tween 80 was used as surfactant. Suspension failed and particles agglomerated and settled.					
ZZZONR113006	200	20	2	5.109	35
Span 83 from this point on. Produced particles. Problem with purge gas					
ZZZONR120706	200	20	2	5	35
Encapsulation success. Heptane dried @ stp, then particles redispersed in heptane					
ZZZONR010307	200	20	2	4.95	335
Successful encapsulation, more particles for drying					
ZZZONR020107	50	5	0.3	6	80
Higher temperature, complete agglomeration of WISCM and polymer. Unsuccessful					
ZZZONR022207	200	20	2	5	35
WISCM settled, problem with magnetic stirring? Polymer layer formed on top of WISCM					
ZZZONR032007	300	20	2	5	35
switch to mechanical stiring. More solvent added to raise level for stir blade					
ZZZONR032207	150	0	3 drops	14.331	50
testing MMA & V70 at higher Temperatures					
ZZZONR032807	200	20	2	5	50
This made polymer, but did not encapsulate. Dried to sticky solid and yellowed rapidly					
ZZZONR041907	200	20	1	see below	35
2.51g MMA / 2.72g BA copolymer. No capsules. Rapid yellowing of suspension					
ZZZONR050107	100	0	4 drops tween 80	see below	40
3.071g MMA 9.112g BMA copolymerization to check if V-70 would copolymerize. 2 Tgs on DSC					
ZZZONR051507	100	0	3 drops tween 80	see below	40
6.03g BMA, 3.003g MMA, another attempt to get copolymer. Low yield, only 48 %					
ZZZONR052207	100	20	0	see below	40
3.078g MMA, 6.12g BMA similar results to ZZZONR051507 copoly shell abandoned					

2.2.2 Synthesis of a “Core Shell” ISP

This section discusses the initially unsuccessful particle synthesis. This approach was initially designed to produce the ideal ISP that of a core shell morphology. This process was not successful at producing ISPs independently but it is presented here because this work is the foundation of the successful synthesis process discussed later in this chapter.

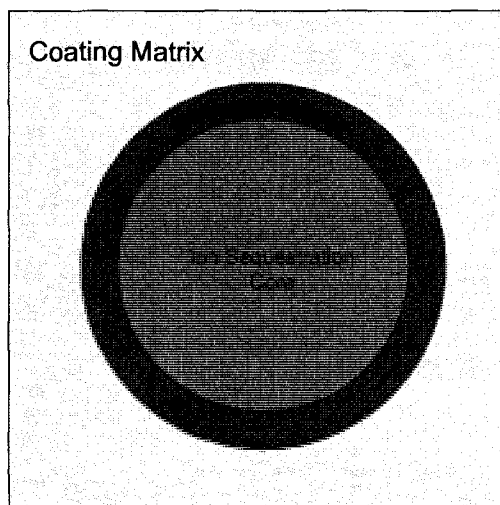


Figure 2.11 Depiction of an Ideal Core Shell ISP

The ideal ISP would be of core shell morphology consists of an ion sequestering solid core material surrounded by a crosslinked polymer shell as shown in Figure 2.11. The shells function is to protect and contain the core material from dissolution and reaction with components of an uncured coating system. The fundamental synthesis of the ion sequestering core is based around the ionic association of phosphoric acid with a linear polyamine inside a high shear field forming microparticles. This ionic association is able to interact by ion exchange with harmful anions involved in the corrosion process, most notably hydroxyl and chloride ions.

Table 2-7: pKa's for Ion Sequestration Core Materials

	pKa ₁	pKa ₂	pKa ₃	pKa ₄	pKa ₅
H ₃ PO ₄	2.16	7.21	12.32		
TEPA	9.68	9.1	8.08	4.72	2.98

The phosphoric acid has three protons that can be utilized for the ionic bonding with the TEPA. However, the pKa for the third proton is 12.32 which is too high for any of the amine moieties present in TEPA to associate. Therefore the amine moieties can only associate with two of the phosphoric acid protons. The acid/base reactions result in a crosslinked network as represented in Figure 2.12. The chemical components are formulated in such a way that there is an excess of amine functionalities after the first acid/base reaction with the phosphoric acid.

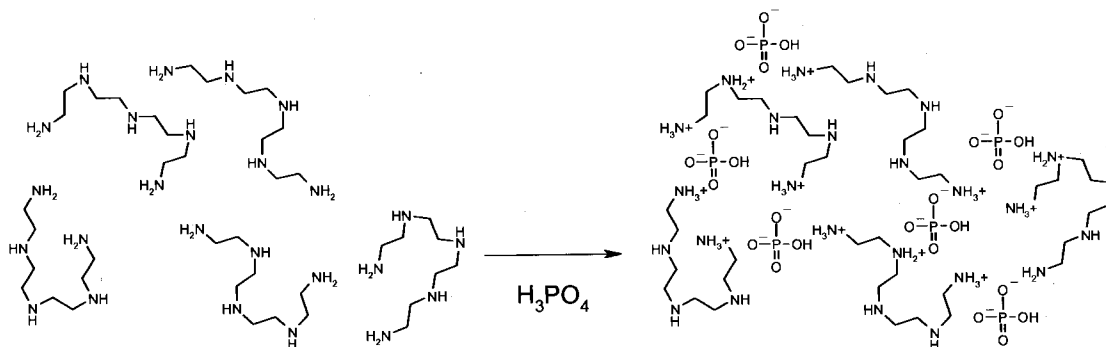
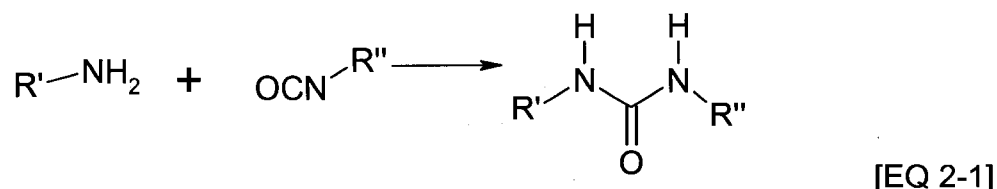


Figure 2.12: Ionic Association of Monomers

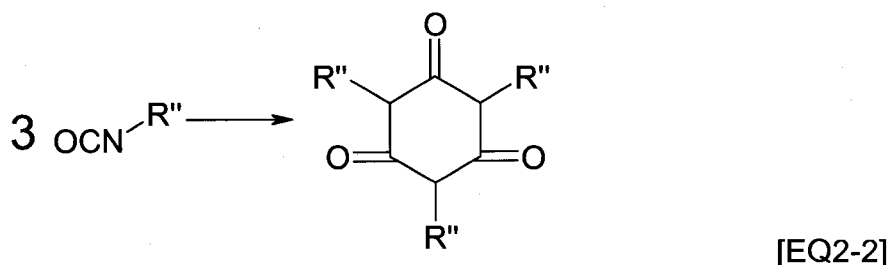
After the first step is completed such that the amines have associated with the phosphoric acid forming the ionic core of the particles, a second monomer is added to the system. This secondary monomer reacts with the excess amines

designed into the core of the initial particles. This should form a hard shell on the surface of the particles. Instead it more likely forms a rigid structure that supports but does not encapsulate the ionic core.

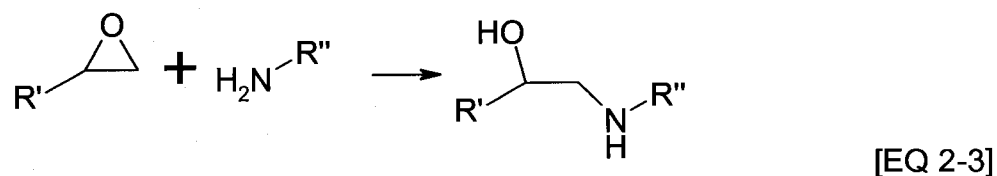
Two different chemicals, isocyanates and epoxides were investigated as they both can react with the excess amines to generate the shell material. An isocyanate moiety reacts with the excess amines to form urea bond (EQ 2-1).



In addition the isocyanate can also self polymerize, with the amine moieties acting as a catalyst, forming isocyanurate bonds (EQ 2-2)



Likewise the core materials excess amines can react with an epoxide by nucleophilic addition to produce an epoxy bond.



The reaction between the isocyanate and primary amines is very fast $K_{ISO-NH_2} \sim 16,000$ (L/mol/s) and highly exothermic with $\Delta H_{RXN} = -197,000$ J/mol¹³¹ at 30C. The speed of this reaction makes working with this chemistry challenging. The epoxy amine reaction is much slower with $K_{EPOXY-NH_2} \sim 5$ (L/mol/s) at 30C

132. The slower epoxy amine reaction provided different problems than the extreme speed of the isocyanate amine reaction.

2.2.2.1 Batch Process Synthesis

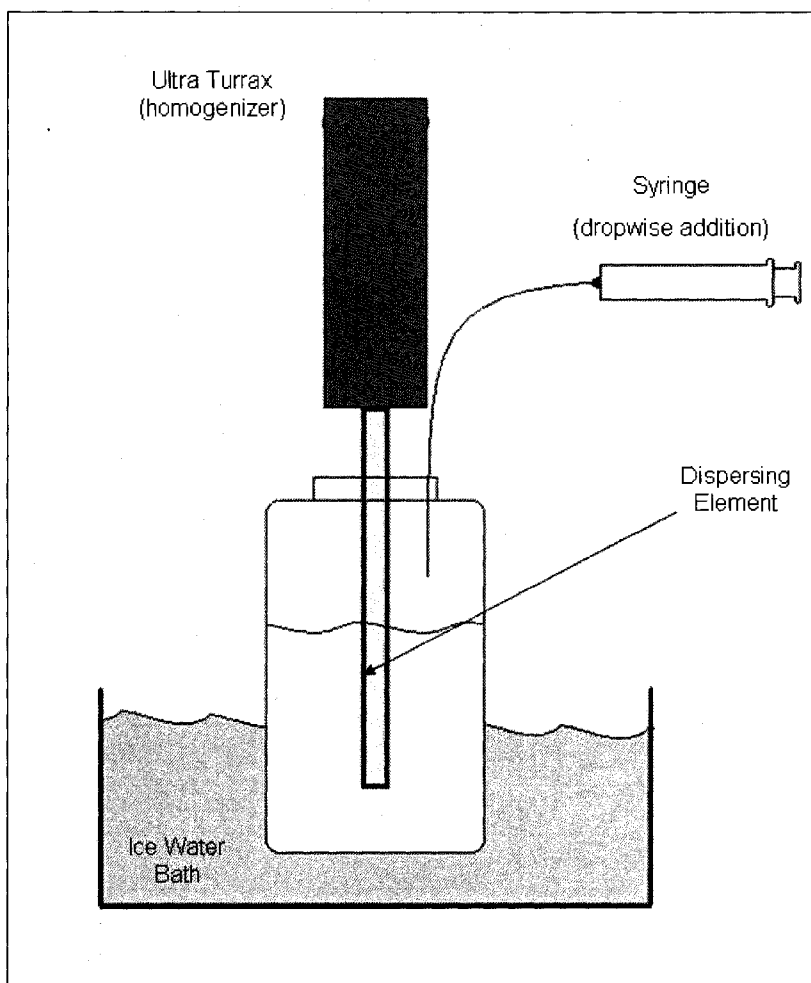


Figure 2.13: Schematic of Batch Process

A batch process (Figure 2.13) with a 10% reactant concentration was selected for the initial experimental synthesis (ZZZONR061504). The early experiments were all formulated with a 30% excess of TEPA over that needed for complete association with the phosphoric acid. The TEPA (19.6g) was dissolved

in 200mL of heptane and placed in the reaction vessel, a 500 mL polypropylene jar. Agitation was provided by an IKA Ultraturrax T-25 High shear mixer at a speed setting of 3 on a scale of 1-6. The reactor was cooled by immersion in an ice/water bath as the acid-base reaction between the amine and the phosphoric acid is exothermic and the Ultraturrax also generates heat. The phosphoric acid (4.68g, 99.9% pure, melted at T=40C) was then added drop wise from above by a gravity feed through a needle. After the phosphoric acid was added the reactor was allowed to mix for 20 minutes with the shear field from the Ultraturrax high shear mixer applied.

This first experiment failed to produce particles. Instead it resulted in two distinct liquid phases. Insolubility of the phosphoric acid and TEPA in the heptane required a change of solvents as the reaction was not proceeding in the inverse phase dispersion as expected. The solvent was first switched to chloroform due to the density as well as increased solubility of the TEPA in this phase. A commercial stabilizer molecule, nonylphenyl pentaethylene glycol (NP-5) was added in an effort to stabilize the suspension. The synthesis was repeated with NP-5 at a concentration of 0.5% by weight of the reactants in the dispersed phase of chloroform. These changes resulted in what appeared under visual observation in a light microscope to be agglomerations of particles stuck together. The ionic bonds formed by the association of the amine with phosphoric acid are not fixed as they would be if they were covalent. It can be deduced that without any covalent bonds to stabilize the particles they can and do agglomerate.

In order to provide the individual particles produced with a more robust structure, a difunctional isocyanate was used to produce a covalently bonded matrix or shell around the core particle. Hexane di-isocyanate (HDI) was selected and used to this end. Experiments were carried out as before, but after the complete addition of the phosphoric acid, HDI (3.998g) was added slowly drop wise from a syringe over a 20 minute period. In later experiments the isocyanate was changed to toluene diisocyanate (TDI) after checking the solubility of several isocyanates in chloroform.

Addressing the health concerns of using chloroform (carcinogenic) as the solvent for these experiments, several other solvents were investigated for the solubility of the reactants. N-methyl pyrrolidone (NMP), dimethyl sulfoxide (DMSO), water and acetonitrile (ACN) were investigated as substitute solvents. ACN was selected based on solubility of reactants and physical properties. It was important that the solvent chosen had a low boiling point to facilitate easy removal during the drying of particles. ISPs are required to be solvent free for their addition into the anticorrosion coatings as the solvent could change the properties of the coating and the Navy has the goal of a solvent free 100% solids coating system.

The first successful synthesis of dry solid ISP (ZZZONR070104) was produced by TEPA (19.5g) in 200 mL of ACN with the addition of Lauric Acid (0.140g) as an alternative stabilizer molecule. Another change was the dilution of phosphoric acid (4.659g) in ACN to 10% concentration prior to addition. Similarly the TDI (4.14g) was diluted to 10% concentration in ACN. The addition

rate of the now dilute reactants was controlled by the use of a programmable syringe pump and a Popper and Sons 50ml glass syringe with a 28 gauge needle. A flow rate of 1.0 mL/min was used.

At best, batch synthesis contained significant agglomerations and coagulum with large amounts of undispersed bulk material synthesized. The rapid reaction of the acid/base as well as the speed of the amine/isocyanate reaction was producing more solid bulk waste material than good particles. In order to overcome the speed of this reaction it was determined that the monomers need to be injected directly into the shear field generated by the ultraturrax tool. The synthesis was changed from a batch process to a semi batch process. Experimental composition details for the work described in this section are presented in Section 2.2.2.3.

2.2.2.2 Semi-Batch Process Synthesis

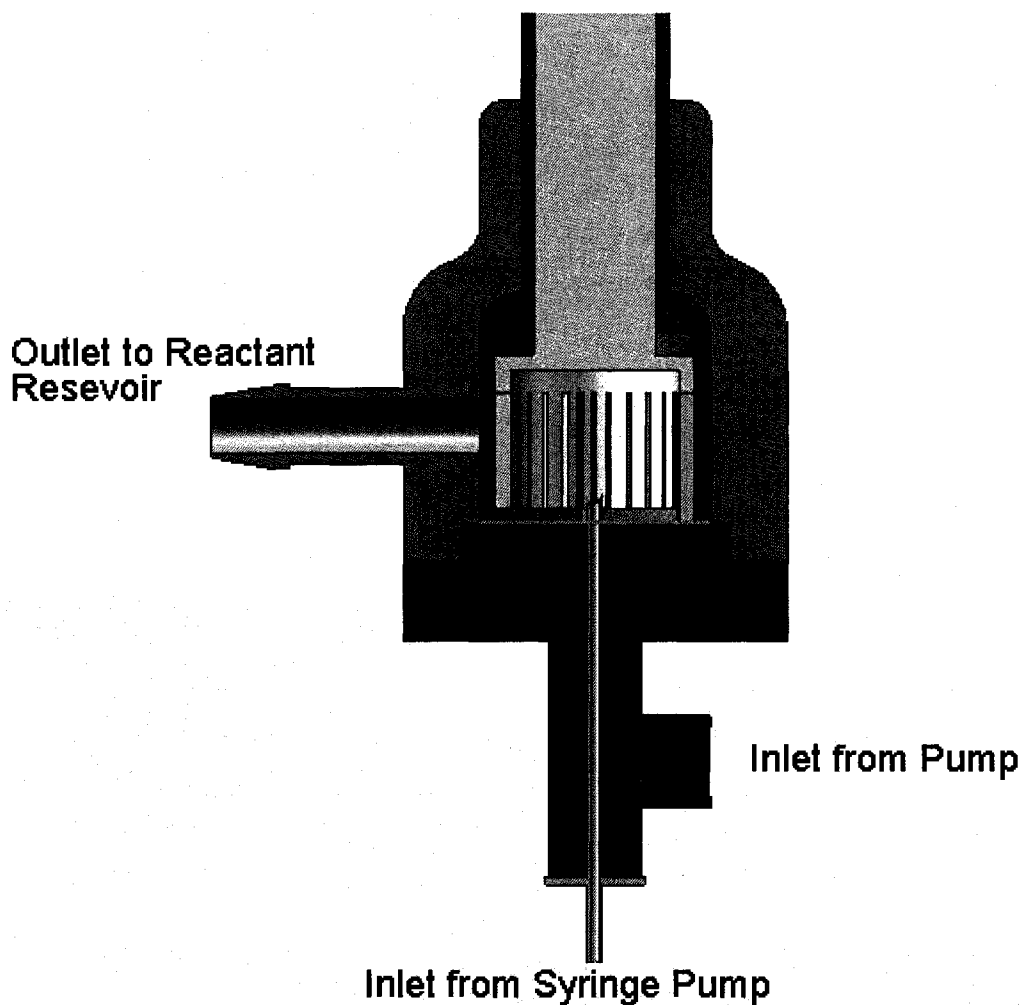


Figure 2.14 Cross section Showing Modified Continuous Cell

The transition from a batch to a semi-batch/semi-continuous synthesis was made possible by the purchase and modification of a continuous flow cell for the Ultraturax. A custom inlet adapter was fabricated to allow for a needle (shown in gold) to disperse the reactants directly into the shear field of the Ultraturax continuous cell as depicted by the red base piece in the cross sectional drawing as Figure 2.14. The Ultraturax rotates the inner shaft with a

crenellated mixer blade at variable speeds ranging from 5,000 to 60,000 RPM and by doing so generates a shear field internally in the center of the cell. By adding the reactants directly into this shear field they were potentially dispersed faster than they reacted resulting in the successful synthesis of ISPs.

Additional process changes included the addition of a peristaltic pump utilized ¼" silicone tubing for circulation of reactants from the reservoir through the cell and back into the reservoir. A mechanical mixer was used to maintain a uniform concentration profile in the reactant reservoir. The semi-batch process schematic is shown as Figure 2.15.

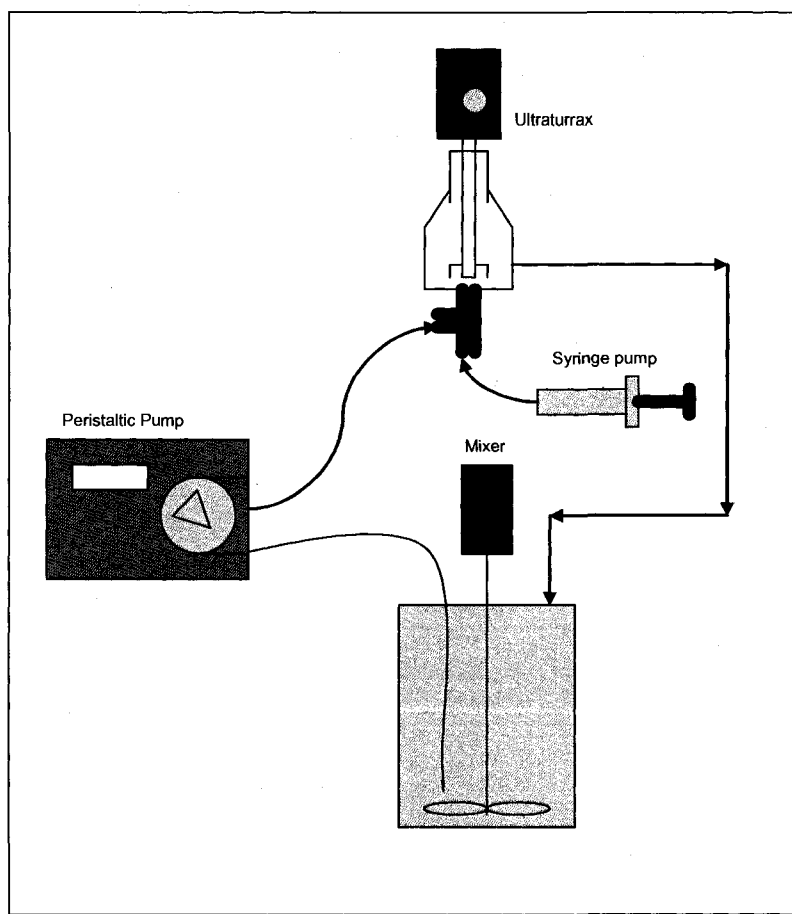


Figure 2.15 Process Schematic Semi-Batch Synthesis

This process had numerous difficulties during development, most of which stemmed from the reaction speed of both the ionic coupling and the encapsulation. The most common failure was a blockage of the needle tip. If the reactants were not ejected from the needle tip at sufficient rate, the reaction proceeded faster than the fluid flow rate and caused a blockage of the needle. Upon determining the appropriate reactant concentrations, flow rates and needle placement the system aspirated the reactants from the needle and syringe by the negative pressure differential generated in the center of the shear field.

The experimental process for synthesis of ISPs by the semi-batch process (ZZZONR040506) starts with the preparation of the three solutions. Solution A consisted of TEPA (15.00g), and mono n-dodecyl phosphate (1.48 g) dissolved in 250 mL of ACN. Solution A was placed in the reservoir and circulated by the peristaltic pump with the speed setting on 45 out of 99 on the pumps arbitrary scale which corresponds to a flow rate of 6.1 mL/s. The ice bath surrounding the reservoir was filled with ice and water. The Ultraturrax was started after the circulation of Solution A began. Solution B, consisting of phosphoric acid (11.65 g) dissolved in 100 mL ACN at 50 C, was injected by a syringe pump into the shear field of the continuous cell. After all of Solution B was injected, circulation was allowed to continue for 10 minutes and the ice in the bath was replenished. Next Solution C, consisting of TDI (10.35 g) dissolved in 40 mL ACN was injected into the continuous cell. After the injection of Solution C formed the shell material the flask was transferred to a rotary evaporator. The solvent was removed by

evaporation at low pressure (<10 mm Hg) and a temperature of 40C. This process, after many iterations and refinements, was successful in producing ISPs of varying size and functional ratios.

2.2.2.3 Summary of Core Shell ISP Experiments

The experimental data for the synthesis of particles described throughout this section are presented in a compact format as Table 2-8 for the batch process and Table 2-9 for the semi-batch process. The experimental designation, mass of reactants and a brief description is presented for each experiment.

Table 2-8: Experimental Details for Batch Process ISPs

Sample ID	Mass TEPA	Mass H3PO4	Mass Encapsulant	Encapsulant	Mass Stabilizer	Stabilizer	solvent (mL)	Solvent
ZZZONR061504	19.5	4.66	0	N/A	0	N/A	200	Heptane
No Particles formed, Separated into two phases								
ZZZONR061504C	19.5	4.66	0	N/A	0.1213	NP5	200	Heptane
No Particles formed, Separated into two phases								
ZZZONR061504	19.5	4.6	0	N/A	0.156	NP5	200	Chloroform
Since the synthesis failed in Heptane Solvent was switched to Chloroform. Un particized liquid but some particles.								
ZZZONR061804	15.75	4.66	0	N/A	0.102	NP5	200	Chloroform
Decreased the amounts of excess amine, no improvement shown								
ZZZONR062104	19.5	4.65	3.998	HDI	0.141	NP5	200	Chloroform
Addition of HDI as an encapsulant/shell material.								
ZZZONR062204	19.5	4.65	17.33	HDI	0.21	NP5	200	Chloroform
More HDI used. Large amount of solid/agglomeration								
ZZZONR062804C	15	4.659	XX	HDI	0.141	NP5	200	Chloroform
Reversed the addition, H3PO4 added first then TEPA dropped into solution. H3PO4 dispersed well. Failure on addition of TEPA.								
ZZZONR070104	19.5	4.659	4.14	TDI	0.14	Lauric Acid	260	Acetonitrile
Switch to Acetonitrile. Pre diluted monomers before addition. TDI replaced HDI as shell polymer. Resulted in particles (TEM Imaged)								

The functional ratio in Table 2-9 is the ratio of amine functionalities to reactive phosphate functionalities to the isocyanate (or epoxide) functionalities. This ratio can provide a sense as to how much phosphate is associated in the core particles which should be related to the ion sequestering capacity of the particles. The experimental variables of mass of amine, phosphoric acid, and

encapsulant that were varied can be more easily understood by this ratio than by the mass of monomers used.

Table 2-9: Experimental Details for Semi Batch Process ISPs

Sample ID	Mass TEPA	Mass H3PO4	Mass Encapsulant	Encapsulant	Mass Stabilizer	Stabilizer	solvent (mL)	Functional Ratio
ZZZONR071404	19.5	4.659	4.14	TDI	0.14	Lauric Acid	280	1:0.28:0.33
Failure. The reaction solidified blocking the outlet. Reaction mixture came shooting out of shaft.								
ZZZONR072004	19.5	4.659	4.14	TDI	0.14	MDP	280	1:0.28:0.33
Change to new stabilizer Mono n-Dodecyl Phosphate								
ZZZONR081004	15	4.66	4.14	TDI	0.143	MDP	280	1:0.36:0.33
Post Cure after rxn at 60C for 1 hr								
ZZZONR081904	19.5	4.66	4.14	TDI	0.141	MDP	280	1:0.28:0.33
Initially thought to be successful but particles did not produce dry particles								
ZZZONR082604	19.5	4.65	4.14	TDI	0.141	Lauric Acid	350	1:0.28:0.33
Worked well! First success. Increase in dilution of H3PO4 in ACN helped								
ZZZONR090704	15	9.06	3.45	TDI	0.138	Lauric Acid	340	1:0.7:0.1
Change of ratios. Not leaving 30% excess amine for reaction with epoxy coating anymore								
ZZZONR091504	15	7.76	10.35	TDI	0.166	Lauric Acid		1:0.6:0.3
ZZZONR092404	15	11.65	10.35	TDI	1.479	Lauric Acid	380	1:0.6:0.3
This is when H3PO4 was switched to Difunctional based on titration and PKA data. First successful fine particles produced								
ZZZONR101104	15	11.65	10.35	TDI	1.479	Lauric Acid	380	1:0.6:0.3
This was a repeat of ZZZONR092404 but with the shear field increased. Previous work was done with UT on 3. This was done at a speed of 6								
ZZZONR102704	15	11.65	20.23	DGEBA	1.899	MDP	530	1:0.6:0.3
Changes were heating of soln A to 28 so there was no chance of H3PO4 crystallizing when hitting colder solvent. Cancelled in process								
ZZZONR102804	15	13.59	18.88	DGEBA	1.899	MDP	530	1:0.7:0.2
UT on 3, after addition of DGEBA 2 hr post cure at 70C. Particles dried								
ZZZONR111604	15	13.588	9.441	DGEBA	1.52	MDP	NR	1:0.7:0.1
After seeing SEM of particles cut the DGEBA by half. 60C 3hr post cure after addition of DGEBA UT:3								
ZZZONR10705	15	11.65	10.35	TDI	1.48	Lauric Acid	380	1:0.6:0.3
UT: 6 this is to make more particles and try reproducibility, same as ZZZONR101104 these particles selected as best based on dry flowability, 1st SISC M								
ZZZONR011105	15	11.65	10.35	TDI	1.46	Lauric Acid	380	1:0.6:0.3
UT: 6 T=30C second repeat of ZZZONR101104								
ZZZONR040506	15	11.65	10.35	TDI	1.48	MDP	400	1:0.6:0.3
This was a redo of previous synthesis to make more particles, UT:6, T=30C, total solid content 6.29%								
ZZZONR040506	15	11.65	10	HDI	1.466	MDP	400	1:0.6:0.3
It was thought that switching back to HDI, a less reactive isocyanate, would allow better particle coverage before polymerization								
ZZZONR051006	15	11.65	13.99	HDI	0.812	MDP	450	1:0.6:0.42
Changing the encapsulant ratio to have more shell material. This was difficult. Reactor solidified as did reactant reservoir.								
ZZZONR051606	15	11.65	13.99	HDI	0.812	Lauric Acid	450	1:0.6:0.42
The reactor outlet plugged. Wet rotary seal went on UT dispersing element. New element ordered								
ZZZONR052406	1.5	1.208	1.456	HDI	0.337	Lauric Acid	450	1:0.6:0.45
Attempt to dilute by 10% to make particles without plugging system								

2.2.3 Solid Ion Sequestration Core Material Encapsulation

Learning from the previous synthesis approaches, it was decided to encapsulate the solid ion sequestration core material (SISC M) particles made during the approach that tried to develop the ideal “core shell” synthesis

investigated at the very beginning of this work. A technique similar to that used for the WISCM encapsulation was used to protect the ISPs described in section 0 by encapsulating them in a shell of PMMA. The early semi-batch synthesis ISPs easily dried to a free flowing powder. However they were not successful resulting in a gelation or solidification when added to the uncured components of the MIL-DTL-24441 coating. This was likely due to rapid reaction and ion exchange between these particles and the components of the coating which created an instant gel/sol upon mixing. Encapsulation by a PMMA shell proved itself in the protection of the WISCM capsules so it followed that it should protect the solid core against harmful ionic and covalent interactions with the coating as well.

Previously produced ISPs were redispersed via sonification and mechanical agitation into heptane (ZZZONR070607). The particles were mechanically redispersed successfully in heptane without the addition of any stabilizer or surfactant. This mixture was placed in a RBF and encapsulated by a process similar to the WISCM encapsulation (ZZZONR070907).

The WISCM encapsulation scheme was modified. Since the PEI had been eliminated we could increase the reaction temperature to 55C and a different initiator, V-65 (WAKO Chemical Co.) was used at this higher temperature. V-65 (Figure 2-16) is an oil soluble low temperature azo-initiator with a 10 hr half life thermal decomposition temperature of 51C. Calculations were done to determine what quantity was needed to produce molecular weights of PMMA in the range of 125,000 g/mol. This synthetic approach finally was able

to reproducibly yield larger quantities of ISPs capable of being incorporated into test coupons for anticorrosion performance evaluation.

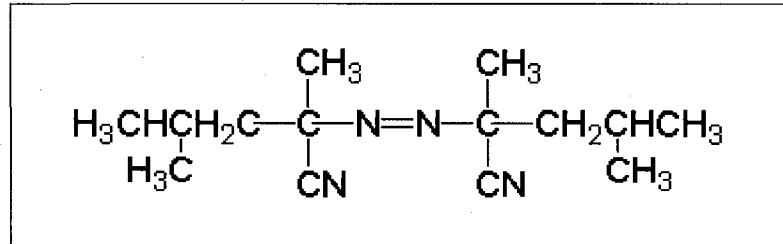


Figure 2-16: Wako Chemical V-65 Azo-Initiator

2.2.3.1 Experimental Procedure

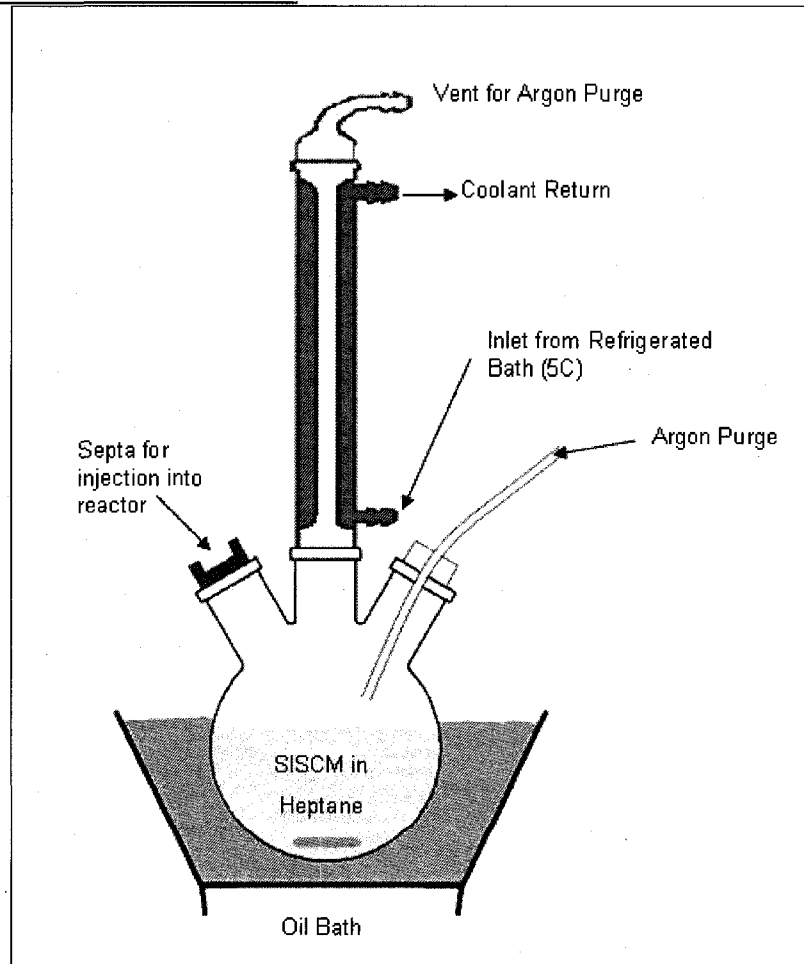


Figure 2.17: Experimental Apparatus for Encapsulation of SISCM

The first SISCM encapsulation utilized previously synthesized dry ISPs particles (ZZZONR070908). The SISCM (2.9017 g of ZZZONR010705 compositional details shown in Table 2-10) were transferred into a three neck RBF containing 100 mL of heptane and a magnetic stir bar. The flask was then gently shaken to provide an initial suspension before being placed in a sonic bath for 20 minutes. This resulted in a uniform re-dispersion of the particles in the heptane. The three neck RBF was then removed from the sonic bath dried of any water.

Table 2-10: Components used in ZZZONR010705

	Mass	Function Ratio
TEPA	15.0	1.0
IPDI	1.0	0.6
TDI	10.4	0.3

It was then placed into an oil bath on a heating/stirring plate. The magnetic stirring was set to 300 rpm, and the temperature to 50 C. A condenser with recirculating coolant at 4 C was placed on the center neck to prevent evaporation of the heptane during the polymerization. The liquid containing the dispersed particles was then purged by a slow steady stream of argon bubbles for 30 minutes through a line and adapter placed over one of the side necks.

The monomer MMA (1.0 g) was injected through the septa covering the third neck on the flask. This was done shortly after the argon purge began so that any oxygen dissolved into the monomer was also purged. The initiator, V70 in early work (0.010g) and V65 later was first dissolved in 2 mL of HPLC grade acetone that had been previously purged with argon, and then diluted with an additional 8 mL of argon purged heptane.

Prior to addition of the initiator, the argon feed was removed from the liquid but left in the reactor providing a continuous blanket of argon to occlude oxygen. The initiator solution was added via syringe through the septa covering the third reactor neck dropwise over 30 minutes. The reaction proceeded for 6 hrs, at which time the temperature controls were turned off and the reactor allowed to cool to room temperature. Magnetic stirring and the condenser were continued until the suspension was transferred to the drying phase.

The encapsulated ISPs were dried on a rotary evaporator. The reaction solution was transferred into a single neck round bottom flask. It was then connected to the rotary evaporator and subjected to a reduced atmosphere of ~ 100 mm Hg at 30C. After the bulk of the heptane was removed the pressure was further reduced to the limit of the vacuum pump and allowed to dry for another one to two hours. The powder indicated that it was sufficiently dry when tapping of the glass resulted in a cloud of light particles floating up from the bulk. This occurred after a period where there was caking and balling of the powder inside of the flask.

2.2.3.2 Variations in Solid Ion Sequestering Core Materials

The Solid Ion Sequestration Core Material(SISCM) had previously been made with TEPA as one of the two ionically associated chemicals that make up the ion sequestering core. By changing this component to a longer chain polyamine it was thought to be possible to further stabilize the core of the particle. The goal of this was to investigate the development of a better SISCM

possibly one that eliminated the need for the protective encapsulation of the SISCM with PMMA.

Table 2-11: PEI SISCM Compositions

	Mass	Function Ratio
PEI A Mn=423	15.0	1
H ₃ PO ₄	6.0	0.6
TDI	5.3	0.3

PEI was purchased with molecular weights ranging from 423 g/mol to 9000g/mol. These PEI were then investigated as a substitute for the TEPA in the original formulation for the SISCM. SISCM (compositional details shown in Table 2-11) was only successfully produced with the 423g/mol PEI, approximately twice the chain length of TEPA (DETONR050). The larger molecular weight PEIs were insoluble in acetonitrile and thus incompatible with the refined synthesis of SISCM particles. The SISCM particles made from the PEI were not capable of being mixed with amine components of a coating system without encapsulation.

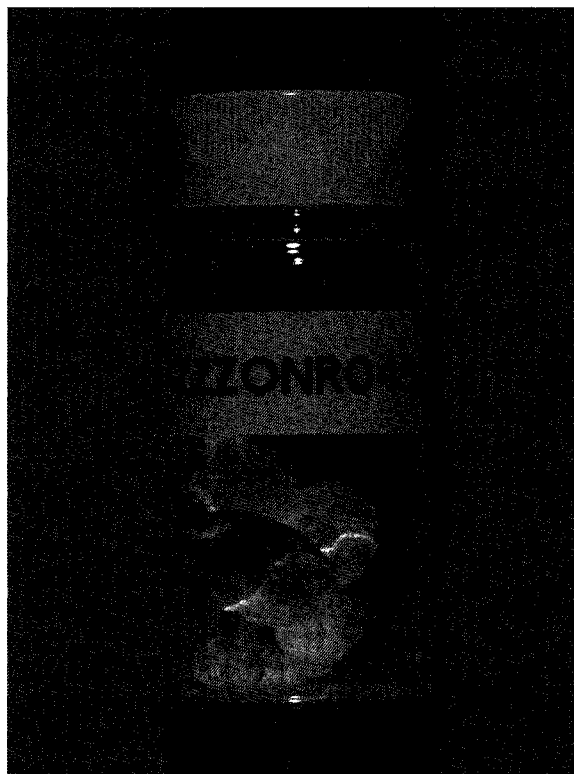


Figure 2.18: Pebble like agglomerations of 90% phosphate SISCM

The ratio of phosphate in the core particles is primarily responsible for the anticorrosion properties. A greater percentage of phosphate in the core particles should result in better protection properties of the ISPs. To this end the SISCM core ratios were changed from 60% of amines coupled to phosphate up to 90%. The 80% particles (ZZZONR030508) were successfully dried and encapsulated. SISCM (ZZZONR043008) with 90% of the amine functionalities associated with phosphate formed large hard pebble like agglomerates upon drying as can be see in Figure 2.18. This is a result of the core not being stabilized enough by the isocyanate structure and ionic exchange and interaction between the individual particles. It was impossible to redisperse the particles without mechanical crushing or grinding and so they were not encapsulated or tested in a coating.

Solid content during SISCAM synthesis was typically 10%. Experiments doubling (ZZZONR042308) and halving (ZZZONR042408) the solid concentration were performed successfully. At 20% solids there was some agglomeration and the mixing in the reactant reservoir was limited by the thixotropic nature of the solution. At 5% solid concentration the synthesis proceeded smoothly. This seemed to produce a finer suspension of particles with less strain, as detected audibly, on the Ultraturrax. In addition to this there was some small difference in the size of particles produced by the two methods as will be discussed in Chapter 3.

2.2.3.3 Summary of SISCAM Encapsulation Experiments

The SISCAM synthesis has produced ISPs in sufficient quantities for adequate testing of anticorrosion properties. The resultant PMMA encapsulated SISCAM particles mixed into anticorrosion coatings successfully. They have been subject to a set of preliminary accelerated aging experiments to determine their enhanced corrosion protection properties as discussed in Chapter 4 Anticorrosion Properties.

New SISCAM particles were synthesized in attempts to control the ratio of phosphate in the core and the effects due to changing the solids content of the process. The experimental data for these SISCAM particles are presented in compact form as Table 2-12.

Table 2-12: Experimental Data for SISCM Core Particle

Sample ID	Mass TEPA	Mass H3PO4	Mass TDI	Mass Stabilizer	Stabilizer	solvent (mL)	Functional Ratio
DETONR043	15	11.65	10.35	1.48	MDP	340	1:0.6:0.3
Failed. The dispersing Elements carbide seal shattered leaving it useless. New one ordered							
DETONR049	15.011 *	6.012	5.687	0.51	Lauric Acid	320	1:0.6:0.3
* This was SISCM with (PEI Mn=423) instead of TEPA. Lauric acid left out. Stirring of reactant reservoir not started							
DETONR050	15.1430 *	6.0076	5.36	0.503	Lauric Acid	320	1:0.6:0.3
redo of DETONR049 with stirring and Lauric acid							
ZZZONR030508	15	15.529	6.9	0.748	Lauric Acid	320	1:0.8:0.2
SISCM with higher ratio of PO4							
ZZZONR031208	15	17.47	6.9	0.78	Lauric Acid	320	1:0.9:0.2
This exp Failed. Tool was ruined. Once again can't produce with more TDI then a 1:1 total ratio of amine: reactants							
ZZZONR042308	15	15.529	6.9	0.748	Lauric Acid	158	1:0.8:0.2
Less solvent, 20% solids, may control primary particle size. Difficult and final solution was thixotropic slurry							
ZZZONR042408B	7	7.25	3.22	0.35	Lauric Acid	320	1:0.8:0.2
5% solids, made a big difference in the ease of synthesis and pumping of solution. Future work should be at 5%							
ZZZONR043008	15	17.47	3.45	0.72	Lauric Acid	700	1:0.9:0.1
5% solids for ionic association, attempt to increase phosphate levels. During drying made small "rocks" ~1cm in diameter							

Experimental details for the SISCM encapsulation experiments are presented in tabular form as Table 2-13.

Table 2-13: Experimental Data for SISCM Encapsulation

Experimental ID	SISCM ID	SISCM Mass (g)	Solvent (mL)	EGDMA (g)	MMA (g)	Temp. (C)
ZZZONR070907	ZZZONR010705	2.9017	100	0	1	50
V70 initiator, first attempt. Mixed with amine component of Mil P coating. DSC shows no Tg of PMMA.						
DETONR045	ZZZONR011105	4.9581	100	0	1.0637	50
particles dried. Scraped during drying when cake formed. Produced fine white powder						
DETONR046	ZZZONR011105	5.008	100	0.04	1.5098	50
0.12g MDP, addition of EGDMA as a crosslinker to particles.						
DETONR047	ZZZONR011105	5.017	100	0.161	1.5119	50
0.12g MDP, 10% EGDMA as a crosslinker to particles.						
DETONR048	ZZZONR011105	5.003	100	0.0759	0.7628	50
0.12g MDP, less total shell material						
DETONR052	ZZZONR011105	5.004	100	0.0316	1.4971	50
syringe needle broke and was replaced with larger diameter needle						
ZZZONR121407	N/A	0	100	0	1.0637	50
this was to generate a sense of Mw profile with the MMA/V70 initiator system						
ZZZONR012208	N/A	0	100	0	1.292	51
test of V65 initiator same as ZZZONR121407. refrigerated bath froze solid and condenser failed. All solvent and monomer lost						
ZZZONR012208	N/A	0	100	0	1.292	51
Redo with condenser at 10C instead of 5C to prevent freezing						
ZZZONR022908	N/A	0	100	0	10.132	50
Making PMMA with new MMA monomer bought to replace they very old MMA used previously. Chasing low Mw. Should be ~125K						
ZZZONR040808	ZZZONR030508	37	400	0	7.447	50
V65 initiator, successful						
ZZZONR042408	ZZZONR042308	37	500	0	7.5	50
V65 used dried to fine powder						
ZZZONR042508	ZZZONR042408B	17.5	300	0	3.75	50
V65, successful. Dried and put into corrosion testing						

2.3 Summary of ISP Synthesis

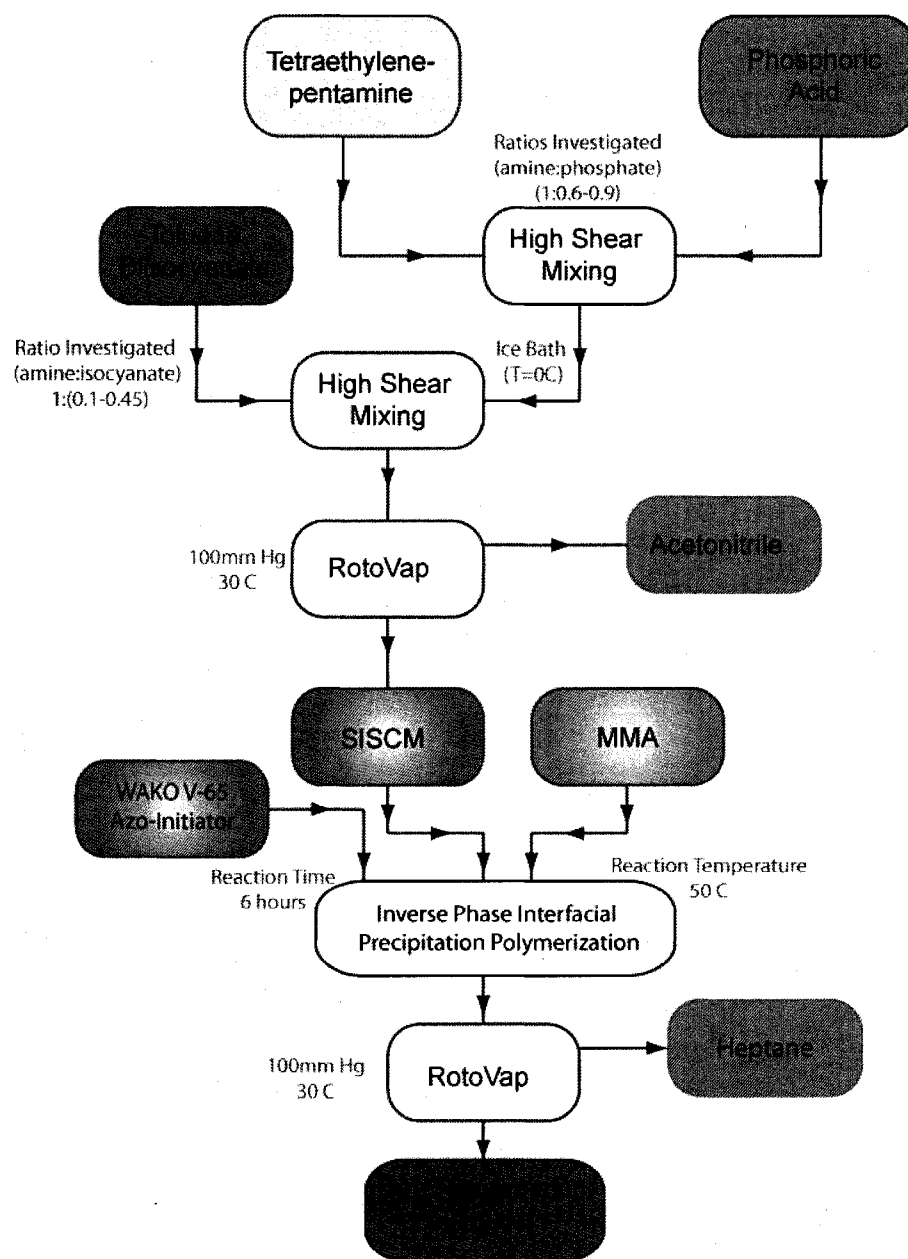


Figure 2.19: Final ISP Synthesis Scheme

The evolution of the ISP synthesis finally lead to the development of the process for the successful production of viable ISPs as outlined in **Error! Reference source not found..** Some of this evolutionary process of synthesis

development was not discussed here as it was not incorporated into the final synthesis process (see APPENDIX 1 and APPENDIX 2). The ISPs synthesized by this final scheme are free flowing particles that can be incorporated into anticorrosion coatings and then evaluated for their corrosion inhibiting properties.

The synthesis process developed has the potential to be scaled up, utilizes low cost readily available raw materials, and has few difficult steps now that a viable process has been discovered. The future of the process would likely involve the transfer of the SISCM particle production from semi batch to a true continuous process. This was attempted briefly as part of this work but it was rapidly apparent that changing the process to a continuous set up would involve a complex engineering solution as well as unavailable process control equipment.

CHAPTER 3

CHARACTERIZATION

This chapter contains details on characterization experiments that were instrumental in the successful completion of this work. The characterization is broken up into two sections. The first of which contains information on the individual components and their interactions. The second section contains characterization details for the ISPs synthesized. Additional supplemental characterization experiments, both successful and unsuccessful are presented in Appendix 3.

3.1 Characterization of Monomers and Surfactants

This section will discuss experiments performed to characterize and better understand the interaction between components used in this work. Without understanding of these basic interactions and reactions between chemical constituents, the synthesis development would never have succeeded. A brief description of the experimental procedure, justification of the needs, and the results is presented in each case.

3.1.1 Reaction Kinetics of DGEBA TEPA

During the initial encapsulation attempts DGEBA was investigated as a reactant. Several semi-batch syntheses were attempted with DGEBA replacing TDI as the original shell material. During these experiments (ZZZONR2704) there was an agglomeration and reaction between particles resulting in a single solid mass. This was thought to be due to the reaction rate between the epoxy moiety and the remaining amines of TEPA being much slower than the reaction between the isocyanate and TEPA. To determine if this was the case the DSC was utilized as a micro-calorimeter to determine the reaction between DGEBA and TEPA.

Two experiments (ZZZONR101104A&B) utilized the DSC in isothermal mode at 30C and 60C. At room temperature, TEPA(1.07g) was mixed stoichiometricly with DGEBA (6.75g) in a 20 mL scintillation vial by hand with a spatula. A DSC pan was then filled with 20 to 40 mg of the mixture, sealed, and placed in the DSC. The DSC was operated in isothermal mode at 30C for 24 hours. This resulted in the data shown as **Error! Reference source not found.** and shows that the cure time for DGEBA with TEPA takes greater than 11 hours at 30C. The clipping of the curve at the beginning of this experiment is due to a lack of data for the time required to mix the two components, prepare the pan and load the pan in the DSC.

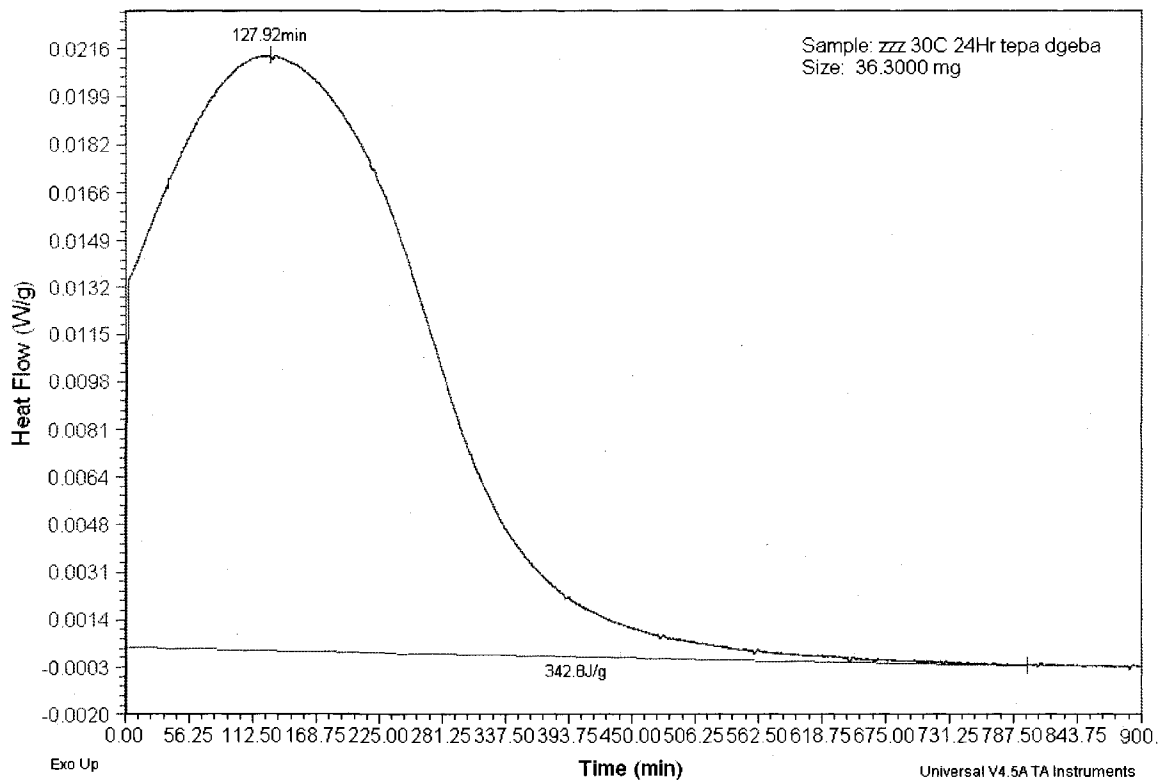


Figure 3.1 Isothermal Heat Flow of DGEBA + TEPA at 30C

The reaction time of 11 hours at 30C was too long. This could be decreased by increasing the temperature. The DSC experiment was repeated but this time with the isothermal temperature set at 60C. The results are shown as Figure 3.1. Once again there is the initial loss of data due to the sample preparation, but as the total enthalpy of the reaction was not of chief interest from these experiments it is unimportant. The 60C experiment showed a full cure of the epoxy was reached by 120 minutes. This data was used to alter the ISP synthesis by adding a two hour post cure at 60C for future DGEBA stabilized ISPs (ZZZONR102804).

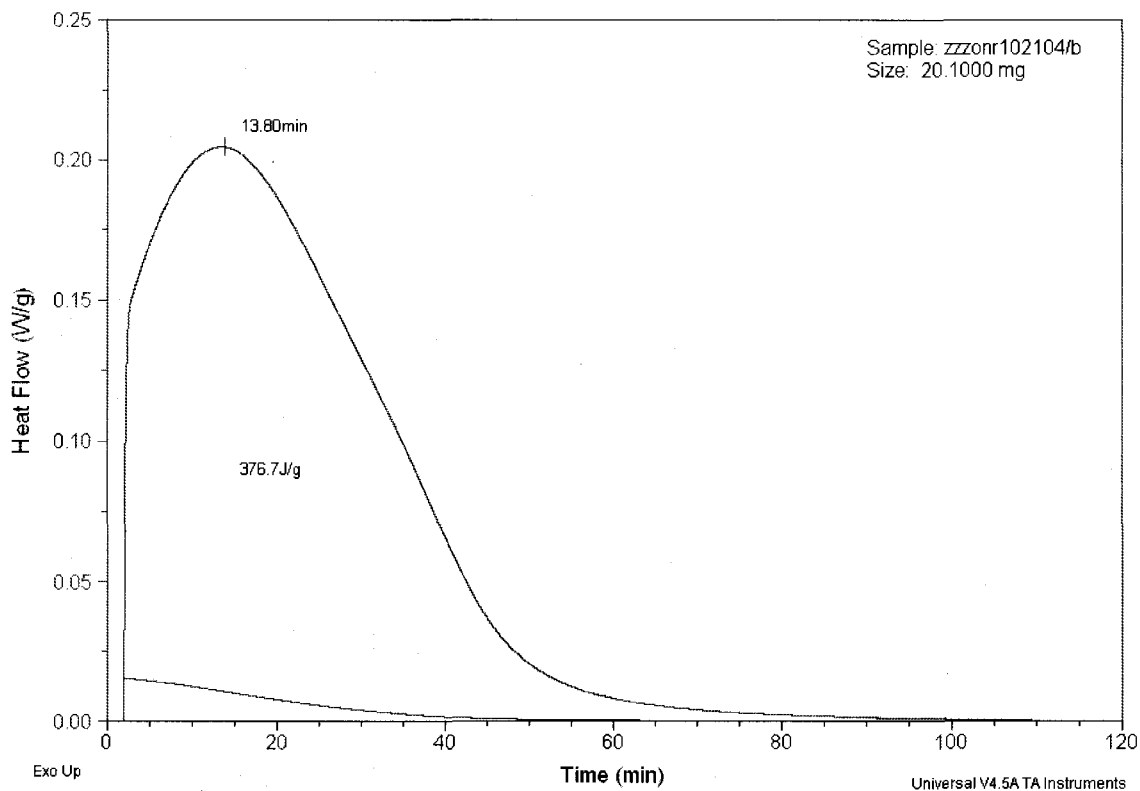


Figure 3.2: Isothermal Heat Flow of DGEBA + TEPA at 60C

3.1.2 Characterization of PMMA Produced by SISCM Encapsulation

The polymer characterization of molecular weight was done by gel permeation chromatography (GPC) in THF. The polymer encapsulant was extracted from the ISPs post encapsulation by dissolution in THF. The THF ISP mixture was subjected to an hour in the sonifier bath which aided in dissolving the PMMA from the particles. The samples were then centrifuged to settle out the insoluble core material. The supernatant, removed by syringe, was concentrated by evaporation prior to injection into the GPC. The GPC molecular weight results are based on a calibration curve generated with polystyrene standards. A representative GPC trace is presented as Figure 3.3.

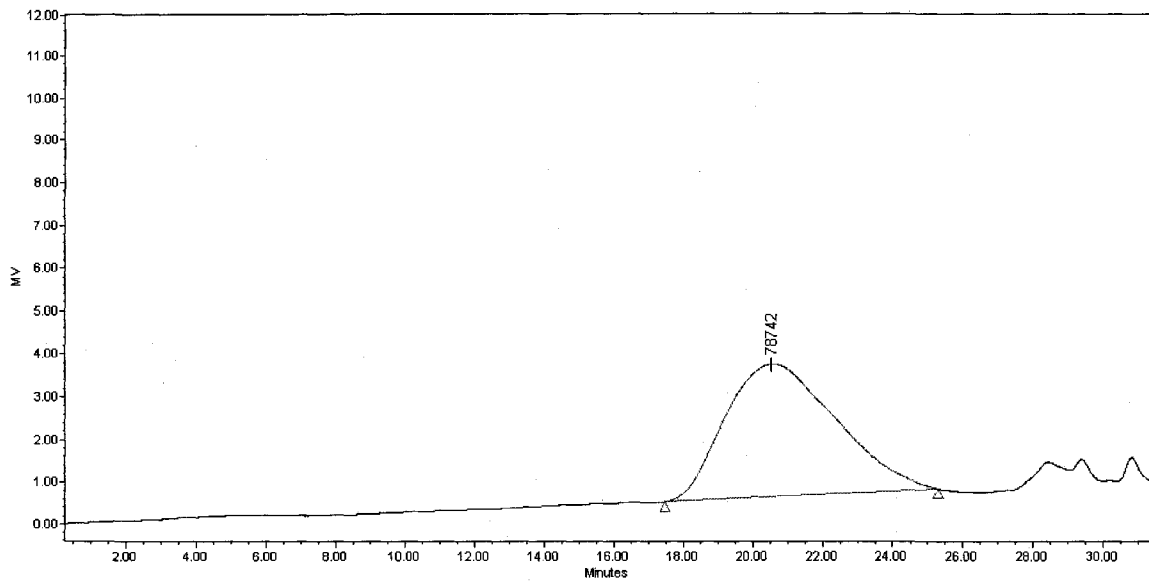


Figure 3.3: GPC Results for ZZZONR040808

Successful encapsulation with varying shell ratio and shell composition was been performed on SISCM synthesized ISPs. The resulting extractions of the encapsulating shell are summarized in Table 3-1. DETONR45, DETONR46, and ZZZONR070907, have varying shells as denoted by the weight percent of encapsulant 17.66%, 23.02% and 25.63%. DETONR47 and DETONR48 have an additional monomer Ethylene Glycol Dimethacrylate (EGDMA) which cross linked the encapsulant polymer and made it resistant to dissolution in solvent. Assuming a uniform coating of the particles, the weight percentage of the outer shell material is directly related to the thickness of the shell.

Table 3-1: SISCM Encapsulation Experiments

Sample ID	SISCM ID	Wt % encapsulant	Mn	Mw	PDI
DETONR45	ZZZONR011105	17.66%	5638	7467	1.32
DETONR46	ZZZONR011105	23.0%	17229	35504	2.06
DETONR47	ZZZONR011105	22.7%	xlinked		
DETONR48	ZZZONR011105	13.1%	xlinked		
ZZZONR070907	ZZZONR010705	25.6%	9210	10349	1.12
ZZZONR042508	ZZZONR042408B	17.6%	35063	61005	1.74
ZZZONR040808	ZZZONR030508	16.8%	42119	86060	2.04
ZZZONR042408	ZZZONR042308	16.9%	30087	58308	1.94

The molecular weights determined by GPC show very low, almost oligomeric, PMMA for the DETONR samples as well as ZZZONR070907. These weights are below the entanglement length of ~20,000 g/mol for PMMA¹³³ resulting in a shell wall with little to no mechanical strength. These resulted in a revision to the process with the change to V-65 as an initiator for ZZZONR040808, ZZZONR042408, and ZZZONR042508 which yielded slightly higher molecular weight PMMA. While the cause of the lower than expected molecular weight of the polymers was not determined specifically, the SISCM is speculated to have some inhibition or possibly radical scavenging effect resulting in the seen molecular weights.

3.1.3 Experimental Determination of PEI Amine Ratio

Commercial PEI is a branched polymer, structure shown as Figure 3.4 and can even contain macrocycles. It is synthesized by the ring opening of ethyleneimine. Literature has reported amine ratios for commercial PEI to be approximated by 25% primary, 50% secondary, and 25% tertiary amines^{134,135,136}. However this is a generalization and amine ratio of PEI can

vary from manufacturer and even from batch to batch. Since the best corrosion protection would be provided by the highest phosphate amount in an ISPs ion sequestering core, it was decided to determine exactly the ratio of amines. More importantly to calculate exactly how much of the PEI could be coupled to phosphate.

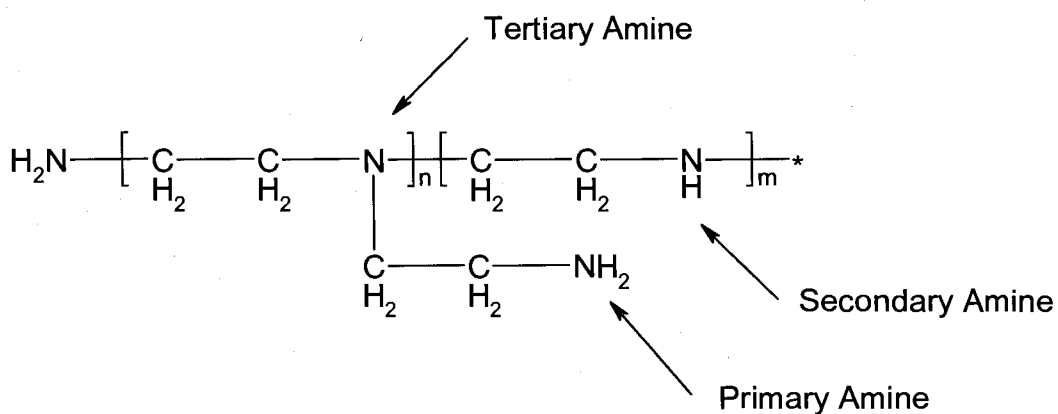


Figure 3.4: Structure of Polyethylenimine

This amine ratio was experimentally determined (ZZZONR080806) by titration with a phosphoric acid solution while measuring the pH of the solution as a function of volume of a phosphoric acid solution added. The plot of the titration curve allowed us to determine the ratio of primary and secondary amines in the PEI from the inflection points of slope change. The change in the slope indicates that the primary and secondary amines have been fully associated.

3.097 g of a 50 wt % PEI (Mn 60,000 g/mol) water solution was added to 100.0 g of high purity water in a 250 mL glass beaker. The beaker was placed on a magnetic stir plate to provide agitation via a 25mm magnetic stir bar. A valved

100mL syringe with the piston removed was filled with a solution containing 6.0947 g of phosphoric acid (99.9% crystalline) in 100.1 g of purified water. This syringe was affixed with an 18 ga needle and suspended above the 250 mL beaker containing the PEI solution. The syringe and needle droplets were previously calibrated to have a drop volume of 0.0357 mL for this solution. Data was recorded by an optical drop counter and pH probe via a laptop and Vernier interface. The system recorded total volume of phosphoric acid solution added and pH of the solution at each drop.

$$X \text{ (g H}_3\text{PO}_4\text{/g PEI)} = V_{\text{drop}}^T [\text{C}_{\text{H}_3\text{PO}_4}] / m_{\text{PEI}} \quad [\text{EQ 3-1}]$$

The data was converted into g of phosphoric acid per gram of PEI by EQ 3-1, where V_{drop}^T is the total volume added dropwise, $[\text{C}_{\text{H}_3\text{PO}_4}]$ is the concentration of the phosphate solution and m_{PEI} is the mass of PEI being titrated. This was plotted against the pH as shown in Figure 3.5. The slope change represents the complete titration of the primary, secondary, and finally tertiary amine. Linear regressions were fit to the regions preceding and following the two primary slope changes and the intercept calculated. This resulted in the primary amines being fully associated at 0.47 (g of H_3PO_4)/(g of PEI) and the secondary amines associated at 1.475 (g of H_3PO_4)/(g of PEI). This translates to a mole ratio of 20.7% primary amine, 64.9% secondary amine and 14.4% tertiary amine for the PEI.

While maximizing the phosphate loading of the core particles was the motivation for determining the amount of phosphate that could be coupled to PEI, the completely coupled PEI has a pH of 2.81. It is known that in the acid region, $\text{pH} < 4$ steel corrosion increases rapidly from dissolution of oxide films. It was thought that having the core particles loaded to this level could increase corrosion rate of the steel rather than inhibit it. For this work a value of 0.6 g phosphate per gram of the PEI was selected as this would ensure the particles would remain slightly basic at a pH of 7.4.

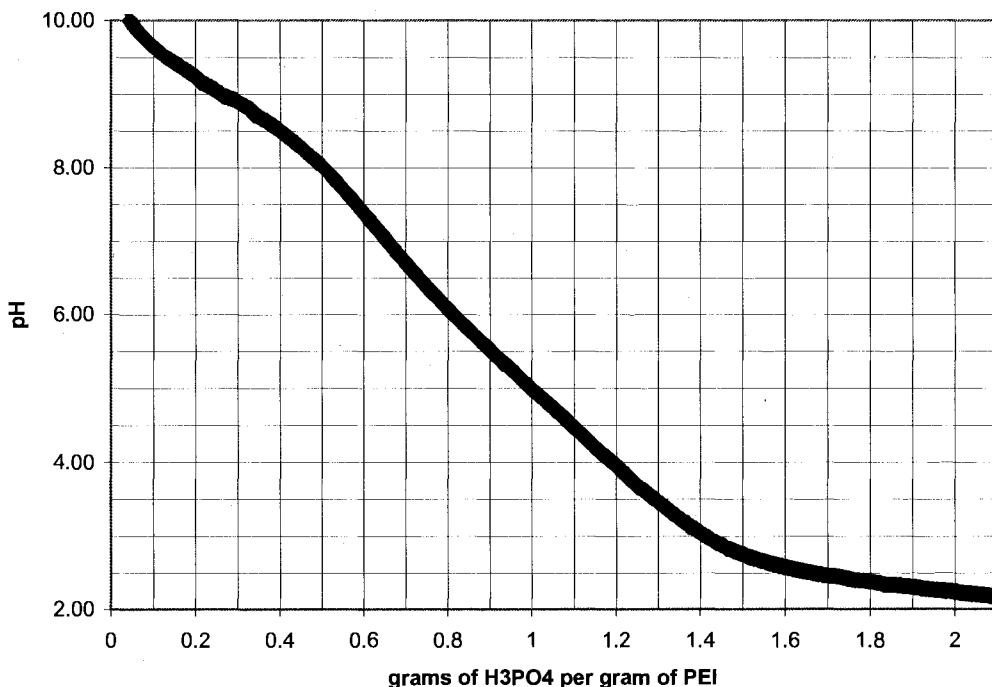


Figure 3.5: Titration of PEI by Phosphoric Acid

3.2 Characterization of ISPs

Characterization of ISPs helped to understand the effects of synthesis changes on the particles. SEM, TEM, light scattering, optical microscopy and sequestering capacity by titration all have been used to characterize the ISPs

synthesized throughout this work. This section will discuss the results of characterization techniques as they pertain to the particles themselves.

3.2.1 Particle Morphology

Scanning electron microscopy was used to understand particle size and morphology throughout this work. Visual light microscopy typically failed to provide sufficient resolution for characterization of ISPs due to their size which ranged from nanometers to hundreds of microns depending on the synthesis parameters.

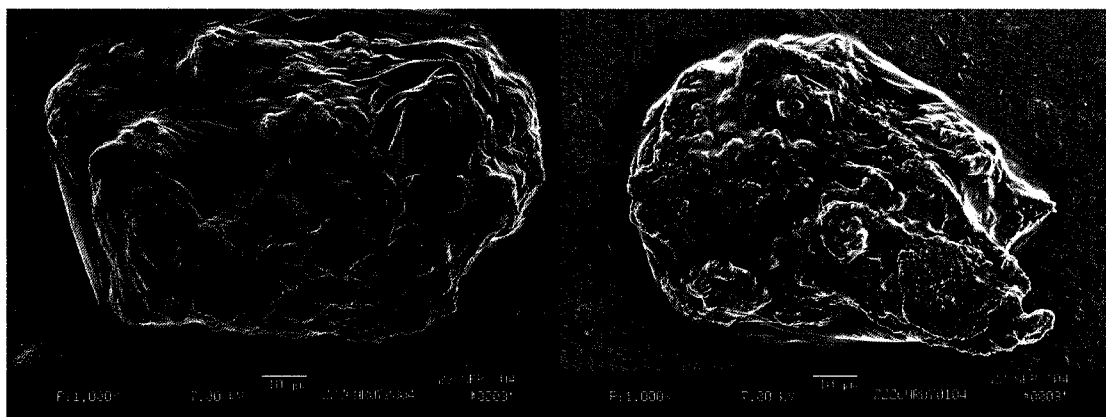


Figure 3.6: SEM of ZZZONR070108, first successful ISPs

The goal of the original synthesis design was to produce particles of a core shell morphology (see 2.2.1). The actual particles produced were not of a uniform concentric core shell morphology as can be seen in the SEM images of two early batch synthesized particles (Figure 3.6). There was a TDI polyurea layer draped over many of the smaller core particles. Instead of a core shell structure as planned, an occluded morphology was synthesized consisting of

many small domains of ion sequestering core particles encapsulated in a polyurea/polyisocyanurate phase as depicted schematically in Figure 3.7.

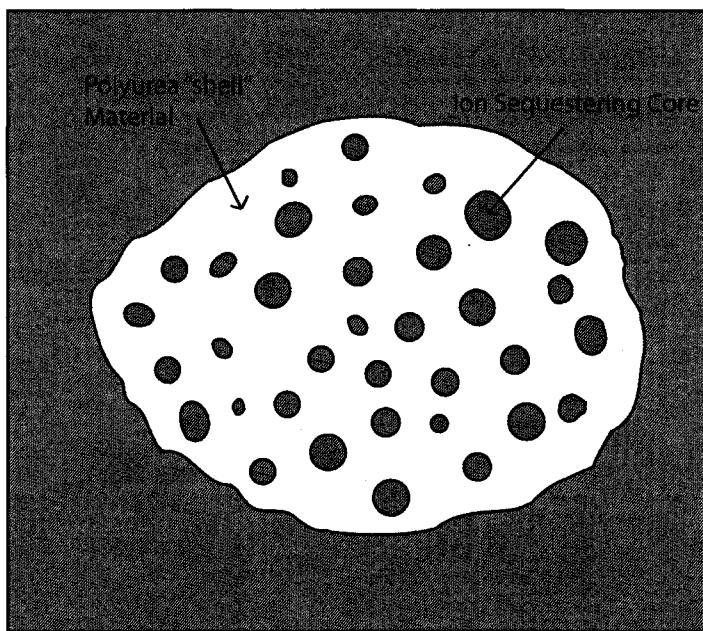


Figure 3.7: Cross Section Schematic of Occluded Morphology of ISPs

Figure 3.8 shows an SEM image of a successful semi-batch synthesized ISP (ZZZONR091504). This ISP was made by encapsulating the ion sequestration core with TDI to form a polyurea shell. The image shows improved encapsulation when compared with the SEM images of the batch synthesized ISPs. The particle is about 1 μ m by 2 μ m in size. This result was typical when comparing the batch and semi-batch process and these images were used in the decision to move forward with the semi-batch development.

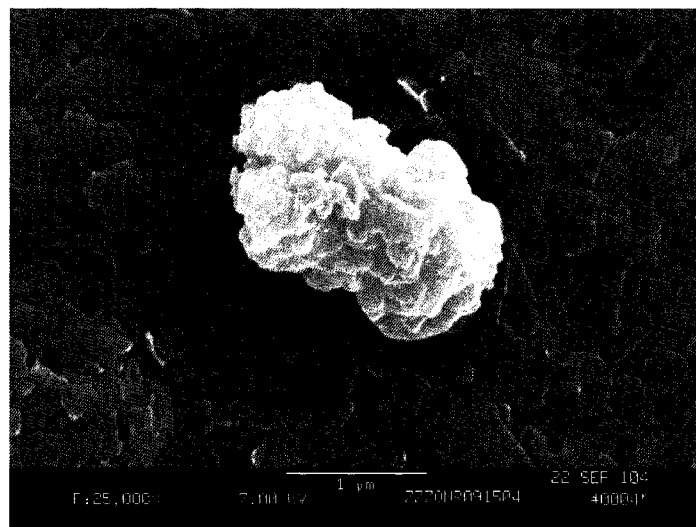


Figure 3.8: SEM image of a Semi-Batch Synthesized ISP

Many of the synthesis experiments resulted in failure to adequately encapsulate the core particles. The result of one such unsuccessful semi-batch ISP synthesis is shown in Figure 3.9. The image shows many small (~100 nm) primary particles adhering to a string of polyurea as opposed to being encapsulated by it. This effect was believed to be caused by the reaction rate of the polycondensation of TDI with TEPA being faster than the transport of the TDI to the interface with the core particle in the shear field generated by the continuous cell.

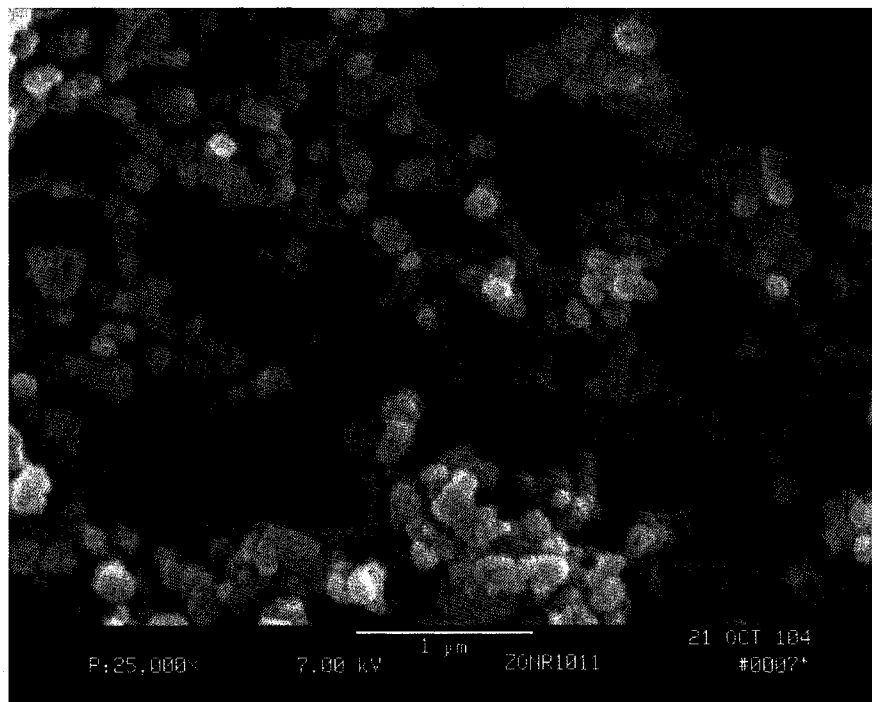


Figure 3.9: SEM micrograph of 50,000x magnification of a polyurea encapsulation experiment

The SEM images provide data on the effect of process changes on the particle morphology. This allowed for the eventual evolution of the semi batch synthesis that was used to produce SISCM for encapsulation in PMMA. It was not possible to adequately protect the ion sequestering material with just the TDI reaction alone.

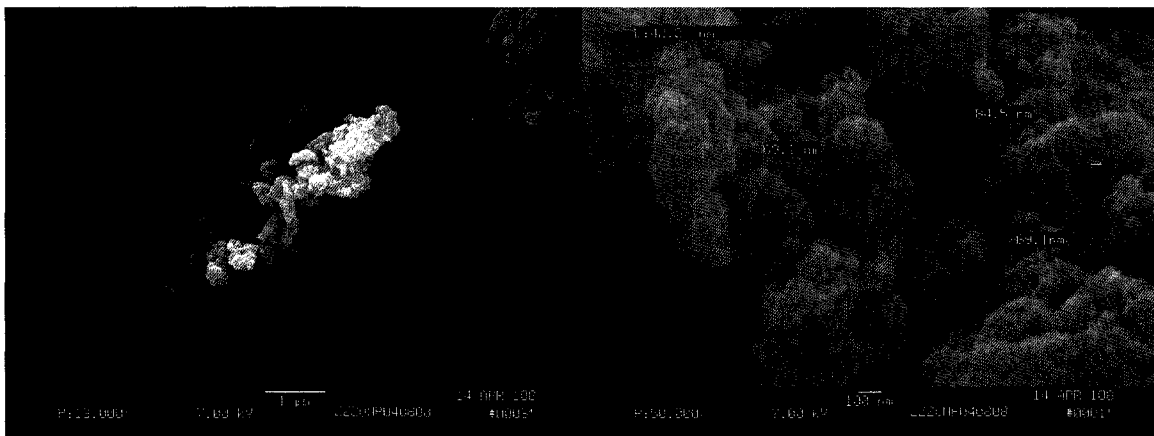


Figure 3.10: SISCM ISP @13,000x and 50,000x

Particles produced by the SISCM synthesis are shown as Figure 3.10 and Figure 3.11. Figure 3.10 shows a discrete particle in the left image and a more magnified view of the particle in the right. The particle consists of many smaller 60-80 nm primary particles stuck together. These primary particles are formed from the ionic association of the amine and phosphoric acid in the first step of the SISCM synthesis. They are then bound together and stabilized but not fully encapsulated by the polyurea formed by the addition of TDI. The final encapsulation with PMMA protects the primary particles from harmful interactions with anticorrosion coating monomers. Figure 3.11 shows a better quality SEM image of the agglomeration of smaller particles typical of the SISCM ISPs.

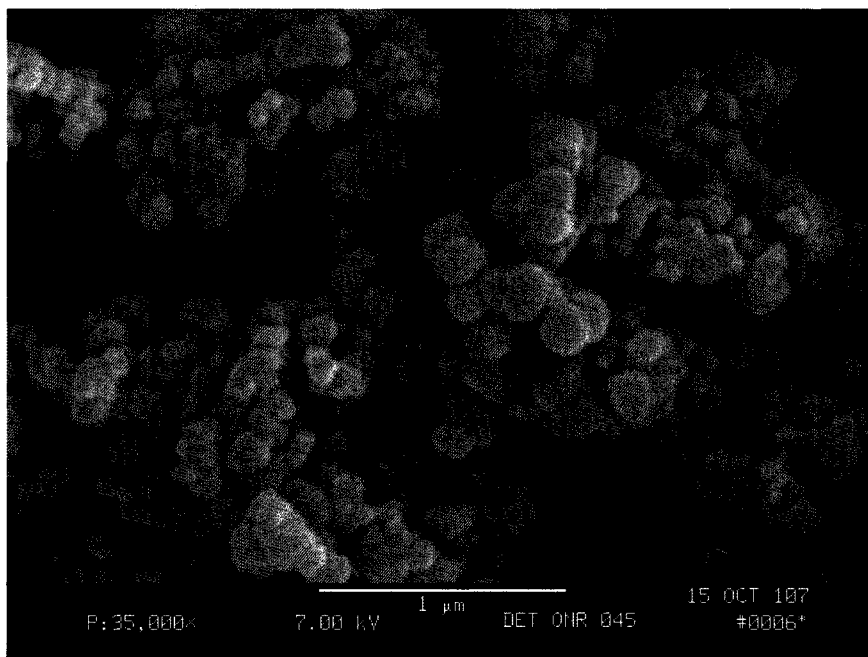


Figure 3.11: SEM of SISCM Synthesized ISPs

One final note on SEM images of ISPs. The particles contain a significant percentage of phosphorus. It was difficult to view particles at high magnification because of a charge build up from the electron beam on the particles which caused them to melt and defocus. The suggested solution to this problem is to use a very heavy gold palladium coating as opposed to the more typical thinner coatings used for SEM.

In an effort to further understand the morphology of the ISP samples were prepared for TEM imaging. Preparation by drying a dilute solution on a carbon film covered copper TEM grid did not allow us to see any detail of the particles. Imaging was tried without staining as well as with ruthenium tetroxide stain. As this did not work, the particles were embedded in an epoxy and cast into a small cylindrical beam capsule for microtoming. These samples were then subjected to negative staining by immersion in a 1% osmium tetroxide solution for 20

minutes. This produced the images in Figure 3.12 and Figure 3.13 of ISPs produced (ZZZONR040808).

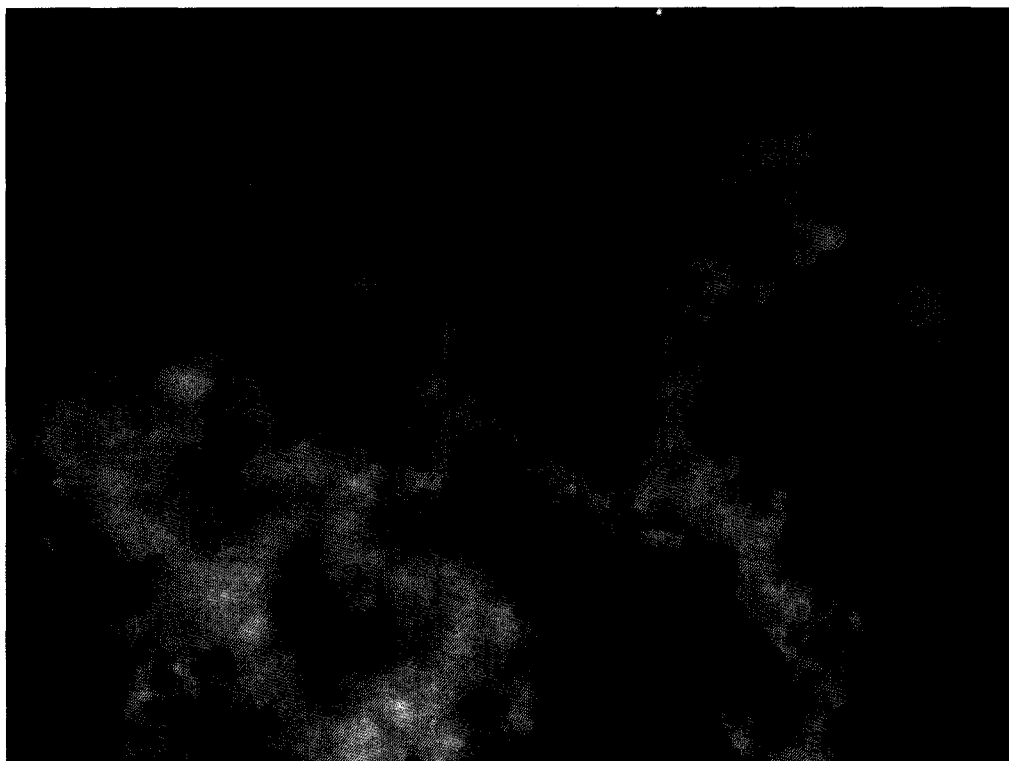


Figure 3.12: TEM of Microtomed ISP at 25,000 x Magnification

The TEM images confirmed the general morphology of the ISPs as not core shell but of the occluded and uneven structure. As it is a thin (50-90 nm typical) section of the particle it provides the information that between the smaller primary particles there is little to no gap or free space. This information was unavailable from the SEM images. These were the best images taken by this technique. TEM was not utilized extensively as the SEM images provided more useful information about the particles synthesized.

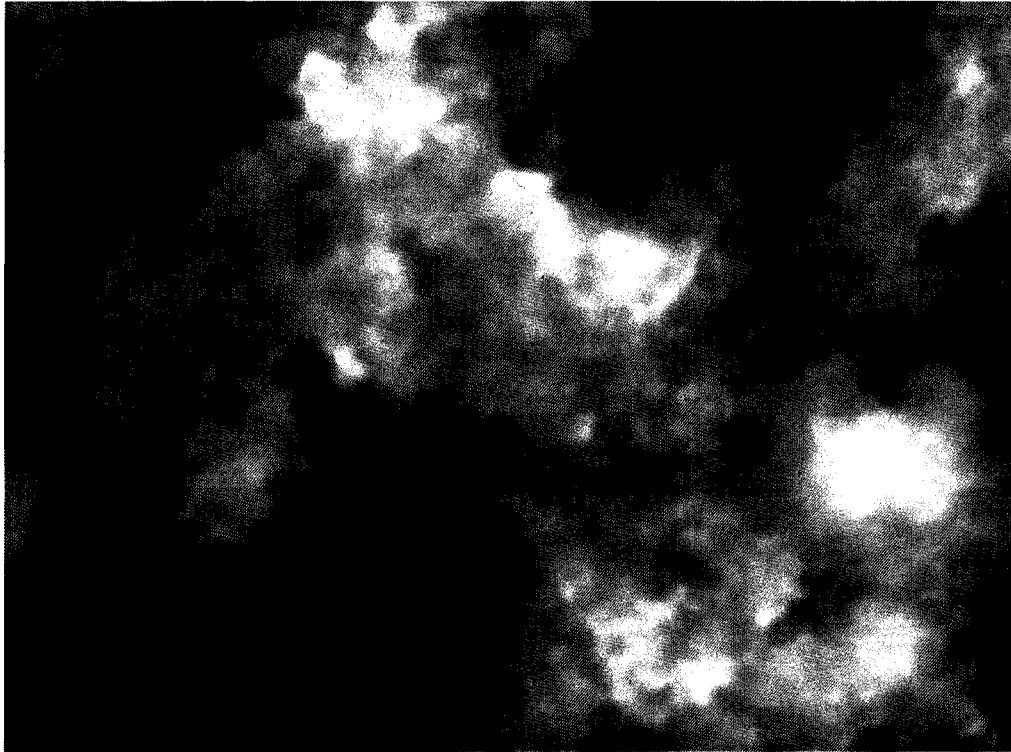


Figure 3.13: TEM of Microtomed ISP at 40,000 x Magnification

3.2.2 Characterization of ISP Size

It was speculated that the size of the ISPs would have an effect on their overall effectiveness in anticorrosion coatings. Moreover, the particles had to be of a small enough diameter that they could successfully be incorporated into an anticorrosion coating. These coatings are typically applied at thickness beginning at 250 μm . Therefore the ISPs had to be smaller than 250 μm , ideally an order of magnitude smaller to be incorporated into existing coating systems without disrupting the film forming characteristics.

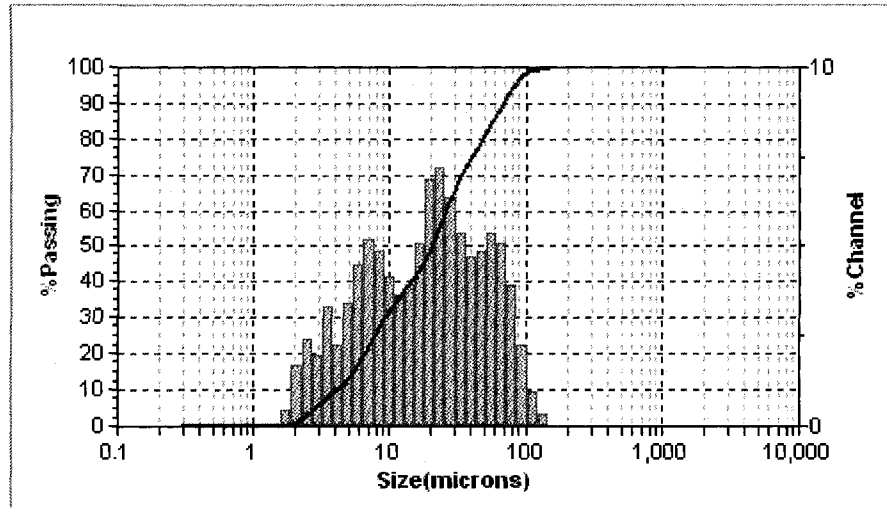


Figure 3.14: Microtrac Size Characterization Data for ZZZONR042508

The characterization of the ISP size distribution was done primarily by light scattering. SEM was used in some cases to verify these results. Particle size was determined on dried ISP which in some cases resulted in larger agglomerates of particles being measured. Early particle size distributions were determined by a Microtrac S3000 particle size analyzer. Later measurements were made on a newer Microtrac S3500 as it replaced the S3000 during the course of this work. A representative plot of the data received from these instruments is shown as Figure 3.14.

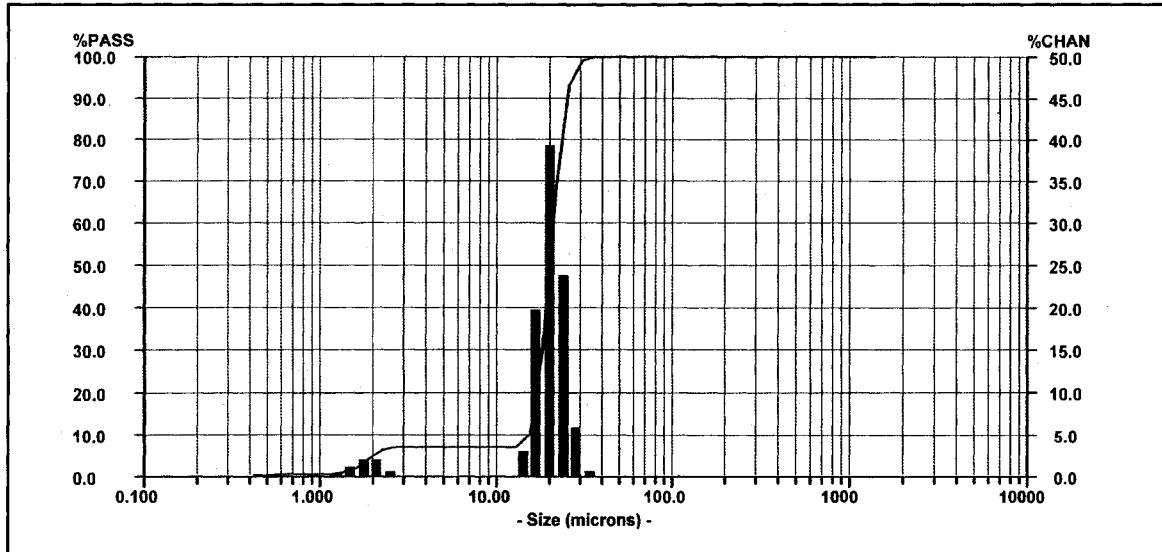


Figure 3.15: Bimodal Distribution for ZZZONR010705 ISPs

The results of the particle size analysis for ISPs synthesized are summarized in Table 3-2. The particle size distributions were in many cases bimodal or even trimodal with a smaller size in the 1-4 um range and a larger size distribution in the 10-50um range as illustrated by **Error! Reference source not found..** These samples were probably truly bimodal. Samples that have small distributions of 1000 um and greater likely contain agglomerations of dry particles that were not adequately separated by the shear induced by the Microtrac prior to the sample chamber.

Table 3-2: Summary of Particle Size Analysis in μm

Sample ID	Peak 1	peak 2	peak 3	peak 4	Dv	Dn	Da
ZZZONR 010705	5.5	20	60	200	50.5	6.126	15.18
ZZZONR 052406	5				19.68	3.391	7.36
ZZZONR 040506	12	200			61.2	3.39	10.49
ZZZONR 080906B	0.1	0.45			146.7	0.1001	0.1186
ZZZONR 080906	2				2.33	2.28	2.32
ZZZONR 040506	5	35	90	400	195.7	3.3	16.5
ZZZONR 050306	3.5	13	45	130	66.06	4.447	27.8
ZZZONR 070104	0.5	1.5					
ZZZONR 011105	10	110	300	1000	433.3	2.267	17.69
ZZZONR GROUND PEI	10	50	150		78.33	3.17	19.26
ZZZONR 032807	120				272	158.6	221.1
ZZZONR 120706	90				1807	100.3	801
ZZZONR 040808	50				405	68	208.8
ZZZONR 010207	300				3740	657	2760
ZZZONR Bently pei ground	10	60	160		62.7	1.77	11.67
ZZZONR 080906	100	500			201	60.6	102.5
ZZZONR 120706	0.6				0.748	0.74	0.745
ZZZONR 111406 20 min sonication	0.15				0.1659	0.1408	0.1552
ZZZONR 111406 40 min sonication	0.1				0.127	0.0965	0.1147
ZZZONR 111406 Post PMMA	0.11				0.1153	0.0962	0.1083
ZZZONR 042408	30				28.22	3.17	10.44
ZZZONR 120706	0.8				0.748	0.737	0.745
ZZZONR 042508	17	300	1200		594.3	2.699	16.84
ZZZONR 040808	19	300	1200		711.8	2.936	20.48
ZZZONR 92404	2	40			26.19	1.81	6.312
ZZZONR 102004	25				26.83	26.05	26.57
ZZZONR 072004	2	20			14.43	0.511	6.482
ZZZONR 110904	4	70			51.46	1.358	22.53
ZZZONR 101104	1.3	11			11.71	1.358	7.038
ZZZONR 011105	0.6	7	70		34.39	0.549	4.29
ZZZONR 010705	4.5	10			5.36	0.785	3.585
ZZZONR 010705b	15				16.25	15.73	16.08
ZZZONR 010705C	20				19.53	0.71	10.56
ZZZONR 070104	4	15			11.83	5.156	9.356
ZZZONR 040501	60	180			53.85	3.102	11.58
ZZZONR 051501	10				23.68	4.706	12.88
DETONR 45	10	60	250		85.49	3.16	11.92
DETONR 47	20	450	1200		761.3	2.682	29.28
DETONR 48	30	400	1200		630.7	2.067	22.48
DETONR 46	20	400	1200		747.9	1.487	15.64
DETONR 45	junk				711.6	3.25	33.68

The encapsulated WISCM was analyzed on a Nanotracer UP250 (Microtrac Inc. North Largo, FL) to determine the particle size distribution. Particles made by this method were significantly smaller than those made by the SISCM synthesis. Typical WISCM particle size ranges were the range 100's of nanometers diameter. A representative result from the Nanotracer is shown as Figure 3-16. The particles for this sample, ZZZONR120706 have a nominal size

of approximately 100 nm. These results are recorded in Table 3-2 along side the other measurements

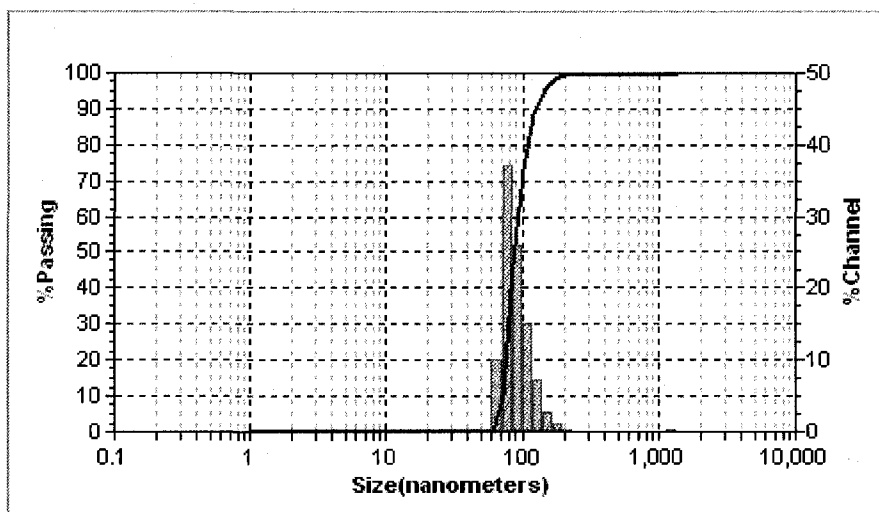


Figure 3.16: Nanotracer Particle Size Distribution for PMMA encapsulated WISCM (ZZZONR120706)

3.2.3 Characterization of PMMA Encapsulation of WISCM

Characterization of the WISCM capsules after the encapsulation with PMMA proved challenging. It was important to determine if PMMA was present and if microcapsules were produced as opposed to a crop of discrete particles. The TGA was used to determine if PMMA was present in the suspension post encapsulation reaction. One might more typically detect PMMA by DSC hoping to detect a characteristic T_g in the range of 105-120C. But because the WISCM particles have a hydrated core, the water would vaporize at 100C causing a possible rupture of the DSC pan and contamination of the DSC cell. Alternative techniques were used to avoid this result.

TGA of a sample of the WISCM was compared to a sample of the PMMA encapsulated WISCM. The results of this experiment are shown in Figure 3.17. The curve for the encapsulated WISCM shows an earlier onset of degradation at 150C which would be indicative of PMMA loss. The difference between the encapsulated vs unencapsulated WISCM is due to the degraded PMMA, The retardation of the decomposition and crossing of the curves at ~650C defies explanation. It would be expected that the PMMA encapsulated sample would remain lower than the unencapsulated for the entire run. These results proved that PMMA had been successfully produced but not if it had encapsulated the WISCM.

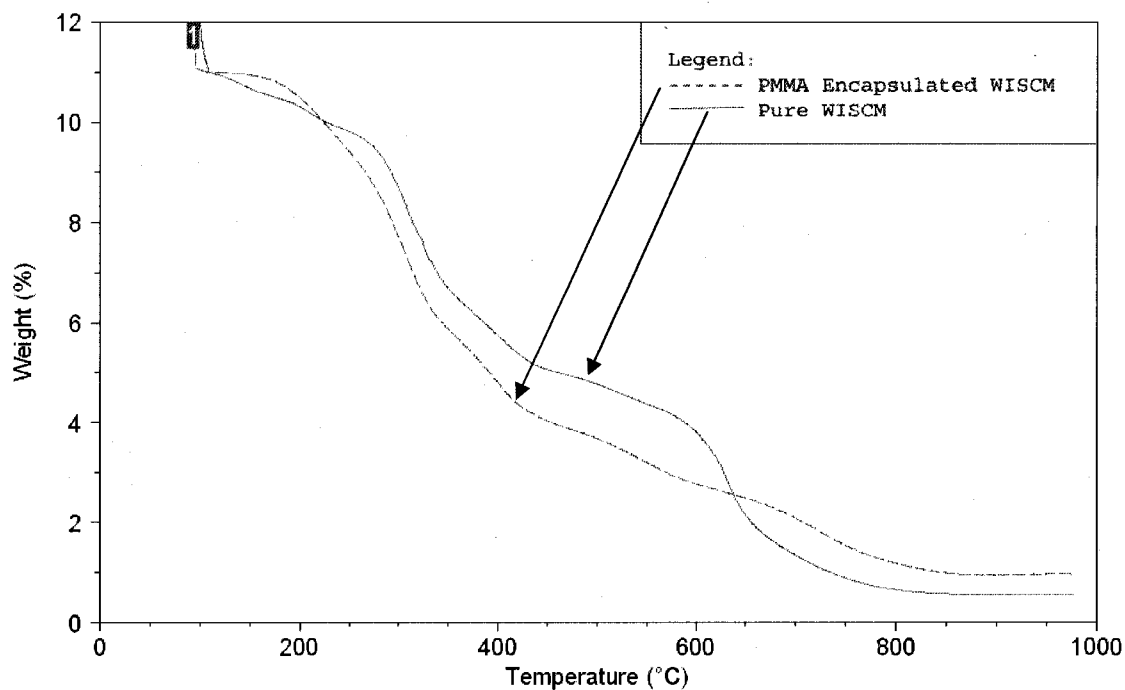


Figure 3.17: TGA Data for WISCM and PMMA encapsulated WISCM

There was concern that the MMA had polymerized forming discrete particles rather than encapsulate the WISCM. After the TGA results showed that PMMA had been polymerized, the heptane was evaporated under a nitrogen purge overnight. This left a solid pancake consisting of the capsules and surfactant. The pancake was then easily redispersed into fresh heptane by simply shaking the flask. This was an indirect proof that the WISCM had been encapsulated by the PMMA. Had the WISCM not been encapsulated by the PMMA a non-dispersible mass would have formed upon drying due to the ionic bonds of the core material exchanging. This re-association into solid agglomerate had been demonstrated many times in unsuccessful experiments.

An optical microscope was used to image the suspension of encapsulated WISCM particles in heptane. The results showed what appeared to be agglomeration of very small particles. It was surmised that there were PMMA capsules containing WISCM as the agglomerated particles did not reform into larger single droplets under the cover slip. A representative image is shown as Figure 3-18. The larger dark ringed spheres are approximately of 3-5 μm in diameter and are likely air bubbles trapped under the cover slip. Due to the small size, as verified by the Nanotrak it is impossible to clearly see the individual particles.

Dyeing the WISCM was attempted unsuccessfully to help show the WISCM particles and their shell. Suspensions of WISCM in heptane were made with ALEXA 647 in solution. The Alexa fluorescent dye phase separated from the solution into a blue liquid phase at the bottom. Likewise, water soluble red dye

was added to the WISCM and dispersed. While it seemed that the dye was in the particles, under the optical microscope there was no detection of the red indicator likely due to the small size of the droplets low yield of the chromophor.

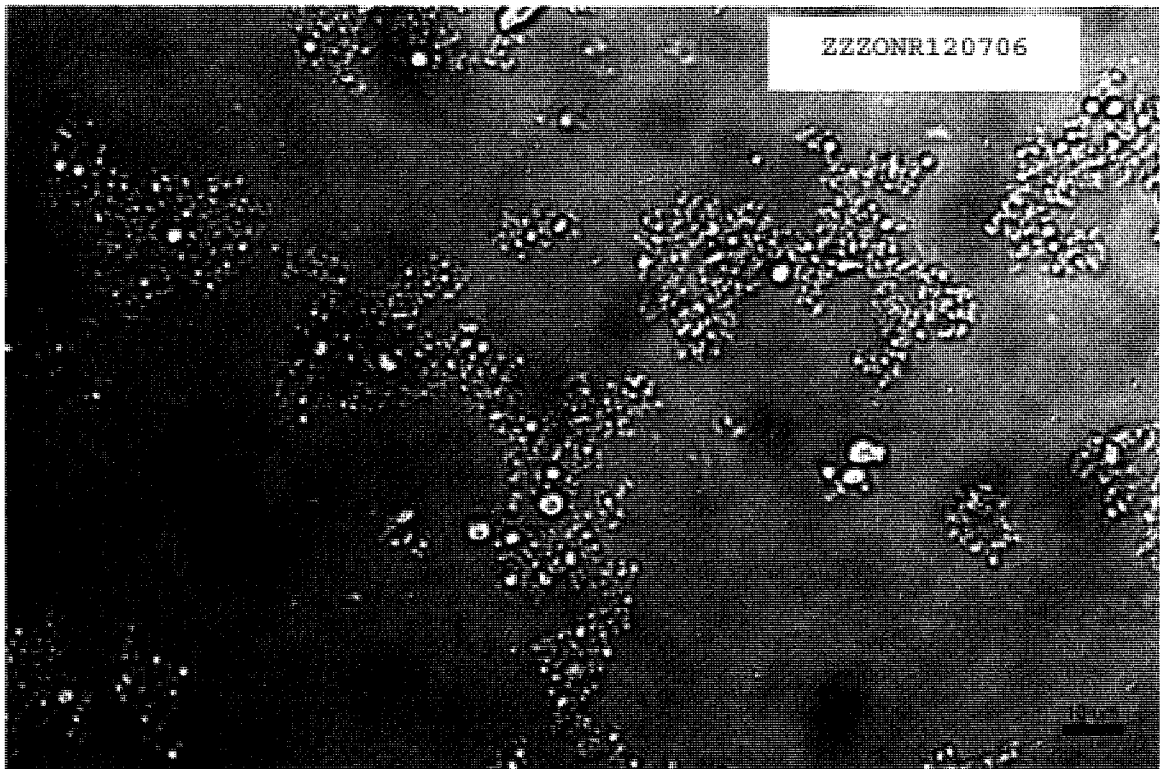


Figure 3.18: Light microscopy image of PMMA encapsulated WISCM

In the end, proof of encapsulation came in the form of successful dispersion of the dried particles into the amine component of the MIL-DTL-24441C coating. The dispersed particles showed no signs of the previously experienced interaction between the ISPs and the coating components. The particles were then successfully incorporated into coated sample coupons (ZZZONR021207) where they were evaluated for their enhanced corrosion characteristics.

3.2.4 SISCM Encapsulation

The success of the encapsulation of SISCM was clearly proven by two different results. Figure 3.19 shows SEM images of a section of SISCM particle (ZZZONR010705) in the upper pair of images. Many primary ion sequestering core particles (90-110nm) make up the agglomerated mass of the larger SISCM as a whole which range from 10-20um in diameter. In the lower images the same particles (ZZZONR0713007) are shown post PMMA encapsulation. There is an increase of the primary particle size (100-150 nm) caused by the layer of PMMA covering the entire SISCM particles. In addition it seems that there are no discrete PMMA particles formed during the polymerization or at least none are found separated from the encapsulated SISCM.

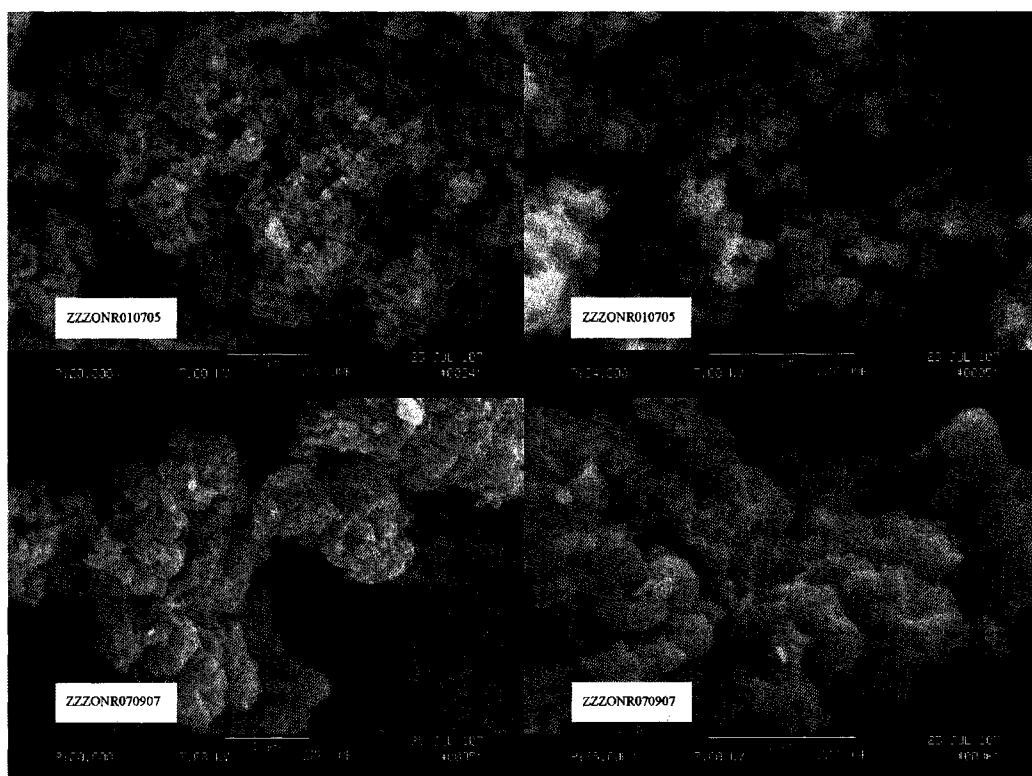


Figure 3.19: SEM of SISCM pre and post encapsulation with PMMA

While the visual changes identified from these SEM provided some proof that the SISCM was encapsulated with a layer of PMMA, final proof of encapsulation came by the successful incorporation of these ISPs into the MIL-DTL-24441C coating.

3.2.5 Characterization of Ion Exchange Capacity

It has proven difficult to quantitatively characterize the ion sequestering properties of the particles produced over the course of this work. A number of different approaches towards characterizing the ion exchange properties of the ISPs were attempted over the course of this work. Most of these were unsuccessful and are discussed in Appendix 3. This section discusses the one successful methodology that allows for comparison between particles to be made based on ion sequestration capacity.

Investigations of anticorrosion pigments reported in literature do not concern themselves with characterization of capacities of the pigments directly. Outside of referencing mass fraction of functional ion, such as to say there is a x wt. % phosphate in the pigment based on the molecular formula, they rely on results garnered from accelerated corrosion experiments. One attempted methodology for the quantification of the ion sequestering capacities of ISPs directly has resulted in success. This method relies on the titration of the ISPs in water to develop a pH profile vs quantity of hydroxyl ions added to the solution.

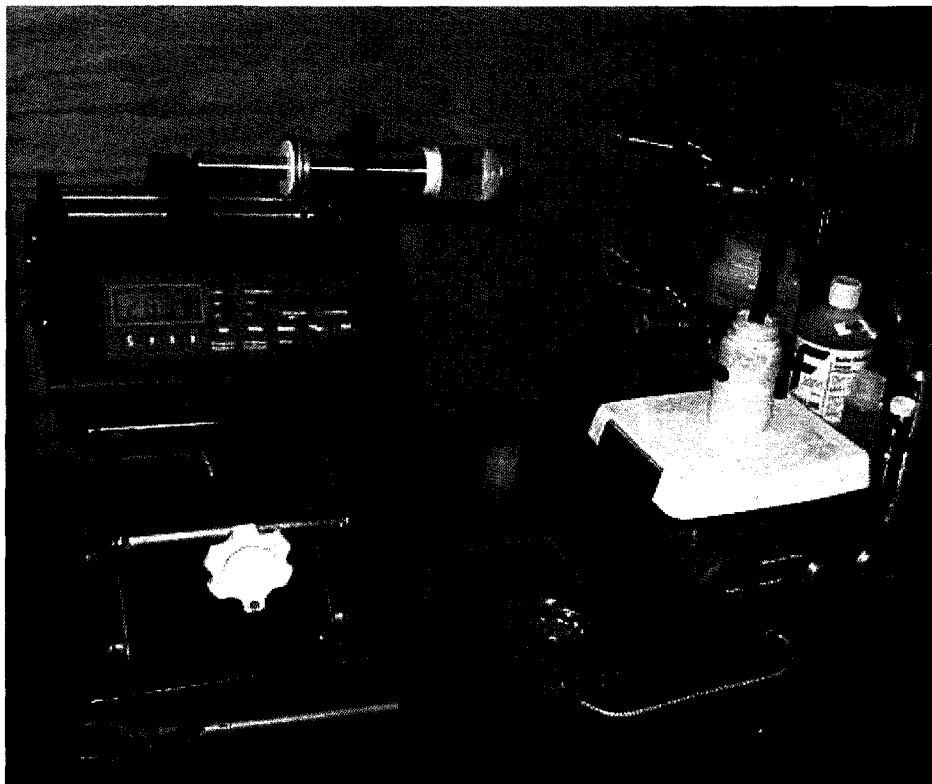


Figure 3.20: Titration Setup for ISP Capacity Determination

The ISPs, dispersed in pure water, were titrated with a calibrated standard solution of sodium hydroxide (61.8623 g/L) by a syringe pump at a rate of 1 mL/min as shown in Figure 3.20. The sequestering capacity was calculated and presented as the mass of OH ions the ISPs absorb on a per gram basis. The pH value of 12 was chosen as the comparison point based on the region of passivation of steel at this pH and in addition to this the titration curves all level off near this pH.

Figure 3.21 shows the titrations of 4 different ISPs from the initial synthesis approaches. The polyurea encapsulated ISPs along with the polyallylamine ISPs showed the best ion exchange characteristics at pH 12 with a buffering capacity of approximately 0.26 grams of ions per gram of ISPs.

These early ISPs show a lower ion sequestering capacity as the formulation was not optimized at this stage of ISP evolution.

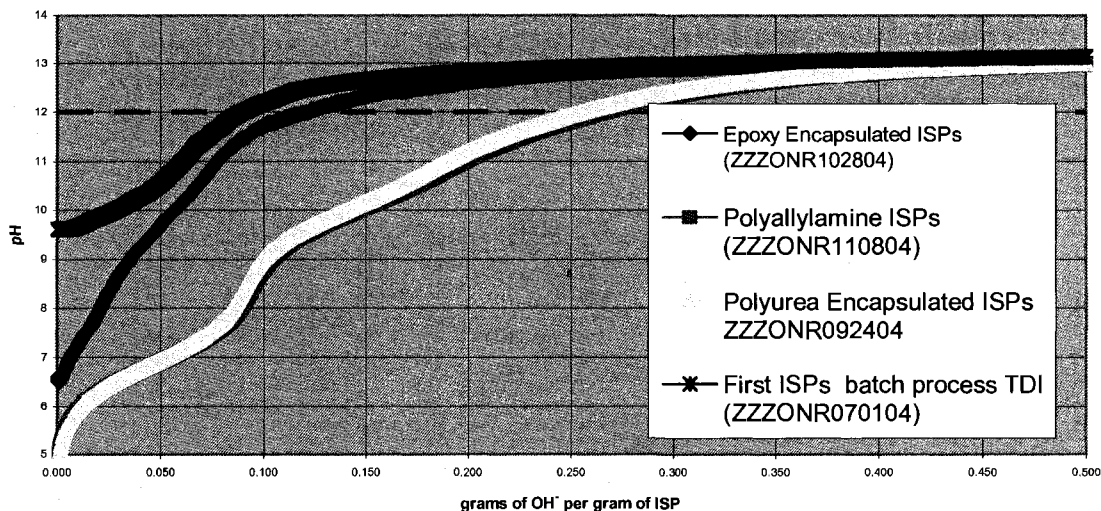


Figure 3.21: Ion Sequestering Capacity of Early ISPs

Particles made by the final SISCM synthesis were titrated and the results are presented as Figure 3.22. These particles show an increased capacity to sequester OH^- ions when compared to the early ISPs produced as shown in Figure 3.21. It is likely that the increased capacity is influenced by the higher phosphate loading used in the SISCM of the later particles. The PMMA shell used to protect the SISCM from harmful interactions with the uncured components of the anticorrosion coating may also play some roll in the enhanced performance as well. This is possibly due to a prevention or retardation of a partial dissolution of the ionic components of the core material.

There is also a distinct difference in the behavior of the PMMA encapsulated particles when placed into the water for titration. Unencapsulated particles mix into the water readily and seem to swell. Whereas the PMMA

encapsulated particles are extremely hydrophobic and try to separate from the water. Strong agitation is required to maintain a semblance of dispersion with these particles during the titration.

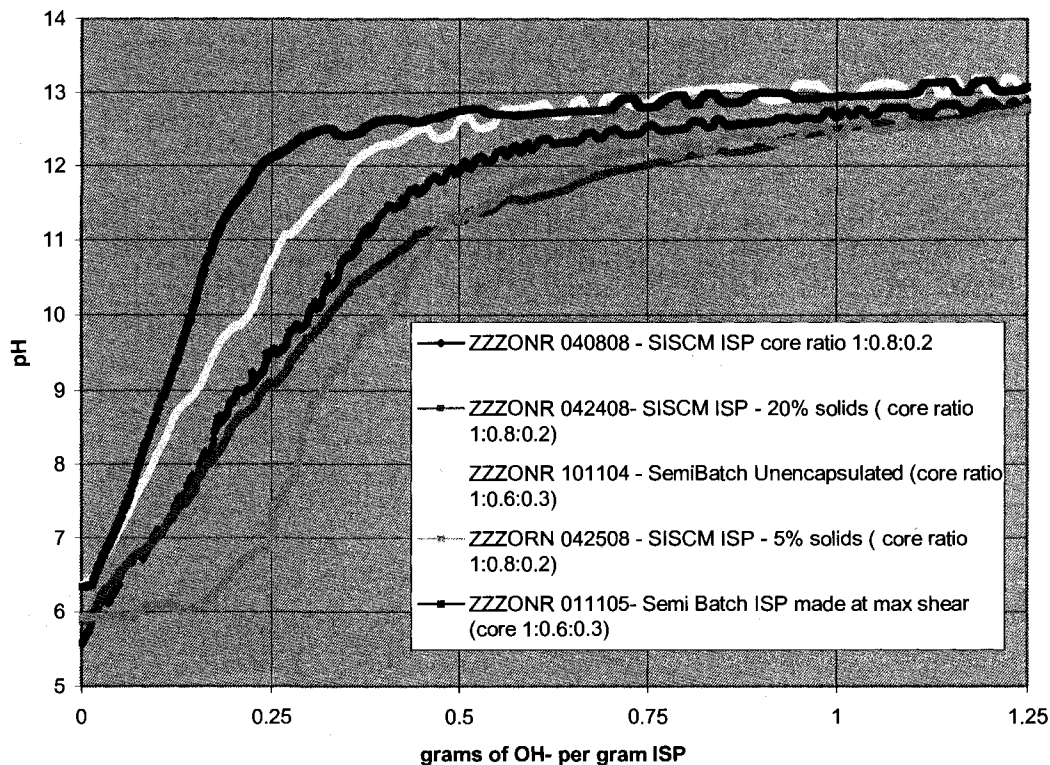


Figure 3.22 Ion Sequestering Capacity of Later ISPs

The values of gram of OH- per gram of ISP at pH 12 are presented for each sample titrated in Table 3-3 for comparison. The data shows that ISPs with lower loading of 1:0.6:0.3 have a decreased capacity at the comparison point of pH 12 when compared to the higher phosphate loaded particles. ZZZONR042408 and ZZZONR042508 show the most ion sequestering capacities. These were the final particles synthesized for this work. In

comparison with the early batch synthesis particles of ZZZONR070104 they show an almost ten fold increase in ion sequestering capacity.

Table 3-3: ISP Capacity at pH = 12

Sample ID	g OH / g ISP	Description of ISPs
ZZZONR070104	0.089	Batch process ISPs
ZZZONR092404	0.255	Polyurea Shelled Semi Batch ISPs with UT on 3
ZZZONR102804	0.124	Epoxy Shelled Semi Batch ISPs
ZZZONR101104	0.354	Polyurea Shelled Semi Batch ISPs same as 092404 but with UT on 6
ZZZONR110804	0.266	Homogeneous (Polyallylamine) ISPs
ZZZONR011105	0.235	Semi Batch process ISPs first used as SISCM
ZZZONR040808	0.575	SISCM ISPs
ZZZONR042408	0.742	SISCM particles made at 20% solids
ZZZORN042508	0.674	SISCM particles made at 5% solids

3.2.6 Diffusion of Chloride Ions Through the MIL-DTL-24441 Coating

The theorized mechanism of ISPs anticorrosion enhancement in a coating is based on diffusion of the passivating ions from the core along with the entrapment of harmful ions as they diffuse through the coating. Therefore the diffusion of these ions through the anticorrosion coating is of interest. Literature containing results on water uptake and diffusion in epoxy has been published since the 1960s¹³⁷. These results are typically derived from experiments based on gravimetry or electrochemical impedance measurement¹³⁸. The values determined from these methods typically vary widely and are inconsistent¹³⁹. By comparison, little has been published about ion transport through the anticorrosion coating.

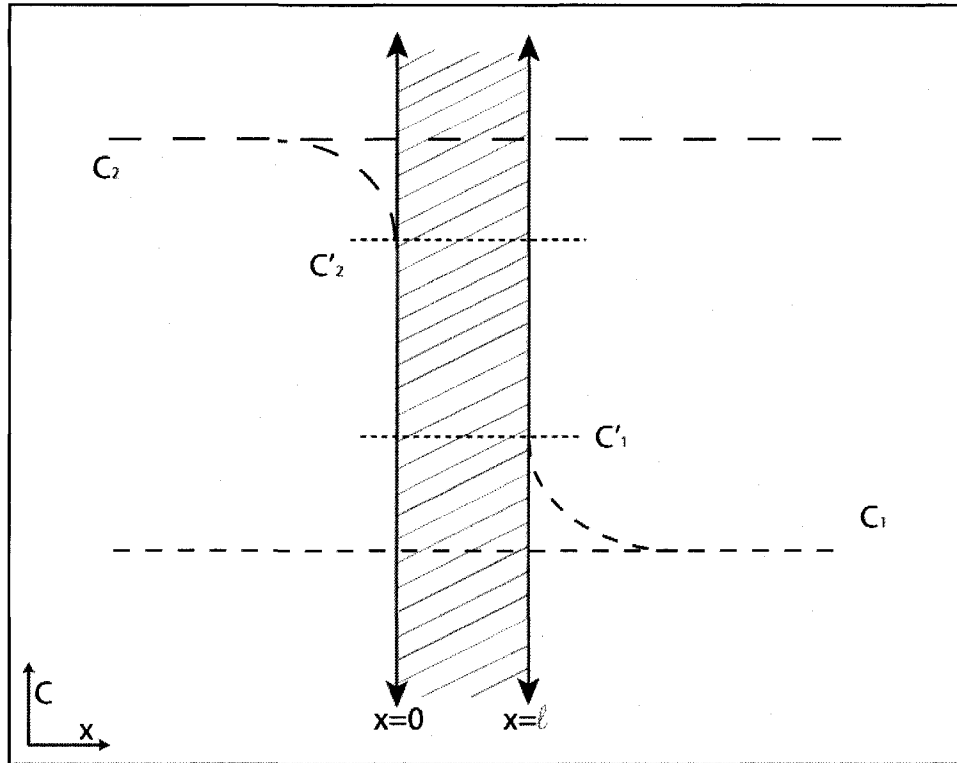


Figure 3.23: Concentration Profile for the Differential Cell

A concentration gradient cell was used to determine the effect of ISPs on chloride transport through the MIL-DTL-24441 coating¹⁴⁰. This method determines the diffusion coefficient from time it takes for a species to pass through a film. The concentration profile for the film is illustrated in Figure 3.23. For these experiments C_2 (the high concentration) was provided by a 5 wt % NaCl solution. For early times the concentration C_2 can be considered as constant, with C'_2 , the concentration at the boundary of the film and salt solution also constant. The initial concentration C_1 was essentially zero as ultra pure water was used.

$$C(x,t) = C'_2 \operatorname{erfc}\left(\frac{x}{\sqrt{4Dt}}\right) \quad [\text{EQ 3-2}]$$

The solution to Ficks second law with time in one direction for this system is presented as EQ 3-2¹⁴¹. Here the concentration C is a function of x and t . The value of $\sqrt{4Dt}$ in this equation represents the characteristic diffusion length, the distance it takes the diffusion front to travel in time t . Rearrangement of the terms results in the solution presented as EQ 3-3.

$$D = \frac{\ell^2}{4t_B} \quad [\text{EQ 3-3}]$$

As the thickness of the coating (ℓ) is known, the breakthrough time can be used to calculate the diffusion coefficient for the film¹⁴². The breakthrough time is the experimentally determined time where the concentration C_1 rapidly increases¹⁴³, deviating from the control sample. This represents the diffusion front having traveled through the thickness of the film.

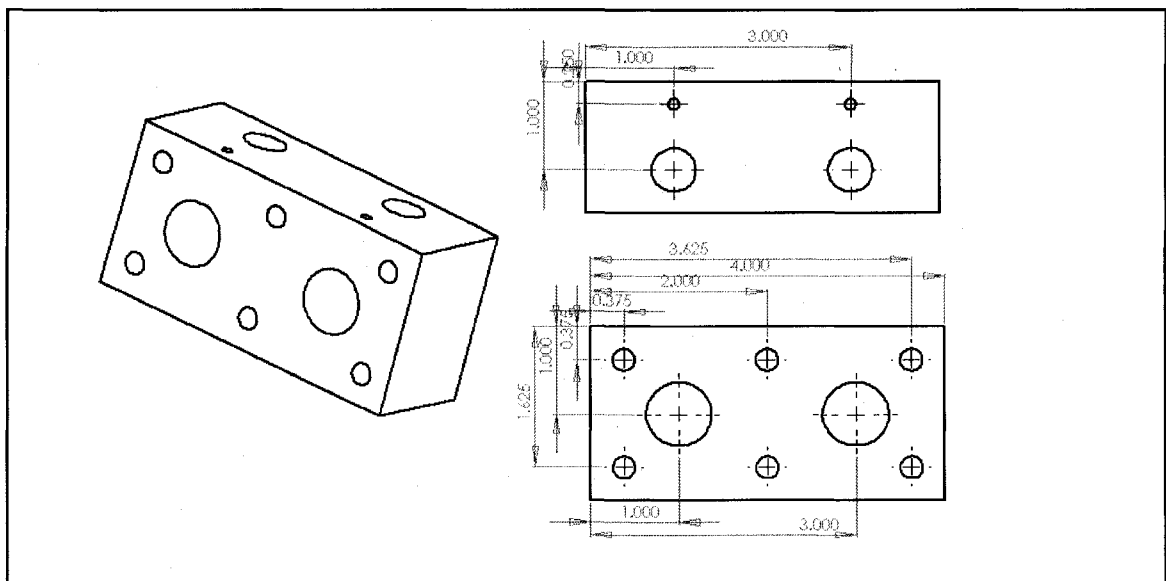


Figure 3.24: Diffusion Cell with Perspective, Front, and Top Views shown

A set of experimental cells were designed and fabricated for the concentration gradient method. These cells consist of four Teflon blocks machined as described in Figure 3.24. The cells were designed to capture an epoxy film between two cell halves. The epoxy films were thin and smooth making no additional gasket material or compound necessary to seal the PTFE cells to the films.

The loose epoxy films investigated were produced by spray application of the MIL-DTL-24441 epoxy coating onto a UHMW PE plate. After the coating was sufficiently cured, well past the gel point and tack free, the coating was carefully peeled from PE plate. The films were then allowed to cure fully while laid flat on the PE plate for at least 72 hrs. The films were cured at room temperature. Coatings were prepared at roughly 0.005" thickness. For each experiment a film was prepared neat (without ISPs) and containing 5 wt % of ZZZONR042508 ISPs.

Conductivity probes (CON-BTA, Vernier Software & Technology, Beaverton, OR) were used to measure the increase in conductivity on the side of the cell containing ultrapure water (C_1). Data was recorded by a Vernier LabQuest stand alone data acquisition system. The diffusion cell set up has two identical side by side solution reservoirs such that the same film could be subjected to a control of pure water and a salt solution simultaneously. One set of cells was used to run samples without ISPs while the other was run simultaneously containing the same film containing 5 wt % ISP. The control was performed to account for any species that might leach out from the coating.

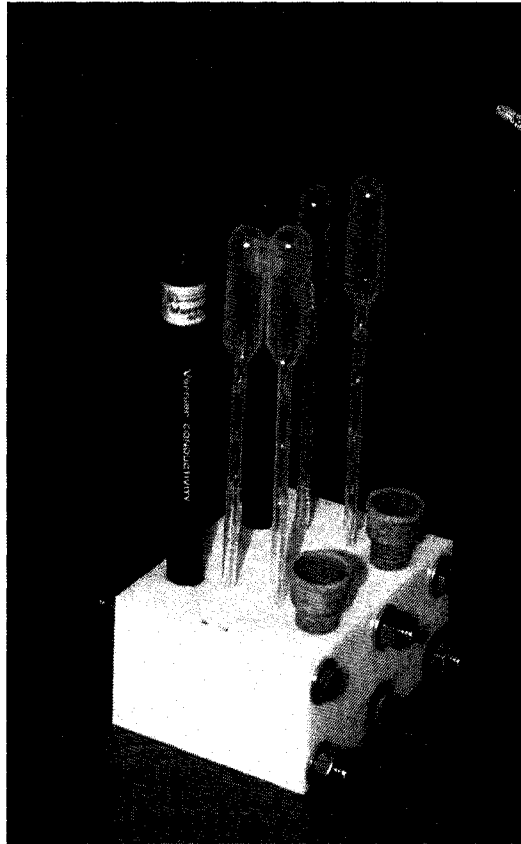


Figure 3.25: Diffusion Cell Experimental Setup

In order to increase the diffusion rate through the epoxy film the experiments were performed at 60C. The test assembly, shown in Figure 3.25 was placed into a water bath at 60 C to ensure uniformity of temperature. The bath chamber also ensured a 100% humid environment which helped prevent vapor loss from the solutions in the cell.

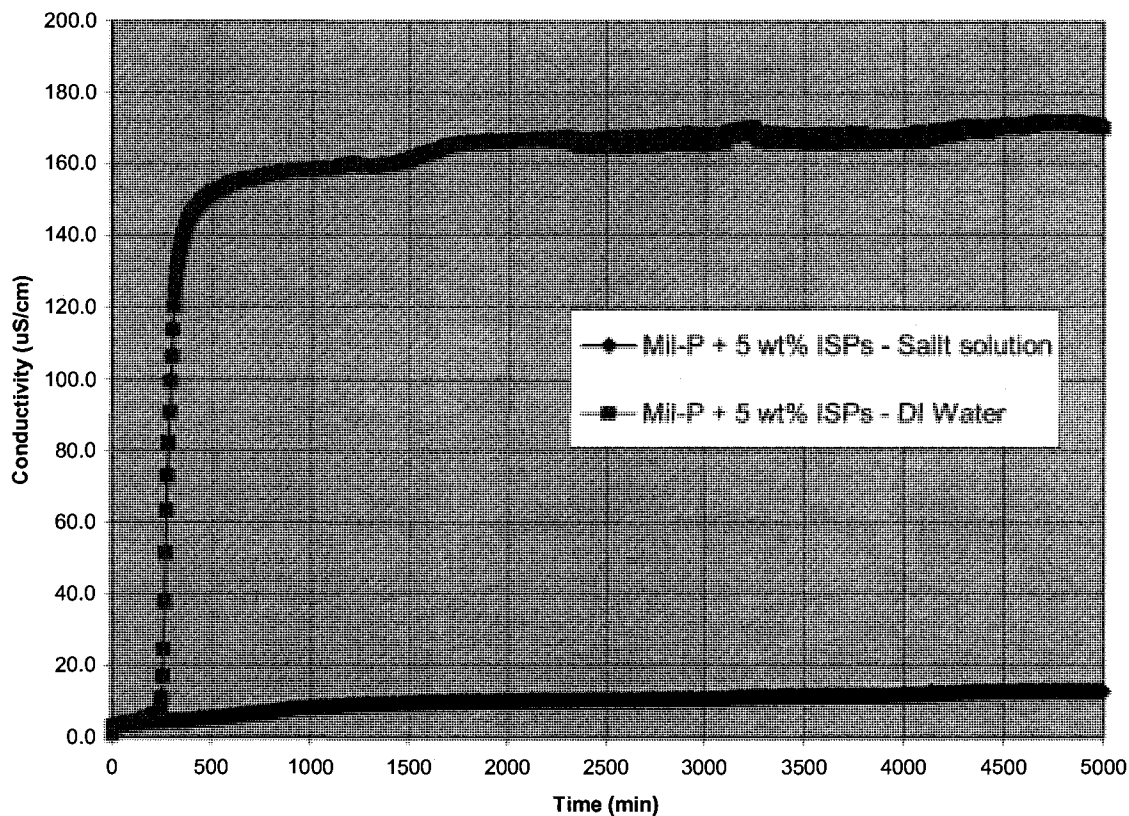


Figure 3.26: Diffusion Cell Results for ISP containing sample (ZZZONR042908)

The data from the diffusion cell experiments was tabulated and plotted as in Figure 3.26. There is a distinct and abrupt breakthrough time for all samples subjected to the sodium chloride solution. This breakthrough time was denoted by the sharp and rapid increase in conductivity that is not present for the control samples containing pure water on both sides of the epoxy film. The breakthrough time and the coating thickness were used to calculate the diffusion coefficient for the epoxy film.

The experimentally determined diffusion coefficients for sodium chloride through the MIL-DTL-24441 film are presented in Table 3-4. The experiment

measures conductivity and it can be inferred that the much smaller sodium ion is transported along with the chloride ion to maintain charge neutrality. The values determined in the first experiment (ZZZONR042908) varied by an order of magnitude from those determined in the second experiment. This could possibly be due to variations in conditions of the film preparation or cure time. The coating films were prepared in small batches. Possibly variations in the measurement of the A, B or solvent component of the coating at preparation resulted in this variation or that the coating was not cured sufficiently in the first experiment. Additionally temperature and humidity control is not available in the laboratories where the films were prepared. Humidity has a large effect on the cured properties of epoxy coatings.

Table 3-4: Diffusion Coefficient of NaCl through the MIL-DTL-24441 Coating

Experimental ID	Breakthrough Time (s)	Film Thickness (cm)	D (cm ² /s)	D _{T=20C} (cm ² /s)
ZZZONR042908				
MIL-DTL-24441	18900	1.52E-02	3.1E-09	2.7E-09
MIL-DTL-24441 w/ 5 wt % ISPs	14700	1.14E-02	2.2E-09	2.0E-09
ZZZONR070208				
MIL-DTL-24441	63600	1.27E-02	6.3E-10	5.6E-10
MIL-DTL-24441 w/ 5 wt % ISPs	83100	1.27E-02	4.9E-10	4.3E-10

One result from these experiments, aside from determination of the diffusion coefficient, is that for both experiments the diffusion coefficient for the coating containing 5 wt % ISPs was ~25% less than that of the neat MIL-DTL-24441 coating. While this could be argued to be within experimental error the 27% decrease for ZZZONR042908 and 24% decrease for ZZZONR070208 could also be explained by the chloride ions being trapped or retarded by the ISPs. These values, converted to T=20C by the well known relationship of $D_1/T_1 =$

D_2/T_2 , are in reasonably good agreement with values from literature for sodium chloride in a pure epoxy film $D = 8 \times 10^{-9} \text{ cm}^2/\text{s}$ and $4 \times 10^{-9} \text{ cm}^2/\text{s}$ ¹⁴⁴.

3.2.7 Diffusion Coefficient Determination by ATRIR

In situ diffusion measurements in polymer films can be determined by attenuated total reflectance infrared spectroscopy (ATRIR)¹⁴⁵. ATRIR is one of very few methods available that allows the *in situ* study of diffusion through coatings. Experiments using ATRIR were performed to determine both the water and phosphate diffusion coefficients through the MIL-DTL-24441 coating. This work follows with some modifications, the method reported by several authors^{146,147}.

Successful ATRIR diffusion coefficient determination requires that the ion under investigation has an IR response. Phosphate has a strong IR response due to PO stretching at $\sim 1100 \text{ 1/cm}$ ¹⁴⁸. These experiments did not provide information on the counter ion diffusion, as sodium does not have any IR response. It is not possible to comment on sodium ion diffusion as it has been reported that it is possible for there to not be a cation diffusing along with the anion during ionic diffusion through polymers¹⁴⁹.

A germanium crystal was utilized on a MIRacle ATR (Pike Technologies Inc.) mounted in a Tensor 27 infrared spectrometer (Bruker Optics) for this work. Germanium crystals for ATR have the highest refractive index ($R_i = 4 @ 1000 \text{ 1/cm}$), resulting in the shallowest depth of penetration (d_p) of the evanescent wave into the sample material¹⁵⁰.

$$d_p = \gamma^{-1} = \frac{\lambda}{2\pi(n_1^2 \sin^2 \theta_1 - n_2^2)^{1/2}} \quad [\text{EQ 3-4}]$$

Where:

$D_p = \gamma^{-1}$ = Depth of evanescent wave penetration into sample

λ = Wavelength of light

Θ = Angle of incidence of the IR beam

n_1 = Refractive index of the crystal

n_2 = Refractive index of the sample

Given a typical refractive index for epoxy coatings of approximately 1.55¹⁵¹ the depth of penetration for the ATRIR system at 1100 cm⁻¹ is calculated using EQ 3-4 to be 0.72 μm . Coatings used for these experiments were on the order of 150 μm in thickness, making the penetration depth less than 0.5 % of the total thickness. This small depth of penetration allowed for a true measurement at the surface of the coating. There is a penalty for such a small penetration of the evanescent wave, it comes in the form of diminished response. Therefore germanium crystals work well only for strongly absorbing bands¹⁵².

$$\frac{A_t}{A_\infty} = 1 - \frac{8\gamma}{\pi[1 - e^{(-2\gamma L)}]} \left[\frac{e^{(-D\pi^2 t)} \left(\frac{\pi}{2L} e^{(-2\gamma L)} + (2\gamma) \right)}{(4\gamma^2 + \frac{\pi^2}{4L^2})} \right] \quad [\text{EQ 3-5}]$$

Where:

t = time

A_t = integral of the IR peak at time t

A_{∞} = integral of IR peak at infinity

L = thickness of the coating

D = diffusion coefficient

The solution to the continuity equation in a polymer film with constant diffusion coefficient has been presented elsewhere¹⁵³. Equation 3-5 takes into account the effect of FTIR-ATR evanescence wave penetration into the coating. Simplifications to this solution resulting in the elimination of γ from the equation can be made provided two conditions are met by the experimental set up and polymer film being studied¹⁵⁴. These two conditions that must be met are described by:

$$4\gamma^2 \gg \frac{\pi^2}{4L^2} \quad \& \quad 1 \gg e^{(-2\gamma L)}$$

It was verified that the epoxy systems and geometries used in this work met these requirements. This allows for a rearrangement of EQ 3-5 into EQ 3-6. A least squares linear regression can now be fit to experimental data plotted. The slope of this fitment to the data allows for the calculation of the diffusion coefficient directly.

$$\ln\left(1 - \frac{A_t}{A_{\infty}}\right) = \ln\left(\frac{4}{\pi}\right) - \frac{D\pi^2}{4L^2}t \quad \text{[EQ 3-6]}$$

The MIRacle ATR has the added feature of removable and interchangeable crystal elements. The germanium crystal was removed from the

ATR assembly and coated with a MIL-DTL-24441 film by airbrush. Post curing of the film, careful measurement of the film thickness was made with a NIST traceable dial indicator accurate to 2.54 μm . After determining the film thickness the crystal was replaced in the ATR unit. A small PTFE cell was fabricated to interface with the ATR unit and provide an ample solution reservoir for the experiments. The PTFE cell was clamped over the coated crystal with an o-ring used to seal against leakage. This entire assembly is illustrated in Figure 3.27. This sectional view shows the cell clamped down on a epoxy coating over the crystal element. The upper hole in the cell is threaded for attachment to the auto tensioning clamp of the MIRacle ATR. The auto tensioning clamp provides precise concentric and parallel alignment as well as a controlled and repeatable clamping force that seals the cell against the epoxy coating.

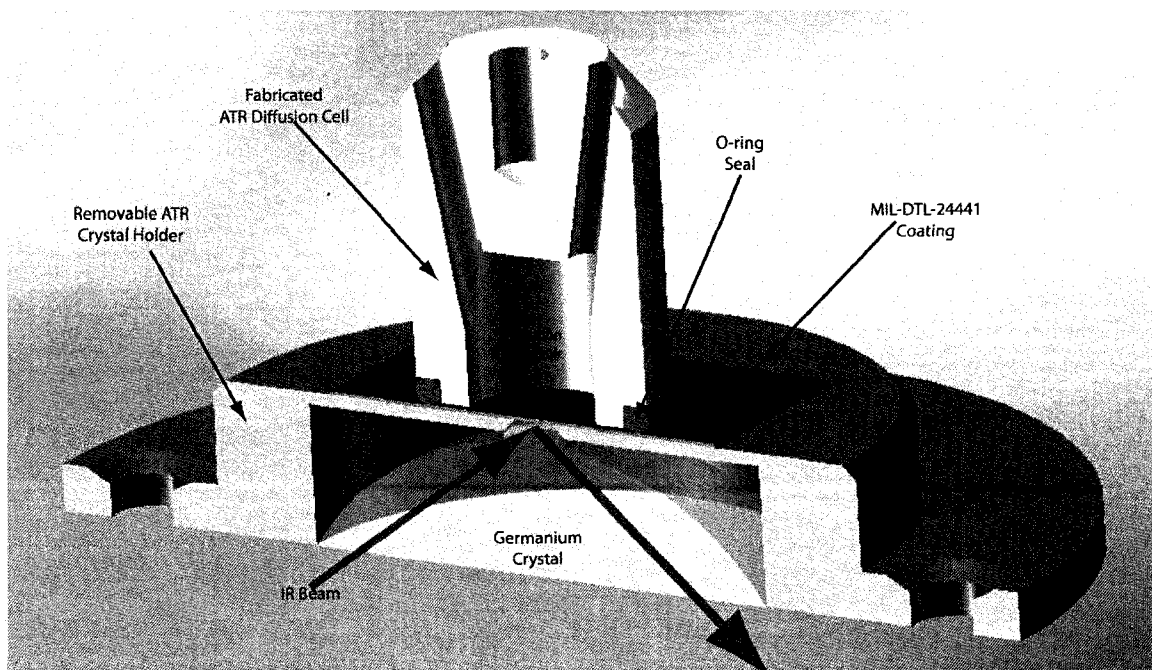


Figure 3.27: Sectional Diagram of Diffusion Cell on ATR Crystal.

Literature reported the use of filter paper to “wick” salt solutions into the area between the coating and a solid anvil¹⁴⁷. A loose film on an ATR crystal requires pressure from an overhead anvil to ensure good contact between the film and the crystal. This good contact is important because of the extremely low penetration depth of the ATRIR technique. While this method provided results it did not account for any decrease in localized concentrations as ions diffuse through the coating or evaporation of liquid from the filter paper. A large (in comparison with the coating volume) reservoir for the solution eliminates any concerns in regard to concentration changes of the “source” solution.

Data acquisition on the TENSOR 27 FTIR was controlled by the OPUS Software Suite which has a built-in feature that allows automated time dependent (kinetic) acquisition of spectra. The first spectra for each experiment were always taken immediately prior to injection of the liquid solution into the cell. This provided us with a baseline point without the possibility for any ion or water diffusion. Two liquids were used for these experiments, ultra pure water, and a 0.25N solution of disodium phosphate. The pure water was only used to pre-saturate the epoxy coatings in the later experiments, ZZZONR080808 and ZZZONR091908.

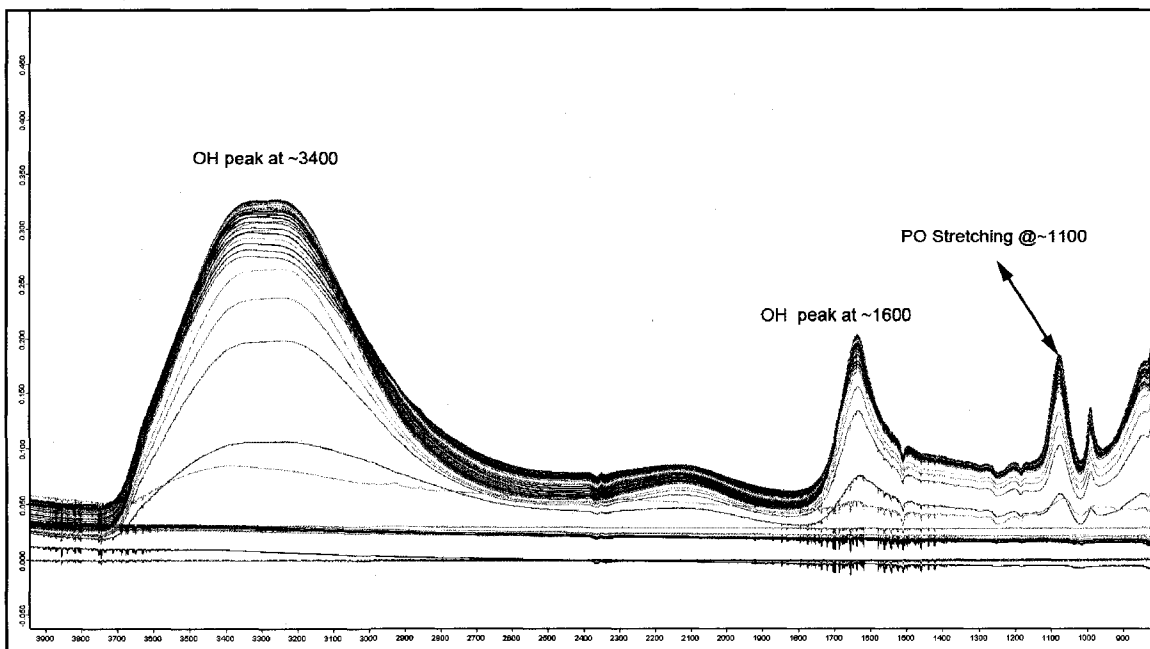


Figure 3.28: Overlay of IR Spectra for ZZZONR062408 (30 minute sampling interval)

The IR Spectra were treated for atmospheric compensation of CO₂ prior to any further numerical treatment. The compiled spectra for ZZZONR062408 are presented in Figure 3.28. In this experiment the MIL-DTL-24441 film is subjected to a 0.25N disodium phosphate solution at room temperature with spectra taken every 30 minutes. The peaks labeled for water (OH at ~3400 cm⁻¹ and ~1600 cm⁻¹) and for the phosphate (PO stretch at ~1100 cm⁻¹) were selected and integrated using the OPUS software. The value of the integral represents quantitatively the amount of functional group present in the sample for each indicated IR response.

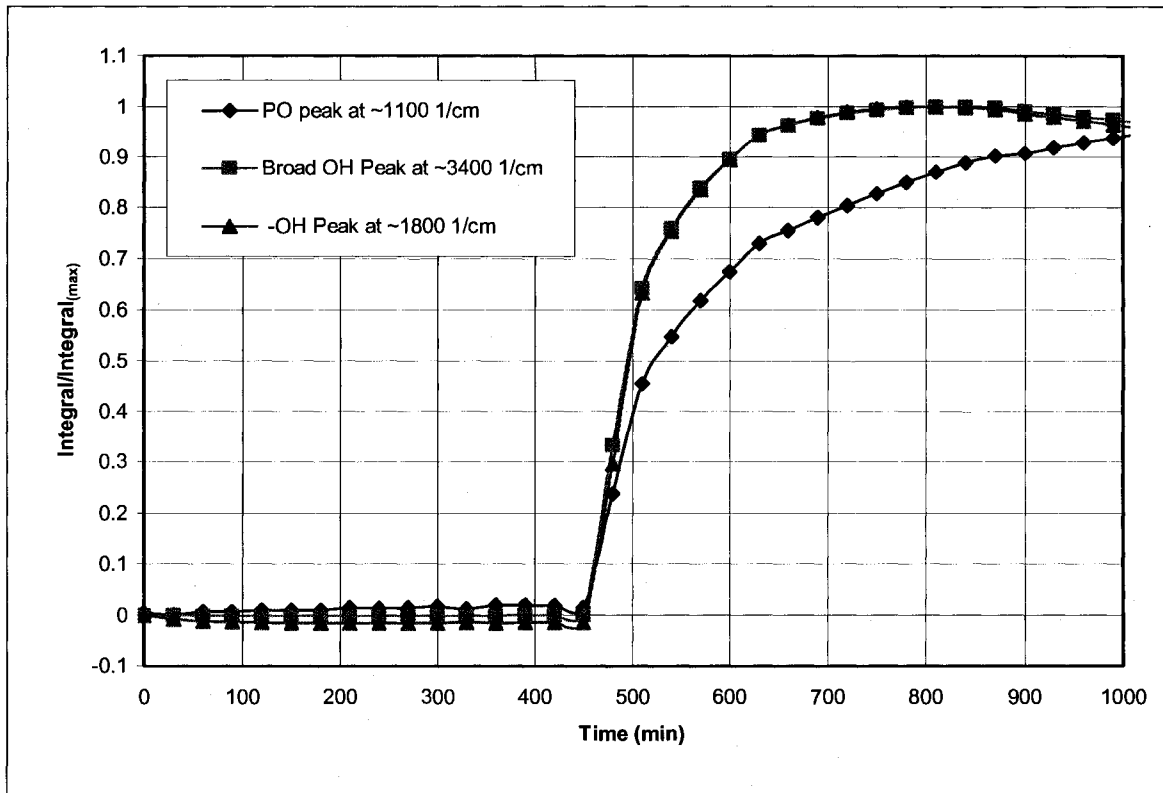


Figure 3.29: Normalized Integral Plotted Versus Time for ATRIR Experiment ZZZONR062408

The integration value for each spectrum in the experimental series was compiled into a single spreadsheet for further numerical treatment. Normalization was performed by dividing by the extrapolated value for the integral at infinity. This was then plotted versus the sample time as seen in Figure 3.29. This shows that the breakthrough time for the phosphate and water is the same. This indicates that the phosphate is transported coupled with the water through the coating, at least in the initial period.

Calculation of the diffusion coefficient was done from a plot of the $\ln(1 - A_i/A_h)$ versus time as in equation 3-5. Solution by this method is only valid for the

steady state or linear portion of the data. Therefore the linear regression is only fit to this portion of the data as shown in Figure 3.30 with the slope equivalent to $-D\pi^2/(4L^2)$. The diffusion coefficient was calculated from the resultant slope.

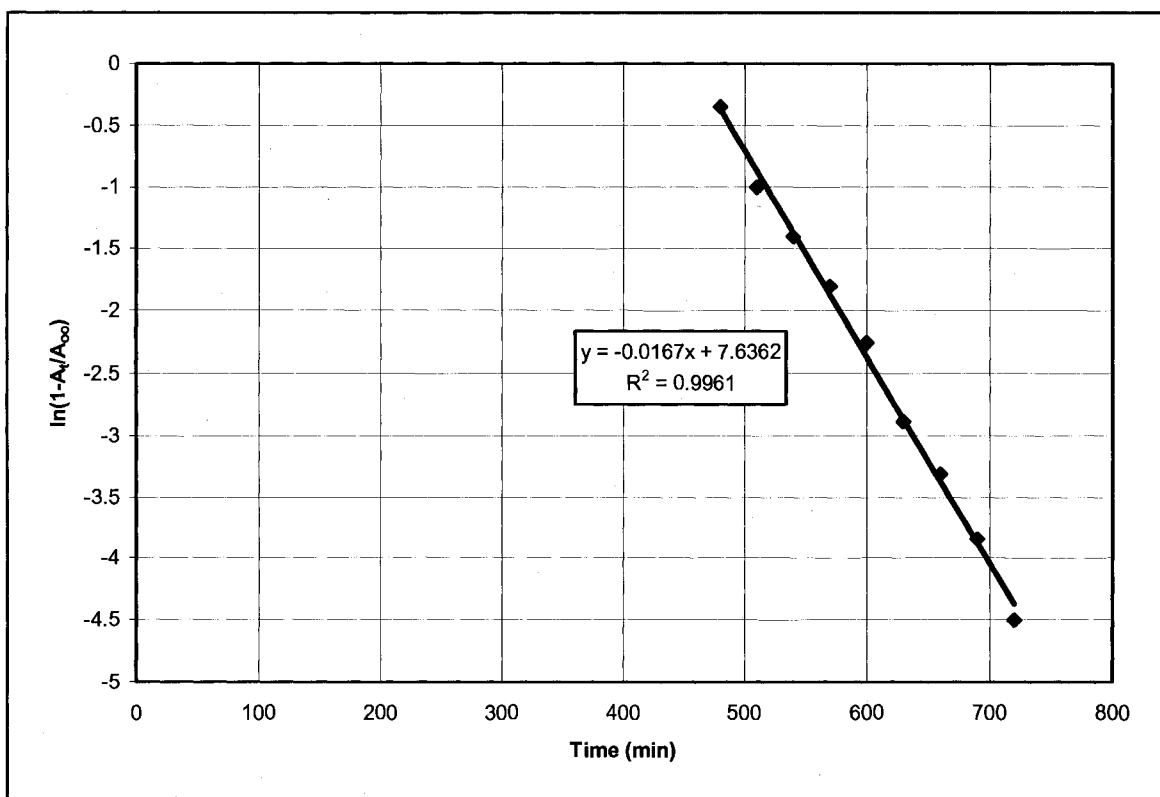


Figure 3.30: Linear Regression for OH band at $\sim 1600 \text{ cm}^{-1}$ in ZZZONR062408

The calculated diffusion coefficient for water from ZZZONR062408 is $D = 2.01 \times 10^{-8} \text{ cm}^2/\text{s}$ which agrees well with values from literature for water in epoxy films which range from 2 to $4 \times 10^{-8} \text{ cm}^2/\text{s}$ ¹³⁸. Table 3-5 contains the values of diffusion coefficients for the MIL-DTL-24441 epoxy coating as determined by the ATRIR method.

The direct coating of epoxy film onto the germanium crystal provided excellent results only for the first experiment to use this method. Unfortunately the germanium was damaged after the first experiment (ZZZONR062408) when the coating was removed from the crystal. Previous experience with ATR used more robust diamond crystal element, as germanium is considerably softer than diamond, damage was done to the crystal in the form of scratches during the removal of the adhered coating. The next experiment (ZZZONR071508) showed a dramatic decrease in signal due to the scratches imparted on the Germanium crystal. This weakening in response resulted in spectra where the water peak could not be successfully integrated. The crystal was then polished as an attempt to alleviate this decrease in IR response while at the same time a new crystal was purchased to replace the damaged one.

ZZZONR080808 was performed with the re-polished crystal. This experiment attempted to decouple the diffusion of the phosphate ion from the water diffusion. This was done by first soaking and saturating the coating with ultrapure water for 24 hrs prior to the start of the experiment. The experiment was then run with the 0.25N disodium phosphate solution. Presaturating the coating with water, by soaking it for 48 hrs prior to the experiment, it proved possible to determine the phosphate diffusion coefficient independent of the water. The signal of the repolished crystal was still considerably weaker than the first experiment with the undamaged crystal.

The same experiment was repeated (ZZZONR091908) with the new germanium crystal, except this time the film was not coated directly on the

crystal. Instead a loose film was clamped against the crystal by the cell. This gave good response and cleaner spectra. The diffusion coefficient determined for this experiment is likely more accurate than the one determined by ZZZONR080808 with the damaged crystal based on the improved response with the new crystal.

Table 3-5: Diffusion Coefficients Determined by the ATRIR Method

Experimental ID	Permeation Time (min)	Film Thickness (um)	D (cm ² /s)
ZZZONR062408			
OH (water)	450	133.4	2.0E-08
PO Stretching	450	133.4	5.3E-09
ZZZONR071508			
OH (water)			
PO Stretching	330	87.6	4.2E-09
ZZZONR080808			
PO Stretching	12.5	155.0	9.7E-08
ZZZONR091908			
PO Stretching	5.5	145.0	1.2E-07

In regards to the phosphate diffusion decoupled from the water diffusion, it becomes clear why one reported value in literature states that the phosphate transport occurs at the same rate as the water¹⁴⁷. With the independent diffusion coefficient an order of magnitude greater than that of the water through the coating it is clear that when no attempt is made to separate the two events with pre-swelling, one does not see the true phosphate diffusion. Figure 3.31 shows the phosphate values from three experiments, ZZZONR062408, ZZZONR080808, and ZZZONR091908 and emphasizes the effect of presaturating the coating with water prior to measuring the diffusion coefficient of phosphate.

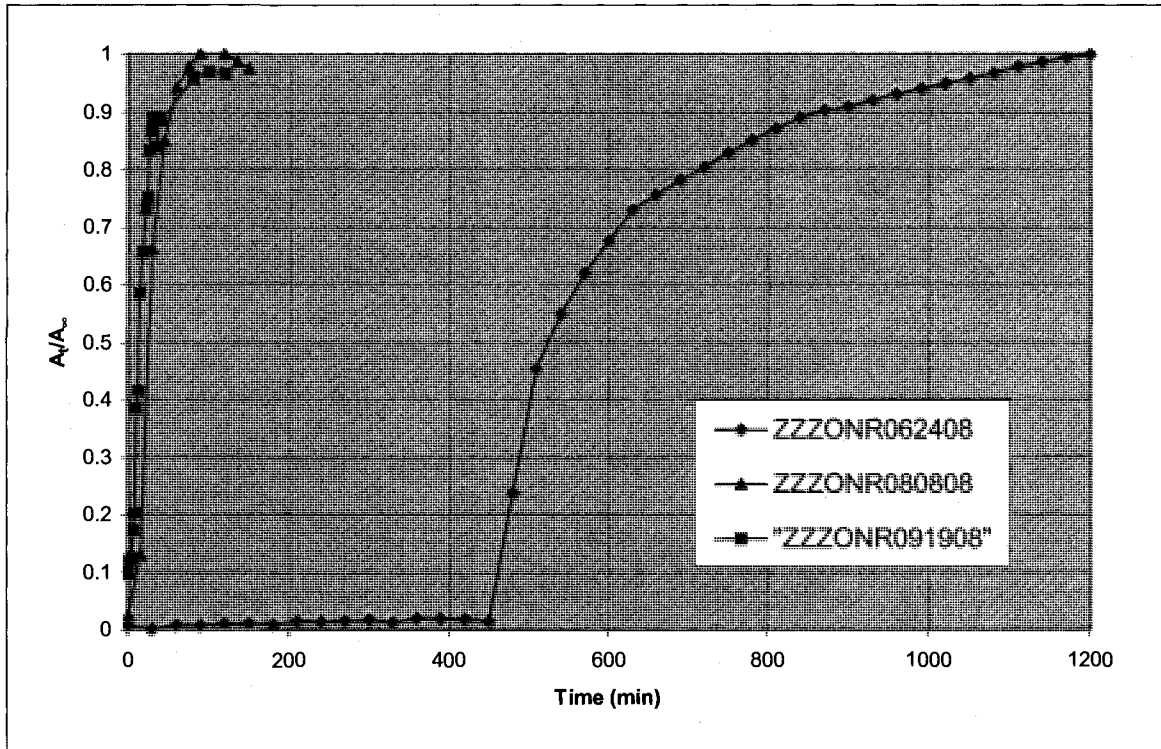


Figure 3.31: Normalized Phosphate Data Coupled (ZZZONR062408) and Uncoupled (ZZZONR091908) from Water

The high value for phosphate diffusion through the coating indicates it is unlikely the enhanced corrosion effects of ISPs are due to the slow steady long time diffusion of phosphate and entrapment of chloride ions. Certainly some of the harmful chloride ions will be retained in the ISP as shown by the decrease in diffusion coefficient determined for sodium chloride by the differential cell method. Given the life time of the coating of a minimum of 7 years (2.2×10^8 s) in a naval applications, and the characteristic diffusion time of phosphate from a point 25 mil from the coating/water interface of 8400 s (2 1/3 hrs) it becomes apparent that another mode of action must be present to explain the enhanced corrosion performance as coatings when loaded with ISPs (as shown in Chapter 4).

ISPs effect on the corrosion performance is speculatively due to the formation of passive films at the steel substrate. The phosphate ions released can interact with the free sites on the iron substrate, especially those that are not coupled to the epoxy coating¹⁵⁵. The epoxy coatings success as an anticorrosion coating is in large part due to the excellent adhesion with the steel substrate. Even on the best of coating applications it is likely that some unadhered or unchelated sites between the coating and the steel substrate remain. These unadhered sites would be the location where the initial corrosion process occurs. A likely mechanism is that phosphate ions released from the ISPs reach these sites and form the many well known and studied passive complexes with the free iron in place of the corrosion products that would otherwise form at these weak spots.

3.3 Summary of Characterization

Characterization of the monomers, individual reactions, and the particles was important during the evolution of the ISP synthesis. Results of characterization techniques allowed for a continual progress towards the development of a successful synthesis route. SEM images were the most useful overall but all of the techniques described in this chapter provided information needed to make this work successful.

It is impossible to develop a new concept, such as ISPs for anticorrosion, into reality without the necessary characterization techniques to understand the effect of developmental changes in the process on the resulting products. In the case where there is no available characterization technique for a new product,

the development of a characterization technique is necessary along with the development of the product.

In this work other characterization techniques attempted some unsuccessfully and are reported in APPENDIX III. These include an attempt at synthesizing longer chain ethyleneamines, prerusted sample coupons, ISP characterization by phosphate detection via (NMR, analytical chemistry/visible spectroscopy, FTIR), NMR determination of primary vs secondary amine competition with phosphoric acid.

CHAPTER 4

ANTICORROSION PROPERTIES

The goal of this project was to produce ISPs that provide enhanced corrosion protection. Proving that the ISPs have enhanced protection properties was critical to the success of this project. Two weeks were spent at the Naval Research Laboratories (NRL) facilities in Key West, Florida acquiring experience and training as part of this work. That time was used to learn most of the Navy's procedures for testing and qualifying new anticorrosion coatings. Hands on training in application techniques and evaluation of testing results provided the experience needed to evaluate the anticorrosion performance of ISPs.

During the time spent at the NRL under the guidance of Ted Lemieux (NRL Corrosion Science Section Head) and Arthur Webb (NRL Marine Coatings Section Head) the preliminary qualification program used to evaluate the ISPs synthesized in this work was defined. Discussions and the extensive experience of the NRL members resulted in the selection of the ISP evaluation program consisting of accelerated corrosion studies based on 1000 hrs of salt spray chamber exposure (ASTM B117), 500 hrs hot (80C) deionized water immersion, and 90 day cathodic disbondment.

This chapter describes the details of preparation of steel coupons for accelerated corrosion study as well as the testing procedures the coupons underwent. The results and anticorrosion properties of the ISPs are presented and discussed as well.

4.1 Preparation of Steel Coupons

It was decided to use the same sample coupon size, surface finish, and materials as those utilized by the NRL. ANSI 1018 steel coupons (4"x6"x1/8") were purchased already prepared for coating. This size was recommended as a minimum acceptable plate size for the accelerated corrosion testing. Smaller steel coupons can have problems related to edge effects. Greater than 50% of all coating failures occur at sharp corners and edges. This is due to rheological properties during film formation resulting in a thinning of the protective film at these points as can be seen in Figure 4.1. The samples ordered were edge ground prior to blasting to help eliminate thinning at the sharp edge.

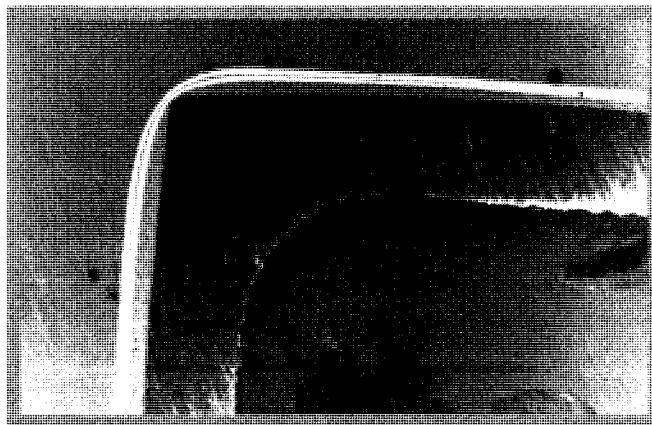


Figure 4.1: Edge Thinning of Epoxy Coating

It is well known that surface preparation is more important than the actual coating system in regards to the successful protection of a steel substrate. The

surface of the sample coupons was specified to meet SSPC – SP5 (NACE 1) white metal blast cleaning as set forward by the Society for Protective Coatings¹⁵⁶. SSPC-SP-5 is a white metal blast cleaned surface that is free of all visible oil, grease, dirt, dust, mill scale, rust, oxides, corrosion products, paint, and other foreign matter. This surface preparation results in the highest possible performance of an anticorrosion coating system as all surface contamination is completely removed. The samples come thermal sealed in heavy polyethylene bags and are certified to SSPC-SP-5 standards.

Samples were purchased from KTA-Tator Inc. (115 Technology Drive Pittsburgh, PA 15275). This source was recommended and used by the NRL in their Key West Facility. All of the steel coupons used throughout this work were of the same size, surface preparation, and material.

4.1.1 Anticorrosion Coating for ISP Performance Evaluation

Four different MIL-DTL-24441C type III coatings were acquired from NCP Coatings Inc. (PO BOX 307, 225 Fort St. Niles, MI 49120). Procuring small quantities of this material was somewhat difficult as standard orders for MIL-DTL-24441 coatings are in the tens or hundreds of gallons. This coating was the standard chosen for this work based on the widespread usage in the past by the Navy and recommendations of the NRL staff. Three of the ordered coatings were standard formulations in green, grey, and white. The fourth was formulated as a clear coating without pigmentation for use with a confocal Raman

microscope. The different colors were purchased to aid in visual identification during multiple coat applications.

The MIL DTL-24441C coating provided excellent protection of the sample coupons. In testing the performance enhancing properties of the ISPs the excellent protection of the MIL-DTL-24441 coating made it difficult to quantify enhancement. It was decided to switch to a less effective epoxy base coating for evaluation of the different ISPs synthesized. A coating system was developed based on DGEBA and TEPA for sample coupon preparation (formulation shown in Table 4-1). This system provided a poor coating baseline so that the evaluation of the corrosion enhancement capacities of ISPs was magnified and thereby more easily quantified.

Table 4-1: Formulation of TEPA/DGEBA Coating System

	Mass (g)
TEPA	18.0
DGEBA	80.9
Toluene	25.0

4.1.2 Coating Application

Producing a good coating on the steel plates was the greatest difficulty in regards to the preparation of sample coupons. The small amounts of materials produced in the laboratory made it impossible to follow the NRL laboratories practice of using commercial sized spray equipment. The minimum quantity of coating accepted by the NRL for evaluation is 5 gallons. In this work samples were prepared in gram quantities, making industrial spray application impossible.

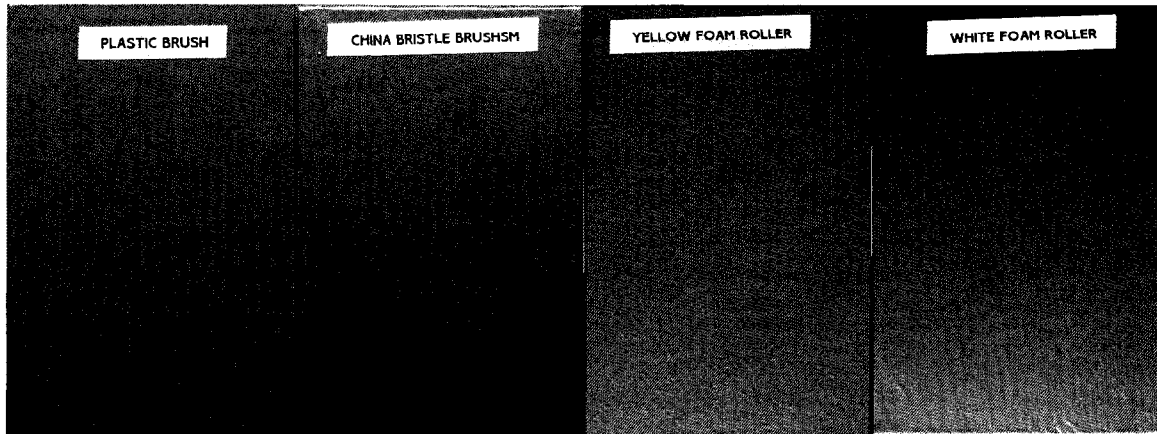


Figure 4.2: Coupons by Different Application Techniques

A range of coating applications was evaluated for their ability to produce good coatings. Several brush and rollers were investigated for their ability to produce good films on the steel substrate with the MIL-DTL-24441 coating. The results of the different application techniques are shown as Figure 4.2. Each application tool left a regular pattern of irregularities in the surface indicating coating regions of different thickness. This would prove problematic as the thin and thick areas could result in polarization of the substrate and artificially increase the corrosion rate. These results determined that no brush or roller application would produce a suitable coating with the MIL-DTL-24441 system.

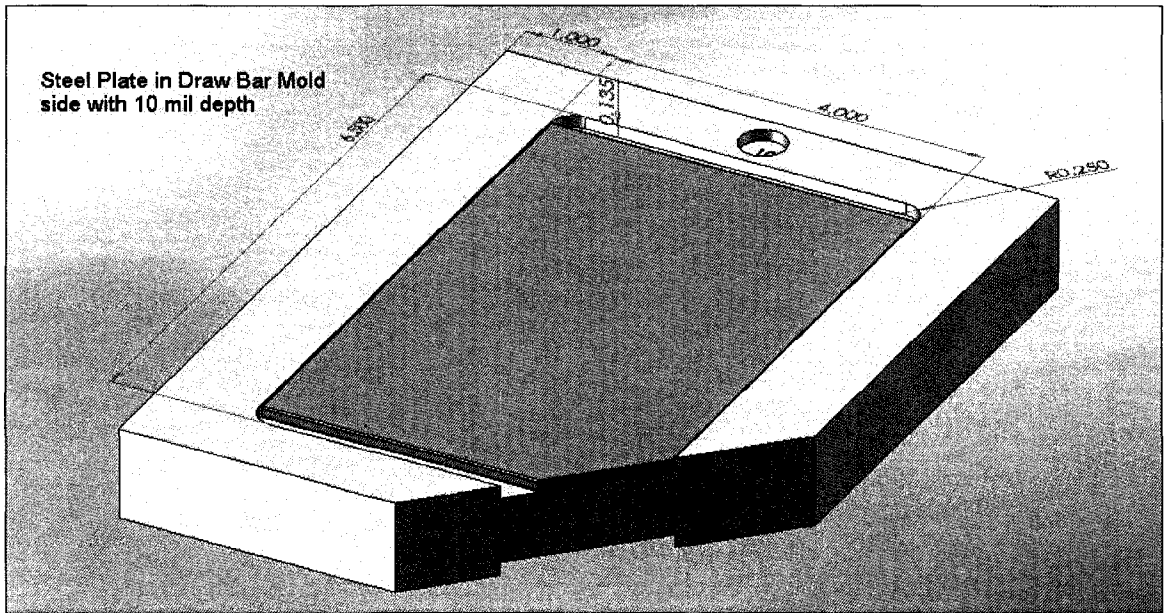


Figure 4.3: Draw Bar Over Plate Mold with Dimensions

A mold was prepared for a draw bar application of the coatings. This was a polyethylene block machined to the specifications shown in Figure 4.3. The steel coupons were placed in the machined recess as shown by the cut away of one corner in Figure 4.3. The mixed liquid coating was poured over the steel coupon and a draw bar pulled across the mold to produce a uniform film. The blocks were machined with two different groove sizes, 10 mil over plate thickness and 20 mil over plate thickness allowing for application of two 10 mil layers if desired.

The draw bar in mold technique was limited to producing only fixed thickness coatings. Later it was decided to move to thinner coatings to help accelerate the corrosion damage. Other problems with the draw bar in mold application technique were sample coupon thickness variation and curvature of the steel coupons. In addition surface irregularities occasionally occurred on

samples prepared by draw bar application as seen in Figure 4.4. It was difficult to get a smooth uniform thickness coating with this application technique.



Figure 4.4: Application Defects on a Draw Bar Application

Following discussion and recommendation of Arthur Webb, the draw bar in mold application method was abandoned in favor of a solvent reduced spray application. This was primarily motivated by the non-uniform film thickness generated by the draw bar method due to variations in the steel coupons. Adding solvent to the coating system changes the film forming and rheological properties as well as affects the protective properties of the dried coating. For the purpose of this work it was decided that this was acceptable due to the scale of sample ISPs produced. Spray application gave control of coating thickness as well as produced excellent uniform films.

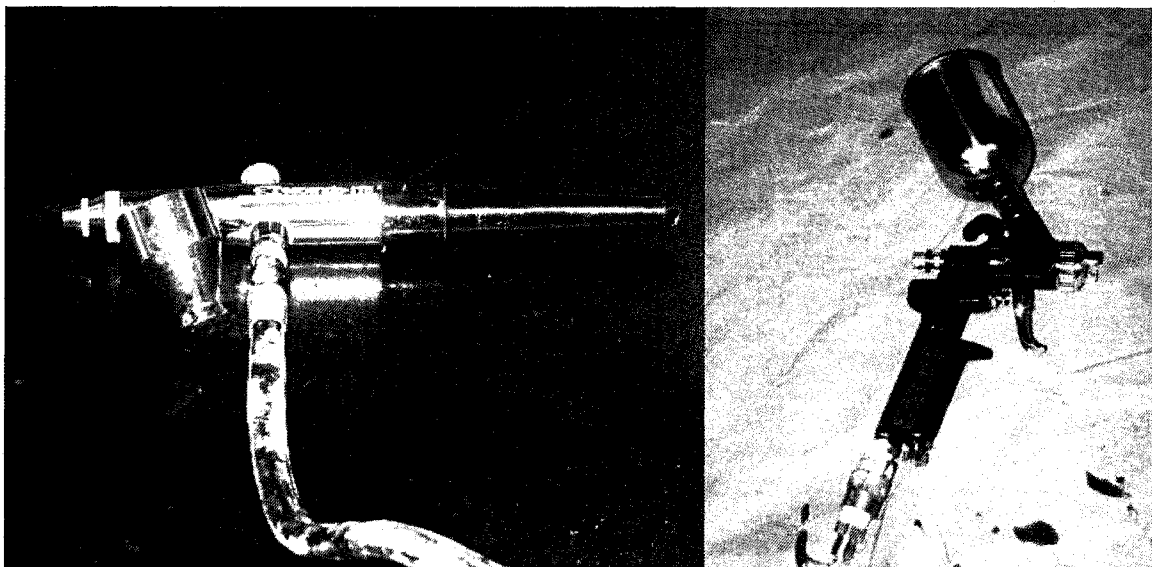


Figure 4.5: Spray Application Tools, Cressendo (left) and Mini Touch up (right)

The two components of the MIL-DTL-24441 coating were mixed together and then 50% by volume of toluene was added as a thinning solvent. Through experimentation it was found that this was the minimum solvent needed to successfully spray the MIL-DTL-24441 onto a steel plate. Steel coupons were positioned at a 45 degree angle by a 90 degree welding magnet during the spray coating process.

The first spray coatings were done with a Cressendo (Model #: 175-7) airbrush manufactured by Badger Air Brush Company (Figure 4.5). The small volume of the airbrush paint cup coupled with the good application control, made this a good application tool for the scale of ISPs synthesized. Unfortunately the limited material transfer rate did not allow for a rapid application. It was difficult if not impossible to apply a single batch mixing to the multiple sample plates required for a given experiment. All samples prepared as part of the same experiment were coated with a single batch mixing of the coating components to

ensure uniformity and eliminate small variations in the ratio of epoxy to hardener between control and ISP test coupons.

The limited material transfer rate was resolved by switching to a AmPro Burgundy Collection Mini Touch-Up HVLP Spray Gun with Regulator (model #: AR6029) shown in Figure 4.5. This spray gun has a fluid reservoir volume of 100 mL. This unit successfully sprayed the sample sizes generated as a course of this project (15-20 mL coating per steel coupon typical). The spray method produces very uniform coatings on the steel coupons as expected and additionally gives a finer control on the thickness of the coating.

In order to amplify the corrosion damage the coating thickness was reduced from the 10 mil generated in the draw bar molds to 3-4 mil wet thickness coating in the spray application. The post B117 scribe evaluation results were more easily quantified with the thinner coating as the corrosion effected area was increased.

4.1.3 Interaction Between ISPs and Coating

Despite the fact that ISPs made by the synthesis outlined in 2.1.1 were free flowing powders it was impossible to re-disperse them successfully into an epoxy based coating for application. At first this was thought to be pigment shock, a phenomenon where the dry pigment added to the coating causes localized reaction and/or agglomerations that can not be dispersed afterwards. Pigment shock is prevented by first dispersing dry pigments in solvent prior to mixing.

When ISPs were added in solvent the effect of the pigment on the amine component was actually worsened and intensified. The ISPs were added to the amine component of the epoxy coating as it was feared they would react with the epoxy component over time. The ISPs had to be stable in one of the coating components as standard shipyard practices make their addition to the coating system at application time improbable at best. The ISPs were associating with the amine components resulting in large agglomerates most likely due to ionic exchange. In the worst cases the ISPs in solvent instantly turned the liquid amine component into a viscous paste, gel, or solid.

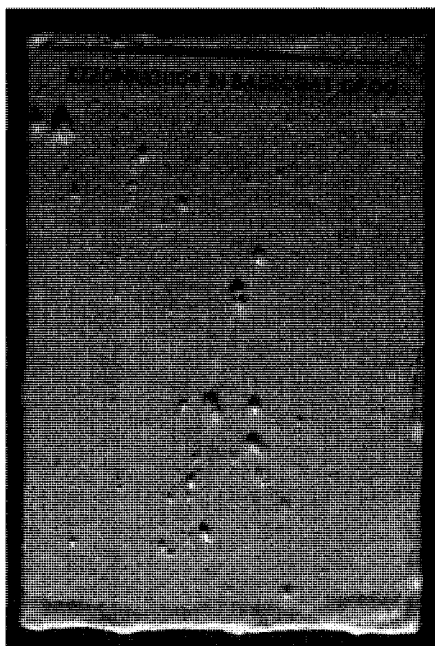


Figure 4.6: Coating Containing Early ISPs

By addition of the dry ISPs (5% by weight) to the mixed MIL-DTL-24441 coating it was possible to prepare a sample coupon shown in Figure 4.6. The agglomerations caused by the pigment can be seen as the large solid

perturbations raised from the coating surface. This was the only sample prepared with ISPs not protected by the PMMA encapsulation step.

4.2 Accelerated Corrosion Experiments

Three qualifying experiments were initially selected to determine the anticorrosion properties of the ISPs. Of these experiments the 90 day cathodic disbondment was abandoned and only the 1000 hr salt fog chamber exposure and 500 hr hot DI experiments were used for all samples.

4.2.1 90 Day Cathodic Disbondment

Cathodic disbondment testing creates a galvanic cell consisting of a magnesium electrode in series with sample coupons in fresh sea water. This experiment tests the destruction of adhesion between the coating and substrate caused by products of the corrosion reactions.

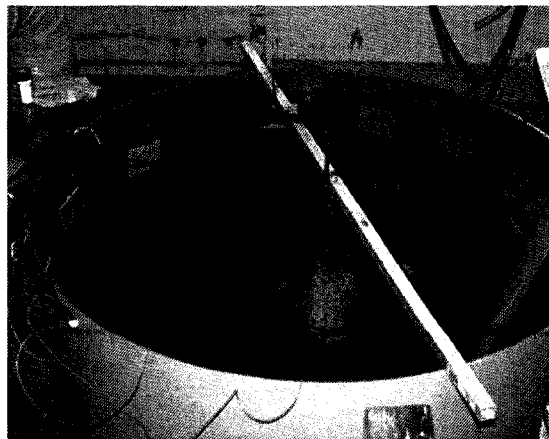


Figure 4.7: Cathodic Disbondment Tank Showing Central Anode and Sample Coupons

UNH has a Coastal Marine Laboratory in Newcastle, NH where we were able to set up a 5 ft diameter tank (Figure 4.7) for cathodic disbondment testing. This site has fresh sea water available and the tank was continually flushed with a slow steady flow. The test method followed ASTM G8, which has a common anode centrally located to all samples in the tank. Sample coupons are subjected to an initial coating defect by a ¼" drilled circle prior to immersion. Samples were labeled on the face as well as additional labeling of the wires going to the anode. Samples were immersed for 90 days, then removed and evaluated.

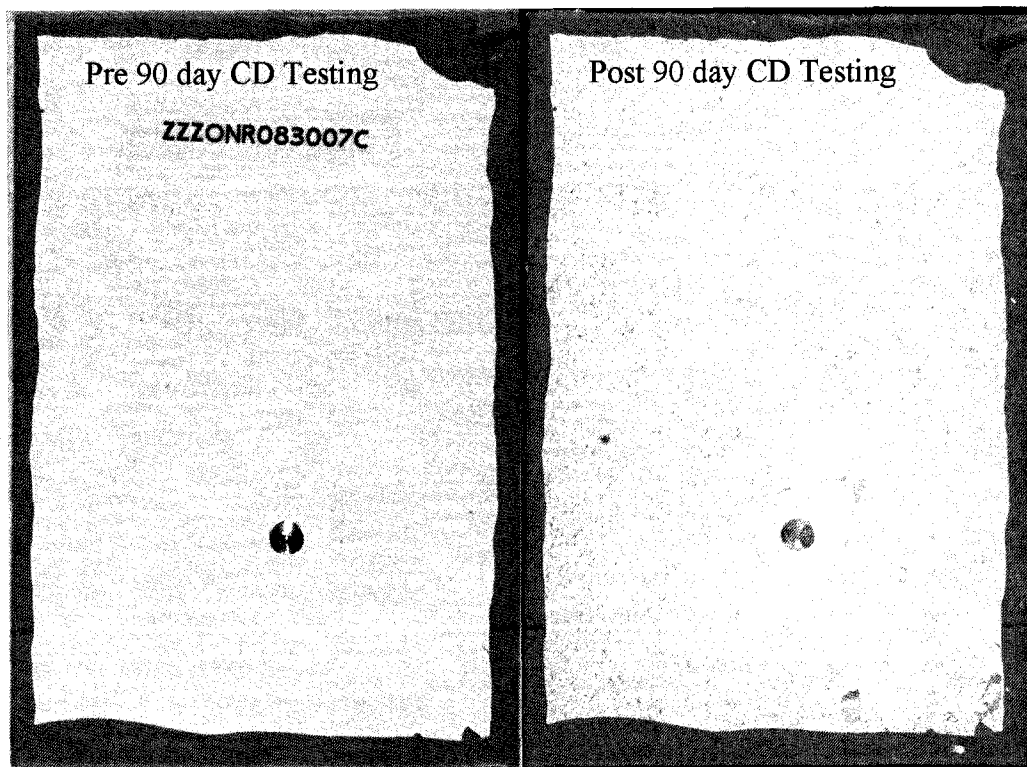


Figure 4.8: 90 Day Cathodic Disbondment Sample Pre and Post Testing

Cathodic disbondment showed no change between those samples containing ISPs and those without. Figure 4.8 shows the typical result from 90 days of CD, the slight discoloration is surface staining/fouling from the sea water. There were no signs of coating disbondment, blistering or corrosion for any sample. Characterization by ASTM D714 – 87 would result in all of the samples being rated at 10 (no blisters). Likewise the ratings for all samples evaluated by ASTM D610 would be 10 (less than or equal to 0.01% rust). This evaluation method was discontinued as the results were uninformative.

4.2.2 1000 hrs Salt Fog Chamber (ASTM B117)

While there is no known coating test or standard that accurately predicts a coatings performance in the field¹⁵⁷, ASTM B117-90: “Standard Test Method of Salt Spray (Fog) Testing” describes the conditions for the most common corrosion test used to evaluate coating anticorrosion performance. The method, involves supporting a sample coupon at an angle of 15 to 30 degrees from vertical in a chamber where they are subjected to a continuous spray of a salt solution at 35C. The salt solution, 5% by weight of sodium chloride in water, is not recycled and the chamber is designed such that condensing droplets do not fall on the sample coupons. A Q-Lab Corporation Q-fog model SSP (Figure 4.9) salt spray chamber was used for this work.

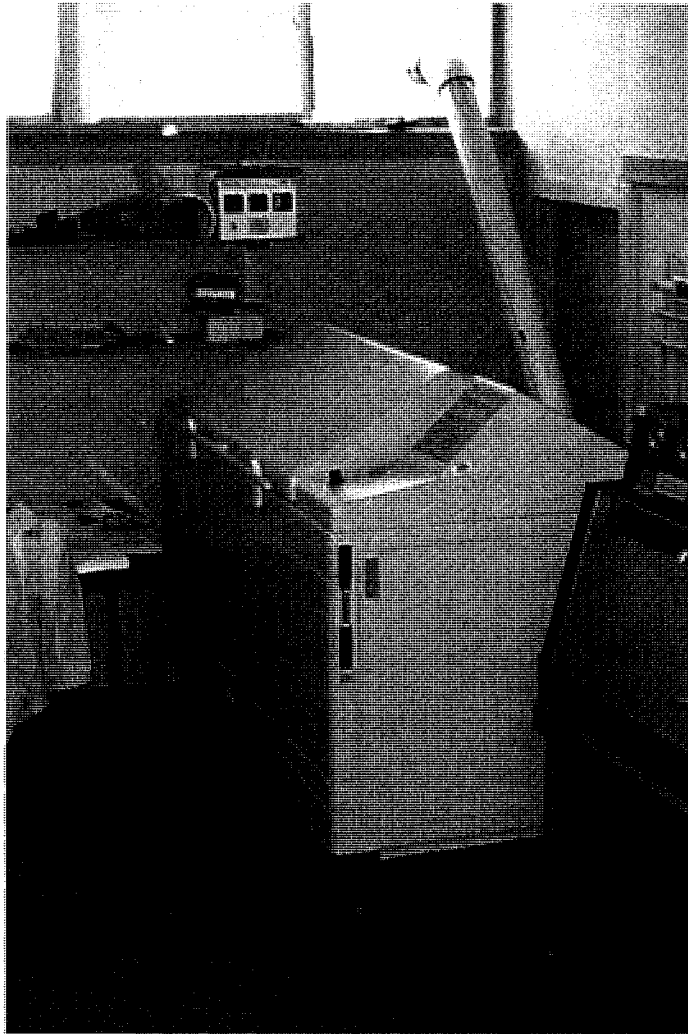


Figure 4.9: Q-Fog Salt Spray Chamber

The samples in Figure 4.10 were prepared using the MIL-DTL-24441C epoxy coating. The samples labeled "a" (left sample) contains with approximately 5 wt % of WISCM ISPs (ZZZONR0100307) whereas the sample labeled "b" (right sample) are for reference (unfilled). The initial samples were scribed 4" with a 1/8" diameter end mill prior to being subjected to B117 conditions for 1000 hrs.

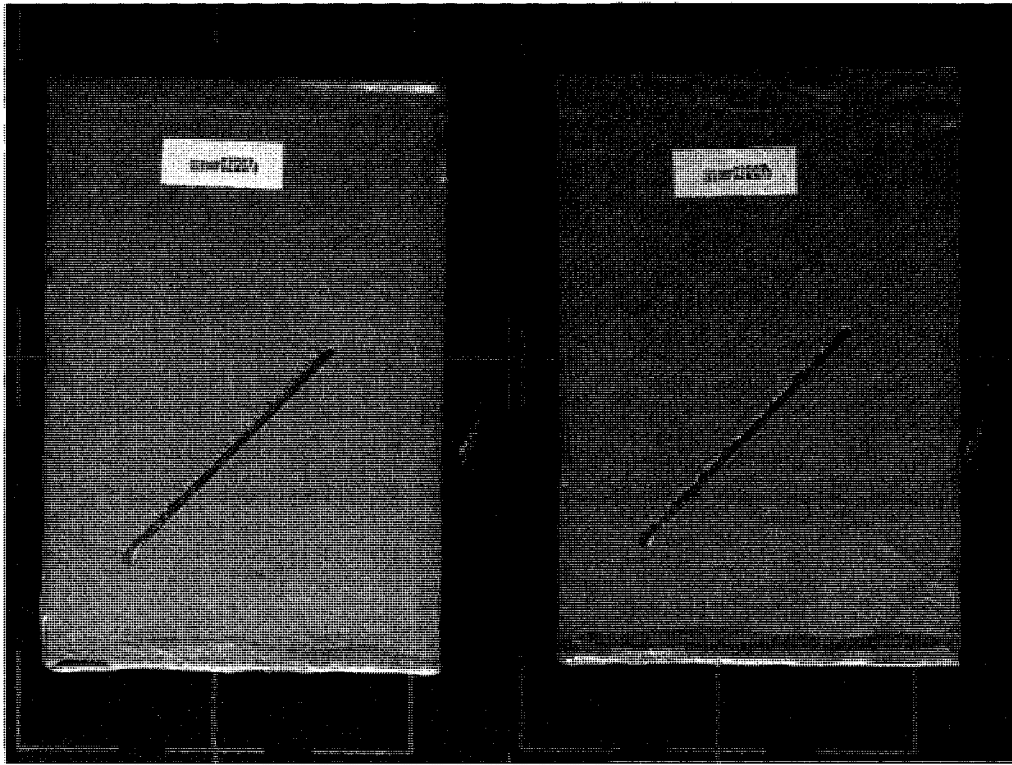


Figure 4.10: Coupons Prepared for Salt Spray



Figure 4.11 Coupons Post 1000 hrs of Salt Spray Exposure

Figure 4.11 shows the same samples as Figure 4.10 after 1000 hrs of exposure in the Q-Fog environmental chamber. The samples were removed; dried; the scribe area scraped; imaged; and evaluated. The scraping is done to remove loose paint and corrosion deposits so that the damaged area around the scribe could be carefully measured and evaluated. The coating and corrosion deposits were removed by hand with a ¼" diameter chisel.

Table 4-2: Rating of Failure at Scribe (Procedure A)

Millimetres	Inches (Approximate)	Rating Number
Zero	0	10
Over 0 to 0.5	0 to 1/64	9
Over 0.5 to 1.0	1/64 to 1/32	8
Over 1.0 to 2.0	1/32 to 1/16	7
Over 2.0 to 3.0	1/16 to 1/8	6
Over 3.0 to 5.0	1/8 to 3/16	5
Over 5.0 to 7.0	3/16 to 1/4	4
Over 7.0 to 10.0	1/4 to 3/8	3
Over 10.0 to 13.0	3/8 to 1/2	2
Over 13.0 to 16.0	1/2 to 5/8	1
Over 16.0	5/8 to more	0

ASTM D1654-92 "Standard Test Method for Evaluation of Painted or Coated Specimens Subjected to Corrosive Environments" is a method for quantifying the damage done during salt spray and other accelerated corrosion experiments. Following the evaluation procedure A as outlined ASTM D 1654, the samples were carefully measured with a digital caliper (Mitutoyo, Model CD-6"C) and recorded. The measurements are recorded as the minimum and maximum damage distance as measured from the pre-scribe. The results of the evaluation are presented in Table 4-3. The ratings are determined by comparison of the measurement value to those in Table 4-2 included in ASTM

D1654. The results for ZZZONR021207 a WISCM based ISP show a 5% improvement in the average minimum rating and a 3% average maximum rating improvement for the sample containing the ISPs.

Table 4-3: Evaluation Results for ZZZONR021207 by ASTM D 1654

ZZZONR021207
as per ASTM D 1654
(Evaluation of Painted or Coated Specimens Subject to Corroive Environments)

Segment	ZZZONR021207A				ZZZONR021207B			
	Min	Rating	Max	Rating	Min	Rating	Max	Rating
A	0.62	8	2.17	6	1.43	7	2.38	6
B	0.95	8	1.53	7	1	7	2.21	6
C	0.87	8	2.01	6	0.77	8	1.89	7
D	0.79	8	1.7	7	0.61	8	1.9	7
E	0.61	8	0.9	8	0.44	9	1.33	7
F	1.11	7	1.58	7	0.98	8	2.53	6
G	0.33	9	1.03	7	1.05	7	1.74	7
H	0.62	8	1.31	7	0.87	8	1.28	7
I	0.39	9	1.26	7	0.75	8	1.3	7
J	0.71	8	1.71	7	1.12	7	1.89	7
Ave	0.70	8.1	1.52	6.9	0.902	7.7	1.845	6.7

Table 4-4: Evaluation Results for ZZZONR082007 by ASTM D 1654

Sample ID	Min Ave	Score Ave	Max Ave	Score Ave	Description
ZZZONR083007A	0.91625	7.75	2.03	6.5	Control with no particles
ZZZONR083007H	0.59625	8.125	1.33625	7.25	~5wt% of ZZZONR070907 ISP encapsulated in PMMA

The SISCM based ISP ZZZONR070907 when added at 5 wt % to MIL-DTL-24441 coating resulted in an average minimum damage score improvement of 3.75% and an average maximum damage score improvement of 7.5% as seen in Table 4-4. The results of salt spray exposure experiments resulted in quantified results showing an improvement caused by the addition of ISPs. Both WISCM and SISCM particles showed improvement over their respective control samples which do not contain ISPs. These results demonstrate that the ISPs aid in the anticorrosion properties when added to the Mil P-24441 coating.

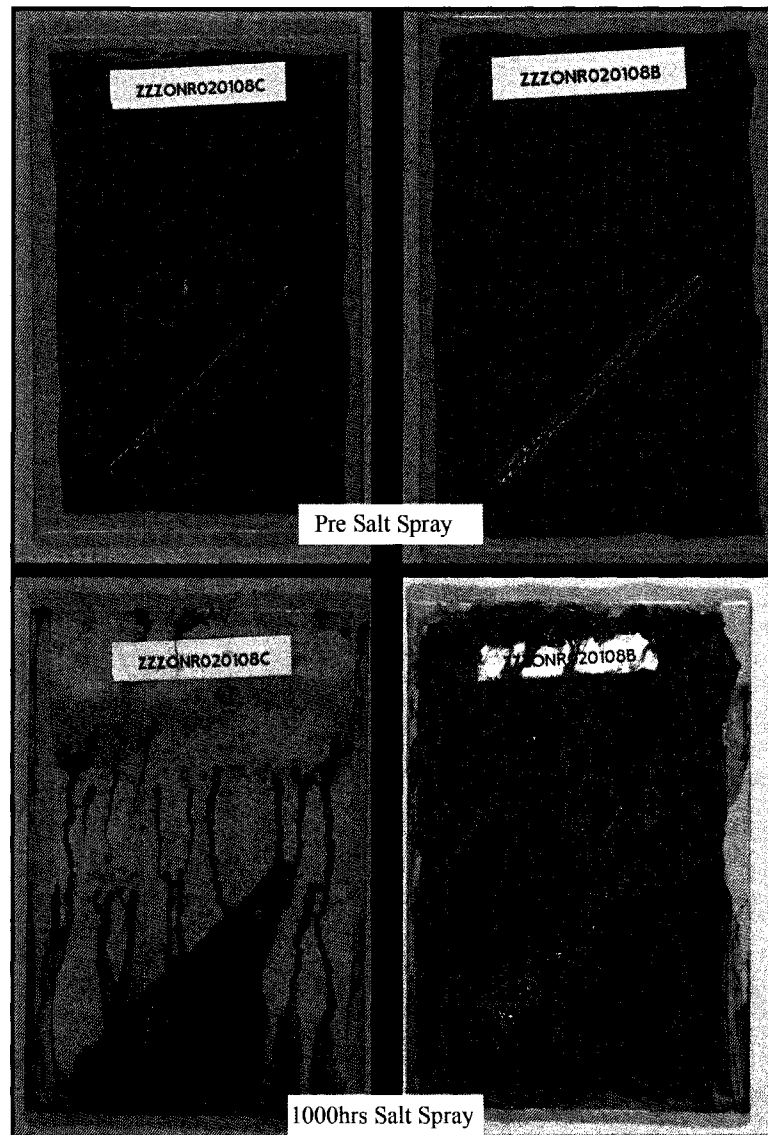


Figure 4.12: Salt Spray Exposure, left samples contains 5 wt % DETONR046 right samples are controls with no ISPs

Figure 4.12 shows the magnified effects of switching to the DGEBA TEPA coating. The increased damage to both samples with the poor coating made it easier to quantify the effect of the ISPs. In some cases this coating system might have been too weak of a coating with plates not containing particles being rated as 0 across the scribe.

Results for the evaluation of all B117 salt spray exposure samples are presented in an abridged format as Table 4-5. In this table, ratings greater than 8.0 are identified in blue, ratings between 8.0 and 7.0 in green, and ratings between 7.0 and 6.0 in yellow to emphasize the increased performance of these samples.

The series of sample coupons in ZZZONR030408 contained ISP loading from 0 to 5 wt %. The plates in this series show an increasing performance with an increasing mass fraction of ISP with the best performance for sample G of this series at 5 wt %.

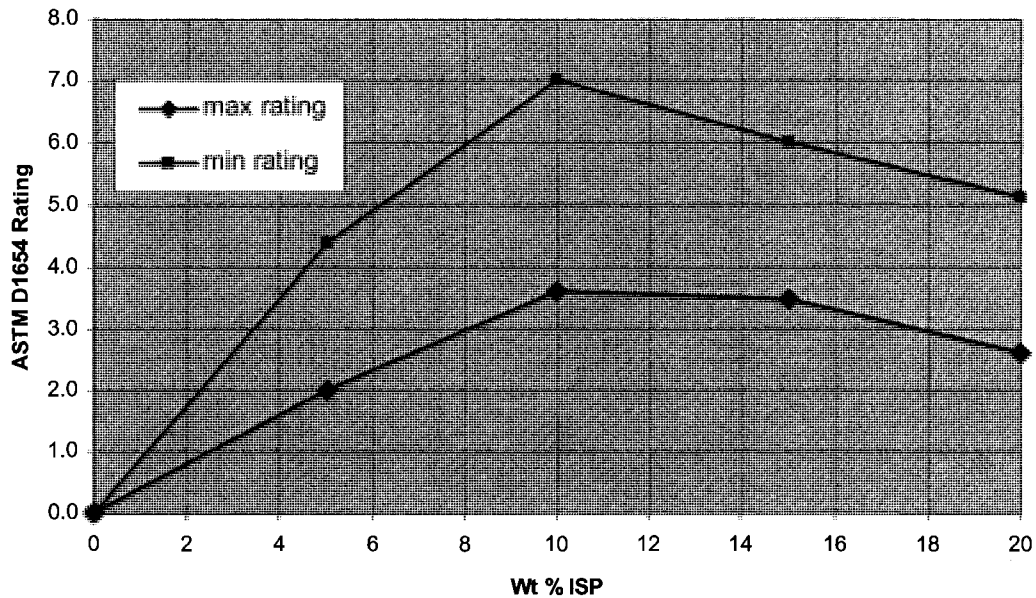


Figure 4.13: Weight % ISPs vs Performance in B117

ZZZONR041408 was a series of experiments with the same particles at higher loading levels up to 20 wt % ISPs with the results shown graphically as

Figure 4.13. This shows that the optimal loading level for this ISP in the coating is 10 wt %. The higher loading levels showed less effective results. The 20% sample was not applied by spray coating as it was too viscous. It was instead poured on to the steel plate and then sprayed with the airstream from the spray gun to a thin layer with the excess coating being blown off the plate. While the CPVC was not determined for ISPs, it is likely that the 20 wt % loading is very near or even beyond the CPVC. This can account for the decreased performance in B117.

The best performance is from SISCM made ISPs ZZZONR042508 at a loading of 5 wt %, sample F of series ZZZONR042608. The remarkable result is not just the average rating of 10 for the minimum, or 7.2 for the maximum damage, but that the unformulated DGEBA/TEPA coating was transformed into a coating comparable to the MIL-DTL-24441 coating.

From the results of the salt spray experiments ISPs generally seem to provide the most effective performance enhancement at 5 or 10 wt % loading of the coating.

Table 4-5: Summary of Salt Spray Plate Evaluations by ASTM D1654

SAMPLE ID	Min	Rating	Max	Rating	ISP ID	wt % ISP	coating
ZZZONR021207A	0.70	8.1	1.52	6.9	ZZZONR010307	5.8	MIL-DTL-24441
ZZZONR021207B	0.89	7.8	1.85	6.7	-----	0	MIL-DTL-24441
ZZZONR083007A	0.92	7.8	2.03	6.5	-----	0	MIL-DTL-24441
ZZZONR083007H	0.60	8.1	1.34	7.3	ZZZONR070907	4.9	MIL-DTL-24441
ZZZONR020108A	1.63	6.9	6.59	4.1	DETONR046	5	DGEBA/TEPA
ZZZONR020108B	16+	0.0	16+	0.0	-----	0	DGEBA/TEPA
ZZZONR020108C	1.21	7.4	2.94	5.6	DETONR046	5	DGEBA/TEPA
ZZZONR030408B	16+	0.0	16+	0.0	DETONR046	0	DGEBA/TEPA
ZZZONR030408C	10.41	0.3	16+	0.0	DETONR046	1	DGEBA/TEPA
ZZZONR030408E	16+	0.0	16+	0.0	DETONR046	2.5	DGEBA/TEPA
ZZZONR030408J	11.36	2.6	26.05	0.3	DETONR046	3.9	DGEBA/TEPA
ZZZONR0304408G	0.90	7.8	2.72	5.8	DETONR046	5	DGEBA/TEPA
ZZZONR041408B	16+	0.0	16+	0.0	-----	0	DGEBA/TEPA
ZZZONR041408D	5.49	4.4	11.54	2.0	ZZZONR040808	5	DGEBA/TEPA
ZZZONR041408F	1.52	7.0	7.20	3.6	ZZZONR040808	10	DGEBA/TEPA
ZZZONR041408H	3.57	6.0	7.09	3.5	ZZZONR040808	15	DGEBA/TEPA
ZZZONR041408J	3.97	5.1	9.48	2.6	ZZZONR040808	20	DGEBA/TEPA
ZZZONR042608B	13.20	1.7	24.90	0.1	-----	0	DGEBA/TEPA
ZZZONR042608D	2.24	6.7	5.04	4.6	ZZZONR042408	2.5	DGEBA/TEPA
ZZZONR042608F	0.00	10.0	1.38	7.2	ZZZONR042408	5	DGEBA/TEPA
ZZZONR042608H	0.39	9.0	2.25	6.3	ZZZONR042408	10	DGEBA/TEPA
ZZZONR042808A	16+	0	16+	0	ZZZONR042508	0	DGEBA/TEPA
ZZZONR042808C	8.162	3.7	15.03	1.6	ZZZONR042508	2.5	DGEBA/TEPA
ZZZONR042808E	0.868	7.8	1.985	6.7	ZZZONR042508	5	DGEBA/TEPA
ZZZONR042808H	0.525	8.8	1.559	7	ZZZONR042508	10	DGEBA/TEPA

The complete data for each salt spray exposure experiment is available in APPENDIX 4. Images of each sample plate taken at intervals from pre exposure through to post exposure are presented in APPENDIX 5.

4.2.3 500 hrs Hot De-ionized Water Immersion

The hot de-ionized water immersion experiments were performed by submerging samples at an angle of 15-30 degrees from vertical in a controlled temperature bath containing de-ionized water at 80C. Samples were removed periodically and images taken on the imaging station recording the progress of

corrosion or lack there of for samples well protected by the coating system. After 500 hrs the samples were removed and imaged one final time.

Table 4-6: Scale and Description of Rust Ratings (ASTM D610)

Rust Grade	Percent of Surface Rusted	Visual Examples		
		Spot(s)	General (G)	Pinpoint (P)
10	Less than or equal to 0.01 percent		None	
9	Greater than 0.01 percent and up to 0.03 percent	9-S	9-G	9-P
8	Greater than 0.03 percent and up to 0.1 percent	8-S	8-G	8-P
7	Greater than 0.1 percent and up to 0.3 percent	7-S	7-G	7-P
6	Greater than 0.3 percent and up to 1.0 percent	6-S	6-G	6-P
5	Greater than 1.0 percent and up to 3.0 percent	5-S	5-G	5-P
4	Greater than 3.0 percent and up to 10.0 percent	4-S	4-G	4-P
3	Greater than 10.0 percent and up to 16.0 percent	3-S	3-G	3-P
2	Greater than 16.0 percent and up to 33.0 percent	2-S	2-G	2-P
1	Greater than 33.0 percent and up to 50.0 percent	1-S	1-G	1-P
0	Greater than 50 percent		None	

The evaluation of corrosion damage for samples subjected to hot de-ionized water immersion was performed as per ASTM D610-01: "Standard Test Method for Evaluating Degree of Rustin on Painted Steel Surfaces". ASTM D610 covers the evaluation of rusted steel surfaces by comparison to visual standards. The numerical rust grade scale is an exponential function of the rust area as presented in Table 4-6 which is included in the standard. The type of corrosion is rated as spot, general, pinpoint, or a hybrid of these three.

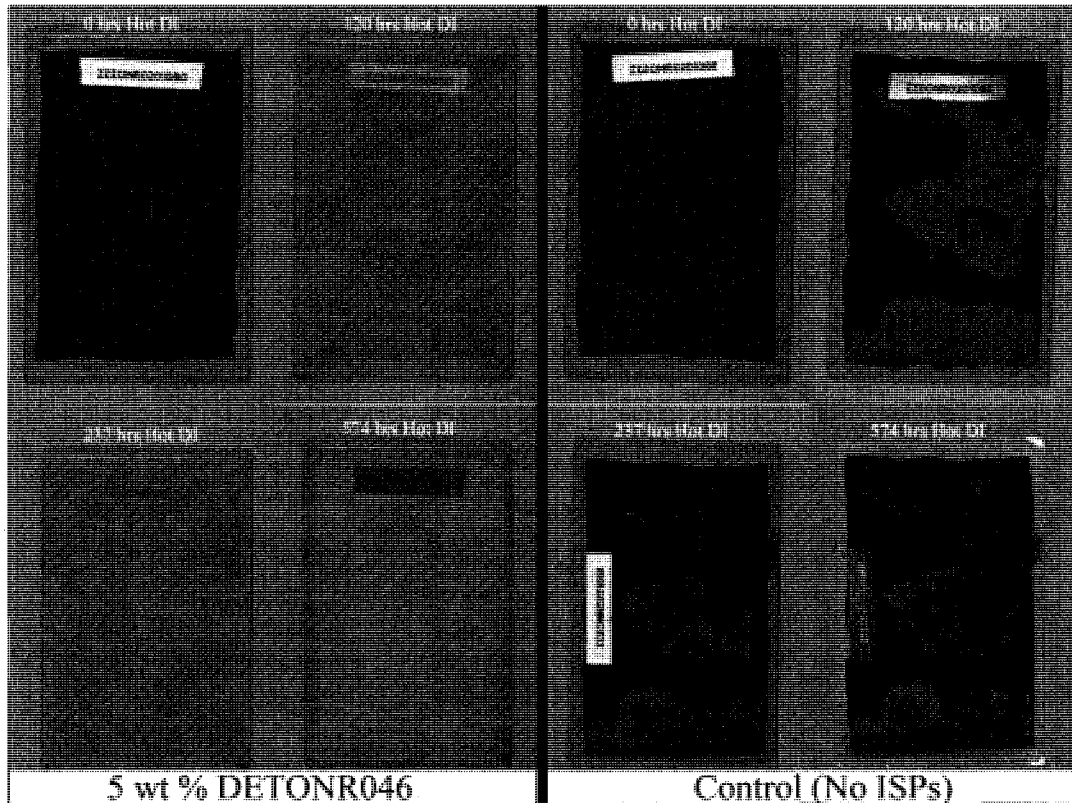


Figure 4.14: Images Hot DI Sample Coupons Showing the Effect if ISPs

Figure 4.14 shows a series of images recorded over the course of evaluation of ZZZONR020108. This was a test using the DGEBA TEPA coating with 5 wt % DETONR046 (D) and without (E). After 574 hrs, sample with 5 % SISCM based ISPs (ZZZONR020108D) was rated at 9P, as there are several small pinpoint areas precluding it from a rating of 10. The control sample (ZZZONR020108E) was given a rating of 1G. The images themselves clearly show the effectiveness of the ISPs enhanced protection of the steel substrate. The same observed improvement due to ISP addition was seen for all samples evaluated during this work.

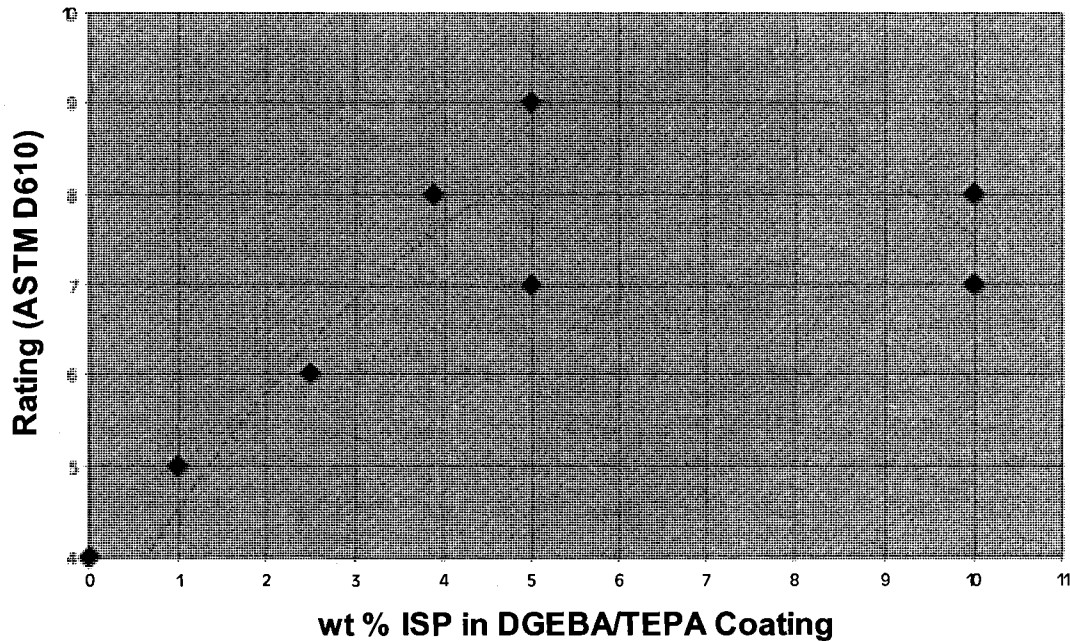


Figure 4.15: Wt % ISP vs. Hot DI Performance

Figure 4.15 displays the experimentally determined rating values versus the ISP loading level in the coating from ZZZONR030408, ZZZONR042608, and ZZZONR042808. Error bars are omitted due to the nature of the data which is relative to the control sample for each experimental batch of sample plates. This shows the best corrosion protection as evaluated by hot DI immersion was experienced at a 5 wt % ISP loading based on the experimental data. As 10 wt % loading was determined to be of greatest protection in regards to the salt chamber experiments, an ideal loading of 7.5 wt % would be a good compromise between the 5 wt % shown by data for hot DI and the 10 wt % maximum for salt spray exposure. Unfortunately no data was evaluated at this loading level during the course of this work. Future work will need to investigate this range to narrow down the best loading level for ISPs in an anticorrosion coating.

Table 4-7: Results of Hot Deionized Water Immersion as per ASTM D610

Experimental ID	wt % ISP	ISP ID	Rating	Notes
ZZZONR020108D	5	DETONR046	9P	3-4 SMALL SPOTS, ALMOST IMPOSSIBLE TO SEE
ZZZONR020108E	0	----	1G	BLACK DISCOLORATION UNDER NON CORRODED AREAS
ZZZONR021607A	2.1	ZZZONR010307	10	NO BLISTERS OR RUST
ZZZONR021607B	0	----	9S	ONE SMALL RUST SPOT
ZZZONR083007B	0	----	10	SOME BLISTERING (FEW SIZE 6)
ZZZONR083007G	4.9	ZZZONR070907	10	SOME BLISTERING (MODERATE SIZE 4)
ZZZONR030408A	0	----	1H	SPOT AND PINPOINT, CLOSE TO A 0
ZZZONR030408D	1	DETONR046	6S	DARKENED SURFACE UNDER COATING
ZZZONR030408E	2.5	DETONR046	6S	DARKENED SURFACE UNDER COATING
ZZZONR030408H	5	DETONR046	9P	
ZZZONR030408I	3.9	DETONR046	8P	8 NOT 9 DUE TO ONE SPOT, COULD BE COATING APPLICATION DEFECT
ZZZONR041408A	0	----	0G	ENTIRE SURFACE RUSTED HEAVILY
ZZZONR041408C	5	ZZZONR040808	6P	
ZZZONR041408E	10	ZZZONR040808	7H	
ZZZONR041408G	15	ZZZONR040808	7H	
ZZZONR041408I	20	ZZZONR040808	8P	SOME BLISTERS (FEW SIZE 6)
ZZZONR042608A	0	----	4G	UNRUSTED AREAS ARE BLACKENED UNDER COATING (MAGNETITE??)
ZZZONR042608C	2.5	ZZZONR042408	6P	
ZZZONR042608E	5	ZZZONR042408	9P	
ZZZONR042608G	10	ZZZONR042408	7P	RUST IS NEAR EDGES WHERE EDGE COATING FAILED
ZZZONR042808B	0	----	4P	GENERAL DARKENING UNDER COATING
ZZZONR042808D	2.5	ZZZONR042508	6H	LARGE CIRCULAR REGION SOLVENT CONTACT @APPLICATION
ZZZONR042808F	5	ZZZONR042508	7S	
ZZZONR042808G	10	ZZZONR042508	8P	

Table 4-7 summarizes all of the results of the hot de-ionized water immersion experiments performed over the course of this work. Images were recorded for each sample plate prior to, during, and post immersion. The image sequences as in Figure 4.14 for each of the hot deionized water immersion samples are presented in APPENDIX 5.

4.3 Summary of Anticorrosion Properties

Sample coupons for testing were prepared successfully by thinning the protective coatings for spray applications. Coatings were applied at a wet thickness of 4 mils on 4" x 6" x 1/8" ANSI 1018 steel coupons prepared and certified at SP5. Both MIL-DTL-24441 and a formulated DGEBA TEPA coating were successfully used to prepare coatings containing ISPs for evaluation.

The anticorrosion properties of the ISPs synthesized have been successfully studied by 500 hrs of hot deionized water immersion and 1000 hrs of salt spray exposure. The results show that the ISPs enhance to varying degrees the corrosion resistance of the coatings to which they are added for all cases. The ISPs synthesized in this work function best in regards to anti corrosion protection in a coating at loading levels of 5-10 wt %.

Actual peak efficiency of the ISPs is likely to change from one coating system to another. Each system would need to be evaluated individually to determine the optimal ratio, with a specific focus on the region between 5 and 10 wt % being studied. This work has provided a methodology for such future evaluations.

CHAPTER 5

CONCLUSIONS & RECOMMENDATIONS

5.1 Conclusions

The SISCM based synthesis of ISPs has been shown to be reproducible, and has successfully produced large enough quantities of ISPs for anticorrosion performance evaluation. This process also has the possibility of being scaled up to produce industrial quantities. The ISPs synthesized meet the requirements needed to be incorporated into existing anticorrosion coatings. With the ever increasing VOC and raw material legislation worldwide these new environmentally friendly and nontoxic anticorrosion pigments can be utilized to develop even better anticorrosion coatings for not only naval, but other applications.

From this work the following can be concluded:

1. Synthesis of the SISCM core particles should be undertaken at 5 wt % solids. This limits the tendency for the continuous cell or other components to become blocked which in turn ruins the synthesis of the core particles.

2. ISPs can be synthesized with core ratios of phosphate to amine moieties as high as 0.8. Ratios of 0.9 and higher form a solid mass upon drying most likely caused by ionic interaction between particles as they dry.
3. A PMMA shell protects the SISCM sufficiently from the harmful interactions that occur between the unencapsulated SISCM and the unreacted components of epoxy based coatings.
4. The diffusion coefficient for water through the MIL-DTL-24441 coating was determined to be $D=2.01 \times 10^{-8} \text{ cm}^2/\text{s}$. This was derived from the ATRIR method and agrees with literature values for diffusion of water through epoxy matrixes.
5. The diffusion coefficient of phosphate through the MIL-DTL-24441 coating was determined by ATRIR to be $1.16 \times 10^{-7} \text{ cm}^2/\text{s}$ independent of water diffusion through the coating.
6. The diffusion coefficient for chloride through the MIL-DTL-24441 coating was determined by the differential cell method to be in the range of 2.7×10^{-9} to $5.6 \times 10^{-10} \text{ cm}^2/\text{s}$ without ISPs. The addition of 5 wt % ISPs to the coating had the effect of decreasing the diffusion coefficient by an average of 25.5%.
7. The best observed corrosion performance in terms of 500 hrs hot DI exposure occurs when ISPs are added at 5 wt % to the coating.

8. The best observed corrosion performance in terms of 1000 hrs of B117 salt spray exposure occurs at an ISP loading level of 10 wt % to the coating.
9. The ion sequestering capacity of ISPs improve with increasing phosphate loading level of the core particle
10. The use of a poor unformulated epoxy coating can help amplify the effects of additives in regards to determination of their corrosion protection enhancement. The use of an unformulated coating eliminates any supplementary effects of additives and anticorrosion pigments in a formulated coating as well as increases the corrosion rate of the steel substrate.
11. The benefit of adding SISCM ISPs to existing “good” coatings was shown by the increase (3-7% by ASTM standard methods discussed in this work) in corrosion performance under the preliminary evaluation periods investigated.

5.2 Recommendations for Future Work

Given the promising results, the development of ISPs should continue and be taken to the next level. The ISPs synthesized in this work have paved the road to a new type of anticorrosion pigment, but the path to industrial implementation is long and has only just begun. The following recommendations for future work should be carefully considered and implemented for the successful continuation of ISPs development in the future.

- The addition of molybdate ions into the initial ion sequestration core should be studied. By adding small quantities of molybdic acid (H_2MoO_4) or phosphomolybdic acid ($\text{H}_3\text{Mo}_{12}\text{O}_{40}\text{P}\cdot\text{H}_2\text{O}$) the protective properties provided by ISPs could be further enhanced. Literature has stated that the molybdate ion has excellent anticorrosion properties and that it works synergistically with the phosphate ion at mass quantities as low as single percentages of the phosphate mass.
- The synthesis process for the SISCM should be converted to a continuous process. This would require the purchase of additional equipment and application of process control to balanced the continuous system parameters. The continuous process when optimized should produce more uniform chemically balanced SISCM particles as there would not be any recycled already formed particles interfering in the synthesis. The encapsulation by PMMA would remain a batch process but this could be scaled up and performed in larger quantities in a 10L reactor.
- ISP containing coatings should be subjected to a larger array of evaluative corrosion testing. The qualifiers chosen and implemented in this study are only some of the many tests applied by the NRL and the original goal was to produce and screen successful candidates to be tested by the NRL. The next phase of study should produce sufficiently large batches (0.5-1.0 kg) of ISPs and send them to the NRL Laboratories

for independent evaluation and testing by the experienced staff at this facility.

- ISPs should be evaluated in different coating types. This study only investigated their effectiveness in epoxy based chemistries. In theory the ISPs could be utilized in a broad array of anticorrosion coatings binder systems. Certainly it should be incorporated and evaluated into urethane, alkyd, and acrylic binder systems.
- The CPVC should be determined for the new continuous process synthesized ISPs as well as for the SISCM based ISPs. The CPVC is determined by an in depth study of different loading of particles into a coating and subjecting the coupons prepared to many controlled corrosion experiments. This would be a project in and of itself but the data is necessary if ISPs are to be successfully implemented commercially.

APPENDICES

APPENDIX 1

HOMOGENEOUS ISPs

This appendix contains the details on the development of homogeneous ion sequestration particles. The material presented in this appendix differs from the body of this work in that the synthesis, characterization, and properties are presented together.

A1.1 Introduction to Homogeneous ISPs

The homogeneous approach provides some useful reference material however the contribution to the successful synthesis development is minor. This work is included for the sake of completeness as well as to provide scientists who might continue this research with the methodologies that were unsuccessful so that resources are not squandered in the future.

The homogeneous ISP was an alternative approach investigated alongside the early batch and semibatch ISPs. Instead of striving for a core and shell morphology this approach attempted to develop a homogeneous particle. This was to be formed by radical polymerization of allylamine coupled to phosphoric acid droplets suspended in heptane. The allylamine would polymerize around the phosphate ions which would act as crosslinks to maintain the structure of the

particle. It was postulated that the ionically coupled network could be further solidified by the addition of covalent crosslinks from the incorporation of the comonomer diallylamine. This rigid network would not release the phosphate ions easily and maintain the structure of the homogeneous ISPs.

A1.2 Synthesis of Homogeneous ISPs

The synthesis of homogeneous ISPs consists of an inverse phase radical polymerization in heptane. The overall process is outlined in Figure A1.1 which shows the basic components and the sequence of the synthesis.

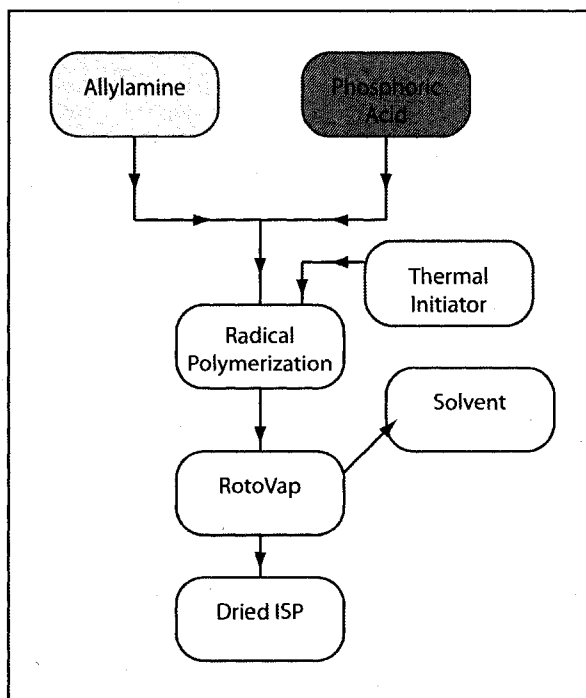


Figure A1.1: Synthesis Scheme for Homogeneous ISPs

Crystalline anhydrous phosphoric acid (mp 42.35 C) was melted at 50C, degassed with an argon purge for 20 min and dispersed in 200 mL of heptane at 50C by the ultraturrax fitted with the immersion tool and placed through the

center neck of a 500 mL jacketed reactor. A condenser at 5 C was used to prevent the evaporative loss from the reactor. Mono-n-dodecyl phosphate was added at 4 wt % of reactants to help stabilize the heptane dispersion.

Allylamine diluted in heptane (10 wt % conc) was then added to the solution and allowed to interact with the dispersed phase of phosphoric acid. The ratio of allylamine to phosphoric acid was calculated such that there were two primary amines for each phosphoric acid molecule. The PKa of allylamine is 9.7¹⁵⁸ and is strong enough to interact with both the first and second proton on the phosphoric acid but not the third.

Table A1-1: Experimental Details for ZZZONR110904

Reactant	Mass (g)	Mw	Moles	Functionality
Allylamine	12.000	57.095	0.210	1
Phosphoric Acid	10.298	97.990	0.105	2
AIBN	0.24			
Mono-n-dodecyl phosphate	0.891			

An argon purge was submerged to remove dissolved oxygen from the heptane and reactants. After 30 minutes the purge was raised above the liquid level but continued to provide an argon blanket to exclude oxygen from the system. A radical initiator, AIBN (dissolved in 1-2 mL of acetone) was added and the temperature was increased to 80C. As the reaction proceeded the milky white suspension yellowed slightly. The reaction was allowed to proceed for a period of 6 hrs after which the temperature was lowered to room temperature. The particles were dried on a rotary evaporator at reduced pressure. The dried powder formed a cake like solid but was easily redispersed into heptane. The quantity for each chemical used for this synthesis is presented as Table A1.1.

A1.3 Characterization of Homogeneous ISPs

Solid state NMR was performed to determine if the allylamine polymerized. Solid state NMR is a useful tool for samples that can not be readily dissolved in a solvent as was the case with the homogeneous ISPs. Typically the signal to noise ratio is not as good as for solvent NMR and the time needed to collect data is considerably longer.

The solid state NMR spectrum for the polyallylamine ISPs is shown as Figure A1.2. Modeling of the theoretical shifts for polyallylamine was done at the UIC facility with the help of Kathy Gallagher. The peak at 30-45 is for the backbone chain carbons. Had there been any unreacted allylamine in the particles there would have been a peaks at ~110 and 140, therefore we can say that there is no allylamine present in the ISPs.

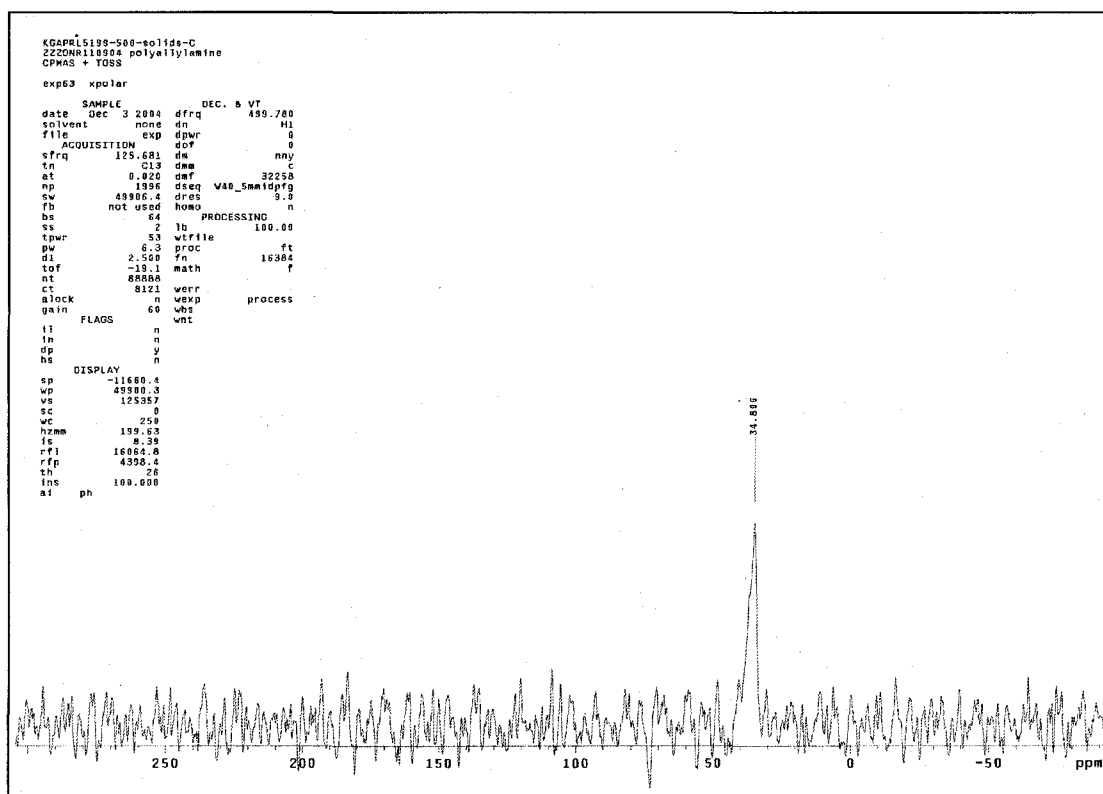


Figure A1.2: Solid State NMR spectra of Polyallylamine ISPs

Liquid NMR was also performed to determine that there was no unreacted allylamine remaining in the solvent post reaction. This sample had the particles separated and removed by centrifugation prior to being run. It was concluded that the allylamine polymerized and was present only in the microparticles. Allylamine is a strong irritant and poses health hazards so the NMR work was done to prove that there is no remaining allylamine in the particles or solvent.

An aqueous GPC (Gel Permeation Chromatography) was set up on an Agilent HPLC system. By analyzing a series of similar monomers of varying molecular weights a calibration table (see Table A1-2) was developed for use with polyallylamine characterization.

Table A1-2: Calibration Data for Aqueous GPC

Chemical	Mw	Elution time
Diethylene Glycol	106.12	32.67
Triethylene Glycol	150.15	30.83
PEG 400	400.00	24.90
Allyl Amine	57.40	38.21
Diallyl Amine	97.16	37.40

The homogeneous ISPs were partially soluble in PBS buffer used with the aqueous GPC set up. A representative plot is shown as Figure A1.3. The molecular weight of the allylamine was found to be approximately 400g/mol. This is not truly a macromolecule but instead oligomers with chain lengths of approximately 8 allylamine units. This was considerably longer than the TEPA used in the encapsulated ISPs synthesis and seemed to be effective at maintaining particle integrity. There is likely some minor crosslinking or other

strong interaction occurring during the polymerization as the particles are not 100% soluble in any common solvent as they should be if there was no crosslinking.

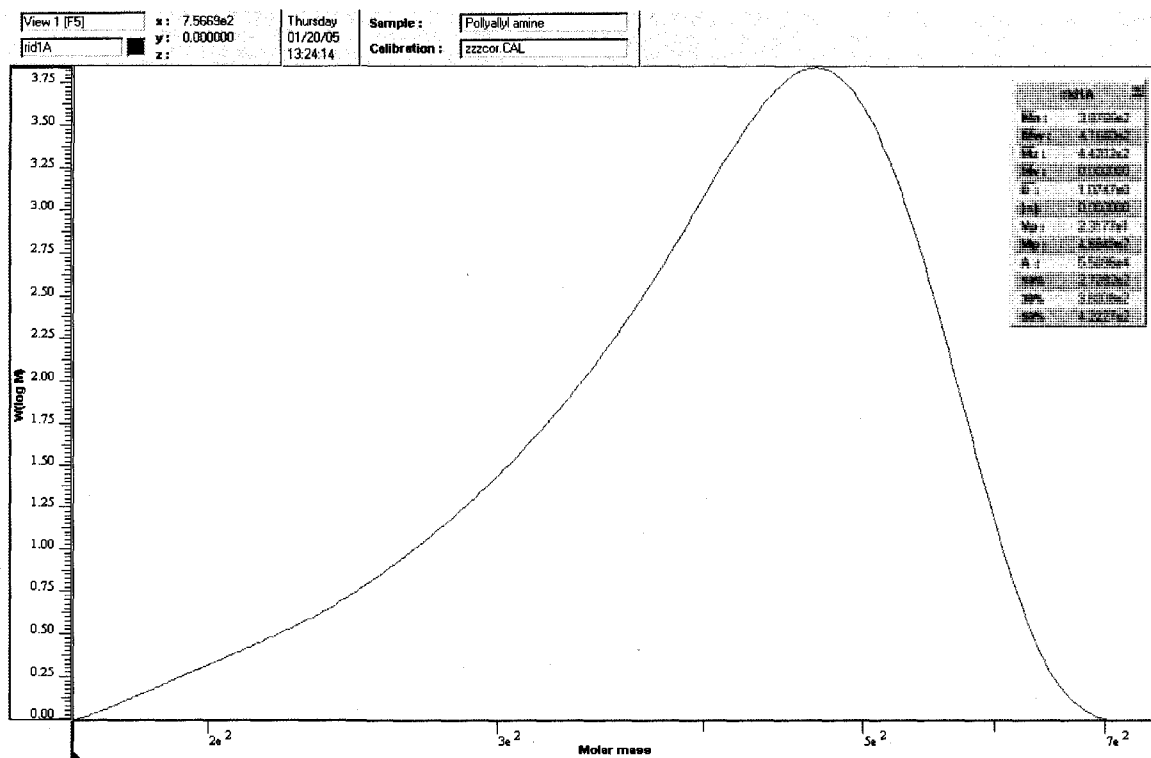


Figure A1.3 Aqueous GPC Results for ZZZONR110904

A1.4 Synthesis Variations

In order to produce longer polymer chains for the homogeneous ISPs, copolymerization of allylamine with maleic anhydride and ethyl vinyl ether were performed. The goal was to determine if it was possible to synthesize higher molecular weight polymer. It was considered that the limited mobility of the associated allylamine may have had a role in limiting the molecular weight of the polyallylamine synthesized. The copolymerization with maleic anhydride

(ZZZONR032105) was unsuccessful at producing high molecular weight polymer. However it was possible to successfully produced larger chains by copolymerizing allylamine with ethyl vinyl ether (ZZZONR032005) with Mn as high as 436,000 g/mol.

Synthesis of a more crosslinked homogeneous ISP was attempted by utilizing diallylamine as a comonomer (ZZZONR022405). The diallylamine was added at a molar ratio of 1 to 4 with the allylamine, while maintaining the total amine to phosphate ratio at 1:1. The addition of diallylamine resulted in an unsuccessful reaction with no discrete ISPs formed. At this point literature was revisited in order to find hints as to the difficulties in polymerizing allylamine.

A1.5 Summary of Homogeneous ISP Approach

The homogeneous particle method produced particles that initially tested as good ISPs by titration (see 3.2.5), but no further investigation into this approach was taken. The decision to abandon this approach and focus on other processes was made after a review of the limited literature on polymerization of allylamine which is reportedly difficult¹⁵⁹. Literature clearly states that there is a well know chain transfer to monomer when trying to polymerize allylamine¹⁶⁰. This chain transfer is degradative and prevents the formation of higher molecular weight in either the homopolymer or copolymers of allylamine¹⁶¹. It seems the only way to produce high molecular weight polyallylamine is by radiation polymerization¹⁶². This limited the probability of success for the homogeneous ISP and the decision to abandon this approach was made early in this work.

APPENDIX 2

SOLVENT/NONSOLVENT POLYMER PRECIPITATION

A2.1 Introduction

This approach towards ISP synthesis relied on a solvent/nonsolvent polymer precipitation to produce particles in the nanometer size range. A polymer is first dissolved, at dilute concentration (~1 wt %), in a good solvent. By slow drop wise addition of the solution into a miscible liquid (a nonsolvent of the polymer) the good solvent disperses and the polymer collapses onto itself precipitating into solid particle. Chemical modification can then be performed to encapsulate the particle.

This appendix will also cover briefly another alternative approach that was investigated as a spin off of the solvent/nonsolvent process. It is possible to make in bulk PEI coupled to phosphoric acid. This material is a hard solid. It was attempted to use a temperature controlled ball mill to grind this material at low temperature into a fine powder, and then encapsulate this powder in a suspension of heptane.

A2.2 Solvent/Nonsolvent ISP Synthesis

For this method to work it was important to first identify a liquid that was a nonsolvent of PEI that was 100% miscible with water, the good solvent. To this end a series of experiments were performed with different polar solvents¹⁶³. In these experiments a 20 mL glass scintillation vial was filled with approximately 15 mL of each solvent investigated. Into this solvent filled vial several drops of a 50 wt % solution of PEI in water was added. The vial was then shaken to provide agitation. The solution was observed and changes noted. The results of these experiments (ZZZONR061306) are presented in Table A2-1. The solvent selected as a nonsolvent of PEI was acetone.

Table A2-1: Nonsolvent of PEI Selection Experimental Observations

Solvent	Observed Change
Methanol	Clear, no change
Isopropanol	Clear, no change
NMP	Initially milky then returned to clear
Acetonitrile	Milky/foggy solution
Acetone	Solution turns white

The same polyethyleneimine (Mn ~ 60,000 g/mol) was used in this work as is discussed in Chapter 2 for use with the WISCM based ISP synthesis. The PEI comes as a 50 wt % solution in water. This solution was further diluted to a concentration of 1 wt % with ultra pure water. The entire synthesis process is illustrated schematically in Figure A2.1 and the description of the experimental procedure (ZZZONR061516) follows.

The 1 wt % solution of PEI was added dropwise via a 20 ga needle affixed to a 100mL glass syringe. The feed rate is controlled by a digital syringe pump at 2mL/min. The droplets were injected into a stirred jacketed reactor containing a 500 mL of acetone at 5C. Symperonic PE/F68 was used as a stabilizer for the suspension at 2 wt % of the reactants. The particles formed as the water was diluted by the acetone and the “dried” PEI collapsed into a small solid particle suspended in the acetone by agitation.

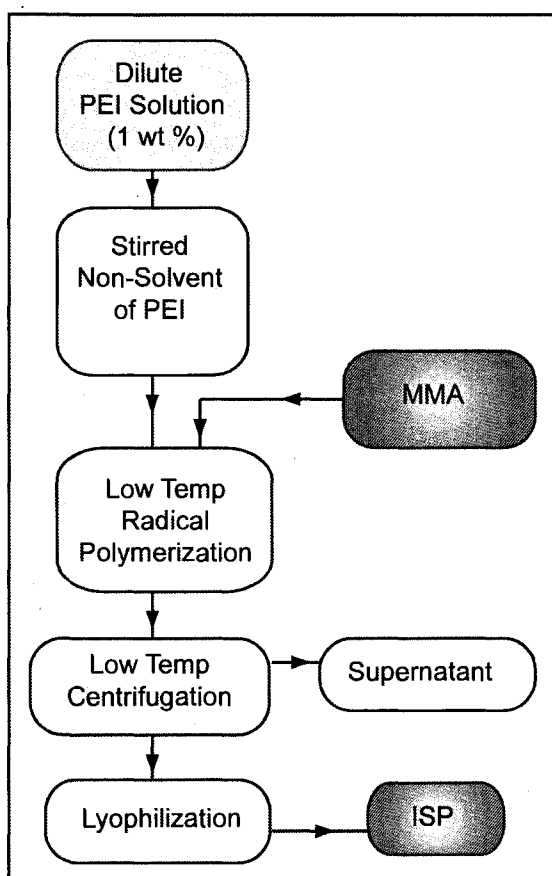


Figure A2.1: Synthesis Scheme for PEI Solvent/Non-Solvent Approach

A dilute solution of phosphoric acid (1 wt %) in acetone was then fed into the suspension of PEI particles by syringe pump. The interaction between the

two solutions forms the ion sequestration core. This core required encapsulation to limit any ionic exchange between the particles so that agglomeration was prevented. Additionally the encapsulating shell would prevent the core from interacting with the liquid amine monomers of the epoxy coating system.

Hexane diisocyanate (HDI) was chosen for the shell material. HDI can polymerize at the surface of the particle both by reaction with unassociated amine moieties of the PEI as well as through self polymerization catalyzed by the amines. The HDI at 1 wt % in acetone was injected into the reactor and allowed to react for 1 hr. Table A2-2 contains the quantity for each reactant used in the experiments discussed in this section.

Table A2-2 Reactants Used for Solvent/Nonsolvent ISP Synthesis

Experiment ID	PEI (g)	H3PO4 (g)	HDI (g)	TDI (g)	Symp. PE (g)
ZZZONE061506	1.5	0.90	0.70	0.00	0.000
ZZZONR062206	3.0	2.43	0.70	0.00	0.124
ZZZONR062806	1.5	0.90	0.70	0.00	0.062
ZZZONR072406	1.5	1.22	0.00	0.57	0.066
ZZZONR080906	1.5	0.00	0.00	0.36	0.000
ZZZONR090106	1.5	0.90	0.00	0.71	0.066

This process produced fine particles in suspension. However upon standard low pressure drying in a rotary evaporator they agglomerated. A successful drying scheme involved lyophilization but due to the volume of acetone and water the process was time consuming. A drying process was developed that utilized low temperature centrifugation to eliminate the bulk of the liquid phase. This drastically reduced the time needed to freeze dry the particles

into a powder. Upon warming the powder agglomerated to form a solid mass. ISPs that required subzero storage were not viable.

As an alternative to the complicated drying process, alternative monomers were considered for the shell material. It was thought that the selection of a different more rigid monomer will produce a shell polymer with a much higher glass transition temperature and eliminate the tendency of the particles to agglomerate. TDI was chosen as this new monomer and particles (ZZZONR090106) were synthesized with TDI as the shell material. This did not result in readily dryable free flowing powder.

Stabilization of the PEI particles prior to association with the phosphoric acid was the next attempted modification to the process. By adding covalent crosslinking to the PEI particles prior to association it was hoped that the mobility and ability to agglomerate would be limited. First an experiment (ZZZONR080906) was done to see if the PEI particles could be stabilized by the addition of TDI without forming coagulum. This was successful and new ISPs were produced with 5% of the amine moieties coupled with TDI prior to the association step. Then an excess of TDI was added post association with phosphoric acid. This experiment (ZZZONR090106) did not produce particles that could be readily dried and stored at ambient conditions.

The water remaining in the acetone was suspected as being the cause of the inability to dry the particles successfully. The acetone, due to a lower vapor pressure, would be removed first during drying. This in effect would concentrate the water which could then solvate the ion sequestering core material. To

prevent this from occurring, the particles were washed by a solvent exchange scheme in order to remove the bulk of water from the system. A SS high pressure ultrafiltration cell was purchased and assembled utilizing teflon membranes typically used for protein purification. After lengthy discussion with membrane manufacturer technical specialists an appropriate membrane was suggested, with the disclaimer that they was no precedent for it being used in this manner. Particles were subjected to washing with 2 complete exchanges of hplc grade acetone. This technique was not successful in preventing agglomeration upon drying, indicating that remaining water re-solvating the core was not the problem.

A2.3 Characterization

A Nanotrak 250, a dynamic light scattering based particle size analyzer was used to characterize the size and distributions for the ISPs produced by this method. The solvent/nonsolvent approach has successfully and reproducibly synthesized particles of 100-200 nm diameters. This size characterization was done on the particles dispersed in acetone. A representative nanotrak result is shown as **Error! Reference source not found.** and is typical of the narrow distributions seen for the solvent/nonsolvent particle synthesis.

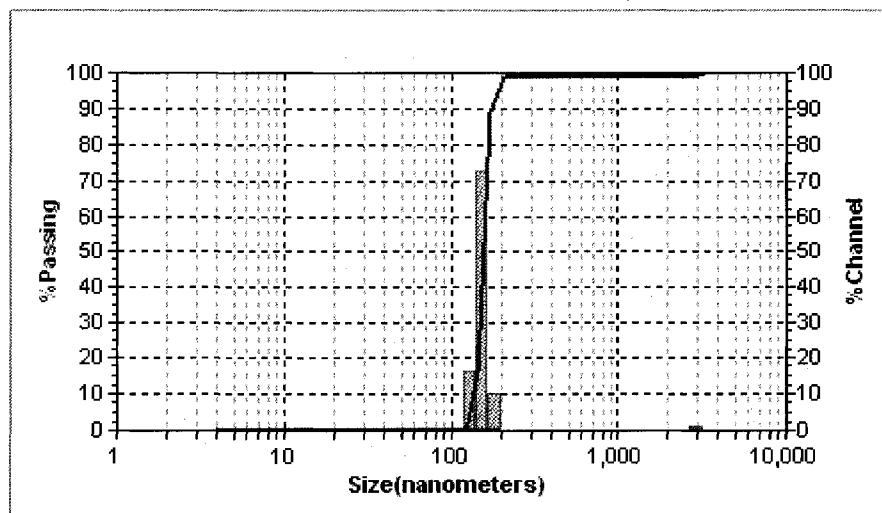


Figure A2.2: Histogram showing particle size for HDI/PEI ISPs (ZZZONR061506)

The solvent/nonsolvent based ISPs had a low temperature glass transition temperature at approximately 11C as shown in Figure A2.3. It was initially suspected that this was due the HDI based shell material and the harder TDI was chosen to replace the HDI. However this change of shell material did not effect the Tg as was expected. The Tg seen for the ISPs with TDI as a shell material actually dropped to approximately 3C as is shown by Figure A2.4.

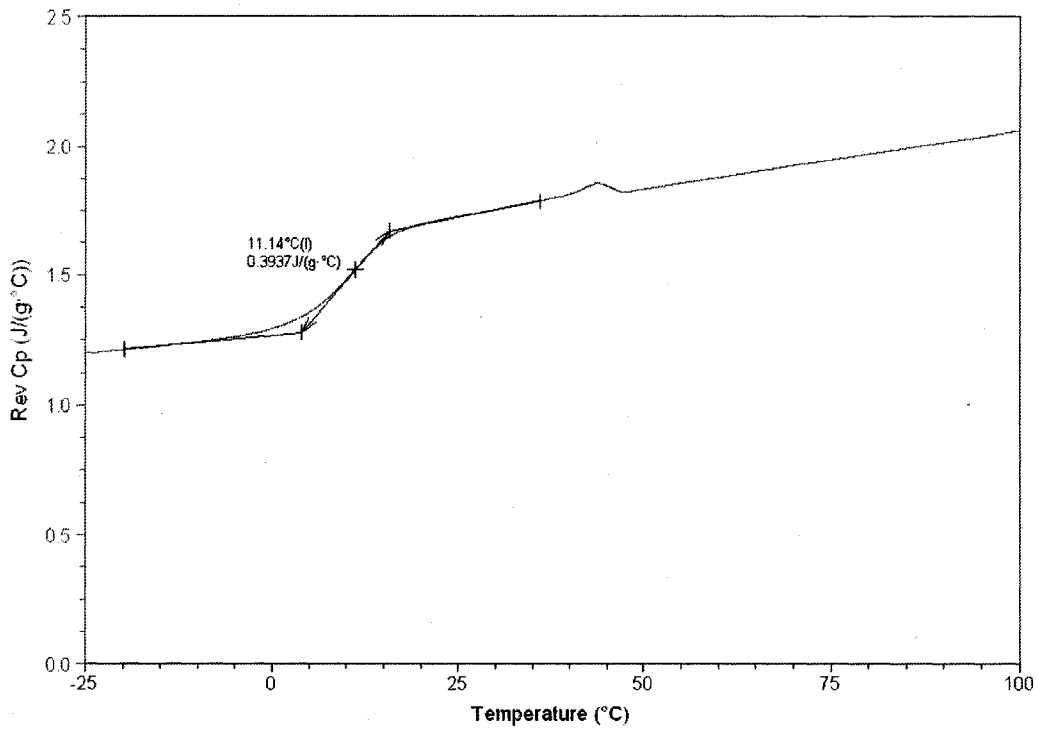


Figure A2.3: DSC plot for ZZZONR06166, HDI encapsulated PEI ISPs

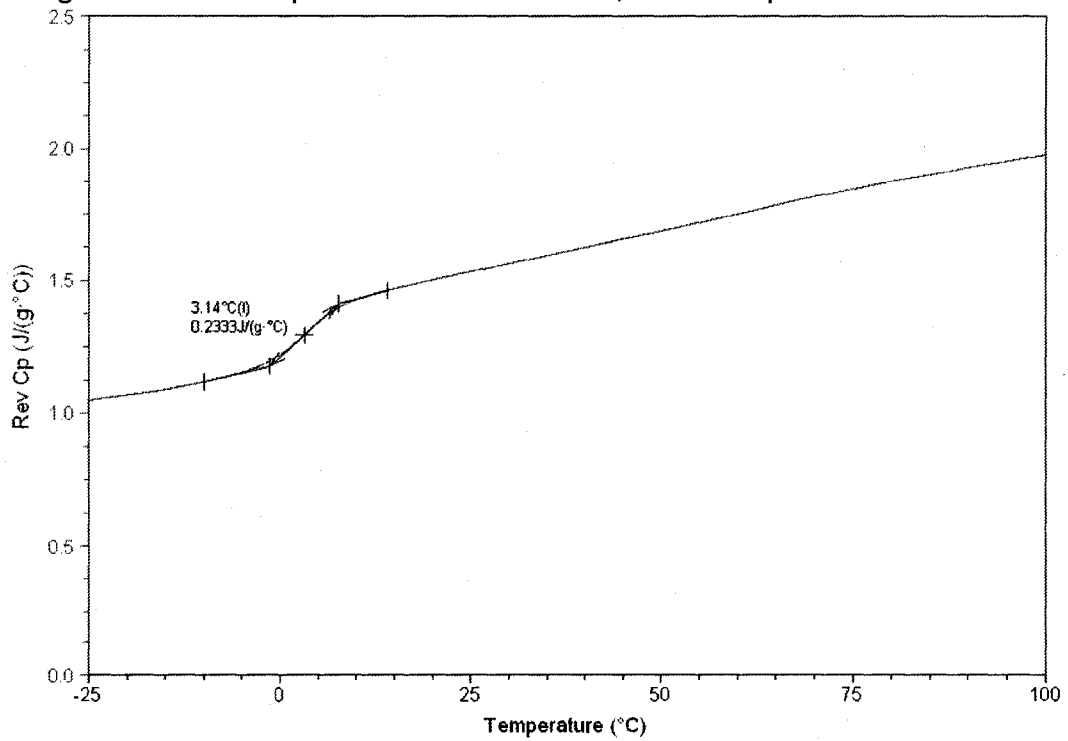


Figure A2.4: DSC plot for ZZZONR072406, TDI encapsulated PEI ISPs

These results were indicative that the low Tg was not of the shell material but instead belonged to the ionic core material. PEI coupled to phosphoric acid was dried at high temperature (100 C) and full vacuum. It was then run on the DSC to determine if the Tg belonged to the core material. There was indeed a transition but not at the expected 3-12 C. Instead the pure PEI/phosphoric acid core had a glass transition at 20-30 C which is slightly higher than that seen for the ISPs. This data is presented in Figure A2.5.

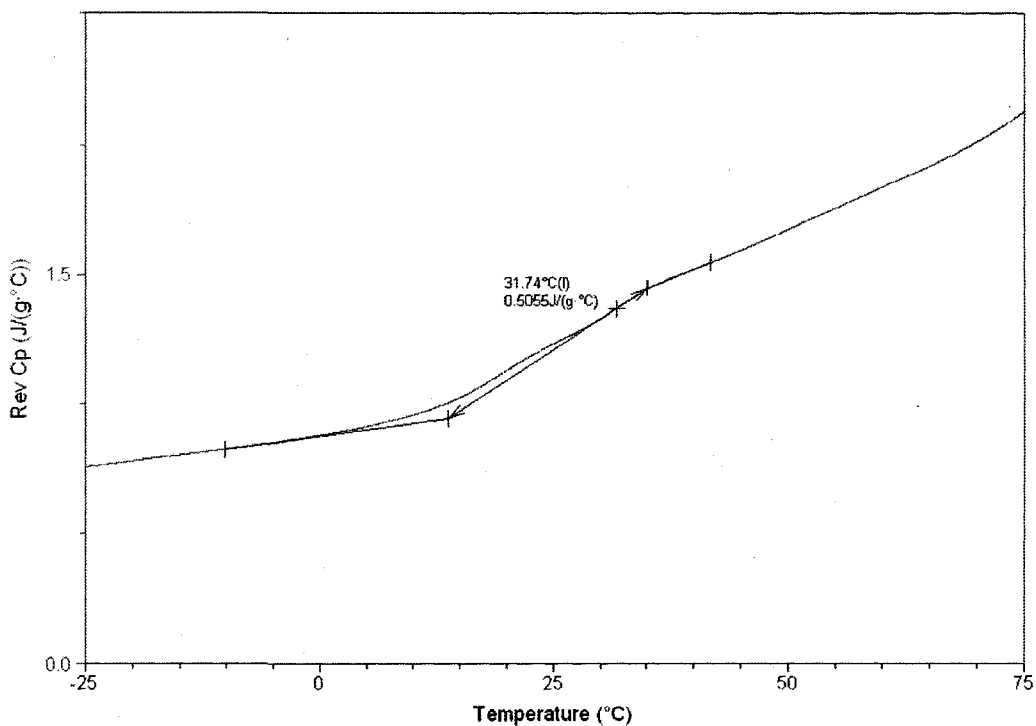


Figure A2.5: DSC showing Transition of PEI/Phosphoric Acid Core Material

The decrease in the Tg for the encapsulated particles could be caused by a hydroplasticization effect of water that was not removed from the core¹⁶⁴. When compared with the drying process used for the pure core material, a much

gentler drying process was utilized for the ISP. It is likely some water remained bound to the extremely hydrophilic core material.

It is also possible that some interaction with the shell polymer resulting in the seen decrease of the T_g. This is unlikely given that the TDI encapsulated ISPs had a lower T_g than those with HDI shells. One would expect the opposite to be true if they were responsible for the shift in the glass transition.

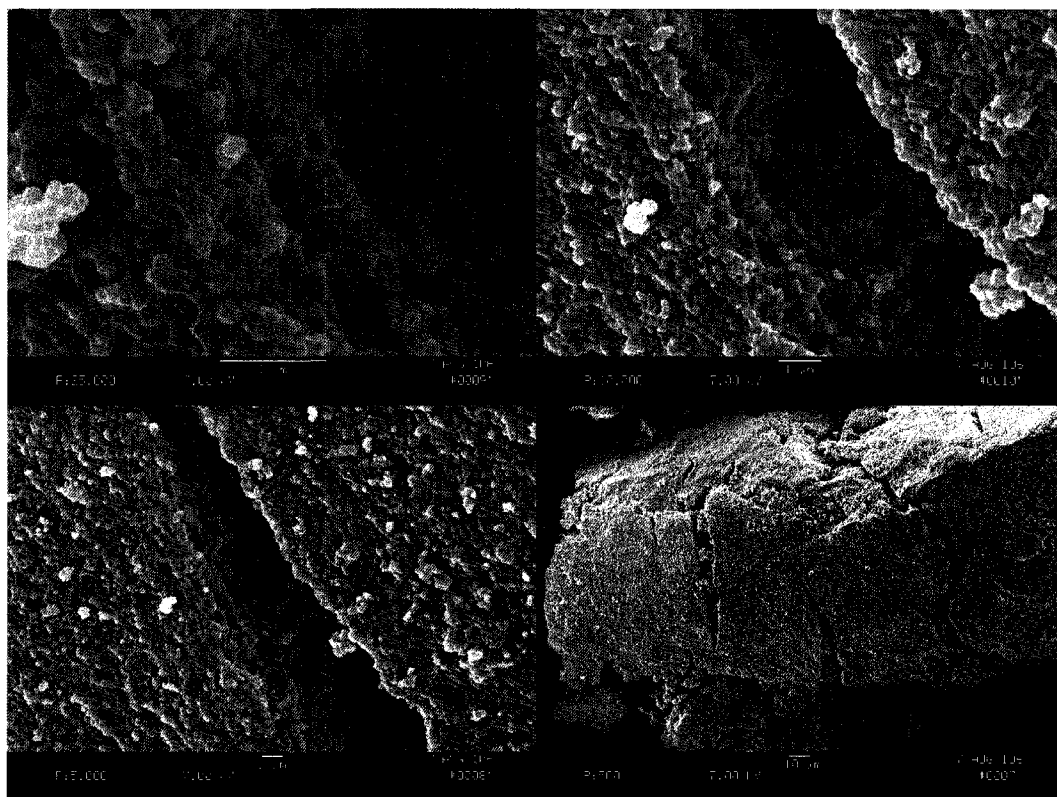


Figure A2.6: SEM images of dried ZZZONR061506

During the early drying attempts the particles were at elevated temperatures and agglomerated. At temperatures above the T_g the core material softens and the shell material was not able to protect the particles. This resulted in the seen agglomeration shown by the SEM images of Figure A2.6.

Similar to what was experienced during earlier attempts to producing core shell ISPs the urea/isocyanurate shell was either incomplete or lacked the strength to sustain the core.

A2.4 Bulk Ion Sequestering Core Based ISPs

The possibility of producing a solid core material consisting of PEI coupled to phosphoric acid was briefly investigated. This material was made by the addition of pure phosphoric acid dissolved in water at 50 wt % concentration to the PEI that comes 50 wt % in water. The solution containing the associated components was then dried at 60C and full vacuum in a rotary evaporator. This produces very hard solid chunks of the core material. First a small batch of 8g total (ZZZONR082906) was produced and then scaled up to produce 100g of bulk material (ZZZONR091106) successfully.

This hard bulk material was then taken to Bentley Pharmaceuticals where a low temperature ball mill was utilized to grind the material into a fine powder. The ball mill went through a programmed grinding cycle of 30 minutes where the temperature was maintained at 5C. Small carbide balls inside a rotating and oscillating carbide chamber perform the actual grinding. This method produced a fine powder while at low temperature and dry. The particle size distribution from the grinding was and is represented in the histogram presented as Figure A2.7. The size ranged from 1um to 200 microns. This sort of wide particle size distribution is a common of ball mill ground powders.

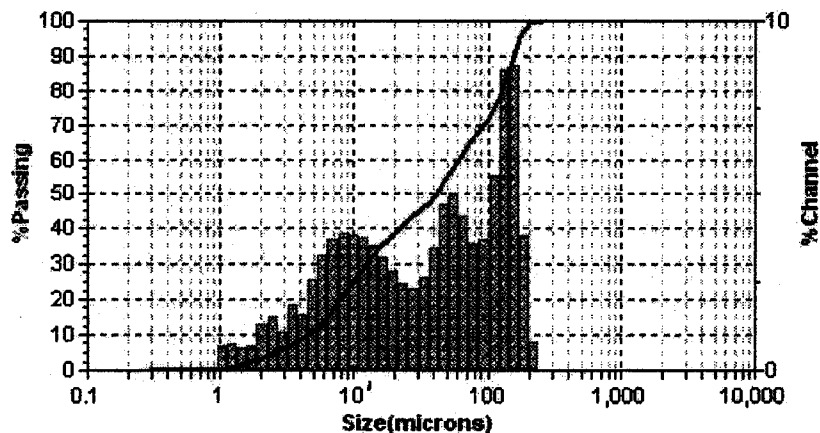


Figure A2.7: Microtrac Particle Size Analysis for Ground Bulk PEI/H₃PO₄

The powder produced from grinding was readily dispersed in heptane. An encapsulation experiment (ZZZONR091906) was done similar to that attempted for the pei solvent/nonsolvent ISPs with MMA and AIBN at 80C. However as the temperature was increased the fine suspension of particles agglomerated into two solid masses on the edge of the reactor. A second experiment (ZZZONR092506) to encapsulate with MMA utilizing V70 initiator at lower temperature (30 C) was also unsuccessful.

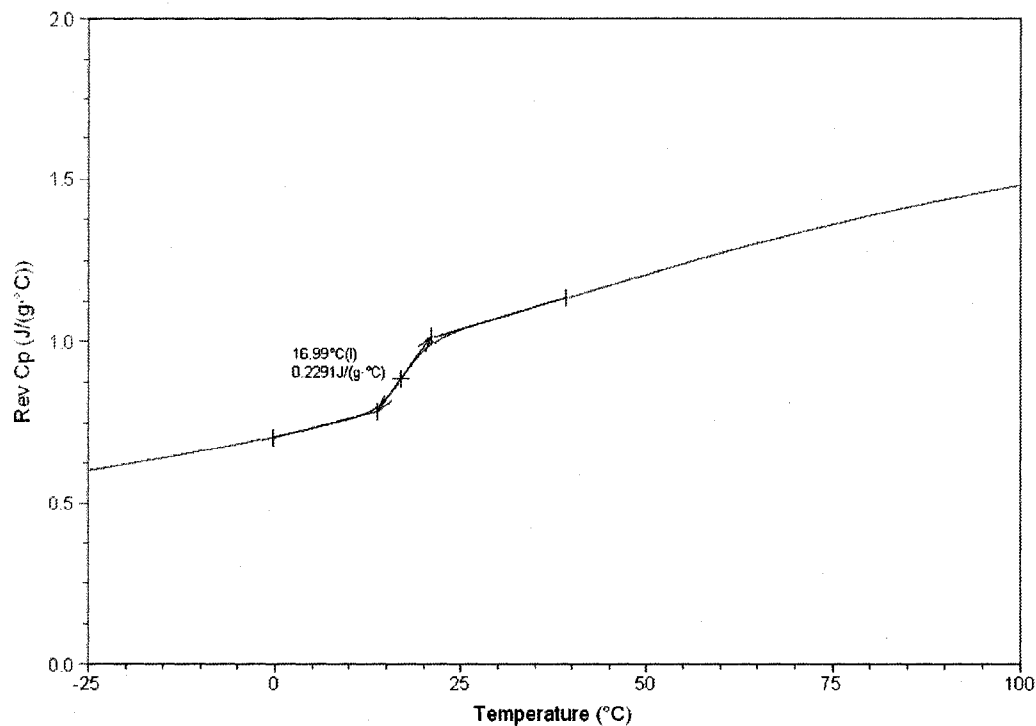


Figure A2.8: DSC for TDI encapsulate ground bulk PEI/H3PO4 particles

It was possible to stabilize the bulk ground particles dispersed in heptane with TDI. These ISPs synthesized from the ground bulk core material likewise contained the low temperature glass transition of the core material as shown in Figure A2.8. This made the drying, handling and manipulation of these ISPs impractical. No further investigation of this method was performed as the research moved towards the WISCM based ISPs.

A2.5 Summary of Solvent/Nonsolvent Synthesis

The solvent/nonsolvent ISPs synthesis and the bulk ISP synthesis method were unable to produce particles that could be dried or manipulated at room temperature. This made the ISPs produced by these syntheses unviable and this work was set aside. The one benign result from this work was the idea behind the WISCM ISP synthesis. The success of the WISCM based ISPs caused this approach to be completely abandoned.

APPENDIX 3

SUPPLEMENTAL EXPERIMENTS

This Appendix contains the description and results of supplemental characterization and properties experimental work that was both successful and unsuccessful done as part of this work. These experiments are of less significance to the complete understanding of ISPs and their synthesis than the material presented in Chapter 3. Additionally, unsuccessful work is shared as it is important to share failures with others. Often times failed research is not disseminated and thus it is repeated only to result, once again in failure.

A3.1 Determination of Primary versus Secondary Amine Reactivity

In order to better understand the competition between the primary and secondary amines in TEPA an experiment was devised which utilized H-NMR (ZZZONR071504). A 50% by mole mixture of a primary amine (n-octylamine) and a secondary amine (diethylamine) was prepared in deuterated acetonitrile (5 mL). A small trace of benzene was added to the solution. This was then divided into two equal parts. To one of these halves sufficient phosphoric acid was added to associate with half of the total amine moieties available. This association formed a solid precipitate of the phosphoric acid coupled with the

amine. The liquid was separated from the solid precipitant by centrifugation, followed by filtration and was then transferred into an NMR tube. A sample of the unreacted mixture of amines was likewise prepared for NMR. The exact mass of the reactants used is presented in Table A3-1.

Table A3-1: Composition for ZZZONR071504

Chemical	Mass (g)	MW (g/mol)	# Mole
diethylamine	0.0906	73.1376	0.001239
n-octylamine	0.1602	129.2448	0.001240
phosphoric acid	0.0202	97.995	0.000412
benzene	one small drop		

The benzene was added to act as an internal standard for comparing the integration values of the proton spectra. The spectra were integrated and then converted by setting the benzene peak to 1.0 for both the reacted and unreacted NMR spectra as it remains unchanged. Spectra were generated on a Varian 500 MHz NMR. Proton NMR is quantitative; therefore the comparison of the integration of the amine peaks give quantitatively the ratio phosphoric acid associated with in regards to primary or secondary amine functionality.

Table A3-2: Peak Integration Values from H-NMR

Chemical Shift	Unreacted	Reacted	
7.4	1.00	1.00	Benzene internal standard (converted to 1.0)
1.03	15.43	15.34	secondary amine peak (CH3) 6H
0.88	9.56	2.65	primary amine peak (CH3) 3H

The results from the NMR experiments are shown in **Error! Reference source not found.** while the before and after spectra with integration values are presented as Figure A3-1 and Figure A3-2 respectively. The primary amine had a

shift of 0.88 ppm. The secondary amine peak was at a shift of 1.03 ppm. The benzene peak used as an internal standard was at 7.4 ppm. The integration of the secondary amine peak was almost unchanged while that of the primary amine dropped by 6.91 (72.3 %) This showed that the phosphoric acid reacted almost exclusively with the primary amine functionalities. This result was expected based on the greater pKa value of the primary amine and the well known reactivity of primary amine over secondary amine moieties but was proven to be true by this experiment.

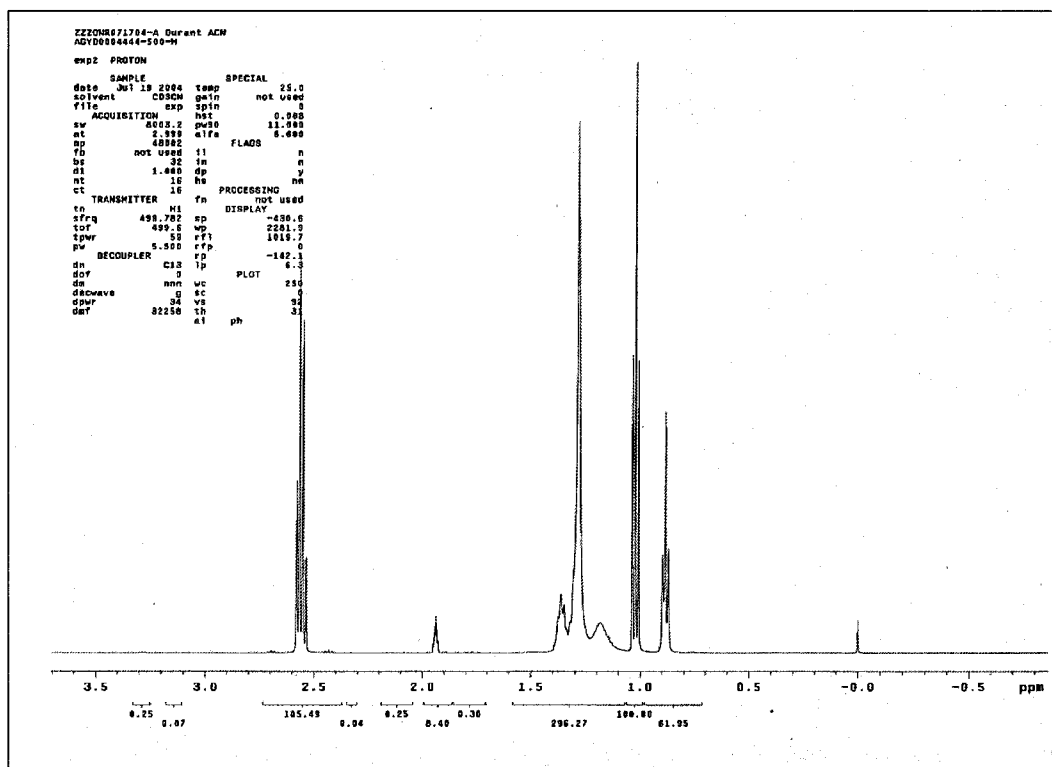


Figure A3.1: H-NMR Spectra before Addition of Phosphoric Acid

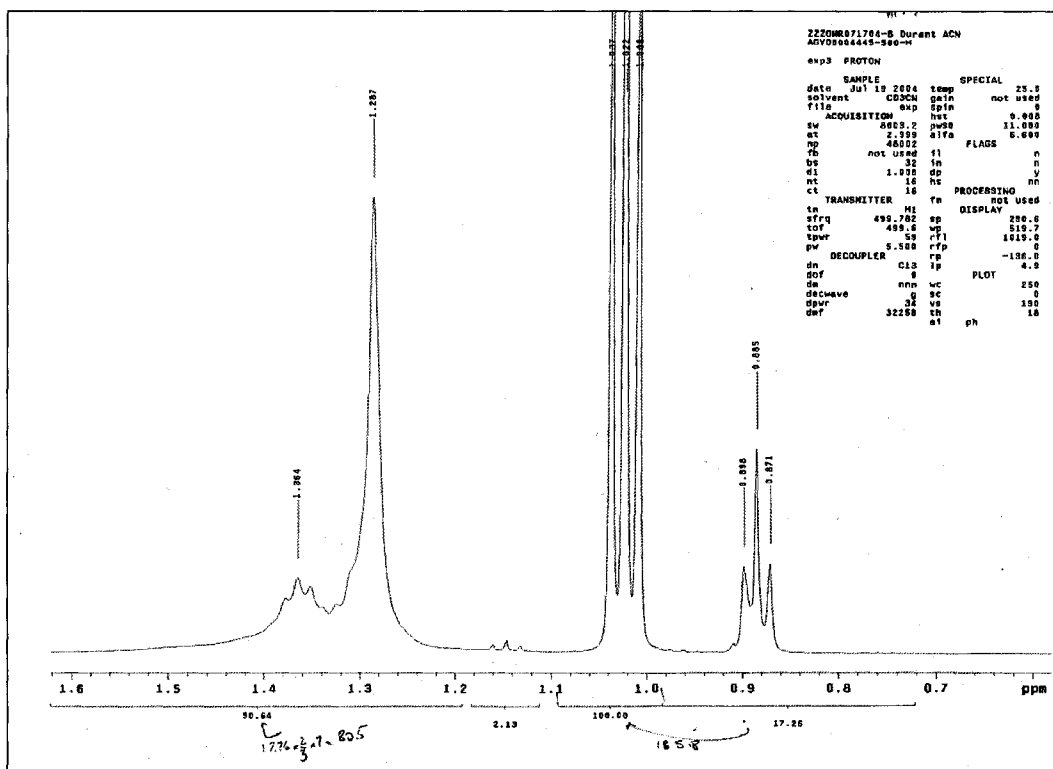


Figure A3.2: H-NMR Spectra After Reaction with Phosphoric Acid

A3.2 Development of Extended Amines

TEPA was the longest available monomer in the ethyleneimine family in a purified form at reasonable cost and quantities. A longer chain ethyleneimine would be beneficial for the synthesis of the ISP core. To this end it was attempted (ZZZONR081604) to double the length of the TEPA by the reaction with TDI as shown in Figure A3.3.

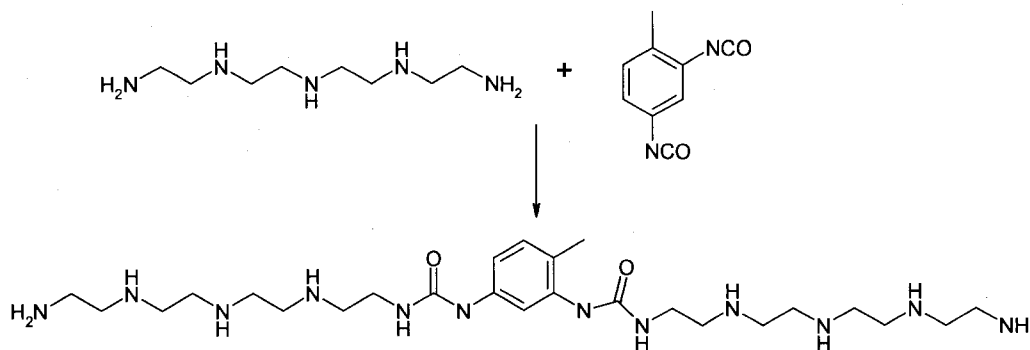


Figure A3.3: Reaction of TEPA with TDI to Synthesize a Larger Monomer

Two dilute solutions were prepared prior to reaction with a 2:1 molar ratio of molecules. The first solution contained 15.0 g TEPA in 100 mL of ACN. The second was made up of 6.90g TDI in 100 mL of ACN. Solution A was placed in an ice bath and allowed to reach thermal equilibrium at 0C. Magnetic stirring provided agitation for solution A in the bath. Solution B was slowly added drop wise to Solution A from above.

Reaction between isocyanates and primary amines occurs at a very fast rate. It was hoped that the low temperature 0 C as well as dilution would slow the reaction rate and allow for the synthesis of a useful longer chain molecule. Useful meaning that the synthesized material would be soluble in ACN so that it could be used in the synthesis of core particles. Unfortunately the resultant material from this reaction was a solid precipitate. The solid precipitate would not melt at temperatures below 100C and was discarded as it was not possible to incorporate the product into the ISP synthesis. Speculatively it was believed the reaction was localized at the droplet of solution B, with a higher ratio of amine to isocyanate in the region of the droplet resulting in much longer

molecule extensions then dimerization, possibly even producing a crosslinked polyurea as the precipitate.

A3.3 Pre-Rusted Accelerated Corrosion

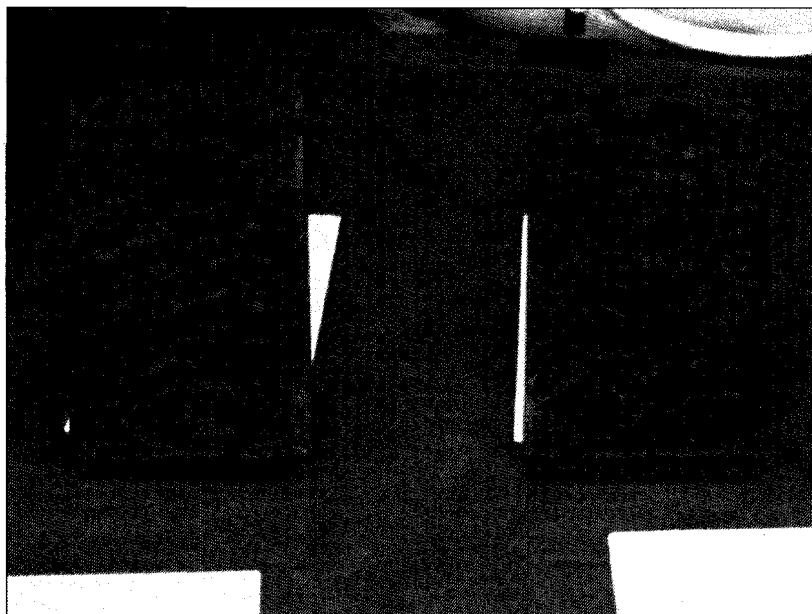


Figure A3.4: Pre-Rusted Plates Prior to Coating

An alternative attempt at increasing the corrosion rate and observable difference between control and ISP containing coatings was done by investigating the use of a pre-rusted steel plate. The pre-rusted coupons were prepared from the standard 4"x6"x1/8" ANSI 1018 steel sample coupons by subjecting them to salt fog chamber for 24 hrs. After the 24hrs in the chamber exposed to standard B117 conditions, the samples had layers of iron oxide on the surface as shown in Figure A3.4. Coatings were applied to the pre-rusted plates by spray application. One coupon was sprayed with a control coating (MIL-DTL-24441) while the other contained ISPs.

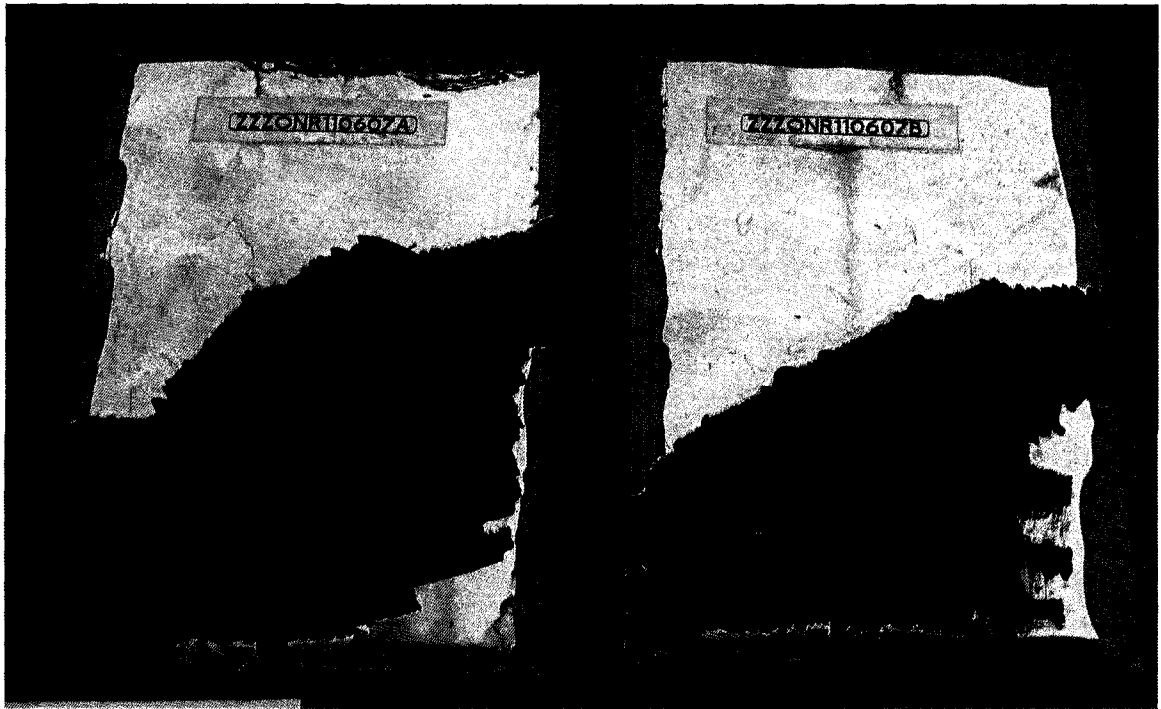


Figure A3.5: Pre-rusted coupon post 1000 hrs B117

The prerusted samples were then exposed to B117 conditions in the salt fog chamber for 1000 hrs. Post scribe evaluation proved impossible as the entire plate was badly corroded (rated 0 by ASTM D1624 and D610) on both sample coupons (see Figure A3.5). It was impossible to differentiate the corrosion damage from the pre-scribe with that caused by the pre-rust treatment. This made post exposure damage quantification impossible. This technique was discarded as not being of any practical utility.

A3.4 Characterization of Ion Exchange by FTIR

Infrared Spectroscopy is a powerful analytical technique that can be used to analyze compounds based on functional moieties. A spectra database of all

the monomers and then reactions between individual monomers was created by running samples on a Bruker FTIR. By setting up this database it was hoped that ISPs could be characterized by their functional groups with qualitative and quantitative results.

The first approach was to use the FTIR to characterize the phosphate ion after it exchanged with a chloride ion in DMSO. A series of controlled samples were run on the FTIR at different concentrations of phosphate. Initially it was expected that this would lead to being able to quantify the P-O stretching peak of the phosphate. However after analyzing the spectra scaled to a reference peak it was determined quantification was not possible as the SO stretch overlaps with the PO stretch at $\sim 1100\text{ cm}^{-1}$. At the time, batch and early semi batch core shell ISPs would swell and agglomerate in water making water not viable as a solvent for this work. This method was discarded for and other alternatives were investigated.

A3.5 Other Techniques for Ion Exchange

This section briefly discusses techniques attempted at ion exchange characterization. Little detail is provided as this information is primarily provided for those who will continue this work in the future to aid them in developing more powerful characterization techniques for the study of ISPs.

It was attempted to characterize the ISPs by monitoring ion exchange through a dialysis bag filled with ISPs stirred in a fixed volume of sodium chloride solution. The issue with this method was how to accurately measuring the

amount of phosphate counter ion released into the solution. Investigating of kits and ASTM standards for biological phosphate determination in water did not provide useful results. These biological determination methods relied on visible spectroscopy and intensity measurement. They are very good at determining very small trace amounts of phosphate. The amount of dilution required with ISP solutions to not oversaturate the spectroscope made this technique impracticable.

The use of an electrochemical reference electrode sensitive in theory to only phosphate was tried. The electrode was also sensitive to chloride ions in solution making this a poor choice for ion exchange characterization. Later an electrode sensitive to only chloride ions was purchased for similar work. This electrode was impossible to standardize with any repeatability. Readings taken from a salt solution in a closed container would fluctuate by 1 or 2 orders of magnitude. This solution was in the center of the probe's supposed range.

P_{31} NMR was investigated. Sample NMR tubes were prepared directly at the NMR station containing deuterated water, both pure and sodium chloride solutions. 5 wt % of ISPs were added directly prior to insertion into the NMR magnet. Timed measurements were performed. Even though this was a liquid NMR experiment the presence of the solid ISPs in the solution proved problematic in terms of spectra acquisition and it proved impossible to determine phosphate diffusion by this method.

APPENDIX 4

B117 SCRIBE EVALUATION DATA

This Appendix contains the data for each sample evaluated following ASTM D1654 scribe evaluation after 1000 hr B117. Each experiment will be presented on a separate page, with all samples from that experiment presented on that single page. The actual measurements data of variation from the scribe line as well as the rating are presented for each sample. This is then averaged and reported and discussed in Chapter 5.

Experiment ID: ZZZONR021207

SAMPLE ID	Min	Rating	Max	Rating	ISP ID	wt % ISP	Coating
ZZZONR021207A	0.7	8.1	1.52	6.9	ZZZONR010307	5.8	MIL-DTL-24441
ZZZONR021207B	0.887	7.8	1.845	6.7		0	MIL-DTL-24441

Sample ID ZZZONR021207A exposure:

Segment	Min (mm)	Rating	Max (mm)	Rating
A	0.62	8	2.17	6
B	0.95	8	1.53	7
C	0.87	8	2.01	6
D	0.79	8	1.7	7
E	0.61	8	0.9	8
F	1.11	7	1.58	7
G	0.33	9	1.03	7
H	0.62	8	1.31	7
I	0.39	9	1.26	7
J	0.71	8	1.71	7

Average: 0.7 8.1 1.52 6.9

Sample ID ZZZONR021207B

Segment	Min (mm)	Rating	Max (mm)	Rating
A	1.45	7	2.38	6
B	1	8	2.21	6
C	0.77	8	1.89	7
D	0.61	8	1.9	7
E	0.44	9	1.33	7
F	0.98	8	2.53	6
G	1.05	7	1.74	7
H	0.7	8	1.28	7
I	0.75	8	1.3	7
J	1.12	7	1.89	7

Average: 0.887 7.8 1.845 6.7

Experiment ID: ZZZONR083007

SAMPLE ID	Min	Rating	Max	Rating	ISP ID	wt % ISP	Coating
ZZZONR083007A	0.92	7.8	2.03	6.5		0	MIL-DTL-24441
ZZZONR083007H	0.60	8.1	1.34	7.3	ZZZONR070907	4.9	MIL-DTL-24441

Sample ID **ZZZONR083007A**

Segment	Min (mm)	Rating	Max (mm)	Rating
A	0.5	9	1.1	7
B	0.58	8	1.34	7
C	1.03	7	2.09	6
D	1.91	7	2.91	6
G	1.33	7	3.55	5
H	0.76	8	1.77	7
I	0.7	8	1.78	7
J	0.52	8	1.7	7
Average:	0.91625	7.75	2.03	6.5

Sample ID **ZZZONR083007H**

Segment	Min (mm)	Rating	Max (mm)	Rating
A	0.21	9	1.89	7
B	0.55	8	1.1	7
C	0.64	8	1.16	7
D	0.56	8	0.72	8
G	0.52	8	0.76	8
H	0.75	8	1.65	7
I	0.88	8	1.5	7
J	0.66	8	1.91	7
Average:	0.59625	8.125	1.33625	7.25

Experiment ID: ZZZONR110607

SAMPLE ID	Min	Rating	Max	Rating	ISP ID	wt % ISP	Coating
ZZZONR110607A	2.40	6.1	7.03	3.8		5.8	MIL-DTL-24441
ZZZONR110607B	2.14	6.3	6.47	4.0		0	MIL-DTL-24441

Sample ID **ZZZONR110607A**

Segment	Min (mm)	Rating	Max (mm)	Rating
A	1.66	7	6.03	4
B	1.03	7	4.91	5
C	1.93	7	3.26	5
D	2.8	6	11.08	2
G	2.35	6	5.75	4
H	2.09	6	7.08	3
I	3.51	5	9.06	4
J	3.86	5	9.09	3
Average:	2.40	6.1	7.03	3.8

Sample ID **ZZZONR110607B**

Segment	Min (mm)	Rating	Max (mm)	Rating
A	3.27	5	6.4	4
B	2.11	6	5.56	4
C	2.35	6	5.9	4
D	1.49	7	4.3	5
G	1.11	7	3.97	5
H	1.55	7	3.65	5
I	3.28	5	6.33	4
J	1.95	7	15.64	1
Average:	2.14	6.3	6.47	4.0

Experiment ID: ZZZONR020108

SAMPLE ID	Min	Rating	Max	Rating	ISP ID	wt % ISP	Coating
ZZZONR020108A	1.63	6.9	6.59	4.1	DETONR046	5	DGEBA/TEPA
ZZZONR020108B	16+	0.0	16+	0.0		0	DGEBA/TEPA
ZZZONR020108C	1.21	7.4	2.94	5.6	DETONR046	5	DGEBA/TEPA

Sample ID ZZZONR020108A

exposure:

Segment	Min (mm)	Rating	Max (mm)	Rating
A	1.14	7	3.53	5
B	1.6	7	13.8	1
C	1.58	7	10.65	2
D	0.88	8	2	7
G	1.56	7	2.47	6
H	1.57	7	5.96	4
I	3.6	5	10.97	2
J	1.1	7	3.3	6

Average: 1.63 6.9 6.59 4.1

Sample ID ZZZONR020108C

Segment	Min (mm)	Rating	Max (mm)	Rating
A	1.63	7	2.36	6
B	0.76	8	2.5	6
C	0.75	8	2.62	6
D	1.22	7	2.59	6
G	1	8	2.25	6
H	1.31	7	3.65	5
I	0.93	8	3.96	5
J	2.09	6	3.55	5

Average: 1.21 7.4 2.94 5.6

B isolated area, I- isolated damage area

Sample ID ZZZONR020108B

Segment	Min (mm)	Rating	Max (mm)	Rating
A	16+	0	16+	0
B	16+	0	16+	0
C	16+	0	16+	0
D	16+	0	16+	0
G	16+	0	16+	0
H	16+	0	16+	0
I	16+	0	16+	0
J	16+	0	16+	0

Average: 16+ 0 16+ 0

total failure of coating

Experiment ID: ZZZONR030408

SAMPLE ID	Min	Rating	Max	Rating	ISP ID	wt % ISP	Coating
ZZZONR030408B	16+	0.0	16+	0.0	DETONR046	0	DGEBA/TEPA
ZZZONR030408C	10.41	0.3	16+	0.0	DETONR047	1	DGEBA/TEPA
ZZZONR030408E	16+	0.0	16+	0.0	DETONR048	2.5	DGEBA/TEPA
ZZZONR030408J	11.36	2.6	26.05	0.3	DETONR049	3.9	DGEBA/TEPA
ZZZONR030408G	0.90	7.8	2.72	5.8	DETONR050	5	DGEBA/TEPA

Sample ID ZZZONR030408B

Segment	Min (mm)	Rating	Max (mm)	Rating
A	16+	0	16+	0
B	16+	0	16+	0
C	16+	0	16+	0
D	16+	0	16+	0
E	16+	0	16+	0
F	16+	0	16+	0
G	16+	0	16+	0
H	16+	0	16+	0
I	16+	0	16+	0
J	16+	0	16+	0

Average: 16+ 0 16+ 0

Sample ID ZZZONR030408C

Segment	Min (mm)	Rating	Max (mm)	Rating
A	16+	0	16+	0
B	16+	0	16+	0
C	16+	0	16+	0
D	11.65	1	16+	0
E	9.16	2	16+	0
F	16+	0	16+	0
G	16+	0	16+	0
H	16+	0	16+	0
I	16+	0	16+	0
J	16+	0	16+	0

Average: 10.41 0.3 16+ 0

No unruined surface on front

Sample ID ZZZONR030408E

Segment	Min (mm)	Rating	Max (mm)	Rating
A	16+	0	16+	0
B	16+	0	16+	0
C	16+	0	16+	0
D	16+	0	16+	0
E	16+	0	16+	0
F	16+	0	16+	0
G	16+	0	16+	0
H	16+	0	16+	0
I	16+	0	16+	0
J	16+	0	16+	0

Average: 16+ 0 16+ 0

Sample ID ZZZONR030408G

Segment	Min (mm)	Rating	Max (mm)	Rating
A	0.82	8	3.17	5
B	1.73	7	2.43	6
C	1.01	7	3.37	5
D	0.4	9	1.63	7
E	0.05	9	1.94	7
F	1.29	7	2.7	6
G	0.53	8	2.75	6
H	1.56	7	3.44	5
I	0.82	8	2.41	6
J	0.81	8	3.4	5

Average: 0.90 7.8 2.72 5.8

Sample ID ZZZONR030408J

Segment	Min (mm)	Rating	Max (mm)	Rating
A	1.68	7	9.83	3
B	6	4	16.22	0
C	8.07	3	45.27	0
D	24	0	37.78	0
E	6.54	4	19.39	0
F	14.42	1	27.81	0
G	3.09	5	32.19	0
H	13.2	1	24.84	0
I	21.23	0	25.5	0
J	15.34	1	21.67	0

Average: 11.36 2.6 26.05 0.3

Experiment ID: ZZZONR041408

SAMPLE ID	Min	Rating	Max	Rating	ISP ID	wt % ISP	Coating
ZZZONR041408B	16+	0.0	16+	0.0	ZZZONR040808	0	DGEBA/TEPA
ZZZONR041408D	5.49	4.4	11.54	2.0	ZZZONR040808	5	DGEBA/TEPA
ZZZONR041408F	1.52	7.0	7.20	3.6	ZZZONR040808	10	DGEBA/TEPA
ZZZONR041408H	3.57	6.0	7.09	3.5	ZZZONR040808	15	DGEBA/TEPA
ZZZONR041408J	3.97	5.1	9.48	2.6	ZZZONR040808	20	DGEBA/TEPA

Sample ID ZZZONR041408B

Segment (mm)	Min	Rating	Max (mm)	Rating
A	16 +	0	16 +	0
B	16 +	0	16 +	0
C	16 +	0	16 +	0
D	16 +	0	16 +	0
G	16 +	0	16 +	0
H	16 +	0	16 +	0
I	16 +	0	16 +	0
J	16 +	0	16 +	0

Average: 16+ 0.0 16+ 0.0

Large areas of deep pitting and flaky oxide covering total area of plate

Sample ID ZZZONR041408D

Segment (mm)	Min	Rating	Max (mm)	Rating
A	4.74	5	11.03	2
B	6.75	4	14.26	1
C	8.79	3	13.95	1
D	4.14	5	12.53	2
G	4.2	5	9.68	3
H	4.52	5	9.07	3
I	6.41	3	11.11	2
J	4.35	5	10.65	2

Average: 5.49 4.4 11.54 2.0

Sample ID ZZZONR041408F

Segment (mm)	Min	Rating	Max (mm)	Rating
A	1.21	7	2.49	6
B	0.99	8	4.14	5
C	0.83	8	3.84	5
D	1.53	7	3.77	5
G	1.35	7	7.29	3
H	2.18	6	10.99	2
I	1.97	7	14.4	1
J	2.12	6	10.65	2

Average: 1.52 7.0 7.20 3.6

Sample ID ZZZONR041408H

Segment (mm)	Min	Rating	Max (mm)	Rating
A	3.18	6	5.96	4
B	3.53	6	11.35	2
C	6.27	4	7.48	3
D	3.47	6	7.31	3
G	3.95	6	6.73	4
H	3.2	6	6.23	4
I	2.93	7	7.05	3
J	2.01	7	4.62	5

Average: 3.57 6.0 7.09 3.5

Sample ID ZZZONR041408J

Segment (mm)	Min	Rating	Max (mm)	Rating
A	3.08	5	6.72	4
B	3.22	5	7.34	3
C	4.66	5	8.58	3
D	2.1	6	7.42	3
G	2.51	6	13.14	1
H	6.84	4	11.58	2
I	5.44	4	11.46	2
J	3.93	6	9.61	3

Average: 3.97 5.1 9.48 2.6

Experiment ID: ZZZONR042608

SAMPLE ID	Min	Rating	Max	Rating	ISP ID	wt % ISP	Coating
ZZZONR042608B	13.20	1.7	24.90	0.1	ZONR0424	0	DGEBA/TEPA
ZZZONR042608D	2.24	6.7	5.04	4.6	ZONR0424	2.5	DGEBA/TEPA
ZZZONR042608F	0.00	10.0	1.38	7.2	ZONR0424	5	DGEBA/TEPA
ZZZONR042608H	0.39	9.0	2.25	6.3	ZONR0424	10	DGEBA/TEPA

Sample ID **ZZZONR042608B**

Segment	Min (mm)	Rating	Max (mm)	Rating
A	9.6	3	22.2	0
B	8.66	3	24.74	0
C	9.19	3	27.44	0
D	16.4	0	35.78	0
E	14.46	1	26.1	0
F	17.65	0	21.5	0
G	23.4	0	31.88	0
H	13.99	1	26.24	0
I	9.61	3	17.71	0
J	9.01	3	15.4	1
Average:	13.20	1.7	24.90	0.1

Sample ID **ZZZONR042608D**

Segment	Min (mm)	Rating	Max (mm)	Rating
A	0	10	1.57	7
B	1.6	7	5.58	4
C	3.52	5	6.6	4
D	5.45	4	9.22	3
E	4.08	5	7.37	3
F	1.78	7	4.83	5
G	0.86	8	3.39	5
H	1.58	7	5.06	4
I	1.94	7	3.84	5
J	1.62	7	2.91	6
Average:	2.24	6.7	5.04	4.6

Dark Magnetite over entire surface

Sample ID **ZZZONR042608F**

Segment	Min (mm)	Rating	Max (mm)	Rating
A	0	10	1.39	7
B	0	10	0.9	8
C	0	10	0.68	8
D	0	10	1.78	7
E	0	10	0.95	8
F	0	10	1.17	7
G	0	10	3.03	6
H	0	10	1.11	7
I	0	10	1.38	7
J	0	10		
Average:	0.00	10.0	1.38	7.2

Sample ID **ZZZONR042608H**

Segment	Min (mm)	Rating	Max (mm)	Rating
A	0.45	9	1.88	7
B	0	10	2.48	6
C	0	10	2.31	6
D	0	10	3.17	5
E	1.16	7	2.57	6
F	0.72	8	1.71	7
G	0	10	1.91	7
H	0.84	8	1.68	7
I	0	10	3.35	5
J	0.77	8	1.4	7
Average:	0.39	9.0	2.25	6.3

one small area of disbondment damage

Experiment ID: ZZZONR042808

SAMPLE ID	Min	Rating	Max	Rating	ISP ID	wt % ISP	Coating
ZZZONR042808A	16+	0.0	16+	0.0	ZZZONR042508	0	DGEBA/TEPA
ZZZONR042808C	8.16	3.7	15.03	1.6	ZZZONR042508	2.5	DGEBA/TEPA
ZZZONR042808E	0.87	7.8	1.99	6.7	ZZZONR042508	5	DGEBA/TEPA
ZZZONR042808H	0.53	8.8	1.56	7.0	ZZZONR042508	10	DGEBA/TEPA

Sample ID ZZZONR042808A

Segment	Min (mm)	Rating	Max (mm)	Rating
A	16+	0	16+	0
B	16+	0	16+	0
C	16+	0	16+	0
D	16+	0	16+	0
E	16+	0	16+	0
F	16+	0	16+	0
G	16+	0	16+	0
H	16+	0	16+	0
I	16+	0	16+	0
J	16+	0	16+	0
Average:	16+	0.0	16+	0.0

Sample ID ZZZONR042808C

Segment	Min (mm)	Rating	Max (mm)	Rating
A	0.87	8	2.17	6
B	2.89	6	5.85	4
C	6.85	4	20.29	0
D	9.94	3	24.7	0
E	12.14	2	19.5	0
F	12.13	2	16.67	0
G	16.5	0	18	0
H	12.4	2	25.5	0
I	5.8	4	12.13	2
J	2.1	6	5.51	4
Average:	8.16	3.7	15.03	1.6

entire plate blackened, large undercut lots of blistering

Sample ID ZZZONR042808E

Segment	Min (mm)	Rating	Max (mm)	Rating
A	0.34	9	1.93	7
B	1.43	7	4.37	6
C	0.99	8	2.24	6
D	1.11	7	2.74	6
E	0.98	8	1.43	7
F	1.09	7	1.5	7
G	0.6	8	1.04	7
H	0.97	8	1.52	7
I	0.62	8	2.33	6
J	0.55	8	0.75	8
Average:	0.87	7.8	1.99	6.7

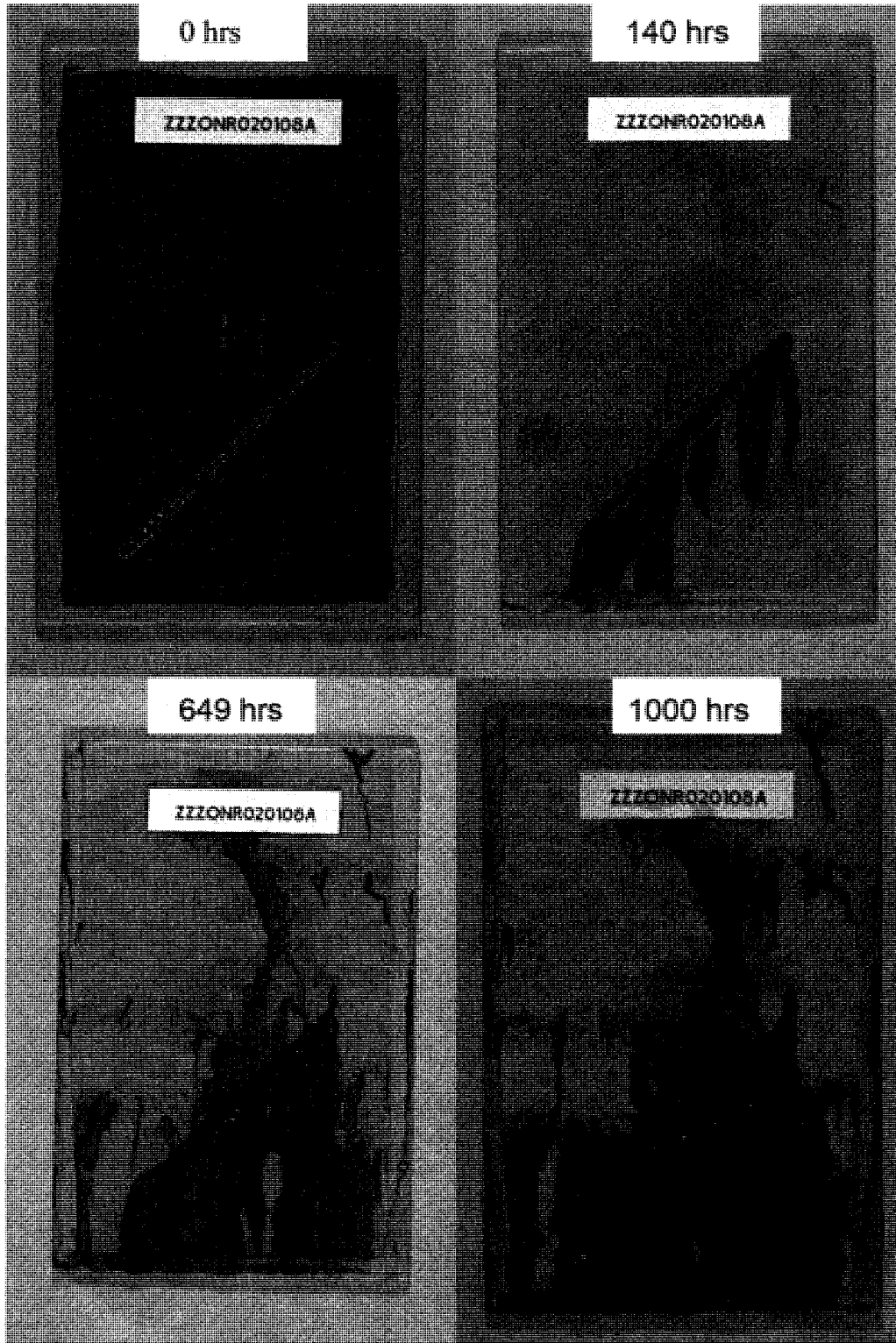
Sample ID ZZZONR042808H

Segment	Min (mm)	Rating	Max (mm)	Rating
A	0	10	0.91	8
B	1.35	7	1.65	7
C	1.05	7	1.7	7
D	0.83	8	1.46	7
E	0	10	0.97	8
F	0	10	1.95	7
G	0.25	9	1.5	7
H	0.45	9	2.15	6
I	1.32	8	2.01	6
J	0	10	1.29	7
Average:	0.53	8.8	1.56	7.0

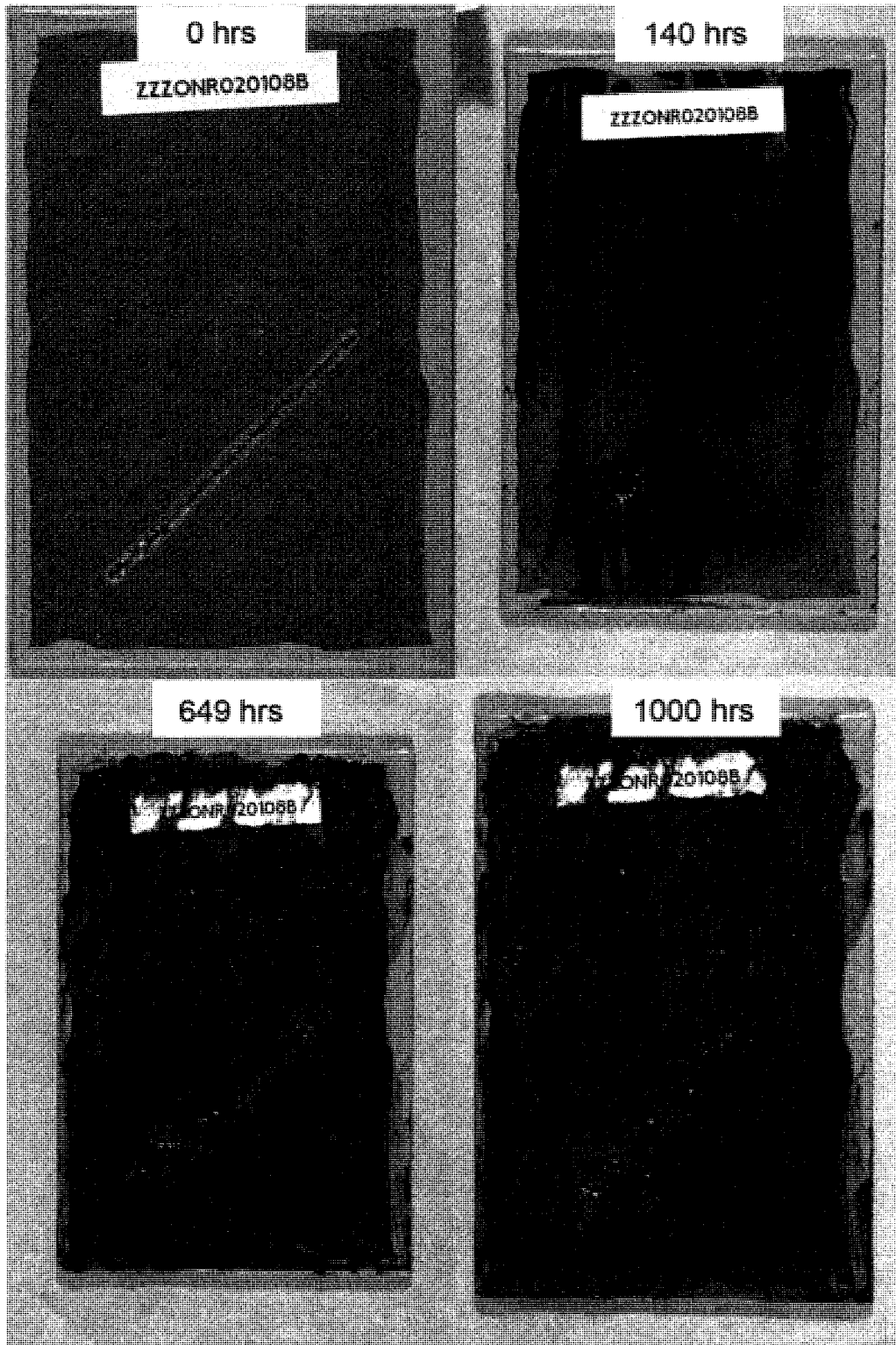
APPENDIX 5

PHOTOGRAPHS OF SAMPLE COUPONS

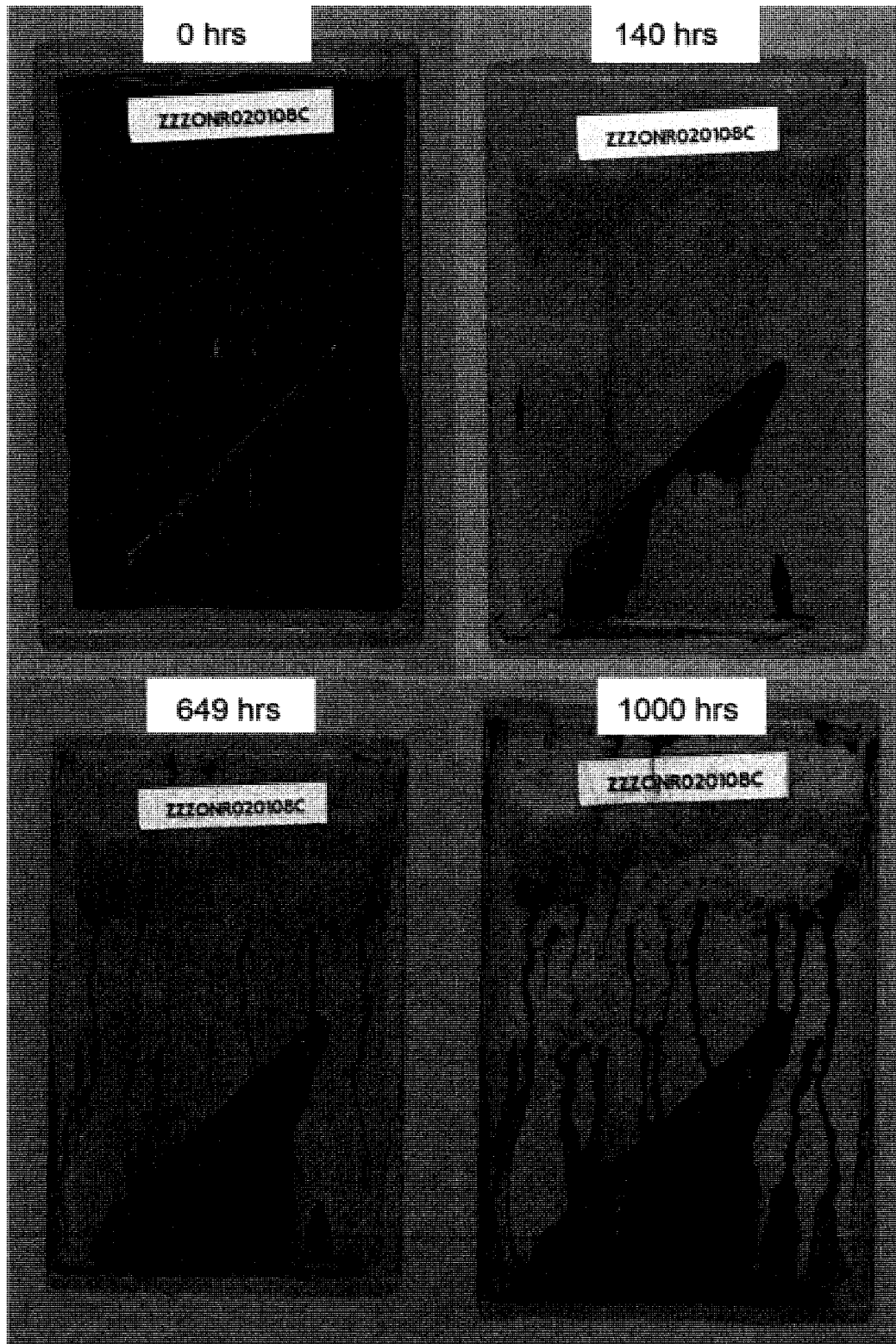
This Appendix contains a series of time laps images for each painted steel sample coupons used to evaluate the anticorrosion performance of the ISPs. Each sample will have a series of four images presented. The images always contain a pre experiment image at time zero in the top left image. Proceeding clockwise from this image will be two intermediate time images where the samples were removed from the experiment briefly and photographed. Finally the bottom right image is of the sample coupon post exposure. Each image in the sequence is labeled with the actual time stamp for that images acquisition time.



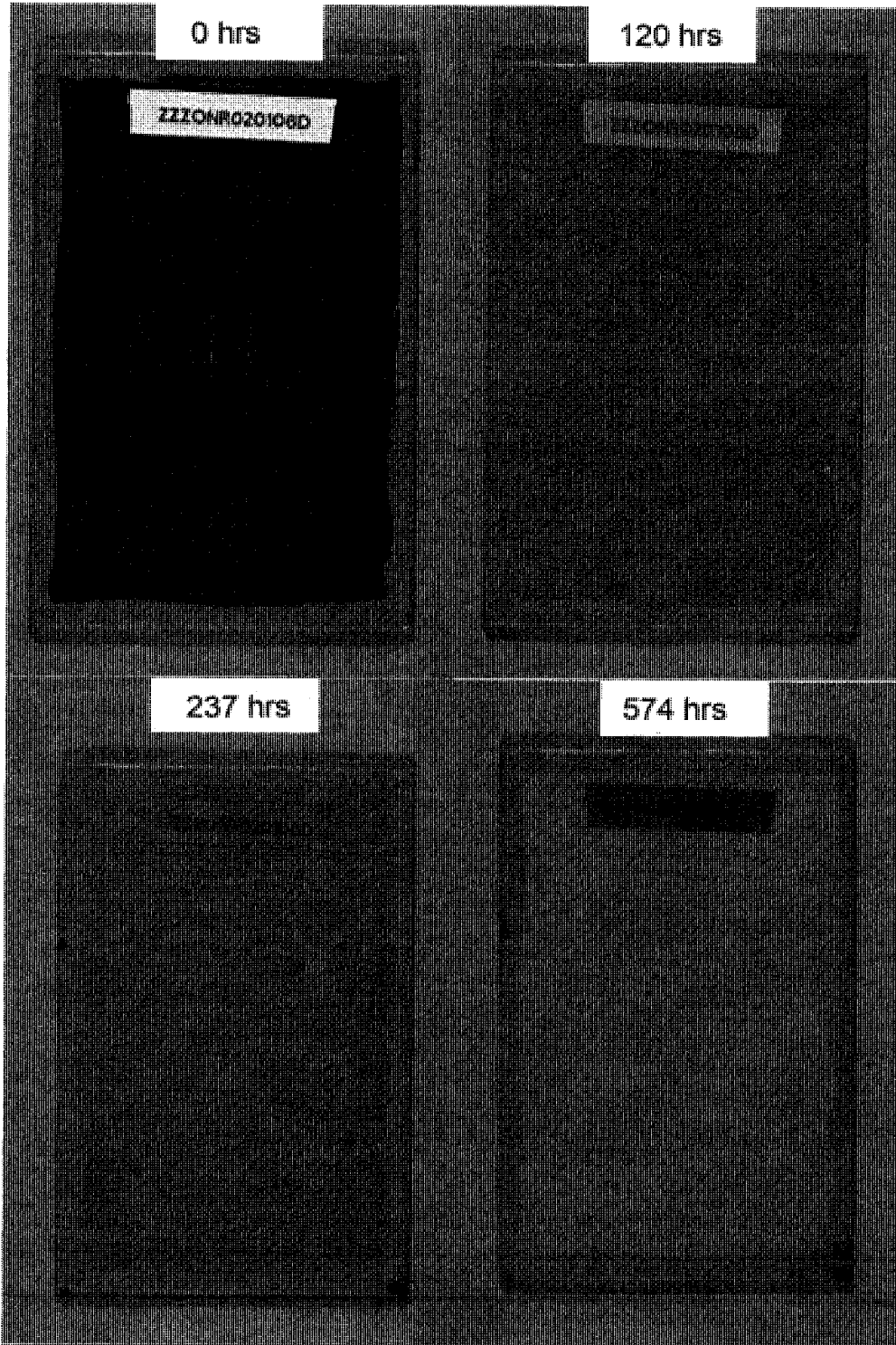
ZZZONR020108A - Salt Spray Exposure - 5 wt % of DETONR046



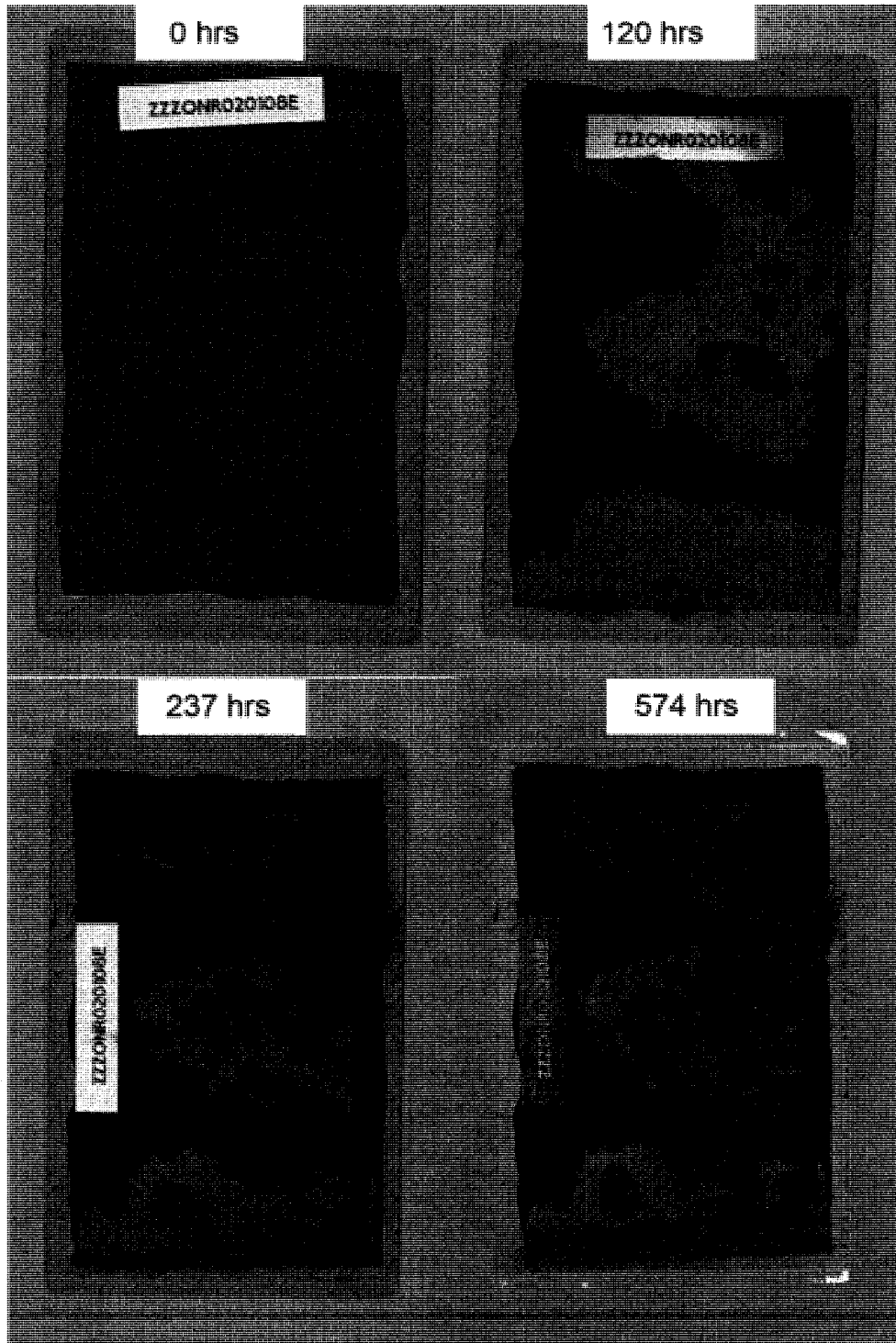
ZZZONR020108B - Salt Spray Exposure - Control



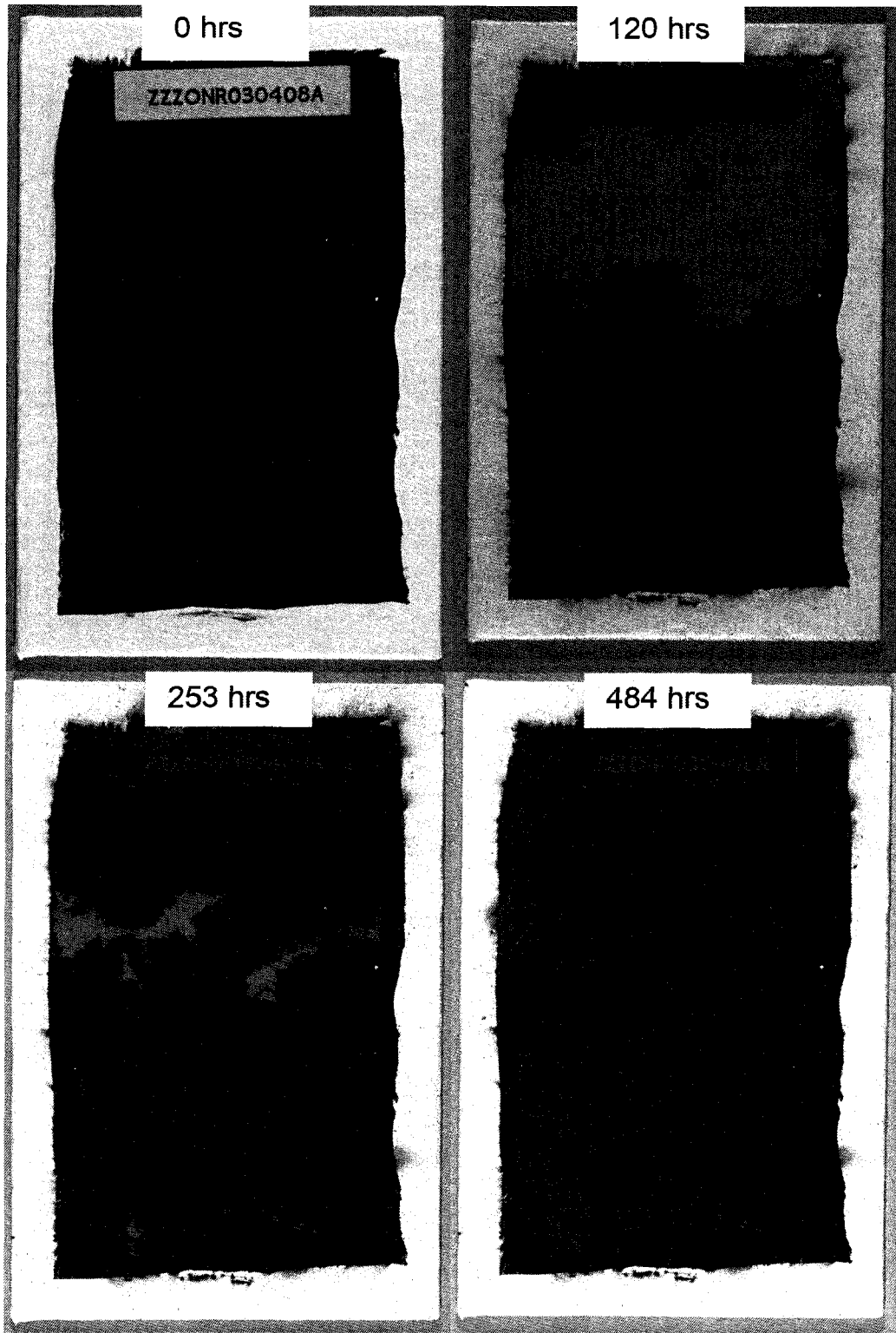
ZZZONR020108C - Salt Spray Exposure - 5 wt % DETONR046



ZZZONR020108D - Hot DI Immersion - 5 wt % DETONR046



ZZZONR020108E - Hot DI Immersion - Control



0 hrs

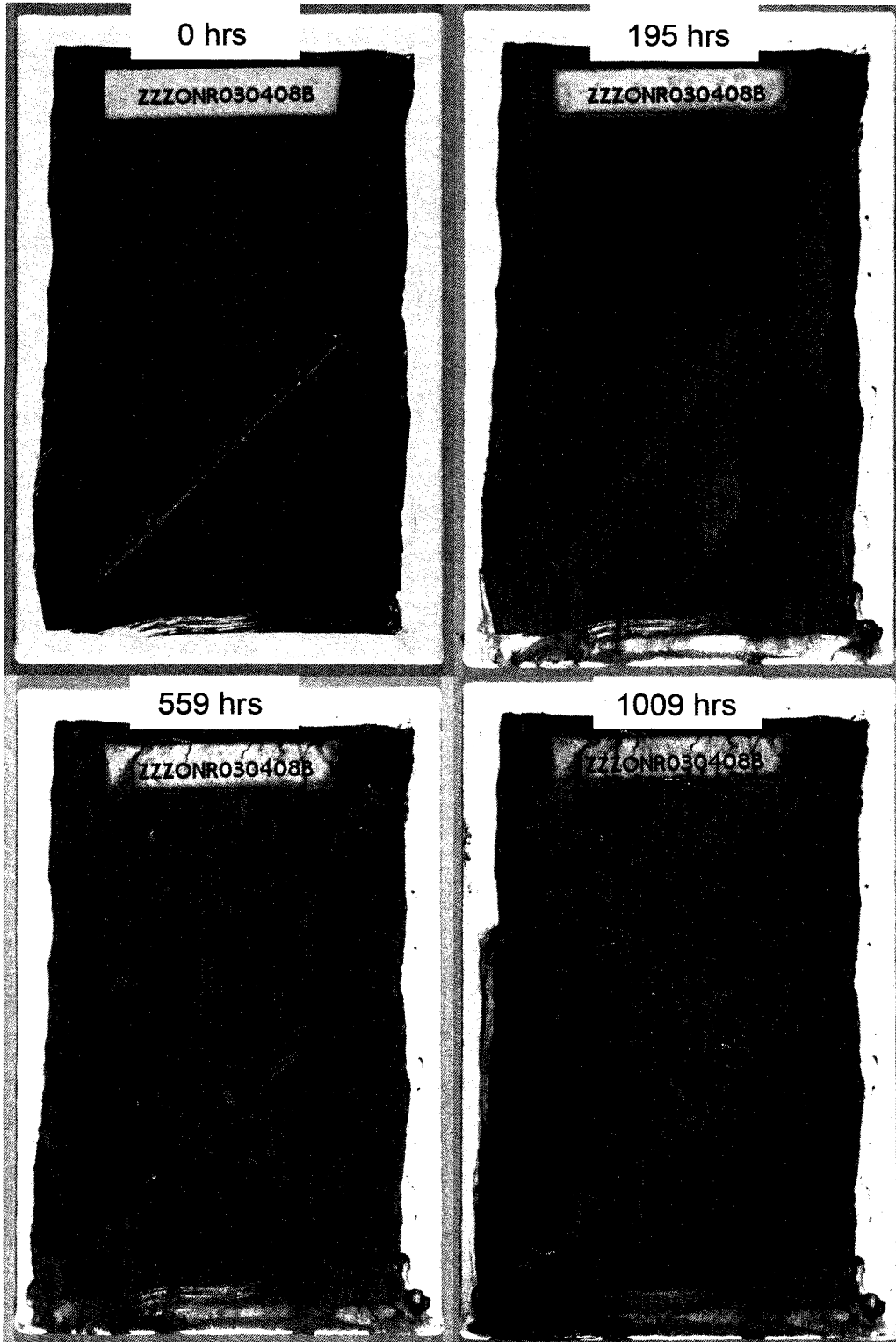
ZZZONR030408A

120 hrs

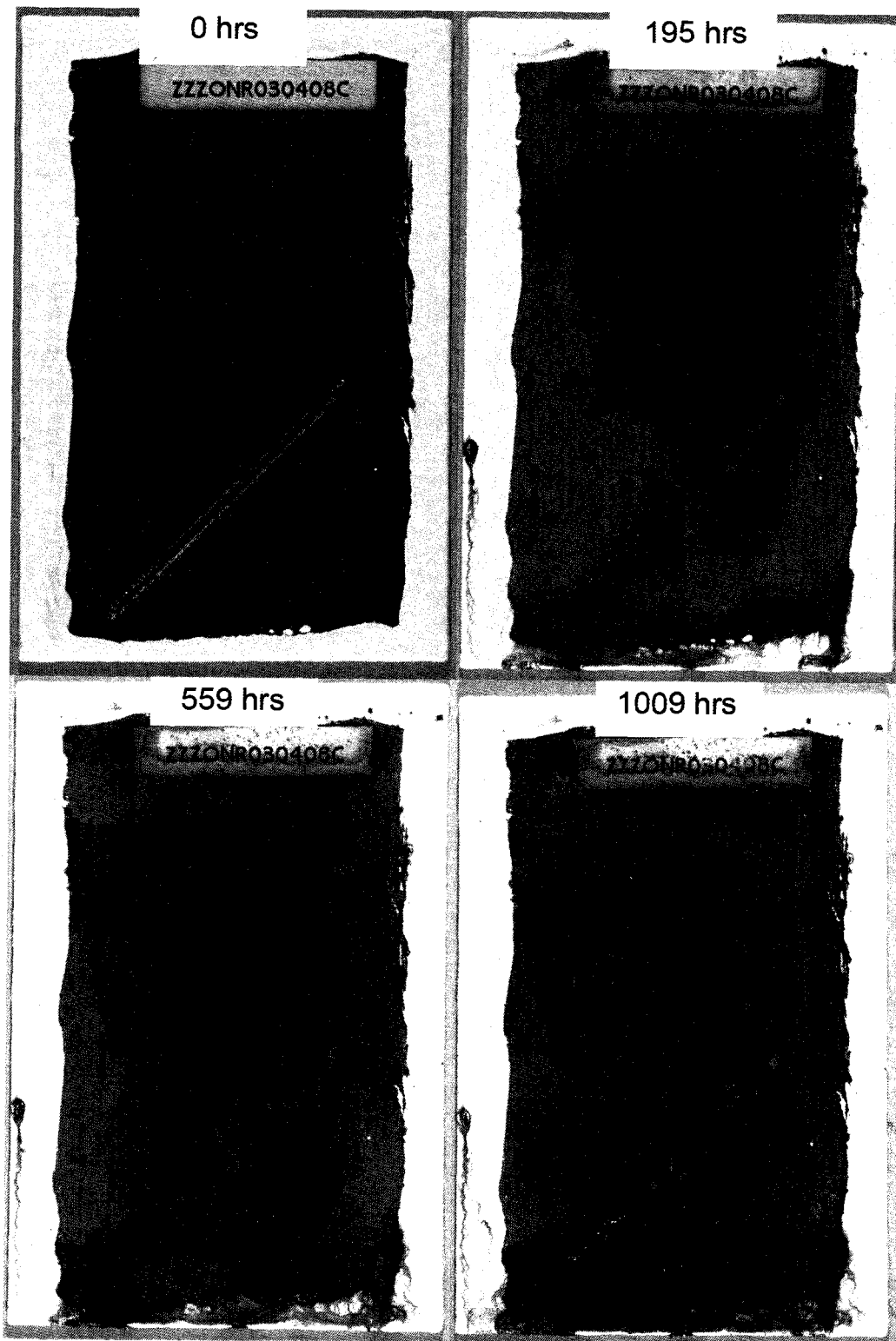
253 hrs

484 hrs

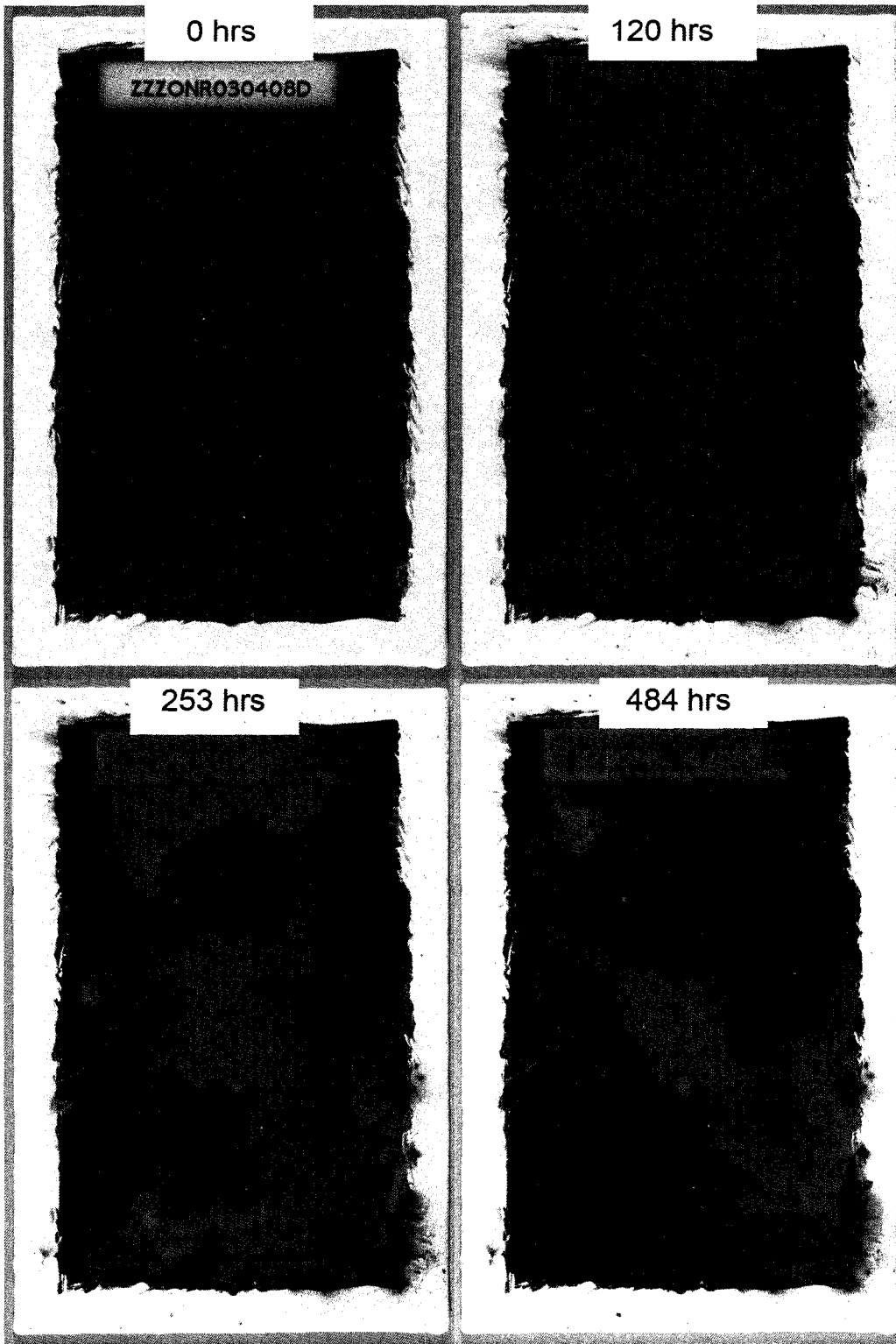
ZZZONR030408A - Hot DI Immersion - Control



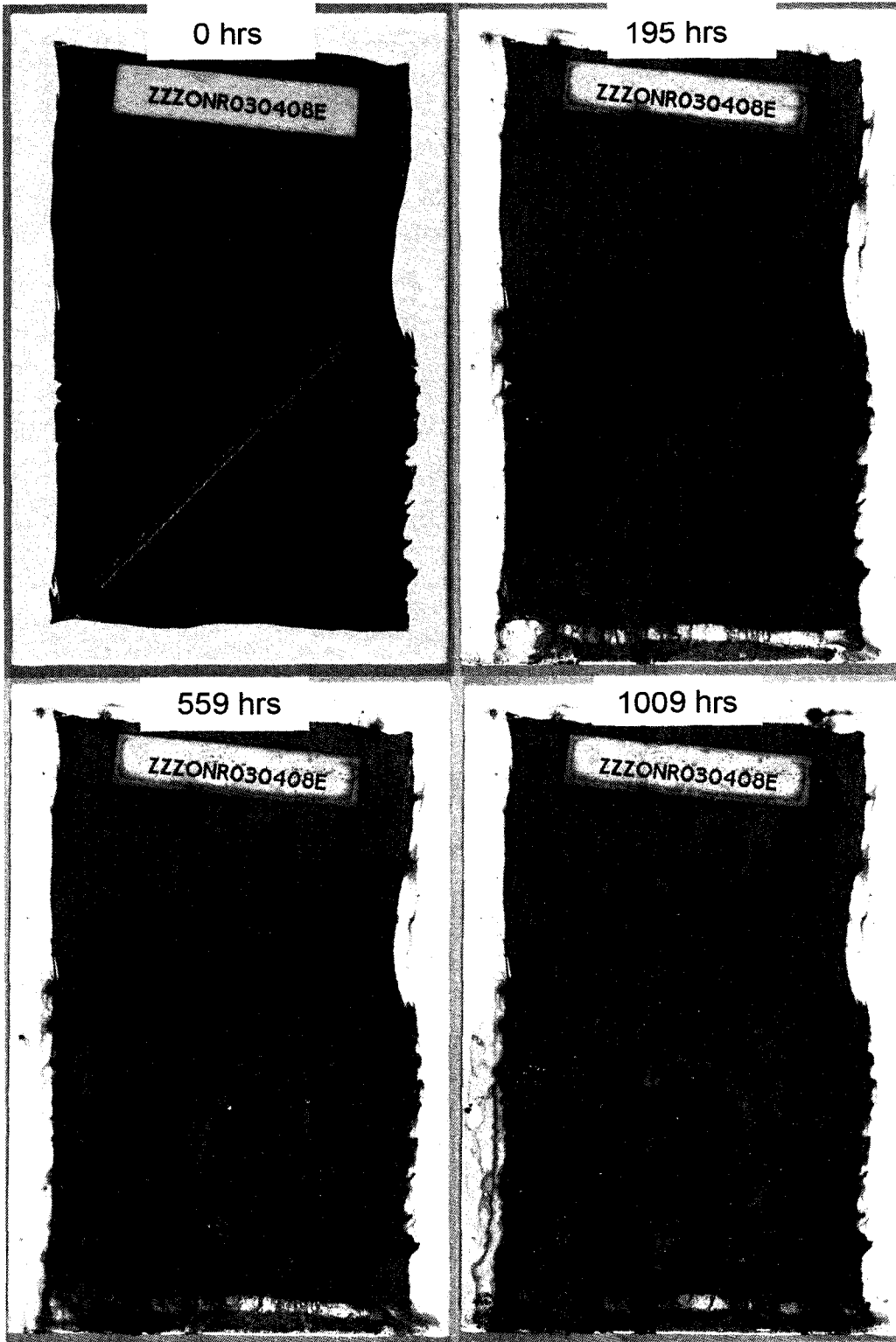
ZZZONR030408B - Salt Spray Exposure - Control



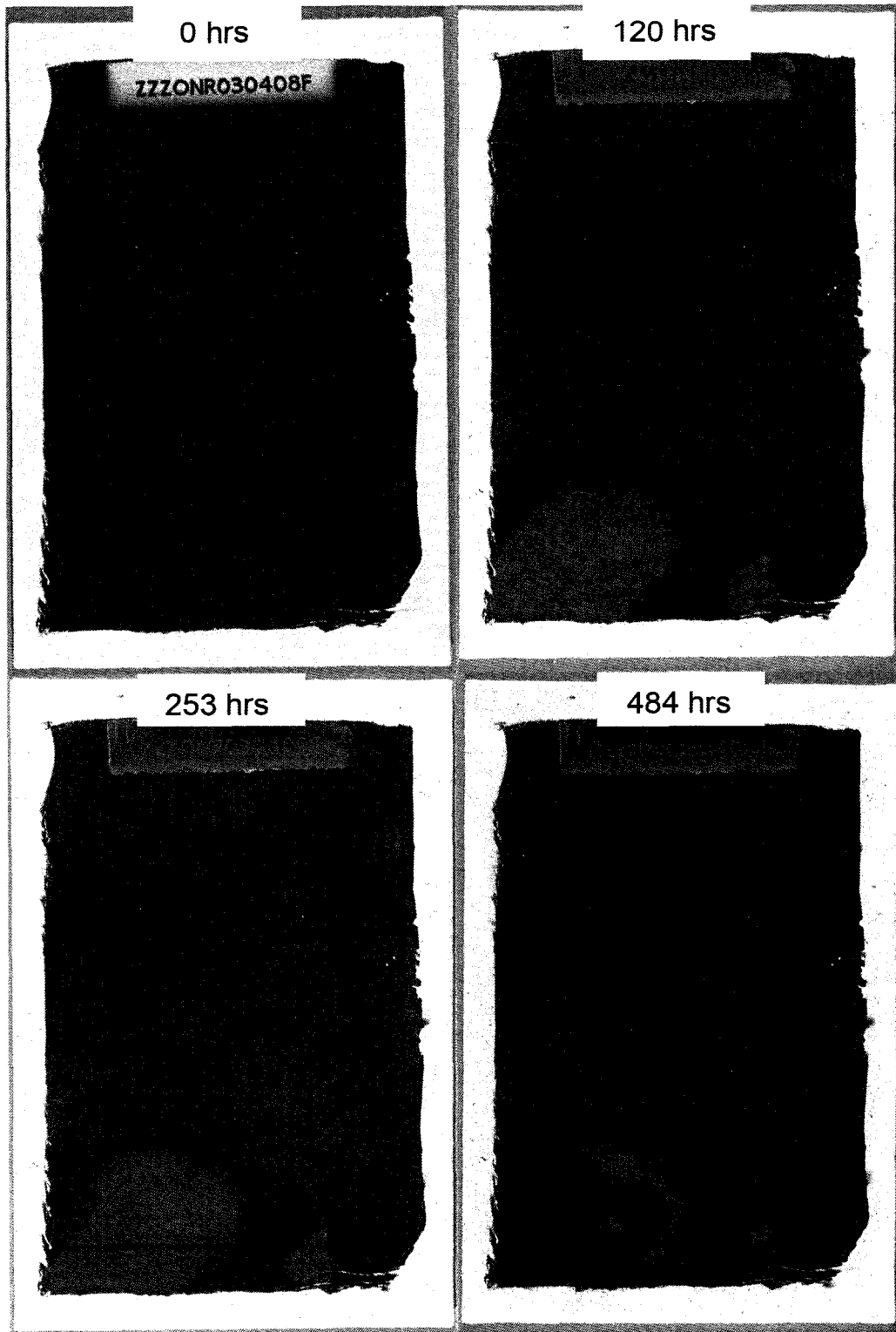
ZZZONR030408C - Salt Spray Exposure - 2.5 wt % DETONR046



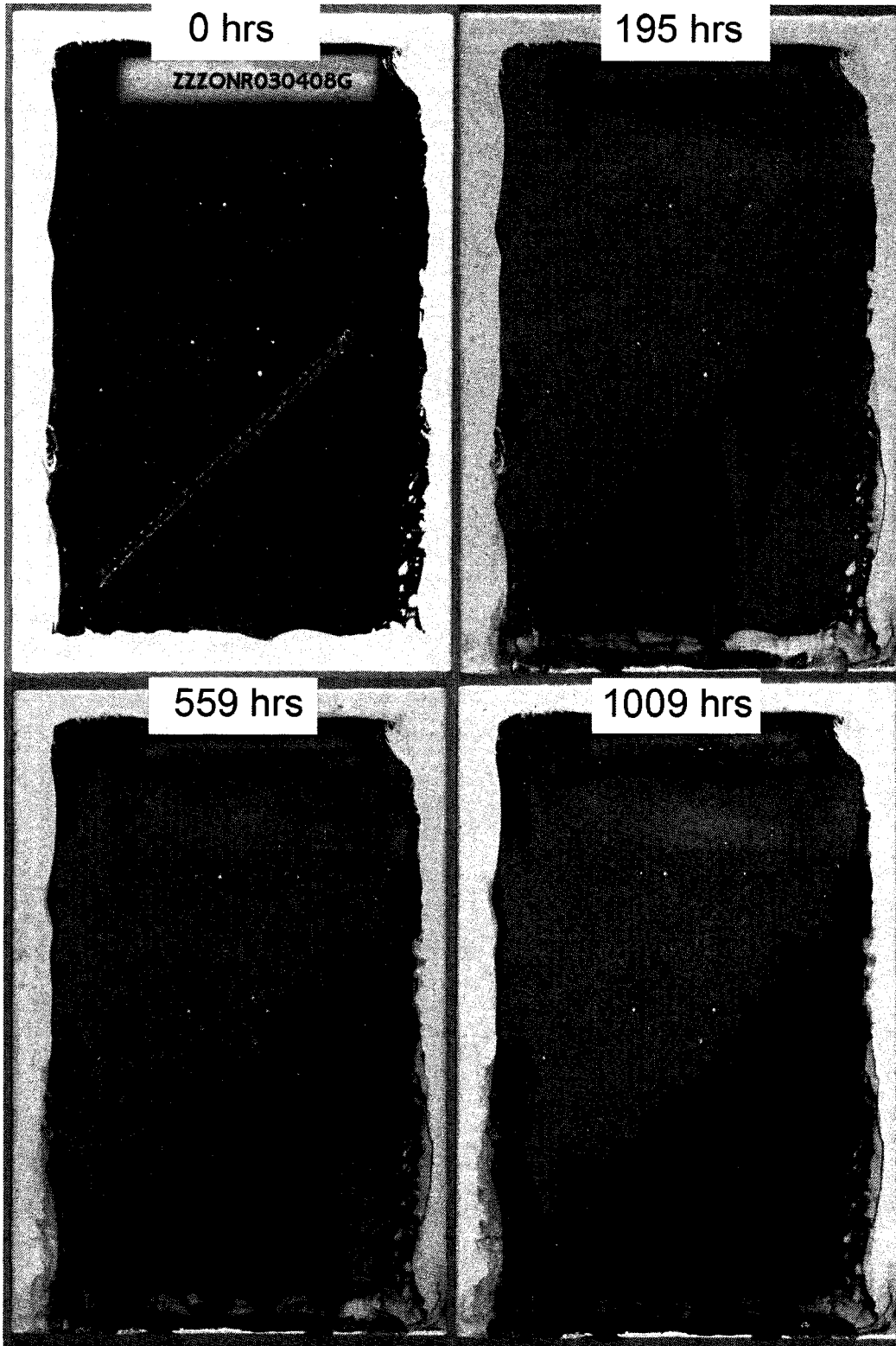
ZZZONR030408D - Hot DI Immersion - 1 wt % DETONR046



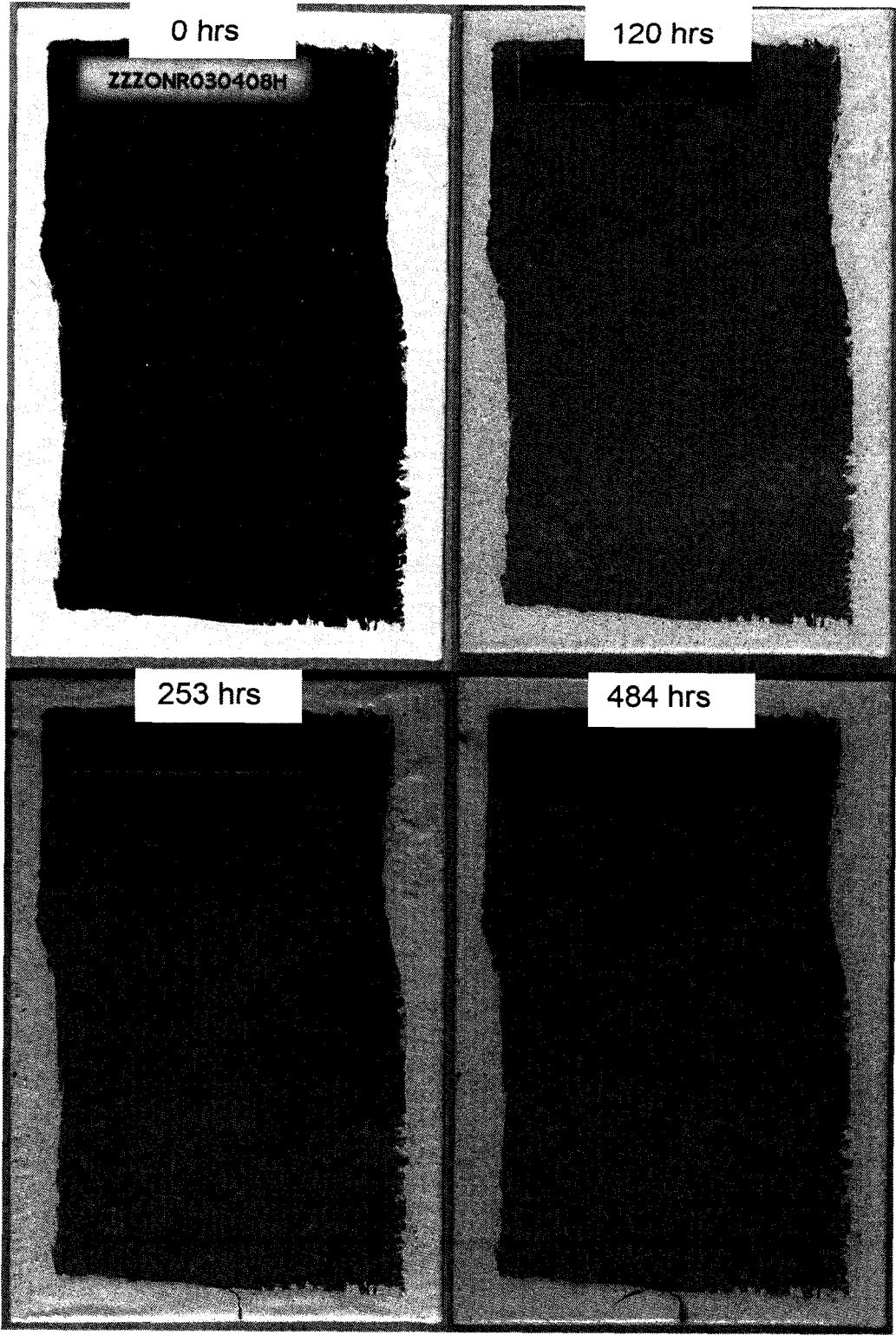
ZZZONR030408E - Salt Spray Exposure - 2.5 wt % DETONR046



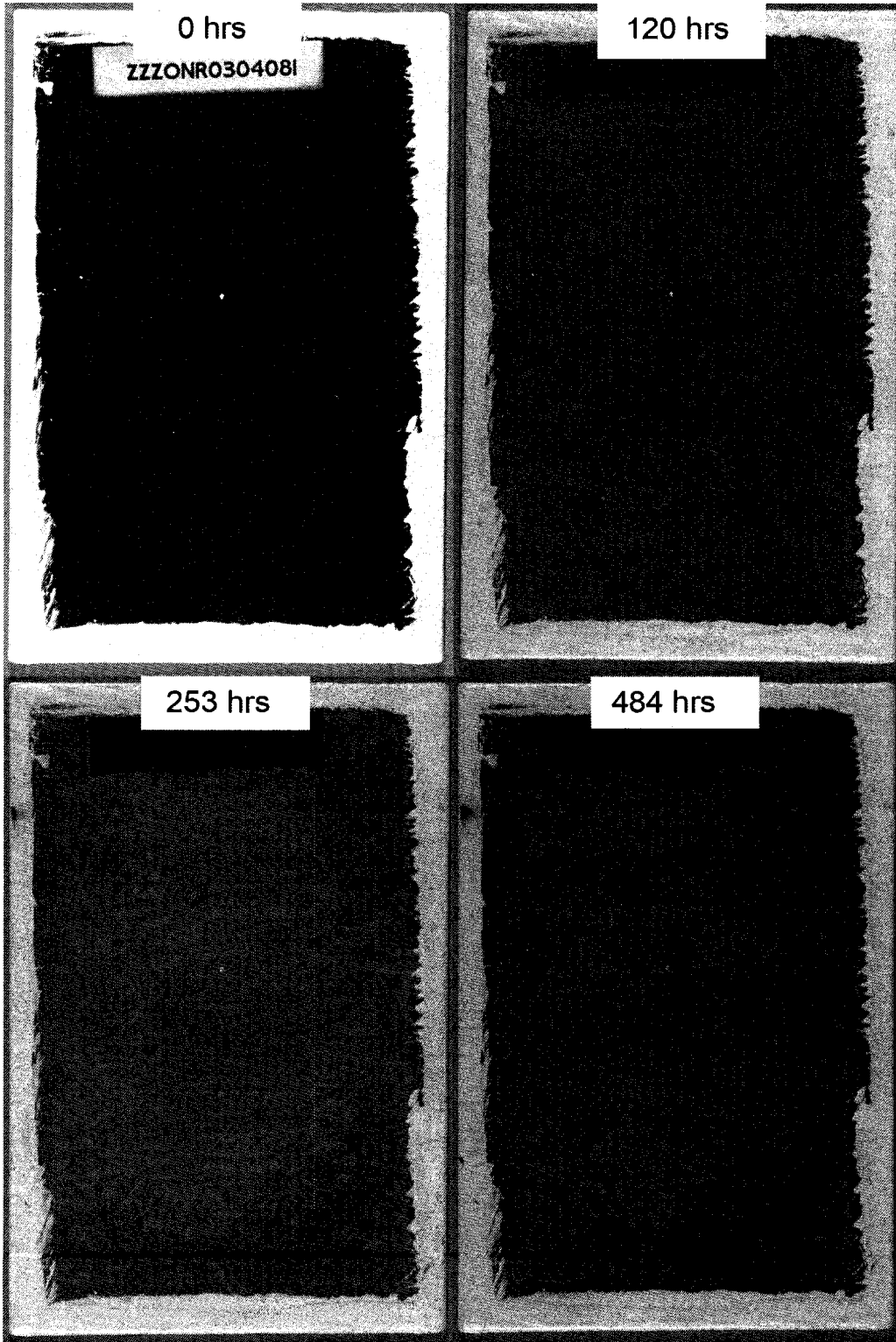
ZZZONR030408F - Hot DI Immersion - 2.5 WT % DETONR046



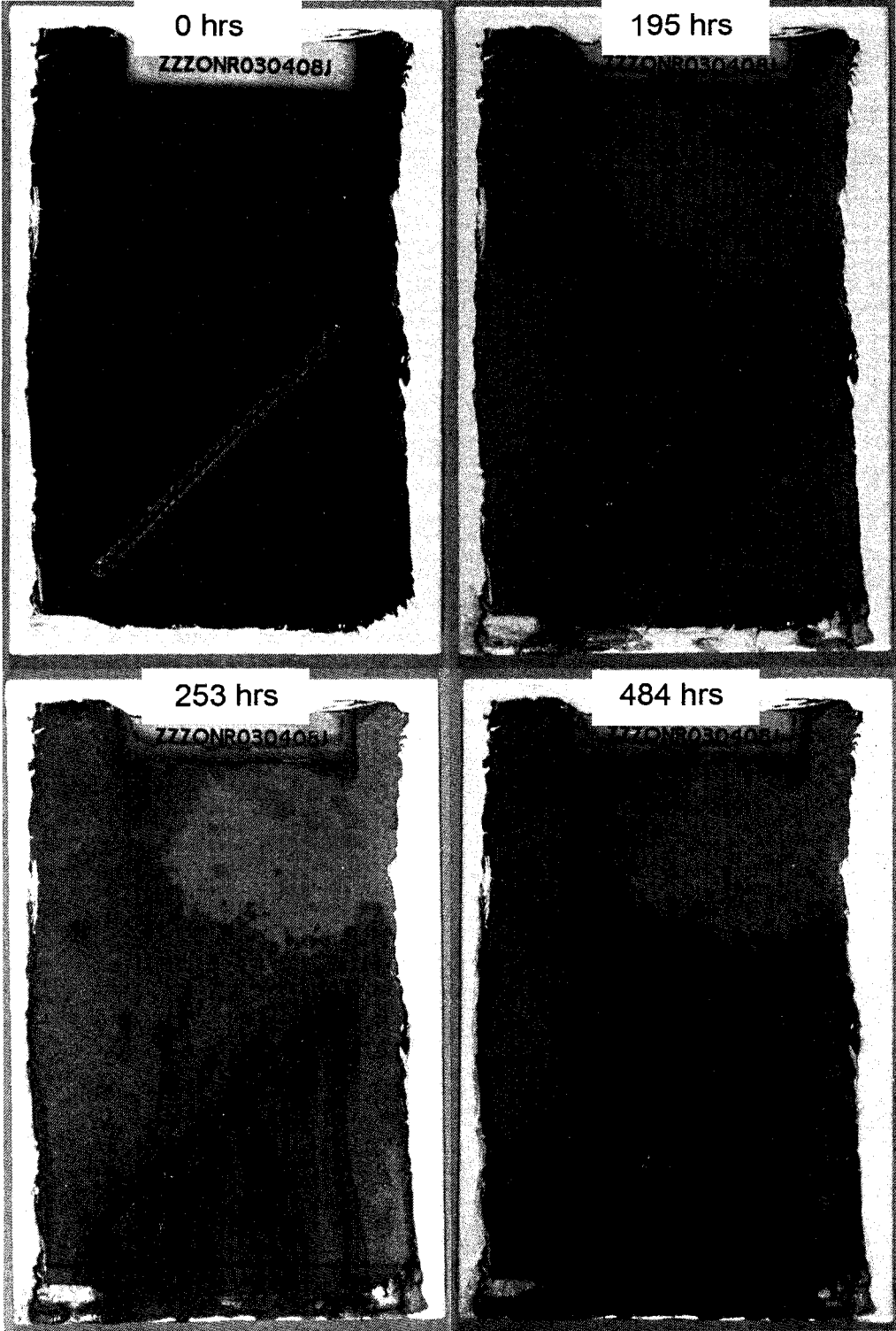
ZZZONR030408 - Salt Spray Exposure - 5 wt % DETONR046



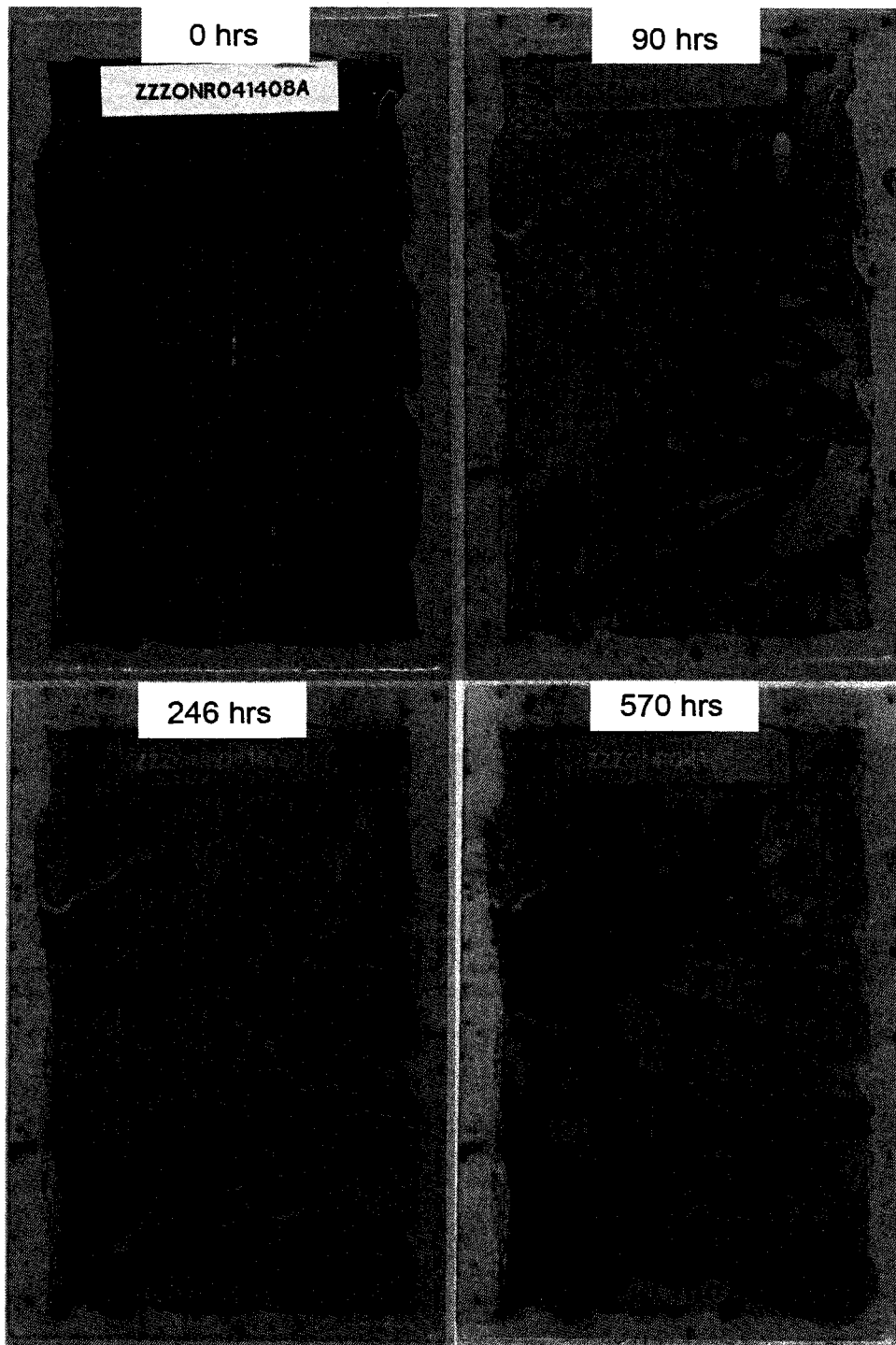
ZZZONR030408G - Hot DI Exposure - 5 wt % DETONR046



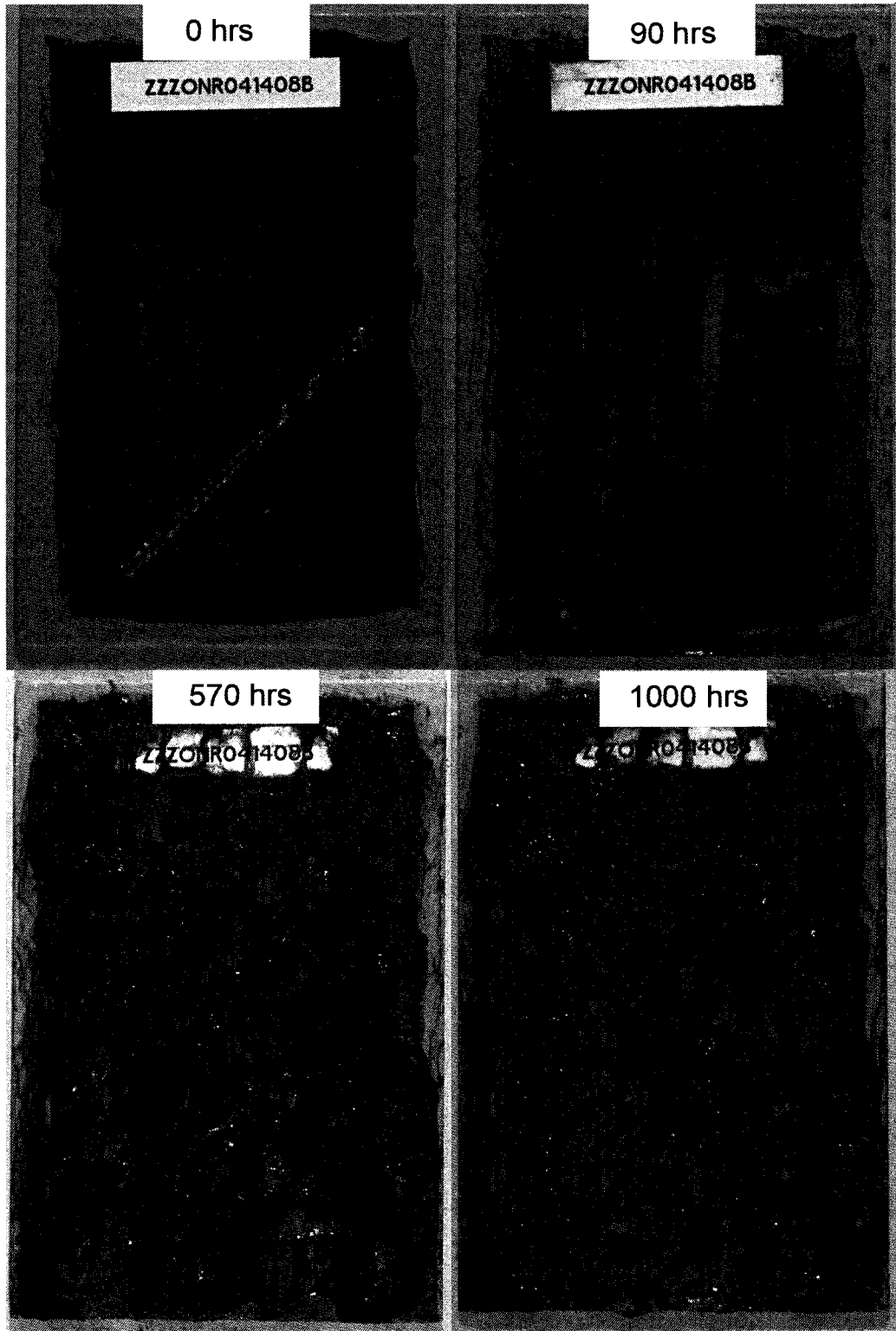
ZZZONR030408I - Hot DI Exposure - 4.9 wt % DETONR046



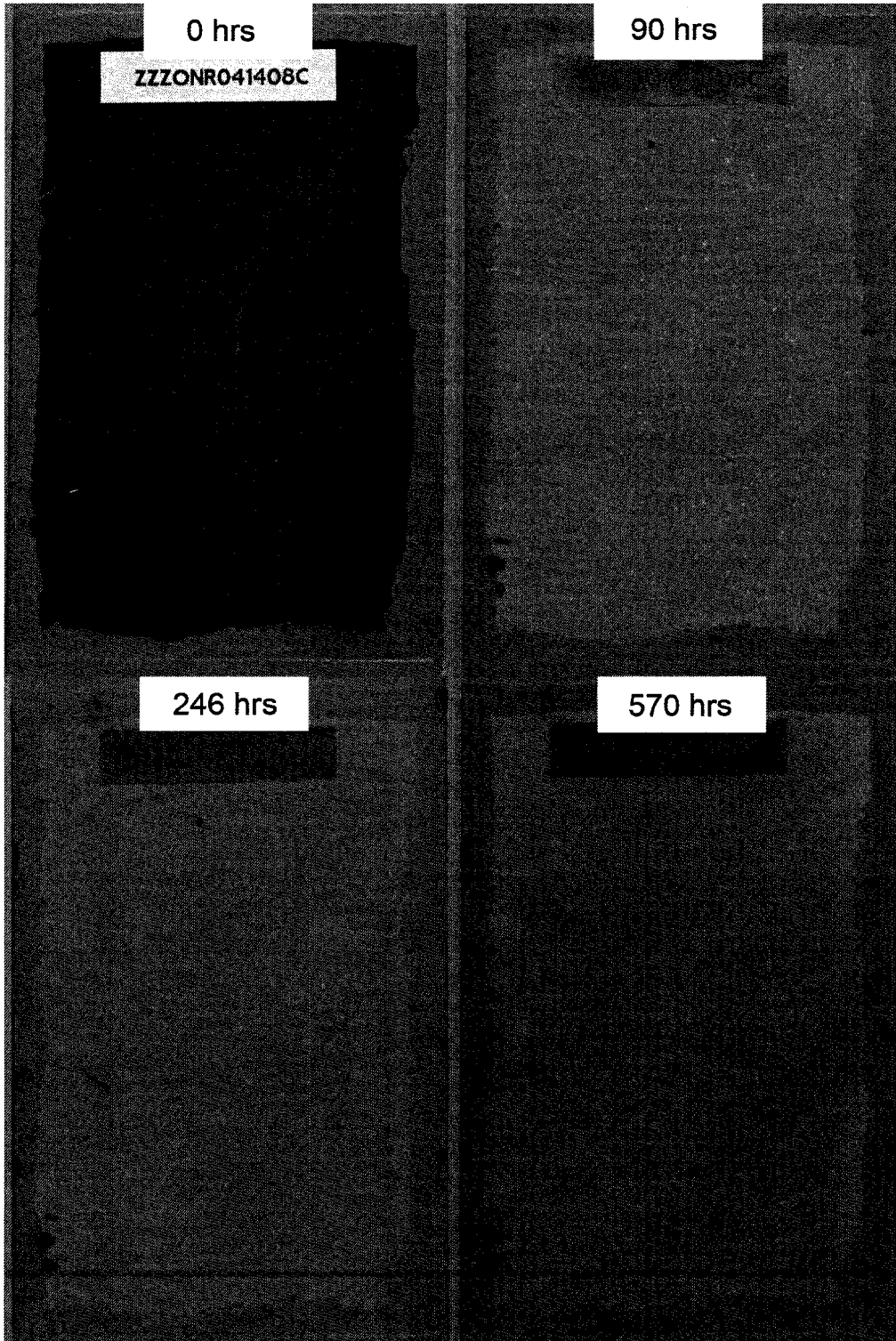
ZZZONR030408J - Salt Spray Exposure - 3.9 wt % DETONR046



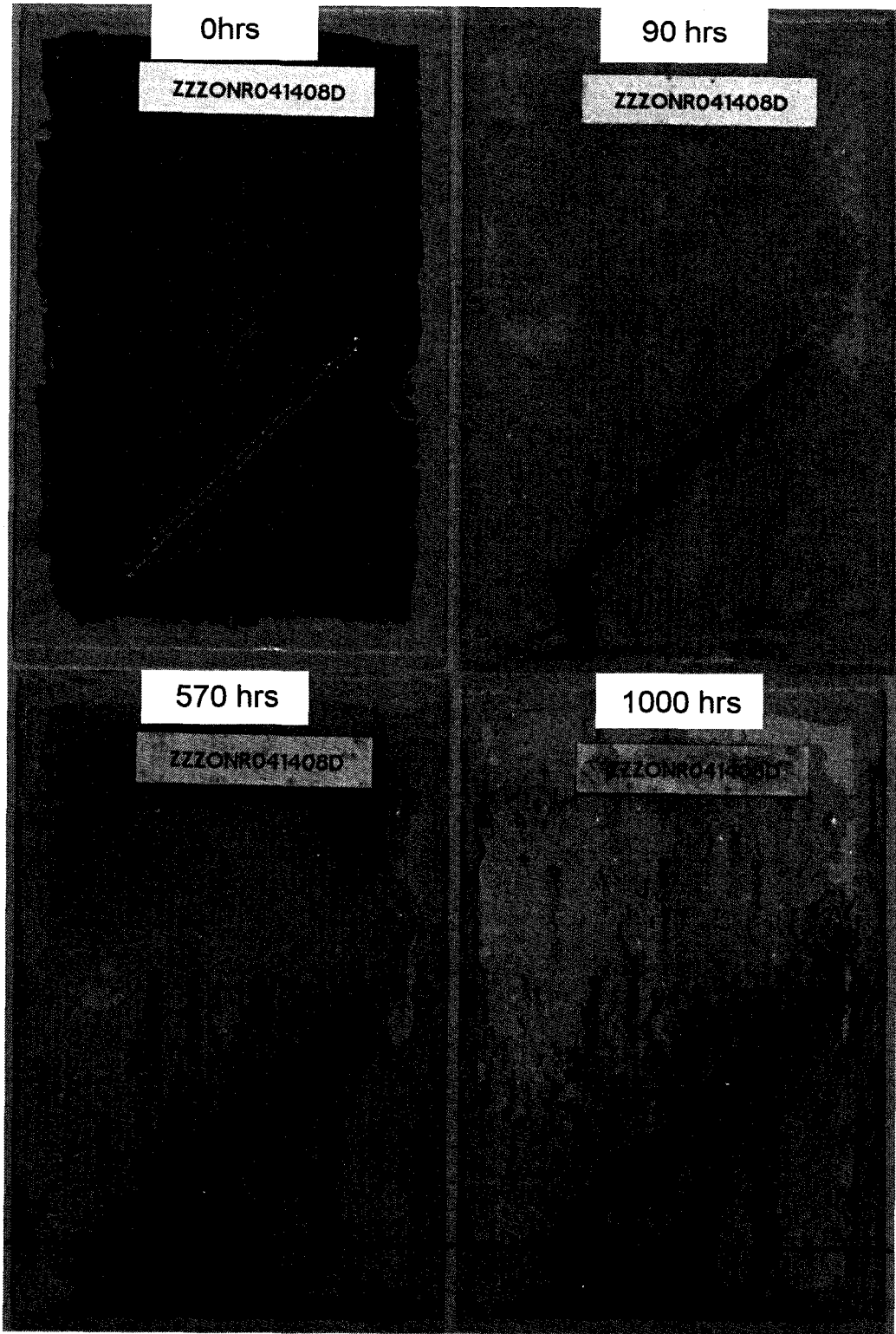
ZZZONR041408A - Hot DI Immersion - Control



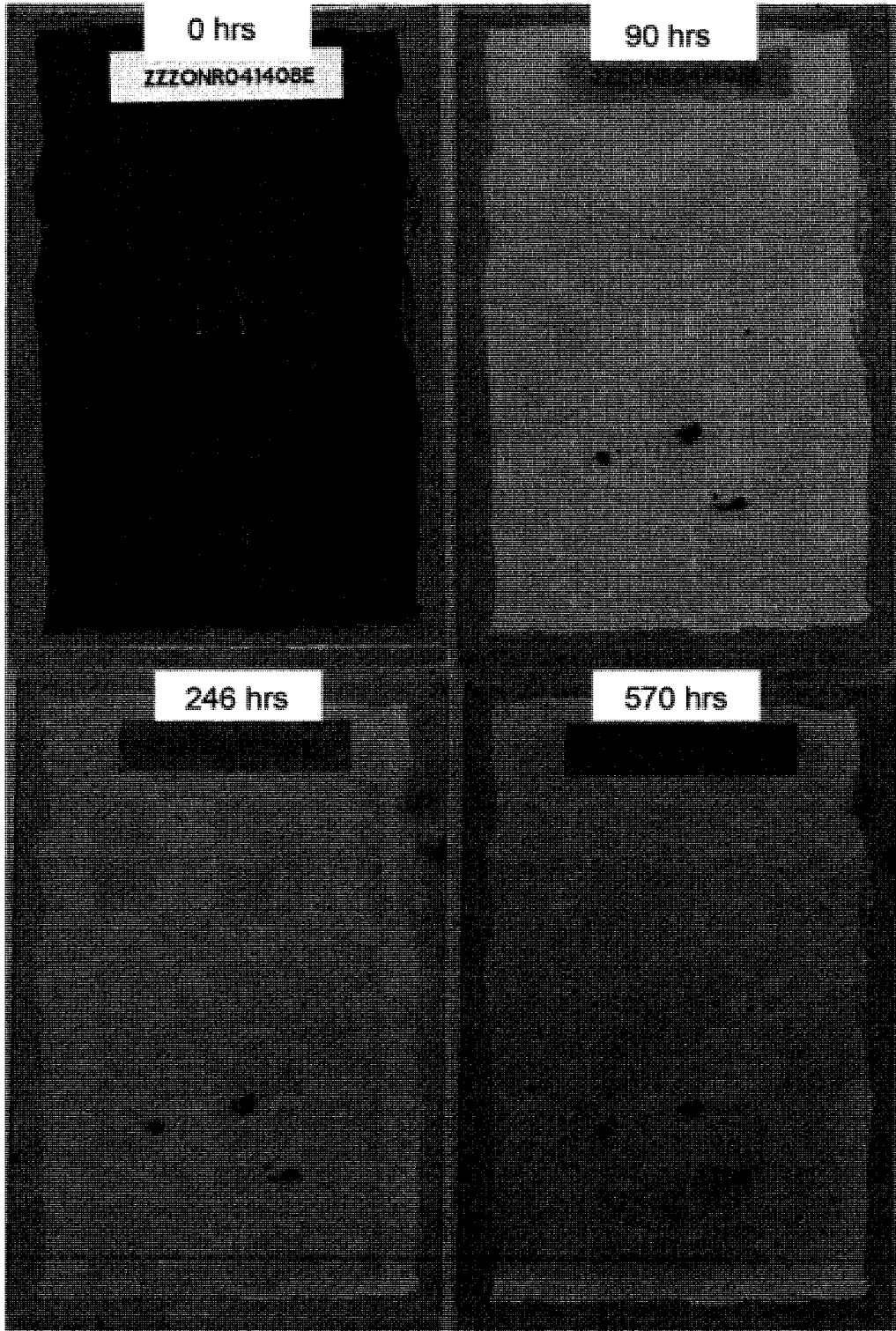
ZZZONR041408B - Salt Spray Exposure - Control



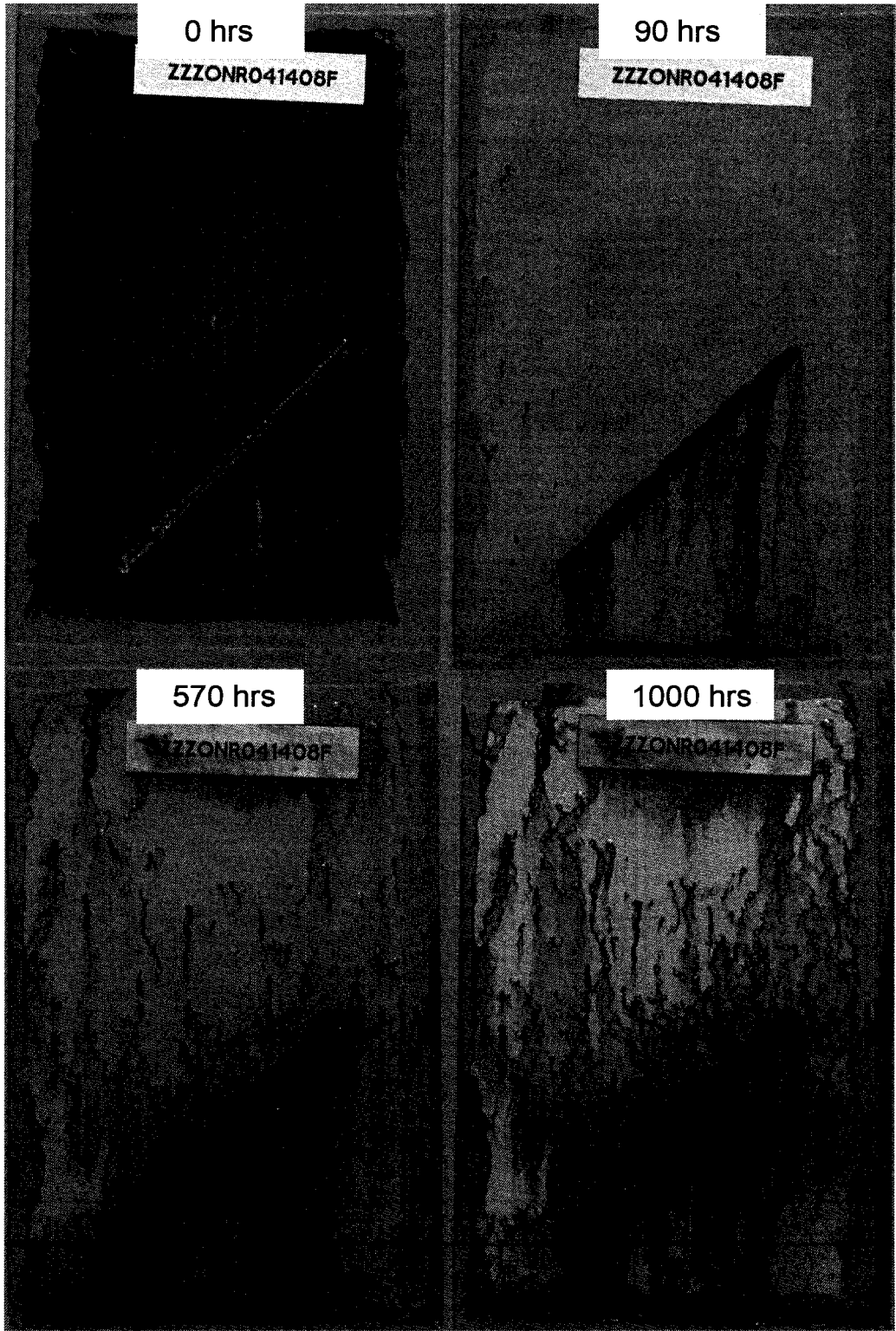
ZZZONR041408C - Hot DI Immersion - 5 wt % ZZZONR040808



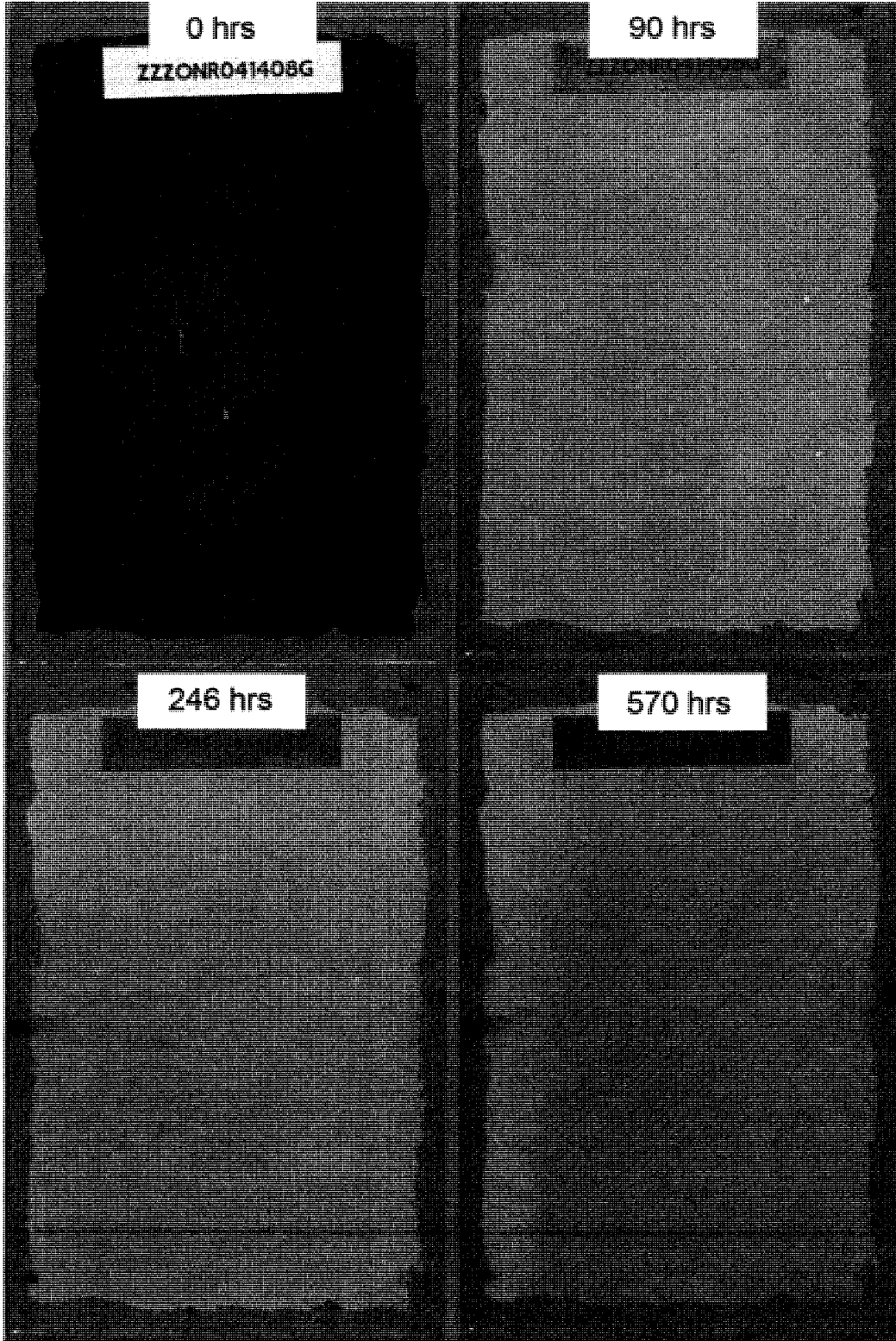
ZZZONR041408D - Salt Spray Exposure - 5 wt % ZZZONR040808



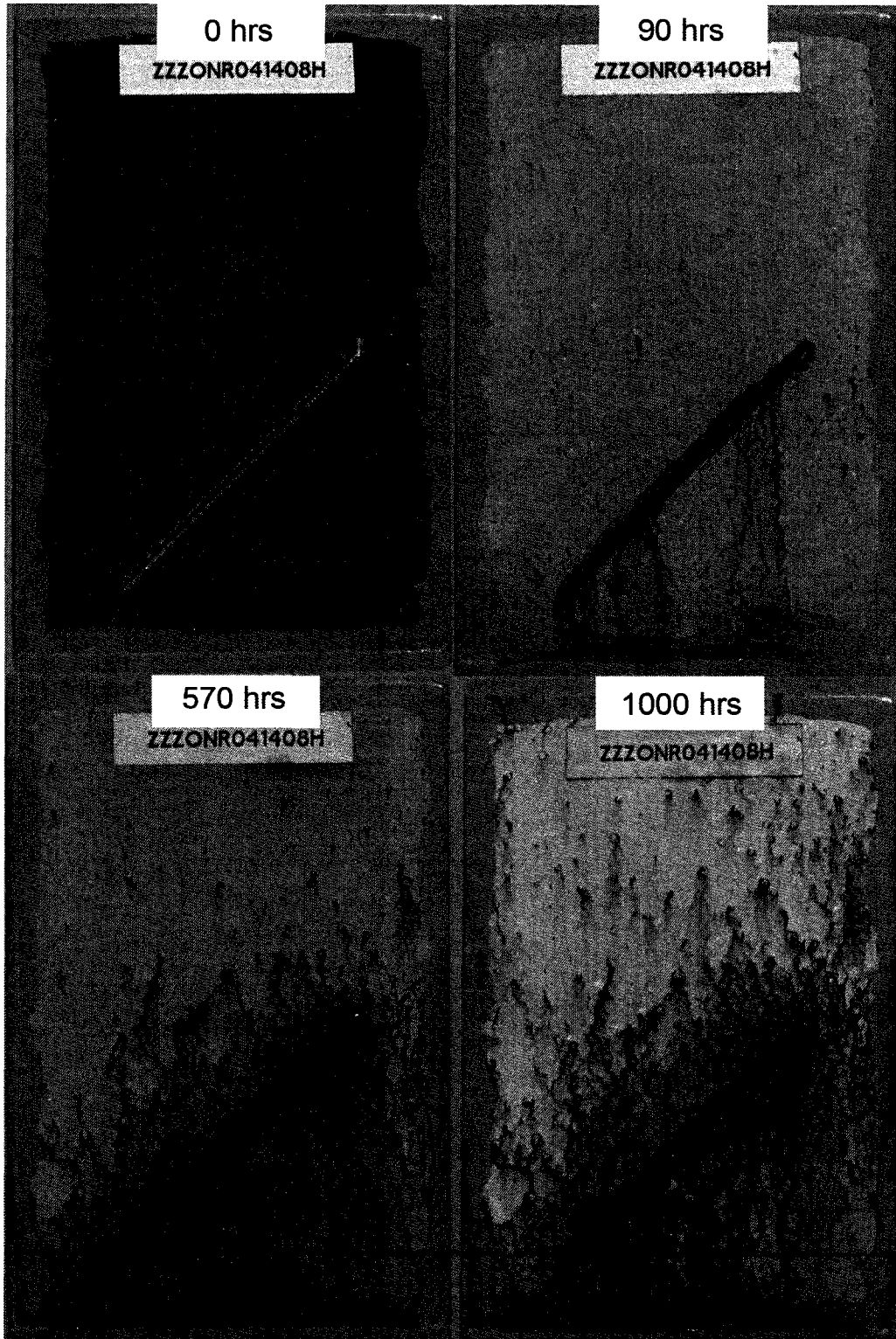
ZZZONR041408E - Hot DI Immersion - 10 wt % ZZZONR040808



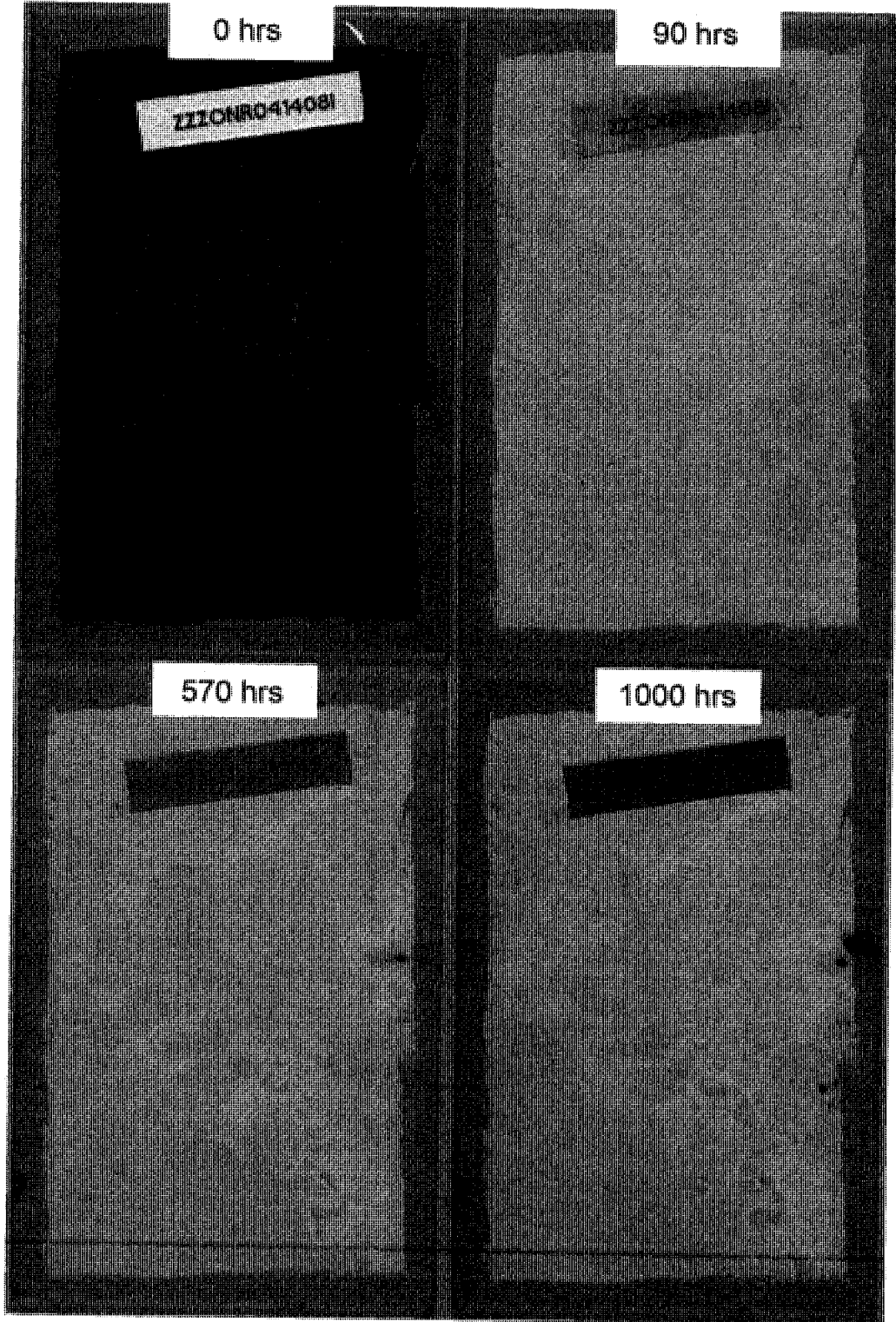
ZZZONR041408F - Salt Spray Exposure - 10 wt % ZZZONR040808



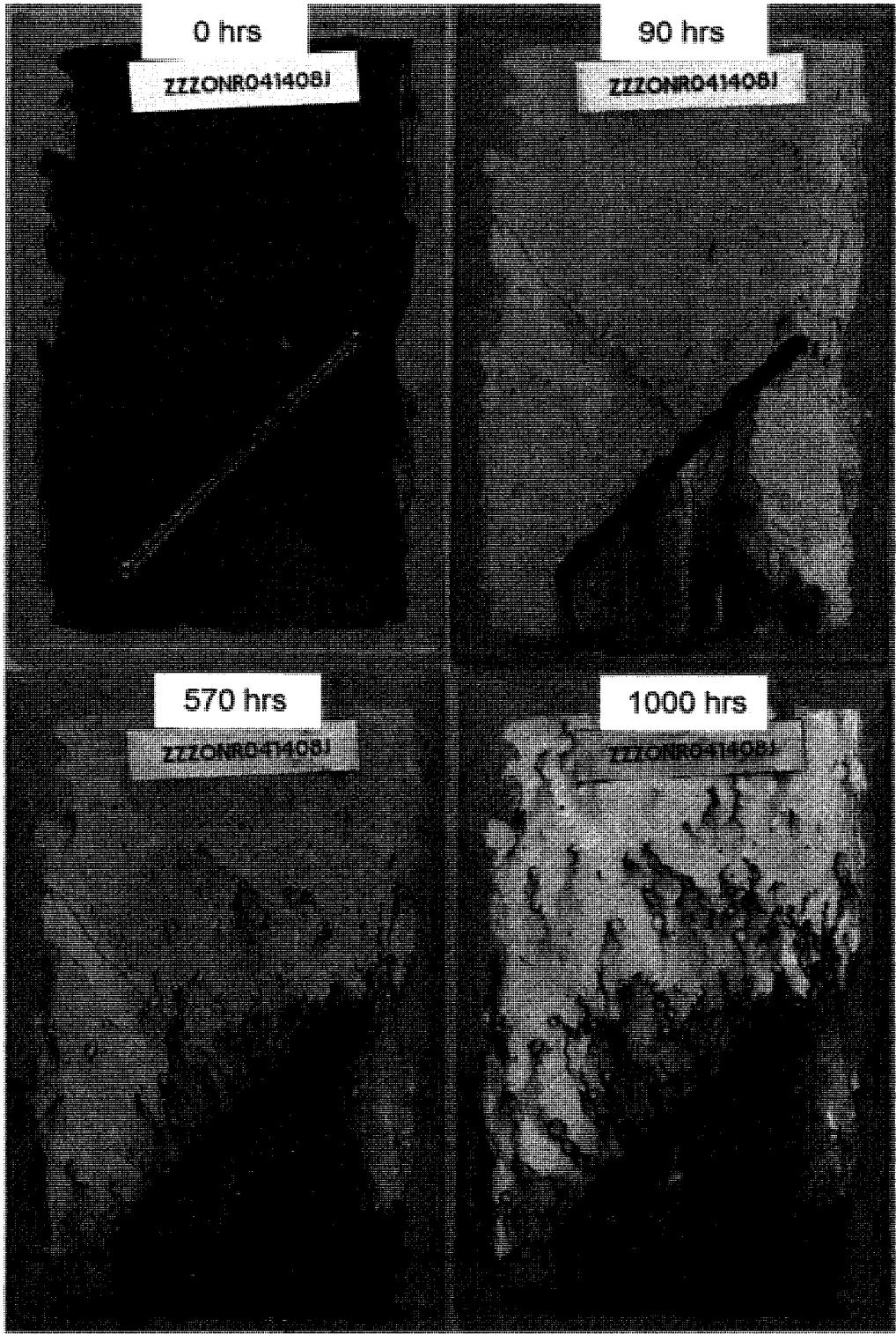
ZZZONR 041408G - Hot DI Exposure - 15 wt % ZZZONR040808



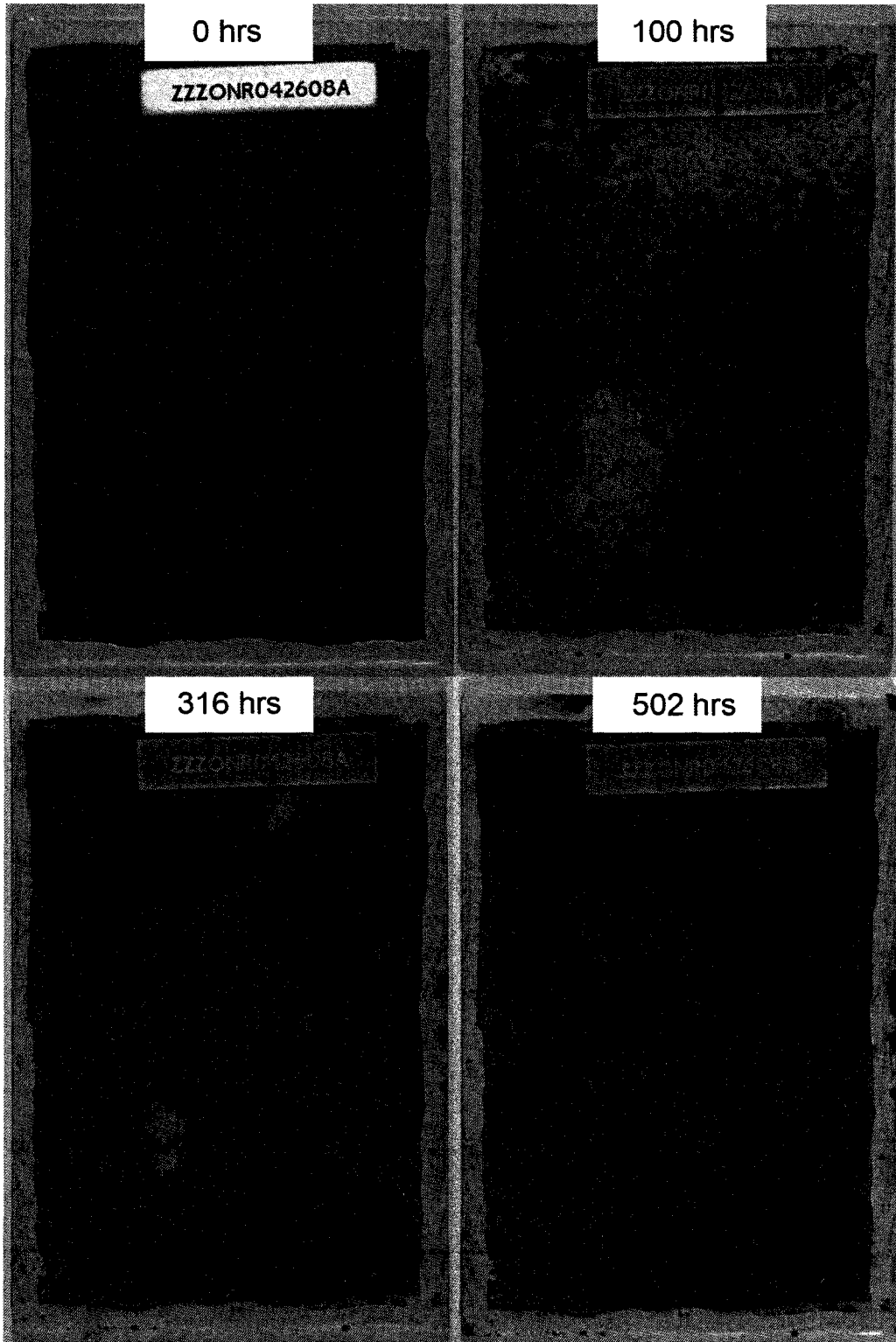
ZZZONR041408H - Salt Spray Exposure - 15 wt % ZZZONR040808



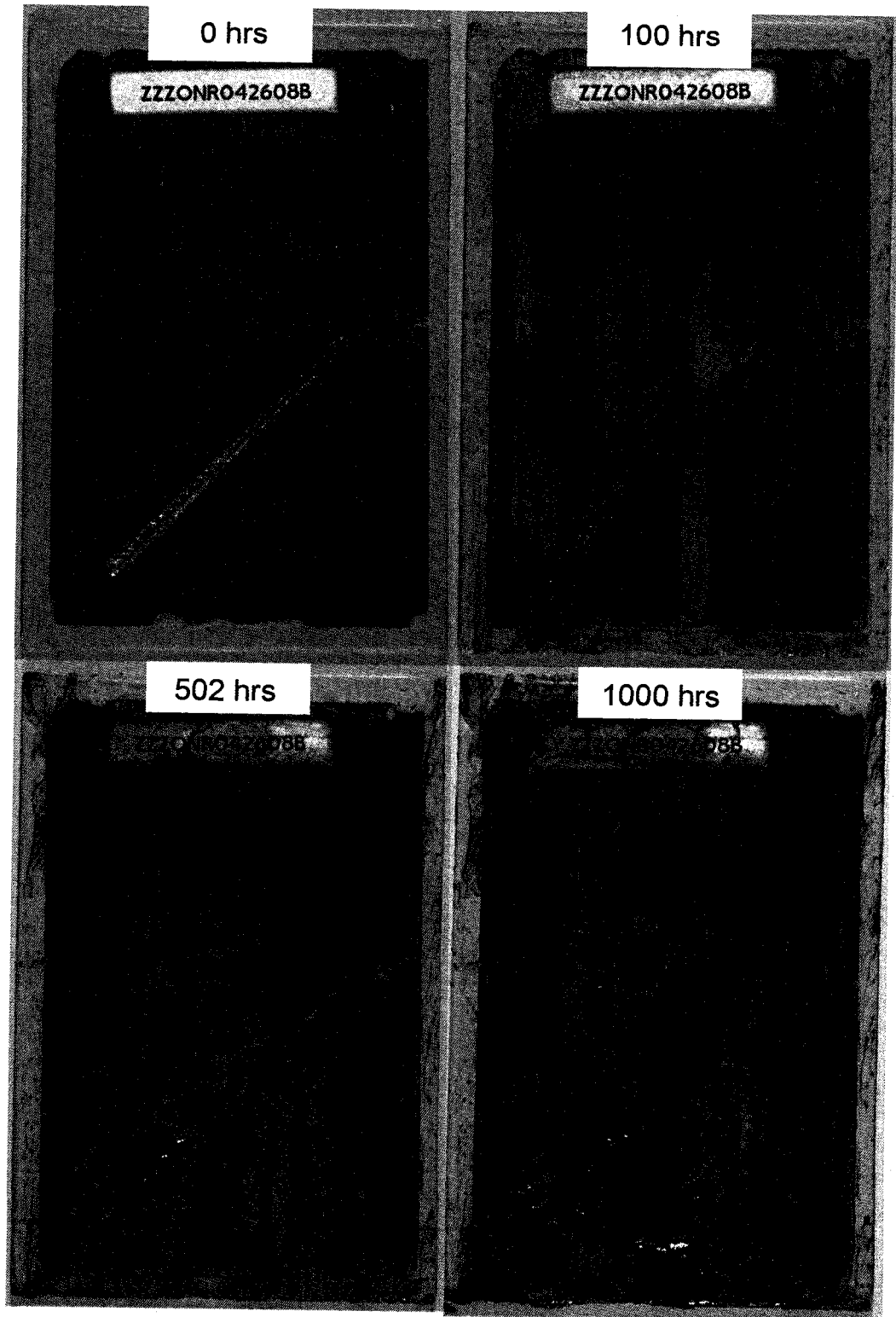
ZZZONR041408I - Hot DI Immersion - 20 wt % ZZZONR040808



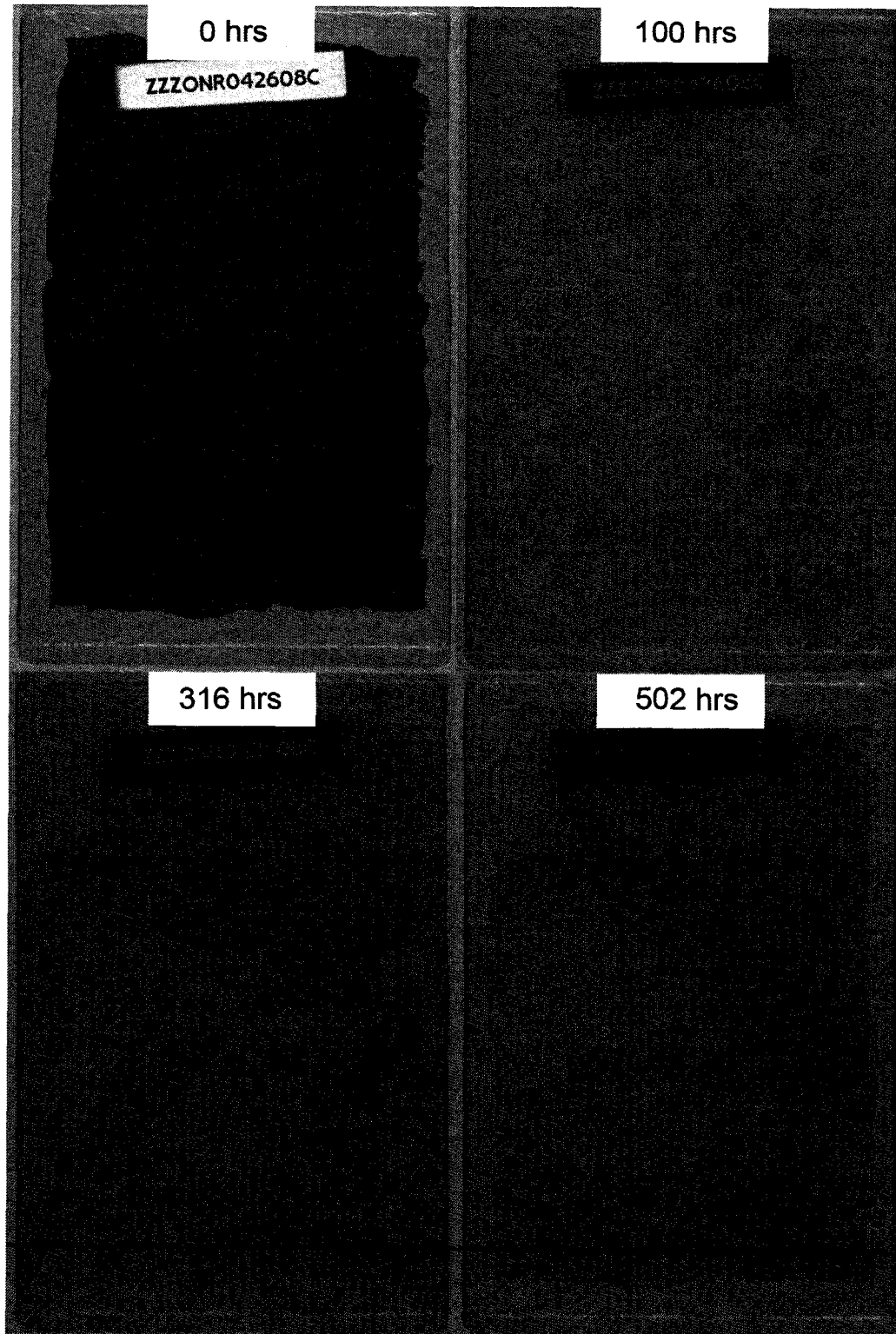
ZZZONR041408J - Salt Spray Exposure - 20 wt % ZZZONR040808



ZZZONR042608A - Hot DI Immersion - Control



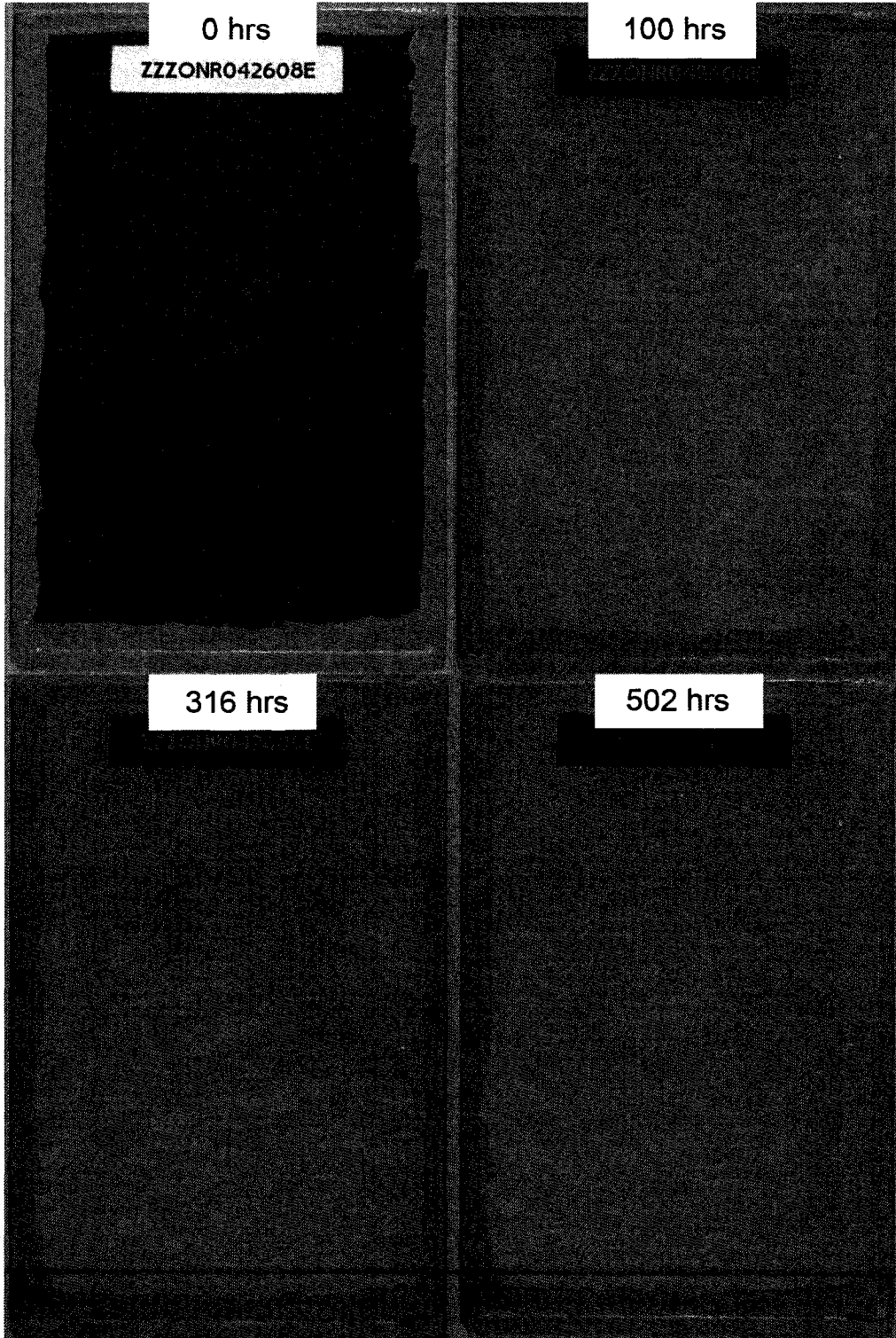
ZZZONR042608B - Salt Spray Exposure - Control



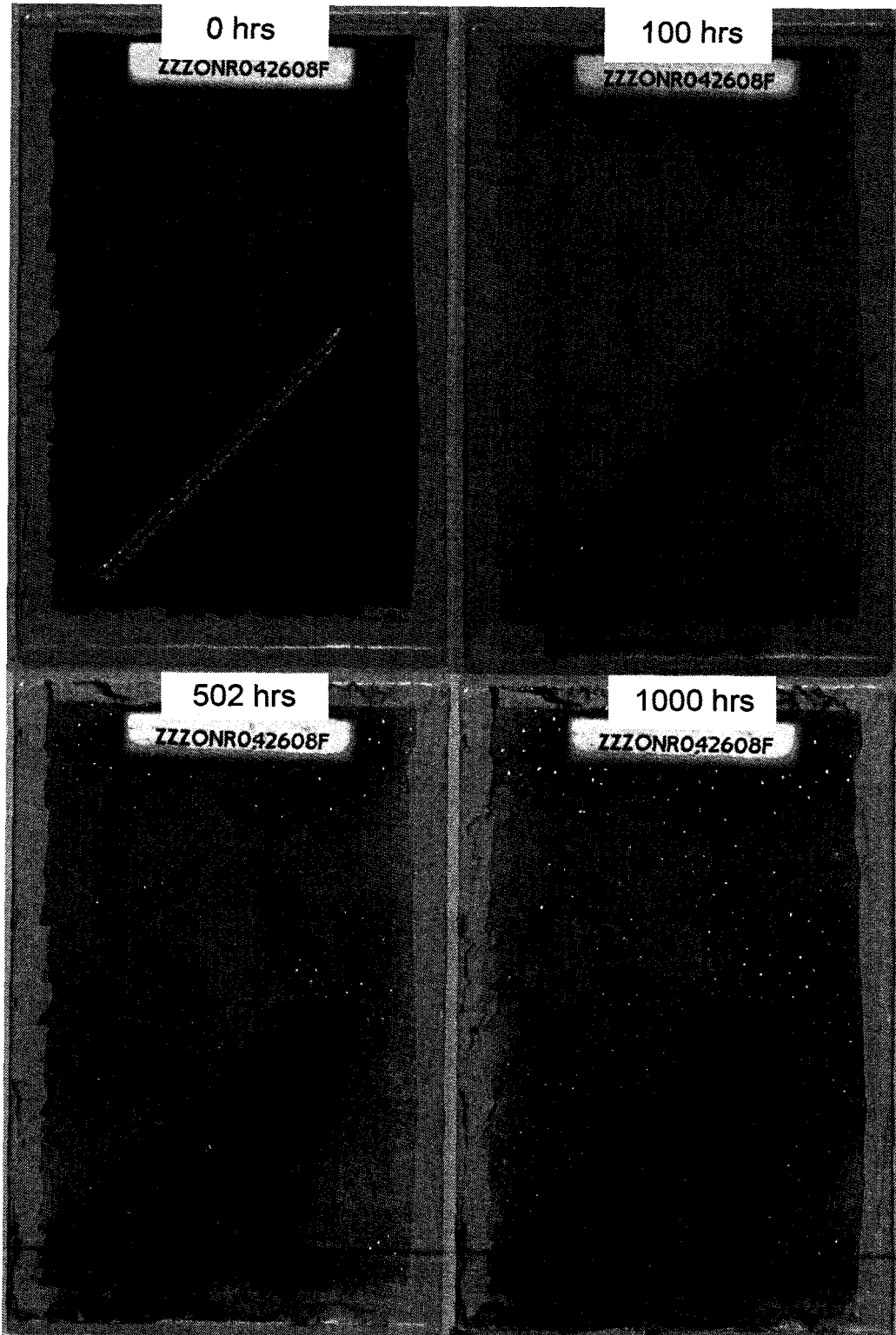
ZZZONR042008C - Hot DI Immersion - 2.5 wt % ZZZONR042408



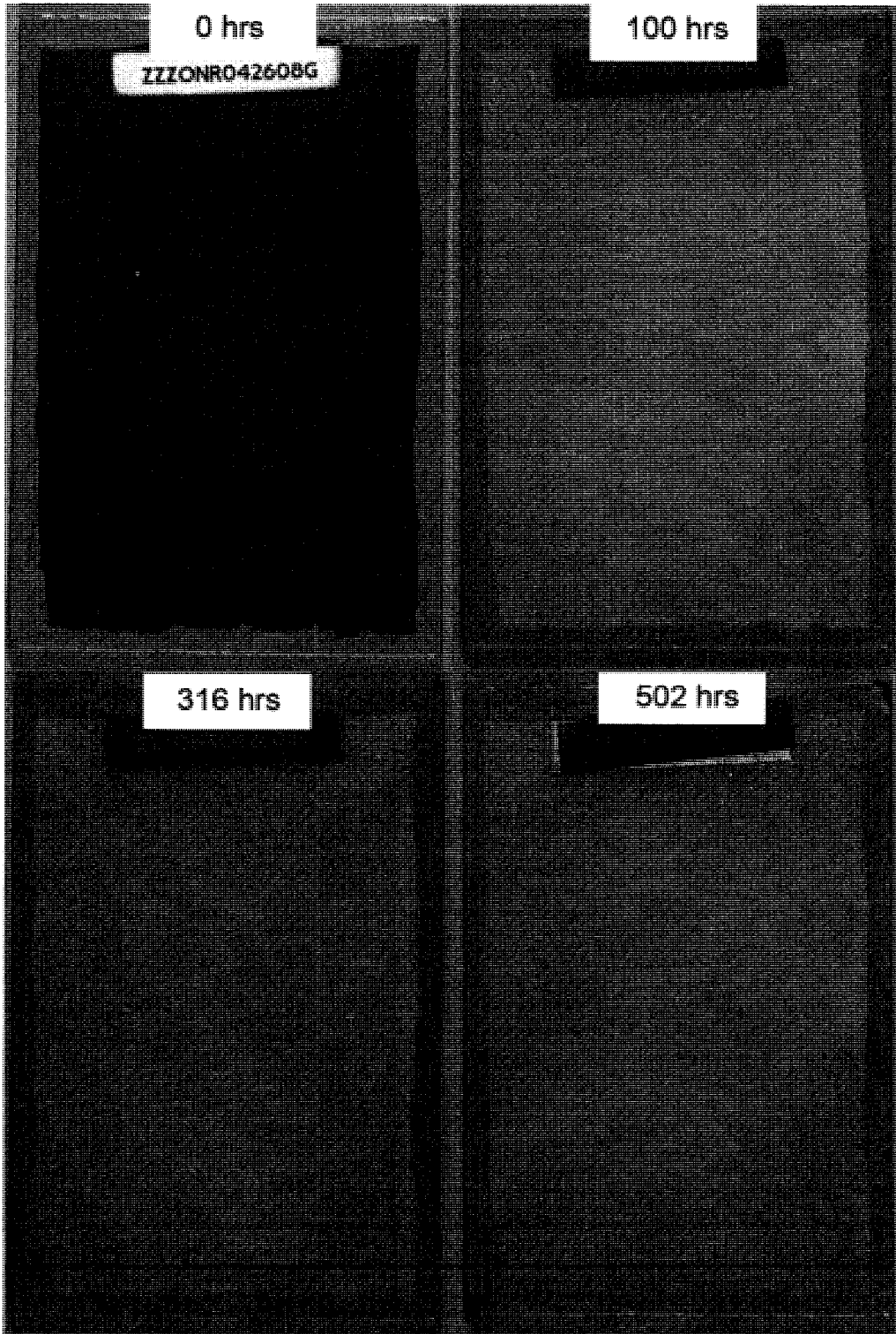
ZZZONR042608D - Salt Spray Exposure - 2.5 wt % ZZZONR042408



ZZZONR042608E - Hot DI Immersion - 5 wt % ZZZONR042408



ZZZONR042608F - Salt Spray Exposure - 5 wt % ZZZONR042408



ZZZONR042608G

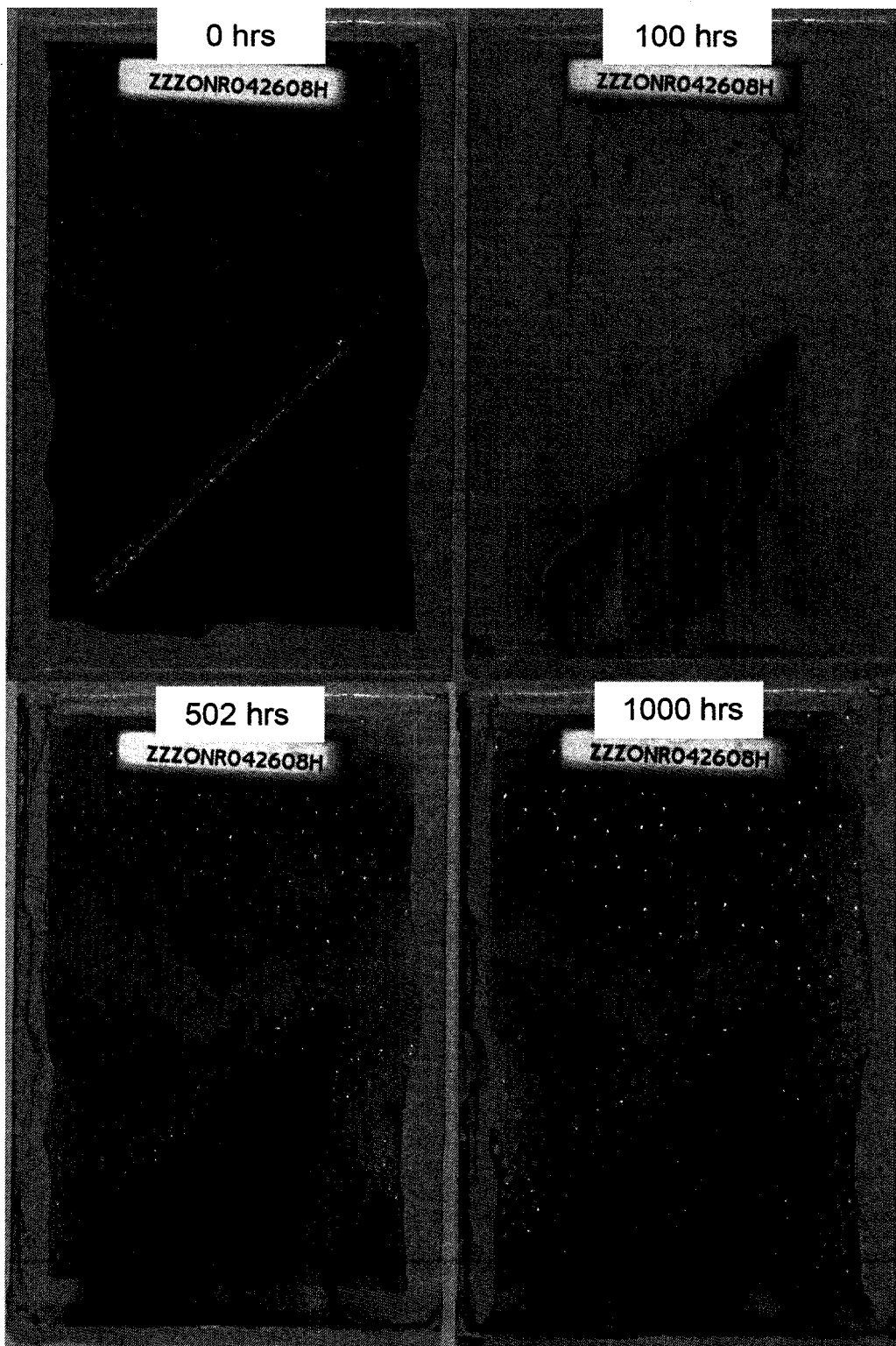
0 hrs

100 hrs

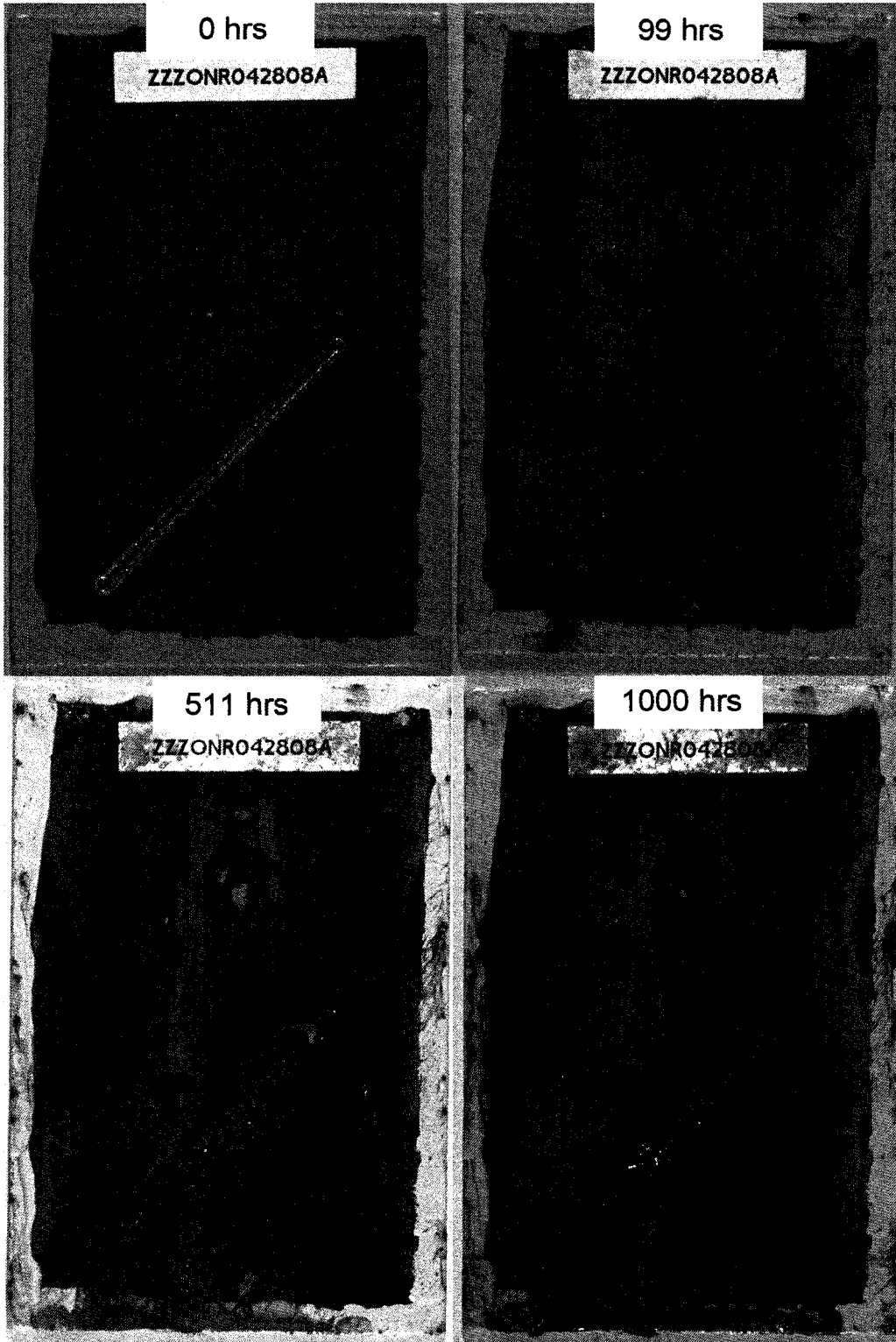
316 hrs

502 hrs

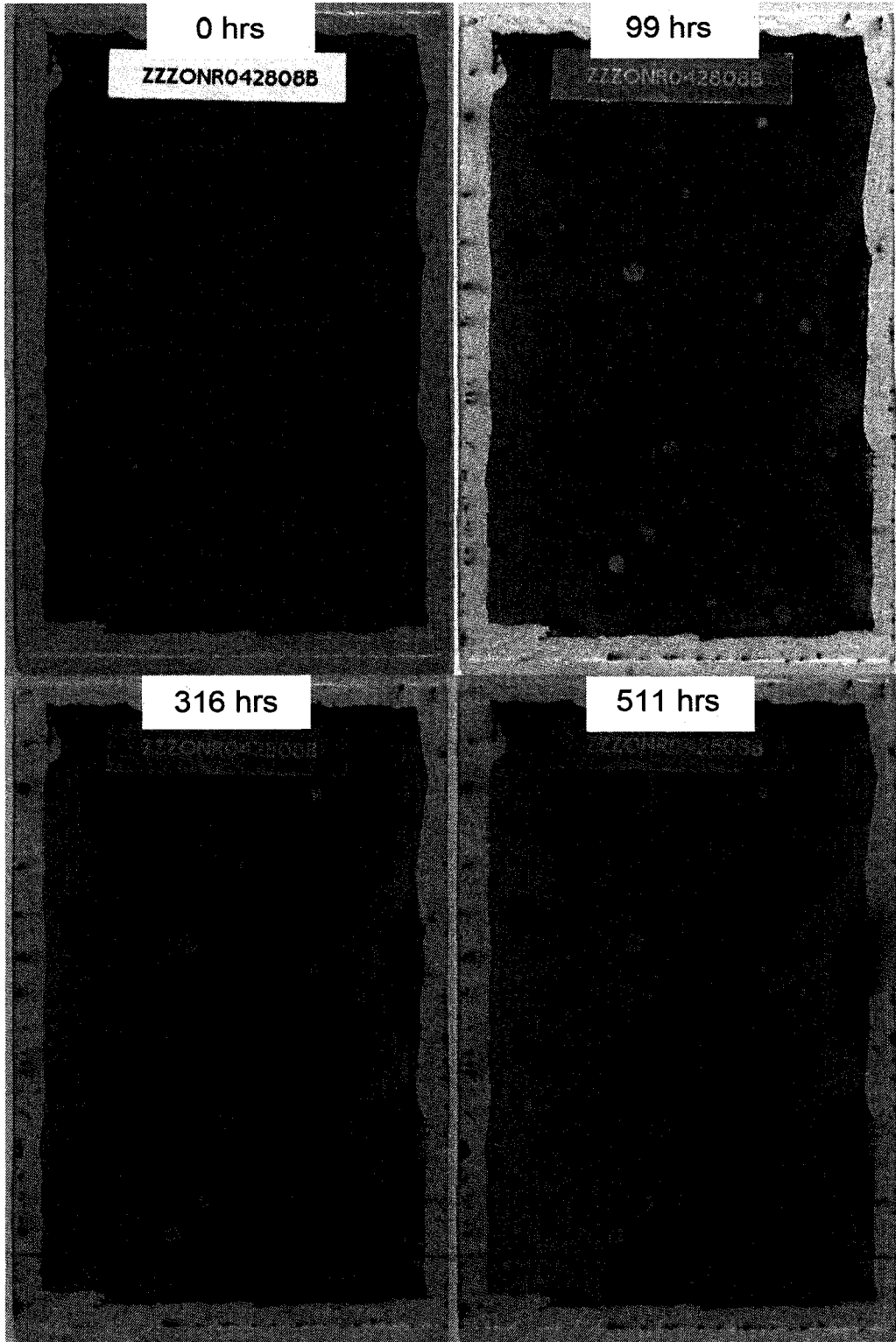
ZZZONR042608G - Hot DI Immersion - 10 wt % ZZZONR042408



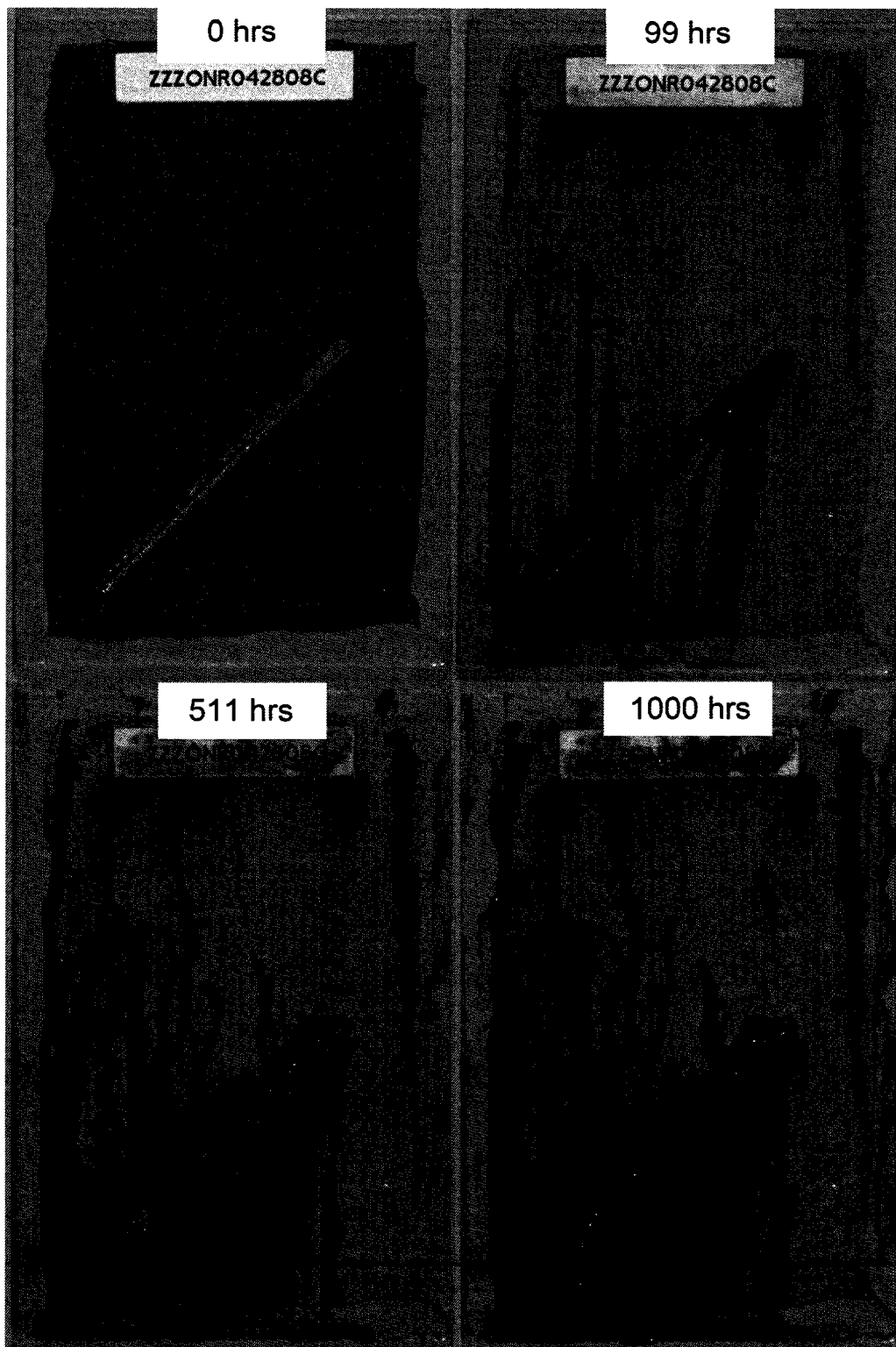
ZZZONR042608H - Salt Spray Exposure - 10 wt % ZZZONR042408



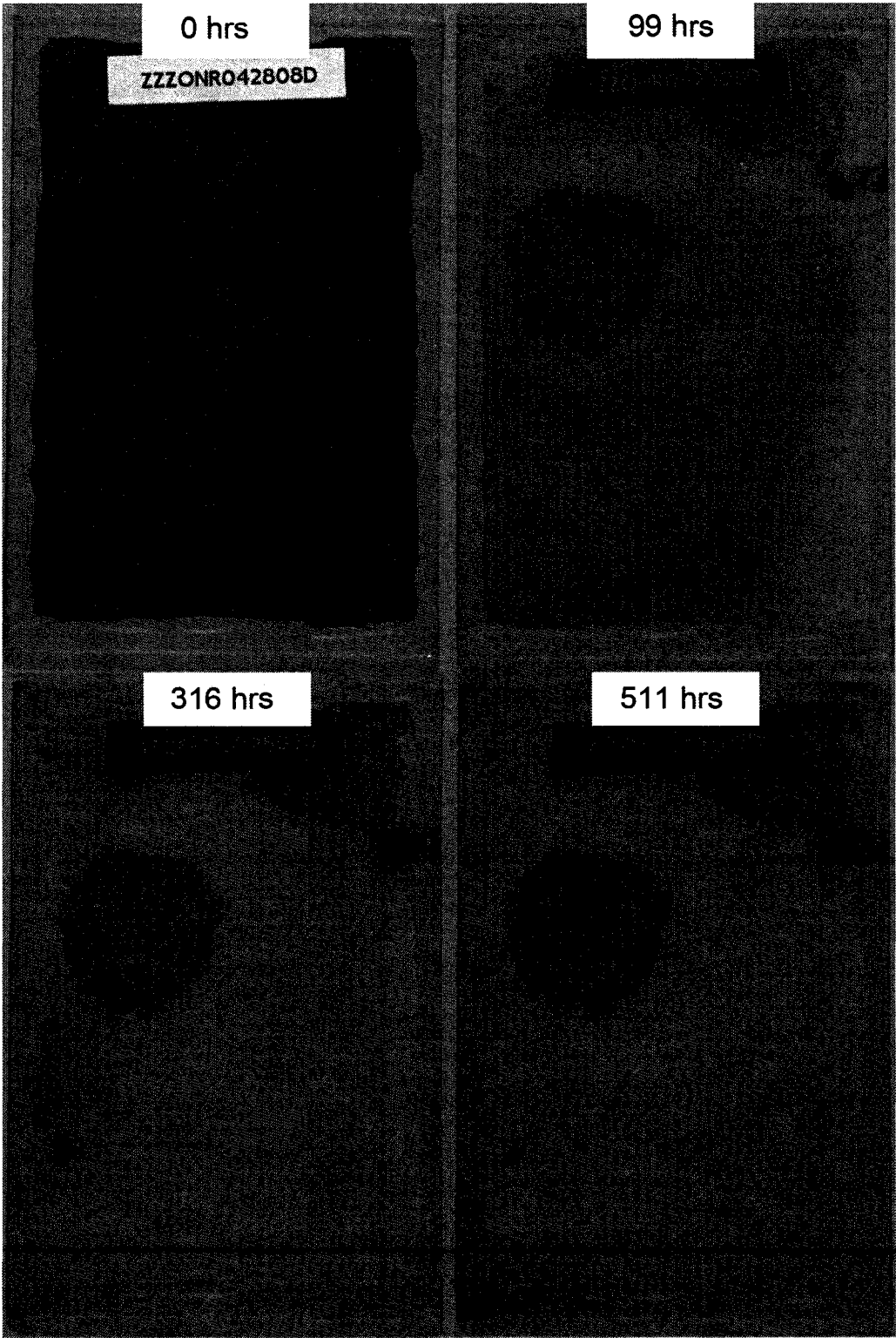
ZZZONR042808A - Salt Spray Exposure - Control



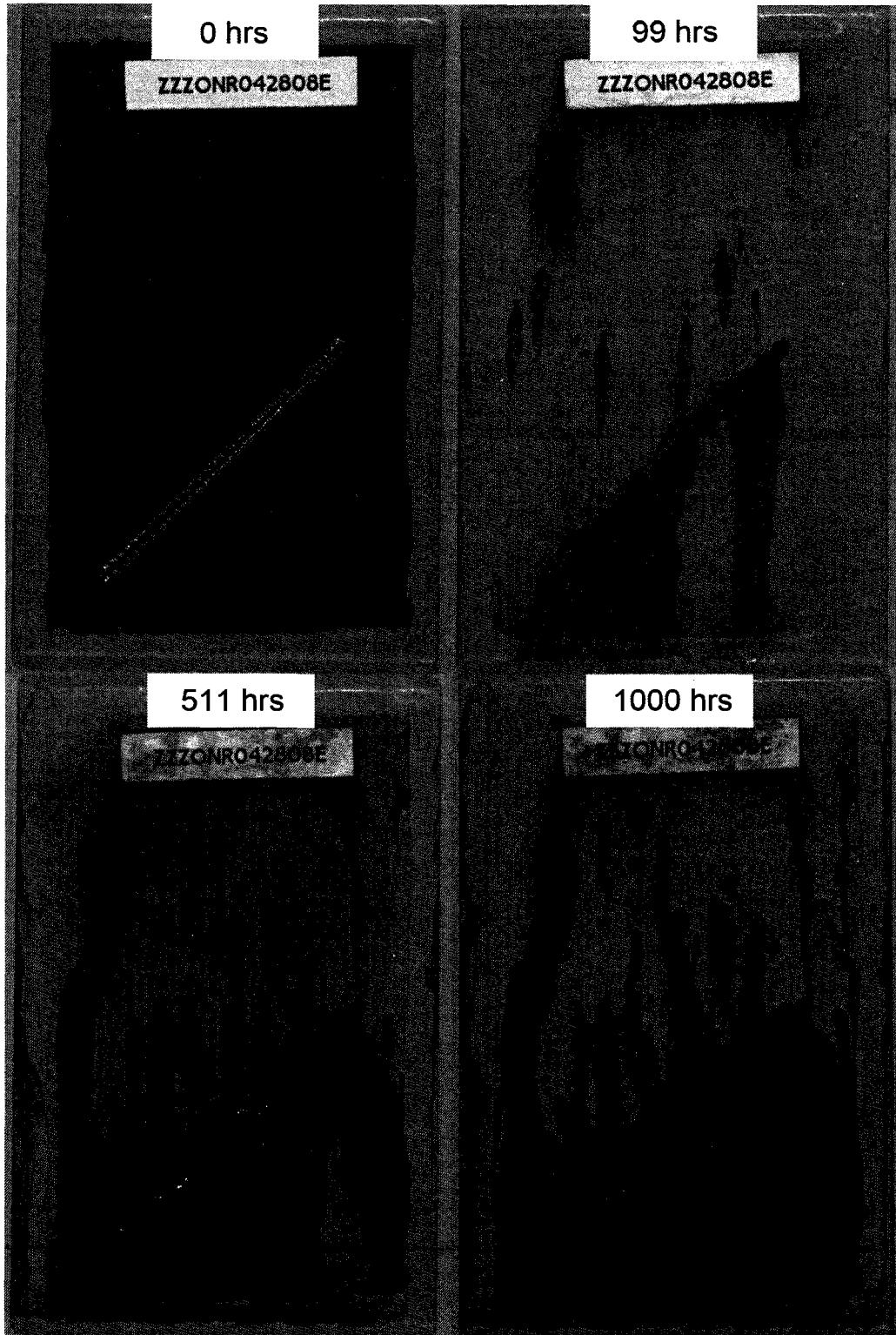
ZZZONR042808B - Hot DI Immersion - Control



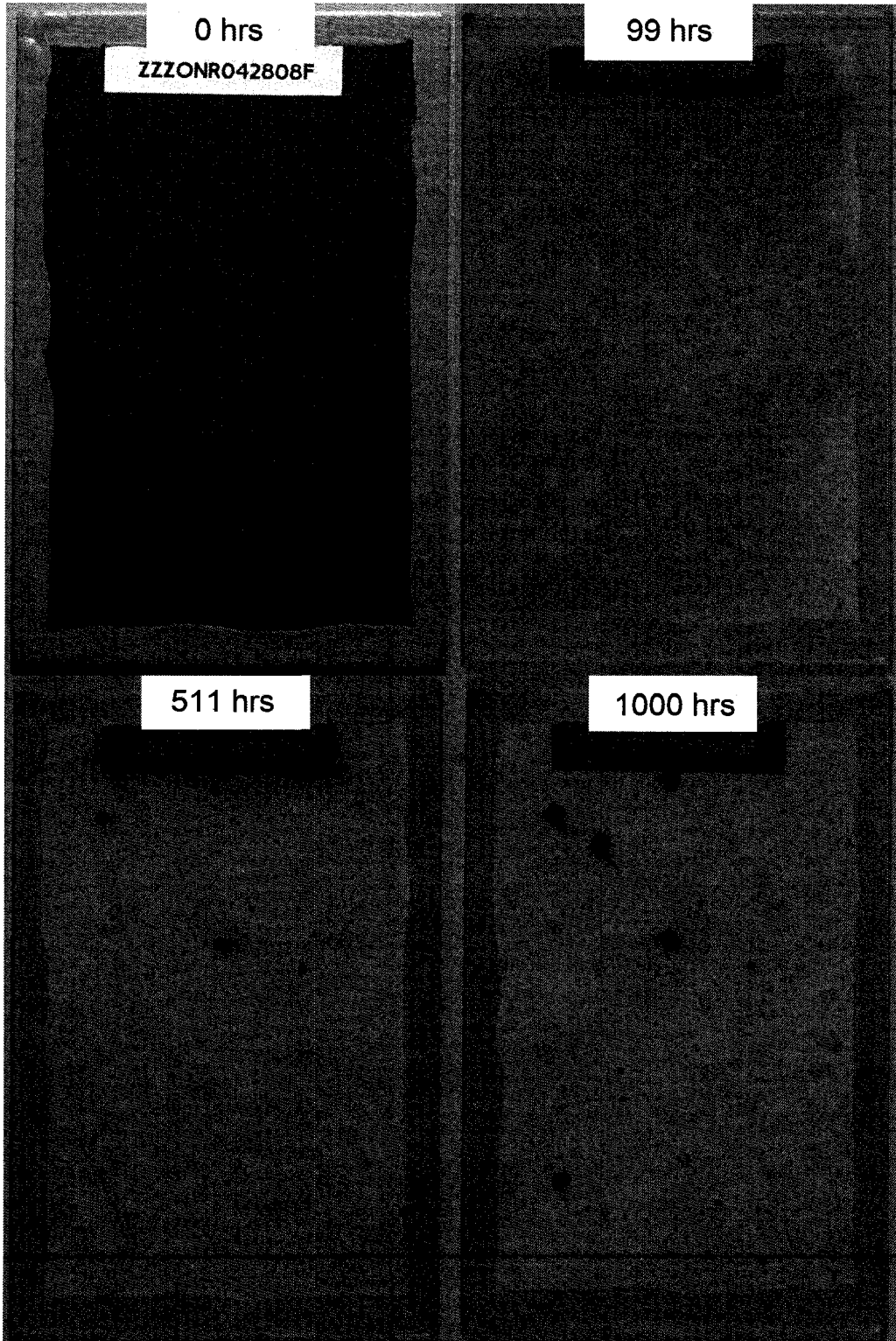
ZZZONR042808C - Salt Spray Exposure - 2.5 wt % ZZZONR042508



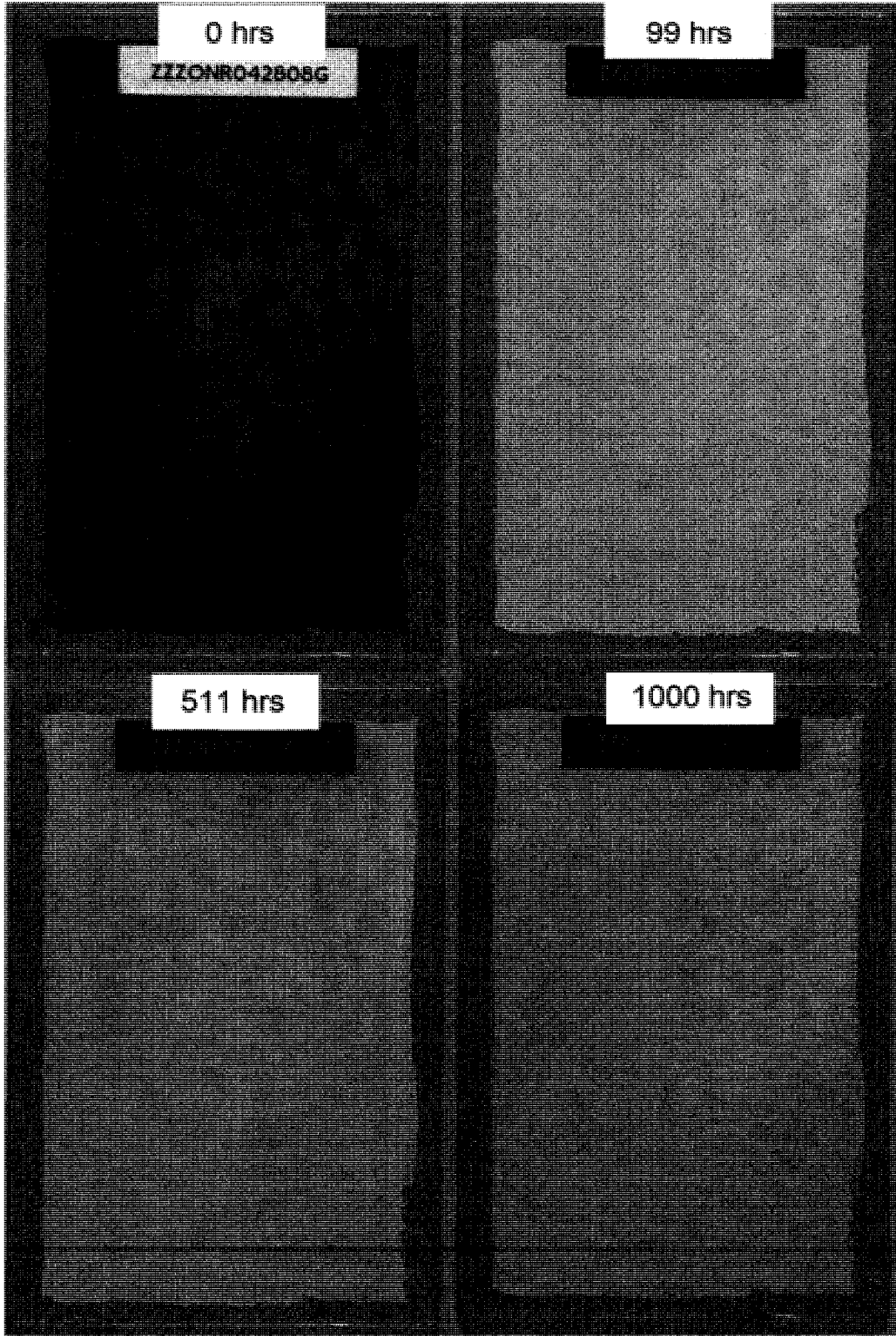
ZZZONR042808D - Hot DI Immersion - 2.5 wt % ZZZONR042508



ZZZONR042808E - Salt Spray Exposure - 5 wt % ZZZONR042508



ZZZONR042808F - Hot DI Immersion - 5 wt % ZZZONR042508



ZZZONR042808G - Hot DI Immersion - 10 wt % ZZZONR042508

REFERENCES

- 1 Virmani, Y. P. ; "Corrosion Costs and Preventative Strategies in the United States" US Dept. of Transportation, Publication No: FHWA-RD-01-156, 2002
- 2 USGAO; "Defense Management Opportunities to Reduce Corrosion Costs and Increase Readiness"
- 3 USDODIG; "Corrosion Prevention for Wheeled Vehicles", DOD Inspector General Audit Report, No. 93-156, 1993
- 4 Lemieux, E., et al; "Remote Tank Monitoring and Inspection Methods" , NRL Annual Review, 2002
- 5 NRL / Materials / Chemistry / Code 6130 / Code 6138 / Research Areas, "Current Areas of Research", <http://chemistry.nrl.navy.mil/6130/6138/researchareas.php>
- 6 Ahmad,Z; "Principles of Corrosion Engineering and Corrosion Control", Ch4, Butterworth-Heinemann, Oxford, UK, 2006
- 7 Whitman, W.; Russel, R.; Altieri, V.; "Effect of hydrogen-ion concentration on the submerged corrosion of steel", Journal of Industrial and Engineering Chemistry, Volume 16, p655, 1924
- 8 Jones, D. A.; "Principles and Prevention of Corrosion", Ch 11, Prentice Hall Inc, Saddle River, NJ, 1996
- 9 O'Grady, W. E.; Bockris, J O'M.; "Interpretation of Moessbauer spectra of passive films on metals", Surface Science, Volume 38, No. 1, p249-51, 1973
- 10 Revie, R.; Baker, B; Bockris, J.; "The Passive Film on Iron: An Application of Auger Electron Spectroscopy", Journal of the Electrochemical Society:Electrochemical Science and Technology, Volume 122, No. 11, p1460-1466, 1975
- 11 Thomas, J. G. N.; Davies, J. D; " Influence of hydrogen carbonate and chloride ions on the stability of oxide films on mild steel in near-neutral solutions", British Corrosion Journal , Volume 12, 2, p108-114, 1977
- 12 Scully, J.; Budiansky, N.; Tiwary, Y.; Mikhailov, A.; Hudson, J.;"An Alternate Explanation for the abrupt current increase at the pitting potential", Corrosion Science, Volume 50, p 316-324, 2008
- 13 Thomas, J.G.N.; "CURRENT VIEWS ON MECHANISMS OF ACTION OF CORROSION INHIBITORS", Practical Aspects of Corrosion Inhibition, Proceedings of a symposium sponsored by the Society of Chemical Industrial Materials Preservation Group, Teddington, Middlesex, England, Feb. 28, 1979
- 14 Chung, K.W.; Kim, K.B.; "A study of the effect of concentration build-up of electrolyte on the atmospheric corrosion of carbon steel during drying", Corrosion Science, Volume 42, Issue 3, p517-531, 2003
- 15 Reffass, M.; Sabot, R.;Savall, C.; Jeannin,M.;Creus, J. ; Refait, Ph. ;"Localized corrosion of carbon steel in NaHCO3/NaCl electrolytes: role of Fe(II)-containing compounds", Corrosion Science, Volume 48, Issue 3, p709-726, 2006

-
- 16 Dexter, S.; "Metals Handbook: Corrosion", Volume 13, 9th Ed., p893 ASM Int., Metals Park, OH, 1987
 - 17 Morcillo, M.; Hernandez, L.; Simancas, J.; Feliu, S., Jr.; Gimenez, S.; "Underfilm corrosion of steel induced by saline contaminants at the metal/paint interface", Journal of the Oil and Colour Chemists' Association , Volume 73, No.1, p24-28, 1990
 - 18 Bregman, J.I.; "Corrosion Inhibitors", Ch 1, The Macmillan Company, New York, NY, 1963
 - 19 Ayala, V.; Ingalls, A.; Genesca, J.; "Mathematical Modeling of Rebar Corrosion in Seawater", Intercor/96 Proceedings, 1st Online Corrosion Conference, 1996
 - 20 Dickie, R.; "An introduction to corrosion control by organic coatings", ACS Symposium Series, Volume 285(Appl. Polym. Sci. (2nd Ed.)), p773-799, 1985
 - 21 Maitland, C.C.; Mayne, J.E.O.; "Factors Affecting the Electrolytic Resistance of Polymer Films", Official Digest , 34, pp972-991, 1962
 - 22 Thomas, N. L.; "The Protective Action of Coatings on Rusty Steel", The Journal of Protective Coatings and Linings, 6 (12), p63-71, 1989
 - 23 Chandler, K.; "Attaining the Potential Performance of Coating Systems in Marine Environments", Marine and Offshore Corrosion, Ch 12 Butterworths, London, UK 1985
 - 24 Scantlebury, D.;" The Dynamic Nature of Underfilm Corrosion", Corrosion Science, Volume 35, No. 5-8, p1362-1366, 1999
 - 25 Hepburn, B. J.; Gowers, K. R.; Scantlebury, J. D.; "Interpretation of low frequency a.c. impedance data for organic coatings on mild steel", British Corrosion Journal , Volume 21, No. 2, p105-108, 1986
 - 26 Mayne, J. E. O.; "Mechanism of anticorrosion action of polystyrene coatings", Journal of the Oil and Colour Chemists' Association,, Volumes 32, p481-487, 1949
 - 27 Schwenk, W.;"Adhesion Loss of Organic Coatings: Causes and Consequences for Corrosion Protection", Corrosion Control of Organic Coatings, Conference Proceedings, p103-10, 1981
 - 28 Hammond, J.; Holubka, J.; Dickie, R.; "Surface Analysis of Interfacial Chemistry in corrosion-induced paint adhesion loss", Journal of Coatings Technology, Volume 51, No. 655, p45-49, 1979
 - 29 Sakashita, M.; Shimakura, T.; Sato, N.;"Ion selectivity and electro-osmosis in porous precipitate films of hydrated iron(III) oxide" Proceedings - International Congress Metals Corrosion, Volume 1, p126-131, 1984
 - 30 Turoscy, R., Leidheiser, H, Jr.; Roberts, J.;"Solid State NMR Studies of Ions in Protective Coatings", Journal of the Electrochemical Society, Volume 139, No.3, p779-783, 1992
 - 31 O'Brien, E.; White, C.; Vogt, B.; "Correlating Interfacial Moisture Content and Adhesive Fracture Energy of Polymer Coatings on Different Surfaces" Advanced Engineering Materials, Volume 8, No. 1-2, p114-118, 2006
 - 32 Tator, K.; "Metals Handbook, Vol 13, Corrosion," 9th Ed, ASM Int., Metals Park, OH, p399, 1987

-
- 33 Gotro, J.; Prime, B.; "Thermosets" Polymer Encyclopedia, Volume 12, p 208, Wiley and Sons, 2004
- 34 Pham, H.; Marks, M.; "Epoxy Resins", Polymer Encyclopedia, Volume 9, p684, Wiley and Sons, 2004
- 35 Ha Q. Pham, Ha Q.; Marks, M. J.; "Epoxy Resins", Encyclopedia of Polymer Science and Technology, Vol. 9, p679, John Wiley & Sons, Inc., 2002
- 36 Cherry, T.; "Navy Preservation Working Group", Carrier Planning Activity Cost Risk Summit, April 24-25 2007
- 37 Wicks, Z. W. Jr; "Coatings", Encyclopedia of Polymer Science and Technology, John Wiley & Sons, Inc., 2007
- 38 Gonzalez, S.; MirzaRosca, I.; Souto, R.; "Investigation of the Corrosion Resistance Characteristics of Pigments in Alkyd Coatings on Steel", Progress in Organic Coatings, Volume 43, p282-285, 2001
- 39 Kalendova, A.; Brodinova, J.; "Spinel and Rutile Pigments Containing Mg, Ca, Zn and Other Cations for Anticorrosive Coatings", Anti-Corrosion Methods and Materials, Volume 50, No. 5, p353-363, 2003
- 40 Johnson, W.; "Cost Effective Pigmentation in Alkyd Primers for Steel: Barrier Anti—Corrosion Mechanism", Journal of Coatings Technology, Volume 66, No. 4, p47-55, 1994
- 41 "Pigment Volume Concentration (PVC)",
<http://www.pslc.ws/macrog/mpm/coatings/pigments/pvc.htm>, May 2008
- 42 Asbeck, W.; Van Loo, M.; "Critical Pigment-Volume Relationships", Journal of Industrial and Engineering Chemistry, Volume 41 p1470-1475, 1949
- 43 Asbeck, W.; "Critical Pigment Volume Concentration Measurements. A Very Fast Method", JCT CoatingsTech, Volume 2, No. 14, p64-66, 2005
- 44 Asbeck, W.; "Dispersion and agglomeration: effects on coatings performance", Journal of Coatings Technology, Volume 49, No. 635, p59-70, 1977
- 45 Braunshausen, R., Jr.; Baltrus, R.; De Bolt, L.; "A Review of Methods of CPVC [critical pigment volume concentration] Determination", Journal of Coatings Technology, Volume 64, No. 810, p51-54, 1992
- 46 Ahmad, Z.; "Chapter 7: Coatings", Principles of Corrosion Engineering and Corrosion Control, p420, Butterworth-Heinemann, Oxford, UK, 2006
- 47 Boggs, L.; Law, D.; Taniguchi, H.; "Rheological properties and Aluminum Flake Orientation in Waterborne Automotive Coatings", Proceedings of the 25th Waterborne, High Solids, and Powder Coatings Symposium, p 30-39, 1998
- 48 DeWit, J.; "Inorganic and Organic Coatings", Corrosion Mechanisms in Theory and Practice, Ch 16, p 611, Marcel Dekker, Inc, NY, 1995
- 49 Mallik, B.; Naik, S.; Khanna, A.; SreeKumar, S.; "High Performance Glassflake Coatings for Aggressive Environments", Paintindia, Annual, p87-98, 2003

-
- 50 Greenwood-Sole, G; "Recent Developments in Glassflake Technology", Polymers in Aggressive and Corrosive Environments, Conference Proceedings, Cologne, Germany, p 15-24, 2004
- 51 Kumar, A.; Wittmar, D.; "Coatings and Cathodic Protection of Pilings in Sea Water: Results of 5 Year Exposure", Materials Performance, Volume 18, No. 12, p9-19, 1979
- 52 Knudsen, O.; Bardal, E.; Steinsmo, U.; "Effect of Barrier Pigments on Cathodic Disbonding Part 1: Aluminum and Glass Pigments", The Journal of Corrosion Science and Engineering, Volume 2, paper 13, 1999
- 53 El-Sawy, S.; Ghanem, N.; "Glass Aluminum Physical Barrier Anticorrosive Paints", Journal of Oil and colour Chemists Assotiation, Volume 67, No. 10, p253-255, 1984
- 54 Knudsen, O.; Stiensmo, U.; "Effect of Barrier Pigments on Cathodic Disbonding Part 2: Mechanism of the Effect of Aluminum Pigments", The Journal of Corrosion Science and Engineering, Volume 2, paper 37, 1999
- 55 Hare, C.; Fernald, M.; "Anti-Corrosive Barrier Pigments", Modern Paints and Coatings, p138-150, October, 1984
- 56 Kruba, L; Stucker, P.; Schuster, T.; "Zinc Flake/Zinc Dust Shop Primer with Reduced Zn content in ethyl silicate binder", Pitture e Vernici, European Coatings, Volume 81, No. 5, p51-58, 2005
- 57 Hochmannova, L.; "Spherical and Lamellar Zinc Dust", European Coatings Journal, p257-262, 2002
- 58 Muller, B.; Langenbucher, J.; "Complete Corrosion Inhibition of Lamellar Zinc Pigment in Aqueous Alkaline Media", Corrosion Science, Volume 45, p395-401, 2003
- 59 Nayak, C.; "Role of Micaceous Iron Oxide in Protective Coatings", Paintindia, Volume 52, No.11, p57-72, 2002
- 60 Carthey, N.; White, K.; "Treatment of Lamellar or Plate-Like Pigments or Extenders with Zinc Phosphate and Anticorrosive Paints Containing Them", EU Pat No: EP 505086, 1992
- 61 Kalenda, P.; Kalendova, A.; Raskova, K; "New Surface Treated Pigments and Fillers with Lamellar Particles in Coatings", Pitture E Vernici, European Coatings, Volume 9, p43-46, 2004
- 62 Emira, H; "Effect of PVC/CPVC ration of Non-Toxic, Platy, Pigments on Corrosion Protection of Acrylic Modified Alkyd Coatings", Anti-Corrosion Methods and Materials, Volume 53, No. 4, 224-231, 2006
- 63 Ahmed, N.; Attia, A.; Selin, M.; "The Effect of Cobalt Oxide on Zinc Oxide in a New Anticorrosive Green Pigment", Anti-corrosion Methods and Materials, Volume 52, No. 6, p 353-364, 2005
- 64 Skoulidkidis, Th.; Vassiliou, P.; Vlachos, S.; "New Anticorrosive Pigments", Developments in Marine Coatings, p132-142,1998
- 65 Augustyn, M.; "Use of Corrosion Inhibitors in Coatings Part 1", Pitture e Vernici – European Coatings, Volume 19, p33-45. 2004

-
- 66 Augustyn, M.; "Use of Corrosion Inhibitors in Coatings Part 2", *Pitture e Vernici – European Coatings*, Volume 20, p37-45, 2004
- 67 Lima-Netoa, P.; de Araujo, A.; Araujo, W. ; Correia, A.; "Study of the Anticorrosive Behaviour of Epoxy Binders Containing Non-Toxic inorganic Corrosion Inhibitor Pigments", *Progress in Organic Coatings*, Volume 62, p344-350, 2008
- 68 Pianoforte, K.; "Anti-Corrosion Coatings: Nanotechnology will play a key role in the corrosion inhibitor market as new technology is developed", *Coatings World*, February, 2007
- 69 Zim, I.; Howard, R. Badger, S. Scantlebury, J.; Lyon, S.; "The Mode of Action of Chromate Inhibitor in Epoxy Primer on Galvanized Steel", *Progress in Organic Coatings*, Volume 33, p203-210, 1998
- 70 Baghini, I.; Lyon, S.; Ding, B.; " The Effect of Strontium and Chromate Ions on the Inhibition of Zinc", *Surface and Coatings Technology*, Volume 185, p194-198, 2008
- 71 Sinko, J.; "Challenges of Chromate Inhibitor Pigments Replacement in Organic Coatings", *Progress in Organic Coatings*, Volume 42, p 267-282, 2001
- 72 Bethencourt, M.; Botana, F.; Marcos, M.; Osuna, R.; Sanches-Amaya, J.; "Inhibitor Properties of "green" Pigments for Paints", *Progress in Organic Coatings*, Volume 46, p280-287, 2003
- 73 Rossotti, H.; "Colour: Why the World Isn't Grey", Princeton University Press, Princeton, NJ, 1983
- 74 Rabinowitz, M.; Hall, G.; " Isotopic Characterization of Six Major Brands of White Basic Lead Carbonate Paint Pigments", *Bulletin of Environmental Contamination and Toxicology*, Volume 69, p617-623, 2002
- 75 Barnes, G.; Davis, A.; "Dissolution of Lead Paint in Aqueous Solutions", *Journal of Environmental Engineering*, Volume 122, No.7, p663-666, 1996
- 76 Mayne, J.; Heyes, P.; "Metal coating compositions", United States Patent 4135934, 1979
- 77 Thomas, N.; "The Protective Action of Red Lead Pigmented Alkyds on rusted mild steel", *Proceedings - Electrochemical Society*, Volume 89, No. 13, p451-467, 1989
- 78 Lindqvist, S.; "Corrosion Inhibiting Properties of Red Lead: Catalytic activity of metallic lead in the repair of the oxide layer on steel due to a polarity change in the bimetal couple lead-steel", *Journal of the Oil and Colour Chemists Association*, Volume 67, No. 11, p288-292, 1984
- 79 Newnham, H. ; "Chemical Reactions in Metallic Lead Pigmented Paint Films", *Protection and Corrosion Metallic Finishing*, *Proceeds of the International Conference*, p342-345, Meeting Date 1966
- 80 Shirsalkar, M.; Sivasamban, M.; " New Anticorrosive Paints for Corrosion Prevention of Metals", *Corrosion and Maintenance*, Volume 2, No. 3, p203-206, 1979
- 81 Kalendova, A.; Kalenda, P.; Vesely, D.; "Comparison of the Efficiency of inorganic nonmetal pigments with Zinc Powder in Anticorrosion Paints", *Progress in Organic Coatings*, Volume 57, p1-10, 2006

-
- 82 Amirudin, A.; Thierry, D.; "Application of Electrochemical Impedance Spectroscopy to Study Efficiency of Anticorrosive Pigments in Epoxy Poyamide Resin", *British Corrosion Journal*, Volume 30, No. 2, p128-134, 1995
- 83 Barraclough, J.; Harrison, J.; "New Leadless Anti-Corrosive Primers", *Journal of the Oil and Colour Chemists' Association*, Volume 48, p341-351, 1965
- 84 Pantzer, R.; "Survey and field of application of lead free anticorrosive pigments", *Anti-Corrosion Methods and Materials*, Volume 22, No. 6, p3-7, 1975
- 85 Robinson, J.; Walsh, F.; "In Situ Synchrotron Radiation X-Ray Techniques for Studies of Corrosion and Protection", *Corrosion Science*, Volume 35, No. 1-4, p 791-800, 1993
- 86 Caprari, J.; Di Sarli, A.; del Amo, B.; "Zinc Phosphate as Corrosion Inhibitive Pigment of Waterborne Epoxy Paints Used for Steel Protection", *Pigment and Resin Technology*, Volume 29, No. 1, p16-22, 2000
- 87 Kwaitkowski, L.; Lutze, A.; Kozowska, A.; "The Influence of Surface Pre-Treatment on Inhibitive Properties of Phosphate Pigments", *Pittura e Vernici, European Coatings*, Volume 81, No. 14, p5-14, 2005
- 88 Zin, I.; Lyon, S.; Pokhmurskii, V.; "Corrosion Control of Galvanized Steel using a Phosphate/Calcium Ion Inhibitor Mixture", *Corrosion Science*, Volume 45, p777-788, 2003
- 89 Deya, C.; Romagnoli, R.; del Amo, B.; "A New Pigment for Smart Anticorrosion Coatings", *Journal of Coatings Technology and Research*, Volume 4, No 2, p167-175, 2007
- 90 Naderi, R.; Attar, M.; "Electrochemical assessing corrosion inhibiting effects of Zinc Aluminum Polyphosphate (ZAPP) as a modified zinc phosphate pigment", *Electrochimica Acta*, Volume 53, No. 18, p5692-5696, 2008
- 91 Lahodny- arc O.; Kaštelan, L.; "Inhibition of Mild Steel by Polyphosphates", *Corrosion Science*, Volume 16, No.1, p25-34, 1976
- 92 Kalendova, A.; "Comparison of the Anticorrosion Efficiencies of Pigments Based on Condensed Phosphates and Polyphosphosilicates", *Anti-Corrosion Methods and Materials*, Volume 50, No. 2, p82-90, 2003
- 93 Deflorian, F.; Felhosi, I.; Rossi, S.; Fedrizzi, L.; Bonora, R.; "Performance of Primers Containing Polyphosphate-Based Ion-Exchange Pigments for the Protection of Galvanized Steel", *Macromolecule Symposia*, Volume 187m p87-96, 2002
- 94 Vetere, V.; Romagnoli, R.; "Role of Calcium Acid Phosphate as Corrosion Inhibitive Pigment", *British Corrosion Journal*, Volume 29, No 2, p115-119, 1994
- 95 Liang, C.; Guoo, J.; Xianqi, H.; "Effects of Mo Composites on the Corrosion Behaviors of Low Alloy Steel", *Journal of Wuhan University of Technology, Materials Science Edition*, Volume 22, No. 1, p12-16, 2007
- 96 Vukasovich, M.; Farr, J.; "Molybdate in Corrosion Inhibition – A Review", *Materials Performance*, Volume 25, No. 5, p9-18, 1986
- 97 Leite, A.; Araujo, W.; Margarit, I.; Correia, A.; de Lima-Neto, P.; "Evaluation of the Anticorrosive Properties of Environmental Friendly Inorganic Corrosion Inhibitors Pigments", *Journal of the Brazilian Chemical Society*, Volume 16, No. 4, p 756-762, 2005

-
- 98 del Amo, B.; Romagnoli, R.; Deya, C.; Gonzalez, J. A.; "High Performance Water-Based Paints with Non-Toxic Anticorrosive Pigments", *Progress in Organic Coatings*, Volume 45, No. 4, p389-397, 2002
- 99 Zin, I.; "Corrosion Inhibition of Galvanized Steel with Inorganic Pigments", *Materials Science*, Volume 35, No. 6, p874-878, 2000
- 100 Veleva, L.; Chin, J.; del Amo, B.; "Corrosion electrochemical behavior of epoxy anticorrosive paints based on zinc molybdenum phosphate and zinc oxide", *Progress in Organic Coatings*, Volume 36, No. 4, p211-216, 1999
- 101 Weinert, L.; "Resistance to Flash Rusting and Corrosion Undercutting of Water-thinned Paint Films Containing Barium Metaborate", *Industrial Finishing and Surface Coatings*, Volume 28, No. 332, p7-12, 1976
- 102 Balakrishnan, K.; Muthukrishnan, S.; Jayakrishnan, P.; Venkatachari, G.; Maruthan, K.; "Studies on the Performance of Barium Metaborate Pigment in Primers", *Transactions of the SAEST*, Volume 28, No. 3, p123-128, 1993
- 103 Hare, C.; "Mechanisms of Corrosion Protection with Surface Treated Wollastonite Pigments", *Paint and Coatings Industry*, p74-81, March 1998
- 104 Kalendová, A.; "Comparison of the Efficiencies of Anticorrosive Pigments Based on Chemically Modified Phosphates", *Anti-Corrosion Methods and Materials*, Volume 49, No. 5, p364-372, 2002
- 105 Snuparek, J.; Kalendova, A.; "Anticorrosion Pigments for Chemically and Thermally Resistant Coatings", *Macromolecular Symposia*, Volume 187, p97-107, 2002
- 106 Vasconcelos, L.; Maia, A.; Margarit, I.; Mattos, O.; Fragata, F.; de Lima Nato, P.; Teixeira, B. Dos Santos, J.; "Comparative behavior of Zinc Phosphates and Calcium Exchanged Paints", *Electrochemical Society Proceedings*, Volume 24, p60-70, 2000
- 107 Shieldex Product Information, W. R. Grace & Co,
<http://www.grace.com/EngineeredMaterials/ProductsAndApplications/Coatings/Anti-CorrosivePigments/SHIELDEXPigments.aspx>, 2008
- 108 "SHIELDEX® AC 3: Non-Toxic Anti-Corrosive Pigment", *Engineering Data Sheet*, BOYSAN, Istanbul Turkey, 2008
- 109 Loveridge, M.; McMurray, H.; Worsley, D.; "Chrome Free Pigments for Corrosion Protection in Coil Coated Galvanized Steels", *Corrosion Engineering, Science and Technology*, Volume 41, No. 3, p240-248, 2006
- 110 Kouloumbi, N.; Moundoulas, P.; "Anticorrosive Performance of Organic Coatings on Steel Surfaces Exposed to Deionized Water", *Pigment and Resin Technology*, Volume 1, No. 2 p74-83, 2002
- 111 Vilche, J.; Bucharsky, E.; Giudice, A.; "Application of EIS and SEM to evaluate the Influence of Pigment Shape and Content in ZRP Formulations on the corrosion prevention of Naval Steel", *Corrosion Science*, Volume 44, p 1287-1309, 2002

-
- 112 Emira, H.; Abdel-Mohsen, F.; "The dependence of the Corrosion Protection of Water-Borne Paints on the Concentration of the Anticorrosive Pigment", *Pigment and Resin Technology*, Volume 32, No. 4, p259-265
- 113 Mayne, J.; "The Use of Inhibitive Pigments in Paints", *Practical Aspects of Corrosion Inhibition*, Proceedings of a symposium sponsored by the Society of Chemical Industrial Materials Preservation Group, p49-53, Teddington, Middlesex, England, Feb. 28, 1979
- 114 Fang, J.; Xu, K.; Zhu, L.; Zhou, Z.; Tang, H.; "A Study on Mechanism of Corrosion Protection of Polyaniline Coating and its Failure", *Corrosion Science*, Volume 49, p4232-4242, 2007
- 115 Armelin, E.; Ocampo, C.; Liesa, F.; Iribarren, J.; Ramis, X.; Aleman, C.; "Study of Epoxy and Alkyd Coatings Modified with Emeraldine Base From of Polyaniline", *Progress in Organic Coatings*, Volume 58, p316-322, 2007
- 116 Attar, M.; Scantlebury, J.; " Polyaniline as a possible inhibitor for the Corrosion of Mild Steel", *The Journal of Corrosion Science and Engineering*, Volume 1, paper 8, 1997
- 117 Kalendova, A.; Vesely, D.; Stejskal, J.; "Organic Coatings Containing Polyaniline and Inorganic Pigments as Corrosion Inhibitors", *Progress in Organic Coatings*, Volume 62, p105116, 2008
- 118 Wessling, B.; "Scientific Engineering of Anti-Corrosion Coating Systems Based on Organic Metals (Polyaniline)", *Journal of Corrosion Science and Engineering*, Volume 1, paper 15, 1999
- 119 Sathiyarayanan, S.; Azim, S.; Venkatachari, G.; " Preparation of Polyaniline – TiO₂ Composite and its comparative corrosion protection performance with polyaniline", *Synthetic Metals*, Colume 157, p205-213, 2007
- 120 Sathiyarayanan, S.; Muthukrishnan, S.; Venkatachari, G.; " Synthesis and Corrosion Protection Performance of Polydiphenylamine", *Journal of Applied Polymer Science*, Volume 105, p 1707-1711, 2007
- 121 Sheih, P.; Massingill, J.; "Fundamental Studies of Epoxy Resins for Can and Coil Coatings. I. Adhesion to Tin-Free Steel", *Journal of Coatings Technology*, Volume 62, No.781, p25-30, 1990
- 122 Adler, J.; "Watching Paint Dry", *Regulation The Cato Review of Business & Government*, Volume 18, No. 4, 1995
- 123 MIL-PRF-16173E; "Performance Specification: Corrosion Preventative Compounds, Solvent Cutback, Cold-Application", September, 2006
- 124 PPI NBR: 63101-00 (REV 22); "Preservation Process Instruction (PPI) Core: Cleaning, Surface Preparation and Painting Requirements for Area to be Prepared", 2007
- 125 Lemieux, E.; "New Preservation Techniques on the Horizon", Conference presentation, MegaRUST, 2007
- 126 Venderbosch, R.; Meijer, H.; Lemstra, P.; "Processing of intractable polymers using reactive solvents. 2. Poly(2,6-dimethyl-1,4-phenylene ether) as a matrix material for high performance composites", *Polymer*, Volume 36, No.6, p1167-1178, 1995

-
- 127 Weijnen, J.; Kemp, J.; Van Der Kolk, C.; "Architectural High Solid Alkyd Lacquers; more than just Solvent Reduction" *Verfkroniek*, 72(4), p14-20, 1999
- 128 Massingill, J.; Waters, D.; "Higher Solids Epoxy Coatings", *Chemtech*, Volume 22, no 4, pp 242-247, 1992
- 129 Mayne, J.;" Further Developments with Epoxyamine Films", *Corrosion Science*, Volume 35, No. 5-8, p1359-1361, 1993
- 130 US Patent 5362914 - Decolorization of polyethylene polyamines using cobalt/copper/chromium, issued Nov, 1994
- 131 Ogier, J. E.; "Polyurethane Polymerization Kinetics" MS Thesis, University of New Hampshire 2004
- 132 Mijovic, J.; Wijaya, J.; "Reaction Kinetics of Epoxy/Amine Model Systems. The Effect of Electrophilicity of Amine Molecule", *Macromolecule*, v27, n26, pg 7589-7600, 1994
- 133 Minkyu Hwang and Kilwon Cho "Effect of chain entanglement on the bulk strength of glassy polymer", Department of Chemical Engineering, Pohang University of Science and Technology, http://www.postech.ac.kr/ce/pail/MinkyuAb_1.htm, 2008
- 134 *Bio-Organic Chemistry*, Volume 22, p318-327, 1994
- 135 Star, A.; Han, T.; Joshi, V.; Gruner, G.; "Polymer Coatings of Nanotube Sensors", *Polymer Preprints*, 44(2) p201, 2003
- 136 Hubbe, M; "Additives and Ingredients, their Composition Function, Strategies for Use ", *Mini-Encyclopedia of Papermaking Wet End Chemistry*, 2006
- 137 Kinsella, E.; Mayne, J.;"Ionic Conduction in Polymer Films I. Influence of Electrolyte on Resistance", *British Polymer Journal*, Vol 1, No 7, p173-176, 1969
- 138 Becker, O.; Varley, R.; Simon, G.; " Thermal Stability and Water uptake of High Performance Epoxy Layered Silicate Nanocomposites", *European Polymer Journal*, Vol 40 p 187-195, 2004
- 139 Philippe, L.; Lyon, S.; Sammon, S.; Yarwood, J. ; "Validation of Electrochemical Impedance Measurements for Water Sorption inot Epoxy Coatings using Gravimetry and Infrared Spectroscopy ", *Corrosion Science*, Vol. 50, p887-896, 2008
- 140 Dullien, F.; Shemlit, L.;"Equations for determining Diffusion Coefficients in Liquid Systems by the Diaphragm Cell Technique", *Letters to Nature*, Vol 187, p767-768, 1960
- 141 "Fick's law of Diffusion", Wikipedia, http://en.wikipedia.org/wiki/Diffusion_coefficient.html, August, 2008
- 142 Lakatos, I.; Lacatos-Szabo, J.; „ Diffusion of H⁺, H₂O, and D₂O in polymer/silicate gels', *Colloids and Surfaces A: Physicochemical Engineering Aspects*, Vol 246, p9-19, 2004
- 143 Halamickova,P.; Detwiler,R.; Bentz, D.; Garboczi, E; "WATER PERMEABILITY AND CHLORIDE ION DIFFUSION IN PORTLAND CEMENT MORTARS: RELATIONSHIP TO SAND CONTENT AND CRITICAL PORE DIAMETER", *Cement and Concrete Research*, Vol 25, p790-802, 1995

-
- 144 Lyon, S.; Phillipe, L.; Tsuousoglou, E.; "Direct Measurement of Ionic Diffusion in Protective Organic Coatings", Transactions of the Institute of Metal Finishing, Vol 84 No. 1, p23-27, 2006
- 145 Fieldson, G.; Barbari, T.; " Analysis of Diffusion in Polymers Using Evanescent Field Spectroscopy", AIChE Journal, Vol 41, No 4, p795-804, 1995
- 146 Li, L.; Chen, Y.; Li, S.; "Water Diffusion Behavior in Epoxy Resins with Various Flourine Contents", Applied Spectroscopy, Vol. 60, No 4, p392-397, 2006
- 147 Philippe, L.; Lyon, S.; Sammon, S.; Yarwood, J.; " InSitu Study of Phosphate Diffusion in Epoxy Coatings Using Attenuated Total Reflectance Infrared Spectroscopy", Corrosion Engineering Science and Technology, Vol 38, No 2, p153-156, 2003
- 148 Socrates, G.; "Infrared and Raman Characteristic Group Frequencies", Third Edition, Wiley & Sons, Ltd. NY, NY, 2001
- 149 Abd-El-Bary, M.; Manson, J.; Goldstien, J.; "Electron Microprobe Investigation into the Diffusion of Ions Through Polymers", Journal of Materials Science, Vol 5, p 898-900, 1970
- 150 "FT-IR Spectroscopy Attenuated Total Reflectance (ATR)", Technical Note, Perkin Elmer Life and Analytical Sciences, 2005
- 151 "Refractive Index Table", Microtrac Corporation, p8, 2006
- 152 "Miracle ATR for FTIR Spectrometers", Pike Technologies, Madison, WI, Sept. 2006
- 153 Fieldson, G.; Barbari, T.; " The Use of DTIR-ATR Spectroscopy to characterize penetrant diffusion in polymers", Polymer, Vol 34, No 6, p 1146-1153, 1993
- 155 Aria, Y.; Sparks, D.; " ATR-FTIR Spectroscopic Investigation of Phosphate Adsorption Mechanisms at the Ferrihydrite-Water Interface", Journal of Colloid and Interface Science, Vol 241, p317-326, 2001
- 156 The Society for Protective Coatings; "SP - Surface Preparation Standards and Specifications", 2008
- 157 Claydon, D.; "Performance Testing of Anti-Corrosion Coatings", White Paper, International Protective Coatings, Akzo Nobel, England, 2008
- 158 "Acute Exposure Guideline Levels for Selected Airborne Chemicals Volume 6, Appendix 1: Allylamine", The National Academies Press, Washington, DC, p12, (2007)
- 159 Shionbekova, S.A.; Nikitina, A. I.; Ergozhin, E.E.; Mukhitdinova, B.A.; Razuvaeva, N.I.; "Activity of Mono- and Disubstituted Derivatives of 1,4-Benzoquinone and Allylamine in Cationic Polymerization", Russian Journal of Applied Chemistry, v 80, n6, p 1012-1014, 2007
- 160 Scherbina, F.; Fodorova, I.; Gorlov, Yu.; " Chain Transfer During Polymerization of Allylamine and its Acyl Derivatives", Highmolecular Compounds, Series A, v12, n9, p2042-2045, 1970
- 161 Drucker, A.; Morawetz, H.; " Amphoteric Polyelectrolytes. III. Copolymerization of Allylamine and Methacrylic Acid", Journal of Polymer Science, vol 78, no 12, p 346-347, 1955

-
- 162 Ergozhin, E.; Hirotsu, T.; Mukhitdinova, B.; Shoinbekova, S.; Nikitina, A.; Razuvaeva, N.; "Cationic Polymerization of a Derivative of Allylamine and 1,2 Naphthoquinone", *Macromolecular Chemistry and Polymeric Materials*, v79, no. 9, pp1506-1508, 2006
- 163 Wang, D.; Li, K.; Teo, W.; "Phase Separation in Polyetherimide Solvent/Nonsolvent Systems and Membrane Formation", *Journal of Applied Polymer Science*, Vol. 71, p1789-1796, 1999
- 164 Snuparek, J.; Kadrnka, B.; Ritz, P.; Quadrat, O.; "Hydroplasticization Effect in Structured Latex Particles Film Formation", *Macromolecule Symposium*, vol 187, p 367-376, 2002